

450

STABLE ISOTOPE STUDIES
OF WATER
EXTRACTED FROM SPELEOTHEMS

STABLE ISOTOPE STUDIES OF WATER EXTRACTED
FROM SPELEOTHEMS

by

CHARLES J. YONGE, B.Sc., M.Phil.

A Thesis

Submitted to the School of Graduate Studies
in Partial Fulfilment of the Requirements
for the Degree
Doctor of Philosophy

McMaster University

February 1982

DOCTOR OF PHILOSOPHY (1982)
(Geology)

McMaster University

TITLE: Stable Isotope Studies of Water Extracted
from Speleothems

AUTHOR: Charles J. Yonge, B.Sc. (Surrey University,
England)
M.Phil. (Surrey University,
England)

SUPERVISORS: Professor Henry P. Schwarcz and
Professor Derek C. Ford

NUMBER OF PAGES: i-xvii; 1-298

ABSTRACT

Calcite speleothems, if shown to be formed under conditions of isotopic equilibrium with their parent seepage waters, can be used to determine relative changes in the past climates from measurement of $\delta^{18}\text{O}$ of the calcite. Furthermore, if $\delta^{18}\text{O}$ of the parent seepage water can be estimated and shown to be equivalent to meteoric precipitation falling at the cave site, then depositional temperatures can be recovered from the temperature dependent oxygen isotope fractionation of the calcite-water pairs. Cave temperatures generally reflect mean annual surface temperatures above the cave. Thus, should the depositional temperature accurately record the cave temperature, then analysis of successive growth layers in speleothems should provide a direct measure of past temperature change at a given site. Estimates of $\delta^{18}\text{O}$ of past seepage water can be made, in principle, because speleothems incorporate seepage water within inclusions as they grow. However, since oxygen in the fluid inclusion water may exchange with that in the carbonate phase, hydrogen isotopes, which cannot exchange, are measured instead. $\delta^{18}\text{O}$ of the original seepage water can then be inferred from δD , if seepage water can be shown to be equivalent to included water, because meteoric relationships exist which link them. Work prior to this study suggested that, following the method outlined above, isotopic temperatures could be recovered from

speleothems.

The early part of this study involved the construction and operation of a mass spectrometer and associated extraction line for δD analyses and some modification to existing apparatus for $\delta^{18}O$ analysis.

Water samples were then analysed from a number of cave sites, mainly in the Eastern U.S., to check the isotopic equivalence of seepage water to meteoric precipitation and observe seasonal isotopic variations in seepage and soil water with respect to meteoric precipitation. The general conclusion reached was that seepage water was equivalent to meteoric precipitation and that no seasonal variation occurred in those caves studied in detail. Study of an Antarctic Ice Core showed that the $\delta^{18}O$ - δD relation of meteoric precipitation during the Wisconsin Glacial Maximum was different from that at present.

The latter part of this study was concerned with the systematics of water extraction and the isotopic measurement of water-calcite pairs from speleothems. A previously developed technique, involving crushing of the sample in vacuum prior to freezing over the liberated water, was found not to be as reproducible as had been stated in the literature, and, as a result, an extraction method by heating was developed to replace it. Although great difficulty was encountered in getting this technique to function, it was found, eventually, to

save time in operation, to liberate up to 2.4 times more water and give greater reproducibility than the crushing method. Attempts to demonstrate the isotopic equality of the two methods was only partially successful however, but both methods seemed to yield water from speleothems that was isotopically depleted with respect to their parent seepage waters.

For the latter reason, experiments were undertaken to characterize the water within the calcite because of the possible presence of structural, isotopically modified water. Petrographic observations left no doubt as to the presence of fluid inclusions from 50 μ m down to unresolvable dimensions but it was questionable as to whether or not all the water lay in these sites. IR, polarized IR and neutron diffraction spectroscopy of powders in the 100 μ m range failed to reveal the presence of oriented water in the calcite lattice although 'liquid' water was still observed.

The isotopic depletion of calcite-bound water with respect to parent seepage water in 'modern' samples was found to be $22.1 \pm 3.9\%$ in δD . This value, when applied to δD profiles of six fossil speleothems to retrieve original seepage water δD , gives rise to calculated calcite-water paleotemperatures that are above zero. Comparison of these modified δD and temperature profiles with other records, such as deep sea and ice cores suggested that paleoclimatic information can be obtained from isotopic studies of speleothems. The mechanism(s) responsible

for the isotopic fractionation of calcite-bound water as it is incorporated into the speleothems during growth is speculated upon as an absorption-like phenomenon but no firm conclusions are reached.

ACKNOWLEDGEMENTS

I would like to thank Drs. Henry Schwarcz and Derek Ford for their suggestion of this project, their willingness to supervise it and their interest in some of the ideas generated from it thereafter. Further thanks are extended to Henry Schwarcz for his critical appraisal of the thesis which resulted in considerable improvement of the original draft. I also extend thanks to Dr. H.G. Thode for his interest in the work and willingness to sit on the supervisory committee.

I would like to acknowledge the following people who also helped me during the research and in the production of the thesis:

Russell Harmon for helping me to set up the water sampling programme.

Tom and Cathy Aley for suggesting seepage water collection sites at the Ozark Underground Laboratory and the conscientious manner in which the samples were picked up at regular intervals.

Mr. Proctor and Mr. Swartz, proprietors of Shenandoah and Indian Echo Caverns respectively, for their willingness to undertake water sampling programmes on their property.

Bob Bowins and Ed Beaver for innovative construction of some of the major electronic components of the D/H mass spectrometer and their friendship outside the professional sphere.

Martin Knyf for intelligent, stimulating discussions and continued enthusiastic help in the laboratory and his friendship. Alf Latham, Mel Gascoyne, Tom Miller and Jake Karakastonoglou for many varied discussions both on and off the topic of this thesis and their friendship. Masa Yamamoto for allowing me to draw freely from his unpublished data, many stimulating discussions and his friendship. Jack Whorwood for excellent photographic production. Len Zwicker for the rock cutting facilities and preparation of thin sections. Sharon Fingland and Linda Hillier for their willingness to undertake the monumental task of typing. Office companions, Peter Vilks and Ishmael Hassan, for listening patiently to my woes and for enjoyable discussions in the coffee lounge. Caving and climbing friends for putting the business of work into its proper perspective.

Finally, Pamela Burns, who quite apart from drafting all the diagrams, undertaking some of the typing and criticizing some of the more difficult english in the thesis, has provided continuing support throughout. It is to her that the thesis is dedicated.

TABLE OF CONTENTS

CHAPTER 1	STABLE ISOTOPE STUDIES OF SPELEOTHEMS	
1.1	Geothermometry	1
1.2	Paleoclimatic Interpretation Based on the Calcite Phase Only	5
1.3	Water in Speleothems	10
	1.3.1 Optical Observations	10
	1.3.2 Extraction	17
1.4	Justification of the Present Study	23
CHAPTER 2	EXPERIMENTAL METHODS	
2.1	Dating of Speleothems	25
	2.1.1 Introduction	25
	2.1.2 Uranium Disequilibrium Dating	28
2.2	Stable Isotope Analyses	33
	2.2.1 Preparation of Samples	33
	2.2.2 Oxygen and Carbon from Calcite	34
	2.2.3 Oxygen and Hydrogen from Bulk Water Samples	35
	2.2.3.1 Oxygen	35
	2.2.3.2 Hydrogen	36
	2.2.4 Oxygen and Hydrogen from Speleothem Water	39
	2.2.4.1 Extraction of Water from Speleothems	39
	2.2.4.2 Oxygen from Small Water Samples	43
2.3	Standards	43
2.4	Mass Spectrometry	45
	2.4.1 602D Instrument for $\delta^{13}\text{C}$ and $\delta^{18}\text{O}$ Analysis	45
	2.4.2 The D/H Mass Spectrometer	46
	2.4.2.1 Description	46
	2.4.2.2 Operation	47
	2.4.2.3 Corrections	48
2.5	Precision and Accuracy	53

CHAPTER 3	METEORIC PRECIPITATION AND RECHARGE WATER STUDIES	
3.1	Meteoric Precipitation and Recharge Water at Cave Sites	56
3.1.1	Rationale	56
3.1.2	Field Program	59
3.1.3	Meteoric Precipitation, Soil and Seepage Water at Tumbling Creek Cave, Mo.	64
3.1.4	Meteoric Precipitation and Seepage Water from Two Other North American Sites	71
3.1.5	Seepage Water from Caves in Other Areas	80
3.2	Antarctic Ice Study	90
3.3	Concluding Remarks	96
CHAPTER 4	STUDY OF WATER IN SPELEOTHEMS	
4.1	Introduction	99
4.2	Petrology of Speleothems	100
4.2.1	Speleothem Morphology	100
4.2.2	Crystal Morphology	102
4.2.3	Fluid Inclusions	108
4.2.4	Origin of Fluid Inclusions	113
4.2.5	Description of Speleothems Analysed in This Study	120
4.2.5.1	Modern Active Deposits	120
4.2.5.2	Ancient, Inactive Deposits	123
4.2.5.3	Age Data	137
4.3	Water Content of Speleothems	137
4.3.1	Review of Previous Work	137
4.3.2	A Comparison of Water Content of Speleothems by Crushing and Decrepitation	141
4.3.3	Water Yields from Partial Extraction by Decrepitation	143
4.3.4	Variations of Water Yield Within Speleothems with Regard to Textural Milkiness	147
4.3.5	Variations in Water Content of Speleothems and Relation to Growth Rates	155

4.3.6	Characterization and Quantification of O and H in Speleothems by IR and Neutron Diffraction Spectroscopy	161
4.3.6.1	Neutron Diffraction Spectroscopy	162
4.3.6.2	IR Spectroscopy	162
4.3.7	The Size and Size Distribution of Fluid Inclusions Based on Observations of Water Yields	175
4.4	$\delta^{18}\text{O}$ and δD of Water Extracted from Speleothems	179
4.4.1	Introduction	179
4.4.2	Isotopic Testing of the Samples for Equilibrium Deposition	181
4.4.3	Comparison of Isotope Ratios of Water from Crushing and Decrepitation Extraction Methods	182
4.4.4	Isotopic Composition of Water Extracted by Decrepitation of Crushed Samples	187
4.4.5	Decrepitation of Hydrothermal Minerals as a Test of the Method of Extraction	188
4.4.6	Decrepitation Temperature Versus δD_i	189
4.4.7	A Comparison of Isotopic Ratios in Cave Drip Water and Decrepitation Water from Modern Speleothems	194
4.4.8	Some Speculation on the Isotopic Composition of Fluid Inclusions	197
4.4.9	A Comparison of Isotopic Temperatures Using δD_i and Cave Temperatures	200
4.4.10	A Comparison of Isotopic Temperatures Using $\delta^{18}\text{O}_i$ and Cave Temperatures	202

CHAPTER 5

THE POTENTIAL OF THE METHOD FOR PALEOTEMPERATURE AND PALEOCLIMATIC DETERMINATION

5.1	Application to Pleistocene Climatology	205
5.1.1	Introduction	205
5.1.2	Speleothems from the Holocene and Sangamon Interglacial Periods	206

5.1.2.1	Holocene Stalagmite from McFail's Cave, N.Y.	206
5.1.2.2	Holocene Stalagmite from Cold Water Cave, Iowa	210
5.1.2.3	Three Mid-Wisconsin Speleothems from Cascade Cave, Vancouver Island	212
5.1.2.4	Mid-Wisconsin Stalagmite from Cold Water Cave, Iowa	214
5.1.3	Paleoclimatic Interpretation	217
5.1.3.1	Holocene Records	217
5.1.3.2	Interglacial/Interstadial Records	225
5.1.4	General Discussion	245
5.2	Application of the Decrepitation Method to Hydrothermal Minerals	251
5.3	The Future	254
REFERENCES		260
APPENDIX I	NOTATION	271
APPENDIX II	OPERATION OF D/H MASS SPECTROMETER AND SUBSEQUENT CALCULATION OF δD	273
APPENDIX III	BULK WATER ISOTOPIC ANALYSES	278
APPENDIX IV	ISOTOPE DATA FROM SPELEOTHEMS AND INCLUDED WATER	285
APPENDIX V	ISOTOPE DATA FROM MINERALS OTHER THAN CALCITE	297

LIST OF TABLES

2.1	Standards used for stable isotope analyses	44
2.2	Analyses of isotope standards and results of replicate analyses	54
3.1	Measurements of the temperature dependence of $\delta^{18}\text{O}$ of precipitation	86
3.2	$\delta^{18}\text{O}$ of seepage water and mean annual precipitation for 20 North American sites	87
4.1	Age date of samples studied	138
4.2	A comparison of water yields from speleothems using crushing and decrepitation modes of extraction	142
4.3	Isotope data for partial extractions of 77151B by decrepitation	147
4.4	Growth rates and water contents for various speleothems	160
4.5	Vibrational modes for calcite	167
4.6	Compilation of water yield data from calcite powders by decrepitation and their IR absorption spectra	174
4.7	A comparison of δD_i and $\delta^{18}\text{O}$ in water extracted from speleothems by crushing and decrepitation	184
4.8	Isotopic temperature and δD_i of modern samples compared to modern cave temperatures and modern δD_s	186
4.9	Isotope ratios and isotopic temperatures of speleothems for which $\delta^{18}\text{O}_i$ was measured	203
5.1	Isotopic compositions, U/Th ages and depositional temperatures for 797MP1	209
5.2	Isotopic compositions, U/Th ages and depositional temperatures for 74014	211
5.3	Isotopic compositions, U/Th ages and depositional temperatures for 74017	213
5.4	Isotopic compositions, U/Th ages and depositional temperatures for 75125, 75123 and 76013	215
5.5	Age and radio-isotope data for fossil speleothems used in this study	216

LIST OF FIGURES

1.1	Variations in the $^{18}\text{O}/^{16}\text{O}$ ratio of speleothems from six areas of North America over the past 200,000 years	9
1.2	D/H and $^{18}\text{O}/^{16}\text{O}$ relationship for cave seepage and spring waters	19
2.1	Decay chains of naturally occurring and artificial radio-isotopes of U and Th	27
2.2	Isochron plots for U-series disequilibrium dating	30
2.3	Apparatus for crushing speleothem samples	38
2.4	System for extraction and collection of water from samples and its subsequent conversion to hydrogen for mass spectrometer analysis	42
3.1	Cave seepage and rain water collection apparatus	63
3.2	Yearly isotopic profiles for soil, cave seepage and meteoric precipitation from Tumbling Creek Cave, MO	67
3.3	Yearly isotopic profiles for cave seepage water and meteoric precipitation from Indian Echo Caverns, PA	74
3.4	Yearly isotopic profiles for cave seepage water and meteoric precipitation from Shenandoah Caverns, VA	76
3.5	$\delta^{18}\text{O}$ versus δD for soil and seepage water and meteoric precipitation for four Eastern U.S. sites	79
3.6	$\delta^{18}\text{O}$ and δD for mean cave seepage of eleven North American sites and one site from South Georgia	82
3.7	$\delta^{18}\text{O}$ versus temperature of cave seepage water and meteoric precipitation for 20 North American sites	85
3.8	$\delta^{18}\text{O}$ and d_t versus depth/age of the Dome C Antarctic Ice Core	92
3.9	$\delta^{18}\text{O}$ versus δD for Wisconsin and Modern Ice from the SWISS/DEEP Antarctic Ice Core	95
4.1	Origin of crystallites and fluid inclusions in columnar calcite crystals	110
4.2	Schematic of cross-section through stalagmite 797MP1	115

4.3	Schematic showing the relationship between 75125 and 76013	130
4.4	Schematic of cross-section through stalagmite 74017	136
4.5	A graph of δD_i versus water yield and temperature and temperature versus water yield for cumulative fractions of water extracted from 77151B by decrepitation	146
4.6	Plot showing water yield, δD_i , $\delta^{13}C$ and $\delta^{18}O_c$ along the axis of 797MP1	151
4.7	Plot showing water yield, δD_i , $\delta^{13}C$ and $\delta^{18}O_c$ along the axis of 74017	154
4.8	Histogram showing water contents of various speleothems	157
4.9	Plot of water content versus growth rate of various speleothems	159
4.10	FTIR spectrum for calcite	165
4.11	IR spectrum of slightly calcined calcite which has been allowed to absorb water	169
4.12	IR absorption spectra for various speleothem samples	171
4.13	Weights of various powdered calcites versus IR absorption for water in the samples	173
4.14	δD_i versus fractional water yields from 77151B at various decrepitation temperatures	191
5.1	$\delta^{18}O_c$ and $\delta^{13}C$ of points along growth bands of 797MP1 and 74017	208
5.2	Plot showing water yields, δD_i , $\delta^{13}C$, $\delta^{18}O_c$ and isotopic temperature along the axis of 797MP1	219
5.3	A comparison of isotopic temperatures and δD_i from 797MP1 with $\delta^{18}O$ of ice from the Camp Century Ice Core, Greenland	223
5.4	Correlations of $\delta^{18}O_c$ and δD_i with isotopic temperature for 74017	227
5.5	Correlations of $\delta^{18}O_c$ and δD_i with isotopic temperature for 797MP1	229
5.6	Plots showing $\delta^{18}O_c$, δD_i , $\delta^{13}C$ and isotopic temperatures of three speleothems from Vancouver Island	232

5.7	Plot showing $\delta^{18}\text{O}_C$, δD_i , $\delta^{13}\text{C}$, water yields and isotopic temperatures for 74017	235
5.8	Comparison of glacial stratigraphic records with speleothems 74014 and 74017	237
5.9	Correlations of $\delta^{18}\text{O}_C$ and δD_i with isotopic temperatures for speleothems 75125, 75123 and 76013	241
5.10	Correlations of $\delta^{18}\text{O}_C$ and δD_i with isotopic temperatures for 74017	244
5.11	δD_i versus $\delta^{18}\text{O}$ for various hydrothermal minerals from the Taulin Ore Deposit, China	253
5.12	Apparatus for simultaneous production of H_2 and CO_2 from small quantities of water	257

LIST OF PLATES

1.1	Detail of large, thorn-shaped inclusions	12
1.2	Detail showing linear fluid inclusions	14
1.3	Fracture surfaces of columnar calcite crystals in speleothems	16
4.1	Mirror Lake #1 under crossed Nicols	104
4.2	Mirror Lake #1 in plain light	104
4.3	View of flowstone 73017 under crossed Nicols	107
4.4	View of flowstone 76010 under crossed Nicols	107
4.5	Fracture surfaces of columnar calcite crystals	112
4.6	View of 75350 revealing length-slow mosaic	112
4.7	Detail of large, thorn-shaped fluid inclusions	117
4.8	View of stalagmite (top) 807CH1 under crossed Nicols	117
4.9	View of flowstone 77151B under crossed Nicols	127
4.10	View of stalagmite 797MP1 (near base) under crossed Nicols	127
4.11	Enlarged view of Plate 4.4	133

CHAPTER ONE

STABLE ISOTOPE STUDIES OF SPELEOTHEMS

1.1 Geothermometry

Speleothems are deposits formed within caves by chemical precipitation. Although a large variety of minerals may occur as speleothems, calcite is most frequently encountered. Deposition of calcite in caves occurs when dissolved CO_2 usually generated in the soil zone, outgasses as seepage water comes into contact with cave air at considerably lower P_{CO_2} . If such deposits can be shown to have grown in isotopic equilibrium with the seepage water, oxygen isotope ratios can be used to recover depositional temperatures. Criteria for recognizing a deposit grown in isotopic equilibrium have been set out by Hendy (1981). Calcite-water geothermometry was originally suggested by Urey (1947) and subsequently applied to marine biogenic deposits by Urey et al. (1947), Epstein et al. (1951) and (1953) and Craig (1965). Since speleothems can also be dated by various means, including U-series disequilibrium methods (see Chapter 2), they have good potential as paleotemperature recorders (Schwarcz et al., 1976).

The paleotemperature scale proposed by Urey et al. (1951) is based on the fact that the equilibrium constant for calcite-water isotopic exchange (K_{cw}) is dependent on temperature; the reaction establishing the constant being:



for which

$$K_{cw} = \{(\text{CaC}^{18}\text{O}_3)^{1/3}(\text{H}_2^{16}\text{O})\} / \{(\text{CaC}^{16}\text{O}_3)^{1/3}(\text{H}_2^{18}\text{O})\} \dots\dots(1.2)$$

or rewritten as

$$K_{cw} = \{(\text{CaC}^{18}\text{O}_3) / (\text{CaC}^{16}\text{O}_3)\}^{1/3} / \{(\text{H}_2^{18}\text{O}) / (\text{H}_2^{16}\text{O})\} \dots\dots(1.3)$$

Because the reaction involves a one atom exchange, at equilibrium

$$R_{cw} = \alpha_{cw} = R_c / R_w \dots\dots\dots(1.4)$$

where α_{cw} is the measured separation factor for calcite-water and R_c and R_w refer to the $^{18}\text{O}/^{16}\text{O}$ ratios measured in calcite and water phases respectively.

The relationship between α_{cw} and temperature (T^{OK}) was experimentally determined by O'Neil et al. (1969) and modified by Friedman and O'Neil (1977) for $\text{CO}_2\text{-H}_2\text{O}$ exchange at 25°C , yielding the relationship used throughout

this work, namely

$$10^3 \ln \alpha_{cw} = 2.78(10^6 T^{-2}) - 2.89 \dots\dots\dots (1.5)$$

If the del form (see appendix (1)) is required then

$$\alpha_{cw} = \{1000 + \delta^{18}O(\text{calcite})\} / \{1000 + \delta^{18}O(\text{water})\} \dots\dots (1.6)$$

or

$$10^3 \ln \alpha_{cw} \approx \delta^{18}O(\text{calcite}) - \delta^{18}O(\text{water}) \dots\dots\dots (1.7)$$

may be applied. Equation 1.7 can be used for convenience in reactions at ambient temperatures since the approximation results in very small error in estimating the fractionation.

The problem almost invariably encountered with ancient deposits is that generally the water phase is absent and assumptions have to be made as to its isotopic composition. Fortunately, speleothems always contain water and if this water can be shown to be an unaltered aliquot of the precipitating solution (an aliquot of the paleowater) then isotopic temperatures can be determined by the above method. However, a problem arises here, too, in that post-depositional exchange of oxygen between calcite and water may occur as the site changes temperature with time. Since small quantities of water are involved (typically 0.03 wt.%), calcite oxygen

would essentially be unaltered but, conversely, the isotopic ratios of water would be radically changed. A way of avoiding this problem is to measure the hydrogen isotope composition instead, because there is no hydrogen in the calcite. To apply this, the relationship between δD (appendix (1)) and $\delta^{18}O$ must be known in order to infer oxygen isotope ratios of the water at the time of deposition. To a first order relationship

$$\delta D = 8\delta^{18}O + d_t \dots\dots\dots(1.8)$$

where d_t is the intercept at time t . $d_0 = 10$, the present day value, may be applied since it fits most data for modern meteoric waters (Craig, 1961 and Dansgaard, 1964). It is assumed above that cave seepage water is equivalent to meteoric water falling at that site. However, evidence is accumulating to suggest that d_t varies both spatially (for example Evans et al., 1978, Harmon et al., 1978, Ambach et al., 1976, Molinari, 1977.) temporally (see 3.2). This subject will be discussed in greater detail in Chapter 3.

Wigley (1975) has shown that caves respond slowly to changes in external climatic conditions such that cave temperatures tend to be one to two year averages of those of the surface above the cave. Speleothems thus respond to secular climatic changes as they grow and in doing so are potentially effective as

paleoclimatic recorders.

1.2 Paleoclimatic Interpretation based on Calcite only

Having described the speleothem geothermometer and alluded to some of its associated problems, it seems appropriate to review paleoclimatic studies based on the calcite phase only. Two approaches are possible with the measurement of both carbon and oxygen isotope ratios. If these are measured along a growth axis of a speleothem then profiles can be obtained which may be interpreted in terms of climatic change for the period of growth. Analyses along a growth layer are used to determine whether or not equilibrium deposition has taken place (Hendy, 1971). Figure 5.1 shows such profiles. Variations in $\delta^{13}\text{C}$ (appendix (1)) may reflect change in vegetation type which contribute CO_2 to the system but this is further complicated by interaction between dissolved carbon species and the bedrock before deposition (Wigley and Brown, 1976). Variations in $\delta^{18}\text{O}(\text{calcite})$ for an equilibrium deposit are due primarily to two factors:

- 1) change in cave temperature,
- 2) change in $\delta^{18}\text{O}(\text{seepage})$.

The first contributes about $-0.25\text{‰}/^\circ\text{C}$ at ambient temperatures whereas the second is variable both from site to site and through time at a given site. Factors affecting $\delta^{18}\text{O}(\text{calcite})$ have been described for example by Harmon et al. (1978) and more exhaustively by Gascoyne (1979). These are summarized below:

- i) temperature dependence of $\delta^{18}\text{O}$ of precipitation

(IAEA, 1979) can yield values from $+0.9\% / ^\circ\text{C}$ for Antarctic snow to as low as $+0.01\% / ^\circ\text{C}$ for Bermuda. Continental sites tend to be around $+0.3\% / ^\circ\text{C}$ which works in opposition to factor 1), the temperature dependence of α_{CW} .

ii) effect of changing storm trajectory on $\delta^{18}\text{O}$ of precipitation. The values and sign of this effect are difficult to assess but climatic modelling has been attempted for North America during the Wisconsin glacial maximum (Gates, 1976). As a result, Harmon et al. (1978) have concluded that since the precipitation regime at the time is equivalent to winters of today in mid-continental U.S.A., then little change in $\delta^{18}\text{O}$ (precipitation) would be expected. That is to say, winter and summer precipitation are separated only by factor i). Whether this situation exists for other parts of the world or applies during glacial/interglacial transitions remains to be investigated.

iii) ice volume effect which causes the ^{18}O content of the oceans to increase in proportion to the ice stored on the continents. The maximum enrichment of ^{18}O in the oceans has been determined as $+1.80\%$. (Shackleton and Opdyke, 1973, Ninkovitch and Shackleton, 1975). Further uncertainty is attached to this effect since the correction depends on matching speleothem dates to deep sea core records.

Thus it may be seen that the uncertainty in magnitude and sign of the temperature dependence of $\delta^{18}\text{O}$ (seepage), and hence, subsequent determinations of $\delta^{18}\text{O}$ (calcite) variations in terms of temperature only is complex and difficult. In

spite of this, considerable contributions to glacial chronology have been made by many workers, principally, Hendy and Wilson (1968), Thompson et al. (1974 and 1976), Harmon et al. (1977, 1978a and 1978b), Gascoyne et al. (1978 and 1980) and Gascoyne (1979).

One further point should be mentioned; Observations of $\delta^{18}\text{O}$ of modern calcite allow $\delta^{18}\text{O}$ profiles to be interpreted in terms of warming and cooling phases. This is possible because there is presently an interglacial maximum; modern calcite $\delta^{18}\text{O}$ thus pertains to a warm period. Peaks and troughs of $\delta^{18}\text{O}$ along the axial profile can be compared to the modern calcite value and the sense of temperature change can be inferred (see for example fig. 1.1). A general conclusion is that for most sites studied speleothems tend to be enriched in ^{18}O with respect to modern and interglacial calcite and $d\delta^{18}\text{O}/dT < 0$, except for caves on Vancouver Island where the trend was found to be reversed (fig. 4.4). This reversal of trends is probably due mainly to factor i) in which the high value of $d\delta^{18}\text{O}/dT$ (temperature dependence of $\delta^{18}\text{O}$ of precipitation) causes the sign to change (Gascoyne, 1980).

The analysis of "paleowaters" from speleothems does, in principle, remove the need to apply factors i), ii), and iii) which lead to uncertainty in $d\delta^{18}\text{O}/dT$ of seepage. Extraction and analysis of fluid inclusions could be used to determine temperatures directly. This important approach and progress made to date is reviewed in the latter part of this Chapter.

Figure 1.1 Variations in the $^{18}\text{O}/^{16}\text{O}$ ratio of calcite speleothems from six areas of North America over the past 200,000 years. The curves were visually fitted to data points uniformly distributed throughout the measured intervals. Vertical arrows indicate $^{230}\text{Th}/^{234}\text{U}$ age control for each composite record. After Harmon, (1975).

1.3 Water in Speleothems

1.3.1 Optical Observations

In thin section, water is observed to be trapped in cavities from 10-15 μm in diameter (plate 1.1). Larger cavities appear to be elongate, tear-drop shape inclusions or negative crystals. Inclusions are numerous in some growth layers and completely absent in others. Elongate inclusions are often oriented at right angles to the growth layers and subparallel to the crystal c-axis suggestive of trapping at compromise boundaries as competitive crystal growth commenced (Bathurst, 1974 and Schwarcz et al., 1976). Although most large inclusions are filled with water, some, when viewed microscopically in polished section, appear to be only partially filled which may be due to leakage or trapping of air bubbles. Some appear to be anastomosing into channels that may account for leakage, should it occur. Cutting of sections may also result in leakage.

Smaller inclusions are more common and tend to be linear (spindle-shaped) cavities (plate 1.2) often closely spaced and parallel to the crystal optic axis, even where the axis itself is not normal to growth layers.

Inclusions that are not resolvable by light microscope are pseudo-pleochroic (ω =mid-brown, ϵ =colourless) and under SEM are seen to be similar to the linear inclusions described above. These are concave and triangular in cross-section (plate 1.3).

Plate 1.1 Detail of large, thorn-shaped inclusions showing marked growth anisotropism and constrictions (arrowed);
Host calcite grew towards the top of the photograph;
After Kendall and Broughton, (1978).

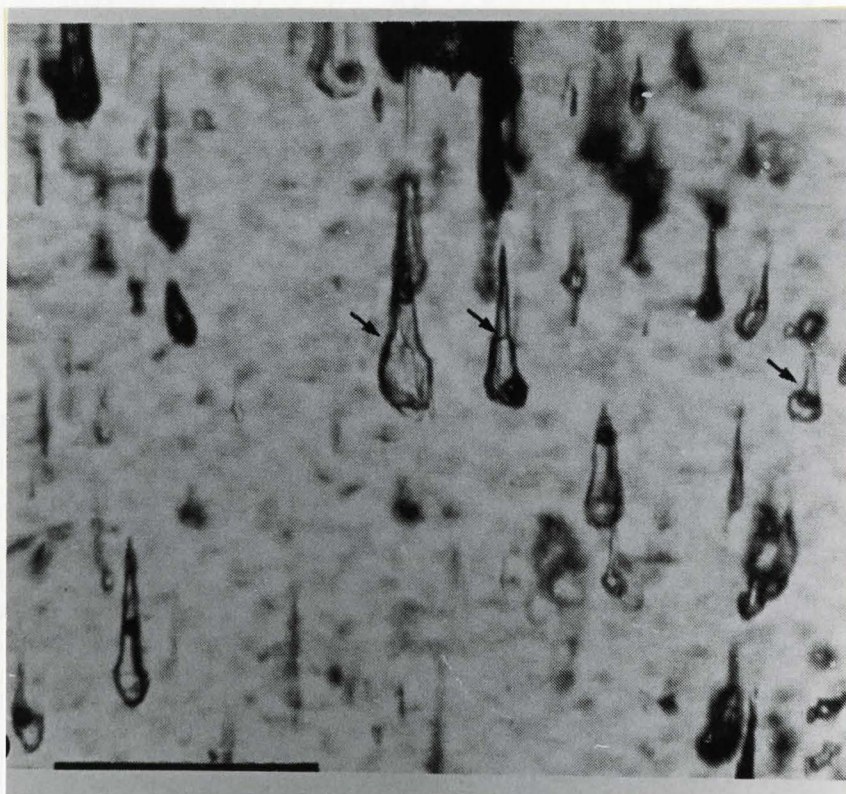


Plate 1.2 Detail showing linear fluid inclusions.

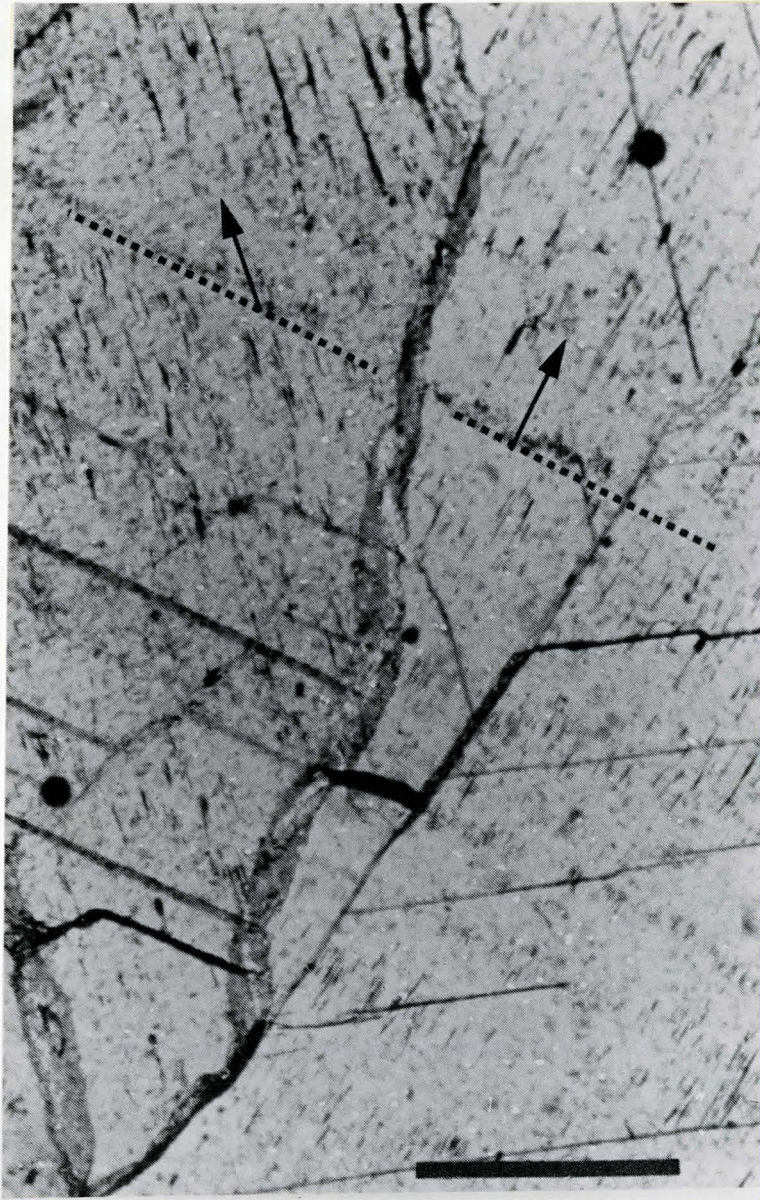


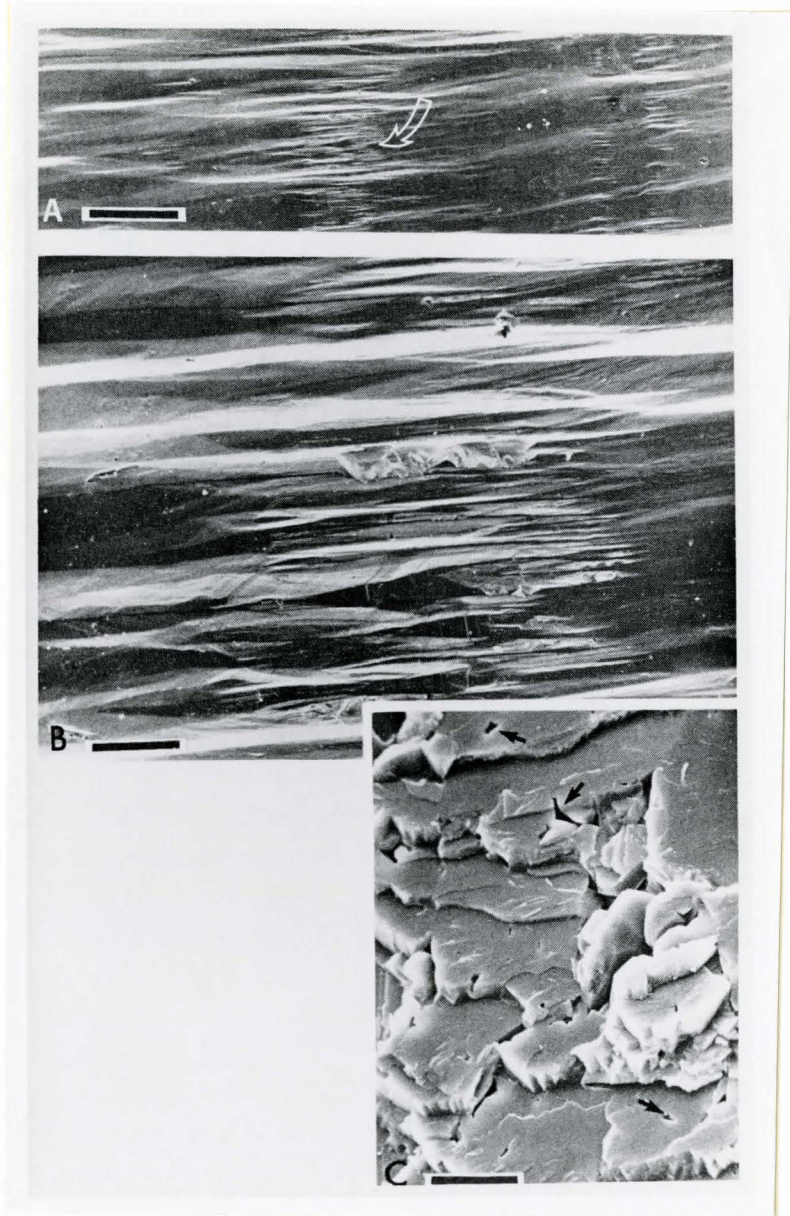
Plate 1.3 Fracture surfaces of columnar calcite crystals
in stalactites.

A: General SEM view to show inclusion-rich layers
(scale = 20 μ m);

B: Detail of A (arrowed), inclusions appear as
spindle-shaped depressions and are interpreted
as parts of elongate cavities that lie between
close-packed, partially coalesced crystallites
(scale = 100 μ m);

C: SEM view of fracture surface oriented normal to
that in A and B, and approximately parallel to
a former growth surface; triangular pores
(arrowed) are interpreted as remnants of former
inter-crystalite spaces (scale = 10 μ m);

After Kendall and Broughton, (1978).



Water is also seen in thin section where rhombohedral terminations occur at growth layer boundaries and sometimes within growth layers themselves where abundant impurities exist.

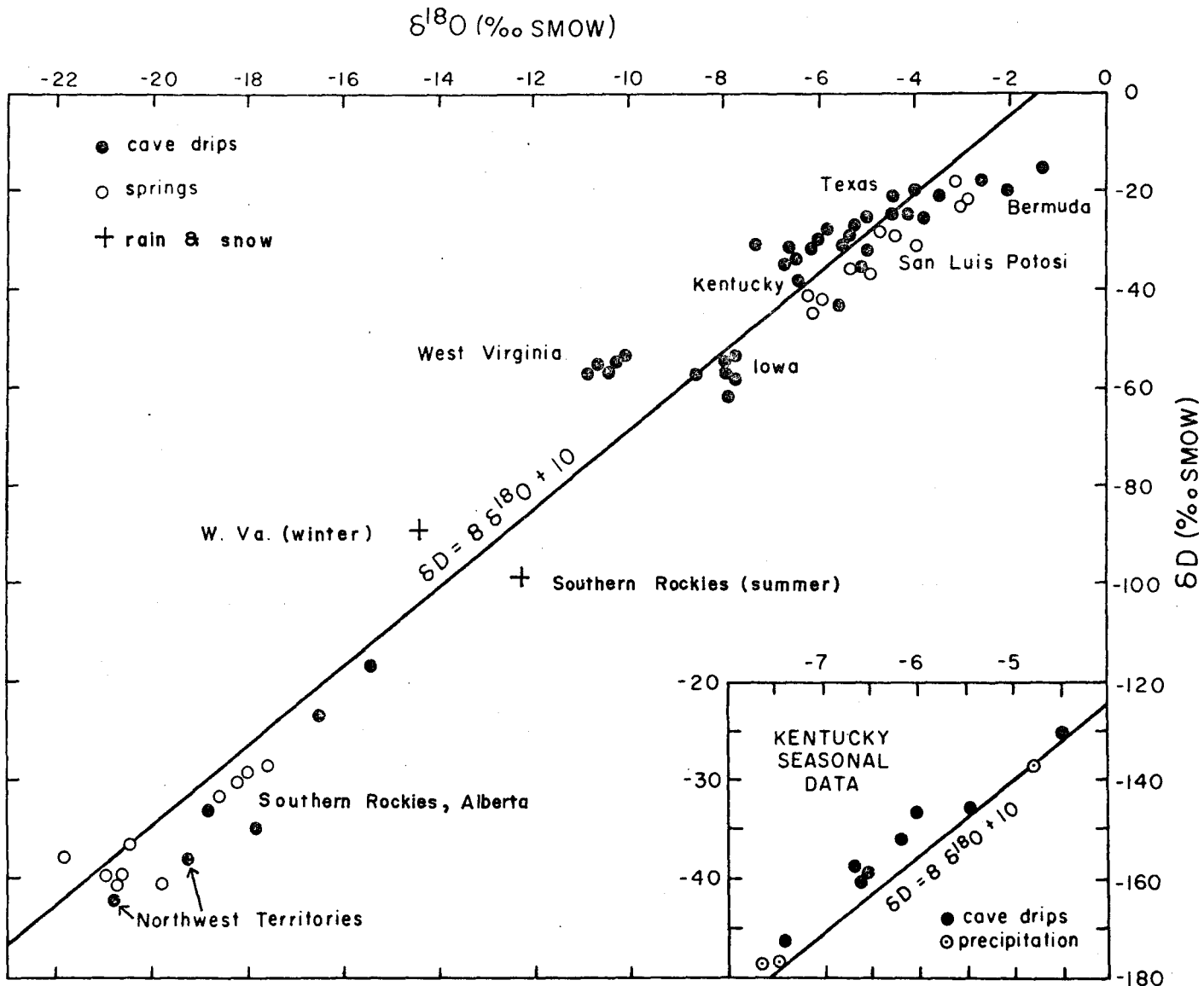
In hand specimens, only the larger inclusions have a milky-white aspect. Where micro-inclusions are present, speleothems may appear quite transparent. Growing stalactite surfaces are rough to the touch, indicative of crystal growth rather than to dissolutional processes. This suggests that the inclusions probably result as crystal growth advances, trapping water between the crystallites. Genetic interpretations of speleothem fabrics will be discussed in Chapter 4

1.3.2 Extraction of water

Water has been extracted from speleothems by crushing the sample under vacuum and transferring the released water vapour to a liquid nitrogen trap. The crushed residue is heated gently at about 200°C to remove any absorbed water (see Chapter 2 for details).

In a preliminary study Schwarcz et al. (1976) made isotopic analyses of what they referred to as "fluid inclusions" in speleothems. They set out to demonstrate that these fluid inclusions were aliquots of meteoric water, first, by showing that cave seepage water and local meteoric precipitation had similar isotopic compositions at seven sites across North America, and, second, by looking at four modern deposits from Bone-Norman cave in West Virginia.

Figure 1.2 D/H and $^{18}\text{O}/^{16}\text{O}$ relationship for cave seepage and spring waters in study areas. Seasonal data from the Mammoth Cave National Park, Kentucky site are shown in the insert (after Harmon, 1975).



In the first case, considerable scatter about the meteoric water line was encountered (fig. 1.2). No regression line was calculated, presumably because of the tendency for each area to generate its own particular relationship. However, their conclusions pointed generally to isotopic equivalence. The study of modern deposits suggested that trapped water was isotopically equivalent to heavier summer precipitation. They suggested that this is due to the tendency for calcite precipitation to take place during the warmer months. In retrospect though, this seems a little odd since subsequent work (see Chapter 3) indicates that at most sites, seepage water represents an integration of at least all annual meteoric precipitation and its isotopic composition does not change throughout the entire year. They went on to study a site in Kentucky to attempt to establish its present day meteoric water line. Temperatures redetermined on the basis of $\delta^{18}\text{O}$ inferred from this "new" meteoric line changed only a small amount ($1.5\text{ }^{\circ}\text{C}$) as compared to those calculated from the global line given by $d_0 = 10$. This amount is insignificant since their claim of precision for the method was $\pm 2\text{ }^{\circ}\text{C}$ (ignoring error in the meteoric water line).

At this point, no check of the integrity of ancient fluid inclusions could be made and post-depositional leakage remained a possibility. However, temperatures calculated from "modern" deposits ranged from 5.4 to $14.1\text{ }^{\circ}\text{C}$, yielding an average of $9.0 \pm 2.3\text{ }^{\circ}\text{C}$ compared to $11\text{ }^{\circ}\text{C}$ for the site today.

Studies of seepage-water soda-straw calcite pairs for five areas gave isotopic temperatures the same as cave temperatures within experimental error.

Given the uncertainty of isotopic temperatures in modern deposits, their findings for old speleothems were roughly in accord with other glacial chronologies. They further observed that temperatures between cold periods rose to values greater than or equal to those today. Bermuda was problematic in that their interglacial temperature of 4 °C is extremely unlikely since evidence from coccoliths suggests temperatures in excess of 10 °C even during full glacials in the region (McIntyre, 1967).

In all the areas studied, except Mexico, the dominant effect on $\delta^{18}\text{O}$ of calcite was found to be α_{cw} which in turn depended only on cave temperature, hence allowing a general interpretation of isotopic profiles in terms of warming and cooling events.

In a further study, Harmon et al. (1979) considered the change in δD through time from five North American sites. A significant change in δD of around 12‰ from the Wisconsin Interstadial to Wisconsin Glacial Maximum was suggestive of the integrity of fluid inclusions. Had they leaked, some sort of homogenization of the record would have been anticipated. Their conclusions pointed towards a depletion in deuterium during glacial periods by a maximum of 45‰ and an average of 12‰ compared to modern precipitation.

Enrichment in deuterium occurred during the last interglacial. They found trends to be the same in different areas and a correlation with foraminiferal records used for determining past ocean water compositions (Ninkovitch and Shackleton, 1975). Comparison with the modern δD contour map of North America (Taylor, 1974) showed a southward shift in contours consistent with that determined for ice margins. In passing, it should be mentioned that a 12‰ decrease in δD during full glacial stands is at odds with some records such as paleowaters from the London Chalk (Smith et al., 1976) and Floridian aquifers (Back and Hanshaw, 1979) and ancient tree rings (Yapp and Epstein, 1977), while agreeing with some other paleowaters (Sonntag et al., 1979, Davies et al., 1968).

In a final contribution, Harmon and Schwarcz (1981), using the data of Harmon et al. (1979), tried to reconcile the fact that 38 out of their 49 fluid inclusion analyses when combined with $\delta^{18}O$ of their host calcites, yield negative temperatures. Using theoretical calculations (Merlivat and Jouzel, 1979) and experimental data (Epstein et al., 1970), they obtained positive temperatures by a shift of the meteoric water line such that d_o is reduced from 10 to 0 (see equation 1.7). In conclusion, they suggested that a continuous change in d_o from 10 to 0 normally occurs over glacial/interglacial transitions and that examination of appropriate ice cores should allow paleotemperatures to be corrected, at least from the

last glaciation.

1.4 Justification of the present study

The possibility of direct determination of isotopic paleotemperatures potentially places speleothems high in importance amongst other Pleistocene paleoclimatic recorders. The need for further work from this point of view is obvious. However, it is not possible to say from the preceding studies whether or not the method really works, although indications are that it has promise. Negative and variable temperature determinations are clearly a problem. Are these really an effect of past meteorological variations or due to some mechanism acting during or after speleothem precipitation? Perhaps such effects are experimental artifacts.

In attempting to answer these questions work has centred on improvement of experimental techniques for extraction and analyses of water from speleothems. The research first required the construction of a mass spectrometer for measurement of D/H ratios. Subsequently, on-line extraction systems that could be modified were developed. New extraction techniques were also attempted and characterization of water within speleothems became an important part of the study.

An initial study of cave seepage water was made to try to elucidate seasonal biases in precipitation and establish geographic variation in meteoric isotopic relationships. Furthermore, an ice core was studied to confirm meteoric isotopic relationships during the Wisconsin glacial

stage.

Given that systematic problems can be overcome, a wealth of knowledge can be obtained from these ubiquitous deposits. Not only could paleotemperatures be worked out, but in addition, secular variations in meteoric precipitation over glacial cycles could be studied and rates of deglaciation assessed. A few temperature determinations made on a given speleothem would allow a detailed $\delta^{18}\text{O}(\text{calcite})$ record to be calibrated and variables affecting $\delta^{18}\text{O}$ of the calcite could be calculated. New extraction techniques could lead to the use of smaller samples thus allowing detailed $\delta\text{D}(\text{water})$ profiles to be generated, too.

As an extra bonus, the new extraction system developed in this study was found to be applicable to other materials besides speleothems; namely to various types of hydrothermal and hydrous minerals.

CHAPTER 2

EXPERIMENTAL METHODS

2.1 Dating of Speleothems

2.1.1 Introduction

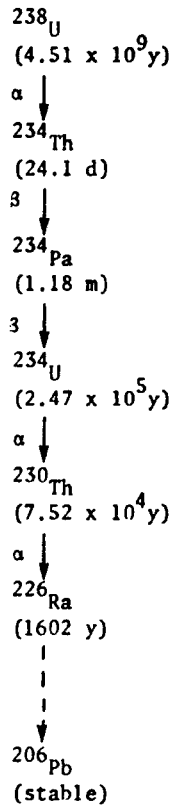
A number of approaches to dating speleothems and travertines has been proposed but only uranium series methods have been widely adopted. Because all the dates referred to in the text were acquired using uranium series dating, it is beyond the scope of this work to go into the more or less esoteric methods or approaches other than to mention them out of interest with appropriate bibliography. They fall into two categories, those employing decay schemes and those utilizing correlative and/or extrapolative criteria. These follow respectively:

i) Electron Spin Resonance (Karakastonoglou, 1981), ^{14}C dating (Hendy, 1969), fission track (Truscott and Schwarcz, 1978), and ^{41}Ca (cosmic rays on travertines, Raisbeck and Yiou, 1979).

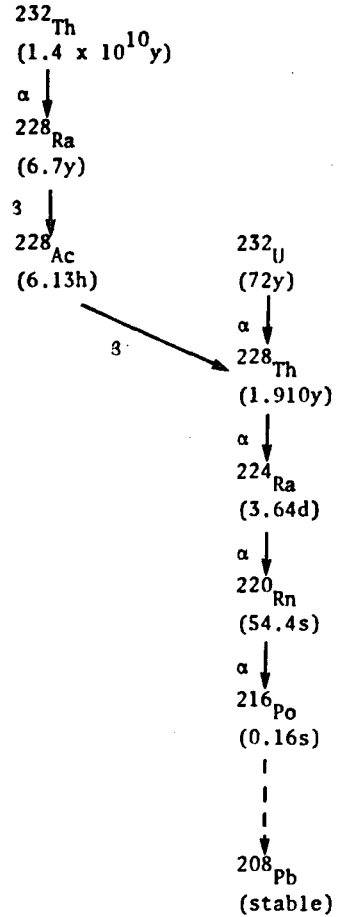
ii) Growth band counting (Broecker and Olsen, 1960), cave stratigraphy (Waltham, 1970), deposition rates of modern deposits (Hendy and Wilson, 1968), and matching of paleomagnetic and stable isotope profiles (Latham et al., 1979 and Harmon, 1975 respectively).

Figure 2.1 Decay chains of naturally occurring and artificial radio-isotopes of Uranium and Thorium.

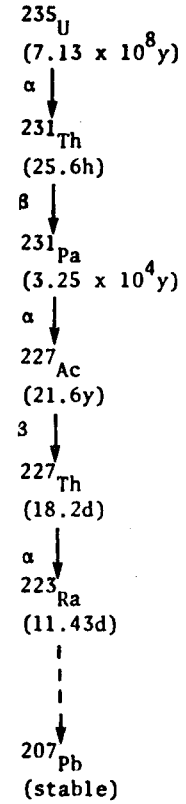
^{238}U SERIES



^{232}Th SERIES



^{235}U SERIES



2.1.2 Uranium Series Disequilibrium Dating

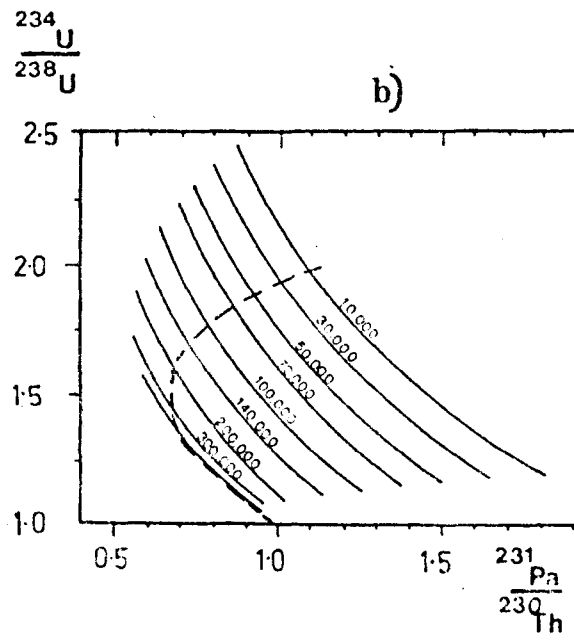
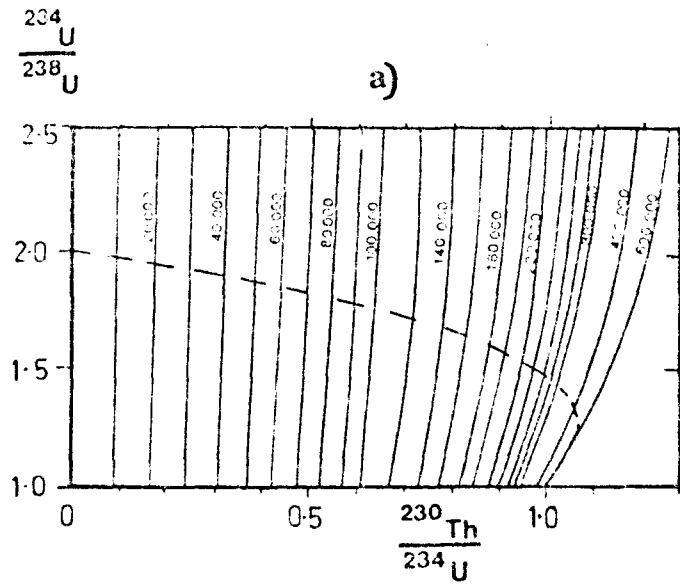
Uranium series dating has generally been reviewed by Ku (1976). Of its application to speleothem dating, there has been a number of contributions: Schwarcz (1980 and 1978), Gascoyne et al. (1978), Harmon (1975) and Thompson (1973). The most exhaustive discussions, including detailed experimental procedures, are of Latham (1981) and Gascoyne (1979). With this comprehensive literature in existence, the principles of these dating methods will be described only briefly.

Since the relevant daughter products, ^{230}Th and ^{231}Pa , of soluble uranium species (Figure 2.1) tend to be highly insoluble, only the parent uranium is transported as a complexed species in groundwater. Consequently, during calcite precipitation, only uranium is incorporated into speleothems, although in practice, some detrital thorium may also be trapped on the surface of the growing speleothem. After a time t , ^{230}Th and ^{231}Pa accumulate and may be used in conjunction with in situ uranium nuclides to determine the time elapsed since precipitation, providing that these daughters have not yet grown into equilibrium with their parent uranium isotopes. Thus, for a speleothem initially containing no ^{230}Th , after time t :

$$\left(\frac{^{230}\text{Th}}{^{234}\text{U}}\right)_t = \frac{1 - e^{-\lambda_{230}t}}{\left(\frac{^{234}\text{U}}{^{238}\text{U}}\right)_t} + \left(\frac{\lambda_{230}}{\lambda_{230} - \lambda_{234}}\right) \cdot \left(1 - \frac{1}{\left(\frac{^{234}\text{U}}{^{238}\text{U}}\right)_t}\right) \cdot A$$

- Figure 2.2 a) Isochron plot of $^{234}\text{U}/^{238}\text{U}$ and $^{230}\text{Th}/^{234}\text{U}$ ratios. Isochrons are in years.
- b) Isochron plot of $^{234}\text{U}/^{238}\text{U}$ and $^{231}\text{Pa}/^{230}\text{Th}$ ratios. Isochrons are in years.

Dashed lines show a typical change in nuclide ratios as age increases, with an initial $^{234}\text{U}/^{238}\text{U}$ ratio of 2.



where $A = (1 - e^{-(\lambda_{230} - \lambda_{234})t}) \dots \dots \dots (2.1)$

(see also Figure 2.2a) and likewise if no ^{231}Pa is present initially then:

$$\left(\frac{^{231}\text{Pa}}{^{235}\text{U}}\right)_t = (1 - e^{-\lambda_{231}t}) \dots \dots \dots (2.2)$$

where ^{230}Th and ^{231}Pa are the daughter products of ^{234}U and ^{235}U respectively, and ^{234}U the daughter product of ^{238}U (isotope abundances are in activity units). λ_{234} , λ_{231} , and λ_{230} are the decay constants for ^{234}U , ^{231}Pa , and ^{230}Th respectively. The half lives for ^{230}Th and ^{231}Pa are 75.2 ka and 32.5 ka respectively and the activity ratio for $^{234}\text{U}/^{238}\text{U}$ is generally greater than one due to preferential leaching of the light isotope from damaged lattice sites during the initial dissolution of bedrock (Gascoyne, 1979).

Equations 2.1 and 2.2 are combined to give:

$$\frac{^{231}\text{Pa}}{^{230}\text{Th}} = \frac{1 - e^{-\lambda_{231}t}}{21.7 \cdot (1 - e^{-\lambda_{230}t}) + B} \dots \dots \dots (2.3)$$

$$\text{where } B = \left\{ \left(\frac{^{234}\text{U}}{^{238}\text{U}} - 1 \right) \cdot \frac{\lambda_{234}}{\lambda_{230} - \lambda_{234}} - (1 - e^{-(\lambda_{230} - \lambda_{234})t}) \right\}$$

where 21.7 is the activity ratio of $^{238}\text{U}/^{235}\text{U}$. Equation 2.3 is represented graphically in Figure 2.2b where it may be seen that the method is applicable back to about 350 ka. Age determination from equation 2.3 may be made without the

addition of a radioactive tracer since the ratio of $^{227}\text{Th}/^{230}\text{Th}$ can be determined directly and ^{227}Th is in equilibrium with ^{231}Pa . However, $^{234}\text{U}/^{238}\text{U}$ must be determined independently.

As mentioned, in practice some detrital ^{230}Th may be carried into the system. Measurement of $^{230}\text{Th}/^{232}\text{Th}$ allows for corrections to be made as ^{232}Th is entirely a detritally derived component. Too much detrital thorium is, however, undesirable when one considers that typical uranium concentrations in speleothems fall in the range 0.1 to 2 ppm and uncertainty in the ^{230}Th concentration leads to larger systematic errors.

The decay of ^{234}U excess into secular equilibrium with ^{238}U unfortunately cannot be used because of the uncertainty of initial $^{234}\text{U}/^{238}\text{U}$ in freshwater systems. This is regrettable because dates back to 1.5 Ma could be obtained, in principle. A means of getting around the problems of initial ratios was conceived by Thompson et al. (1975) for samples whose age range fell on either side of the $^{231}\text{Pa}/^{230}\text{Th}$ limit of 350 ka and using initial ratios determined from the datable portion of the sample. Unfortunately, $^{234}\text{U}/^{238}\text{U}$ ratios fluctuate too much in time and space for this approach to be tenable (Thompson et al., 1975a). An alternative approach suggested by H.P. Schwarcz is to leach ^{234}U , derived from in situ ^{238}U , from damaged lattice sites in hope that authigenic ^{234}U is more retentive; but the effectiveness of this has yet

to be established.

Preparation of samples for radiochemical analysis is undertaken as follows: Part of the speleothem required is dissolved in concentrated HNO_3 along with the tracer containing an equilibrium mixture of ^{232}U and ^{228}Th . Uranium and thorium are coprecipitated on $\text{Fe}(\text{OH})_3$, separated by ion exchange resins and then plated out by evaporation of a solution of TTA on a steel disc. Their alpha activities are counted on silicon barrier detectors and yields determined by isotope dilution methods.

2.2 Stable Isotope Analyses

2.2.1 Preparation of Samples

Isotope measurements were either made on samples of water or calcite. Bulk water samples needed no prior preparation since concentrations of dissolved salts were not sufficiently high to warrant purification.

Speleothem samples were generally sectioned axially to reveal growth bands and then sketched or photocopied. Powders for oxygen and carbon analysis were obtained by drilling after the speleothem axis had been located and well delineated growth bands selected (see Figure 5.3). Drilling of these areas was carried out using drill sizes down to 1mm in diameter, depending on sample size required and this, in turn, depending on the choice of temperature for subsequent acid reaction (25 or 50 °C; see section 2.2.2). Samples for water extraction, on the other hand, were cut from a 0.5 to

1 cm thick slice taken parallel to the axis. Cubes or similar shapes typically from 0.2 to 0.5 g in weight were then cut from the same places as the powders had been obtained, using a diamond band saw. The band saw, designed to cut around corners, could be used to follow growth layers of quite complex shape (see Figure 4.2, for example).

2.2.2 Oxygen and Carbon from Calcite

Two methods were adopted for measuring these isotopes in calcite involving the release of CO_2 on reaction with 100% orthophosphoric acid at a given temperature. The first method requires about 25 mg of sample powder and reaction at 25°C in an evacuated flask for 12 hours. The gas generated is dried via three passes through a $\text{CCl}_4/\text{CHCl}_3$ /dry ice trap and the yield checked manometrically before subsequent removal to the mass spectrometer for analysis (after McCrea, 1950 and Craig, 1957). The second method utilizes an on-line system, environmentally controlled at 50°C . Successive aliquots of sample powder are reacted for 15 to 20 minutes in small chambers that can be removed from the vacuum line following each injection and reaction of the acid which is delivered from an internal reservoir. Drying of the sample gas is done via one pass through the cold trap en route to the mass spectrometer (after Shackleton, 1979). This latter method requires some caution since calcites of radically differing isotopic composition, run one after the other, can be subject to some memory effect. CO_2 liberated from the

50°C reaction is 0.98% lighter in ^{18}O than that from the 25°C reaction. Reaction temperatures are maintained to better than $\pm 0.5^\circ\text{C}$. All results quoted are expressed with respect to VSMOW and PDB standards for oxygen and carbon respectively (section 2.3).

2.2.3 Oxygen and Hydrogen from Bulk Water Samples

2.2.3.1 Oxygen

Oxygen isotope ratios of meteoric precipitation, cave seepage, and soil waters (designated 'bulk samples') were determined on CO_2 equilibrated with 2 ml of sample at 25°C. A drop of concentrated H_2SO_4 was added to enhance the equilibration process (after Epstein and Mayeda, 1953).

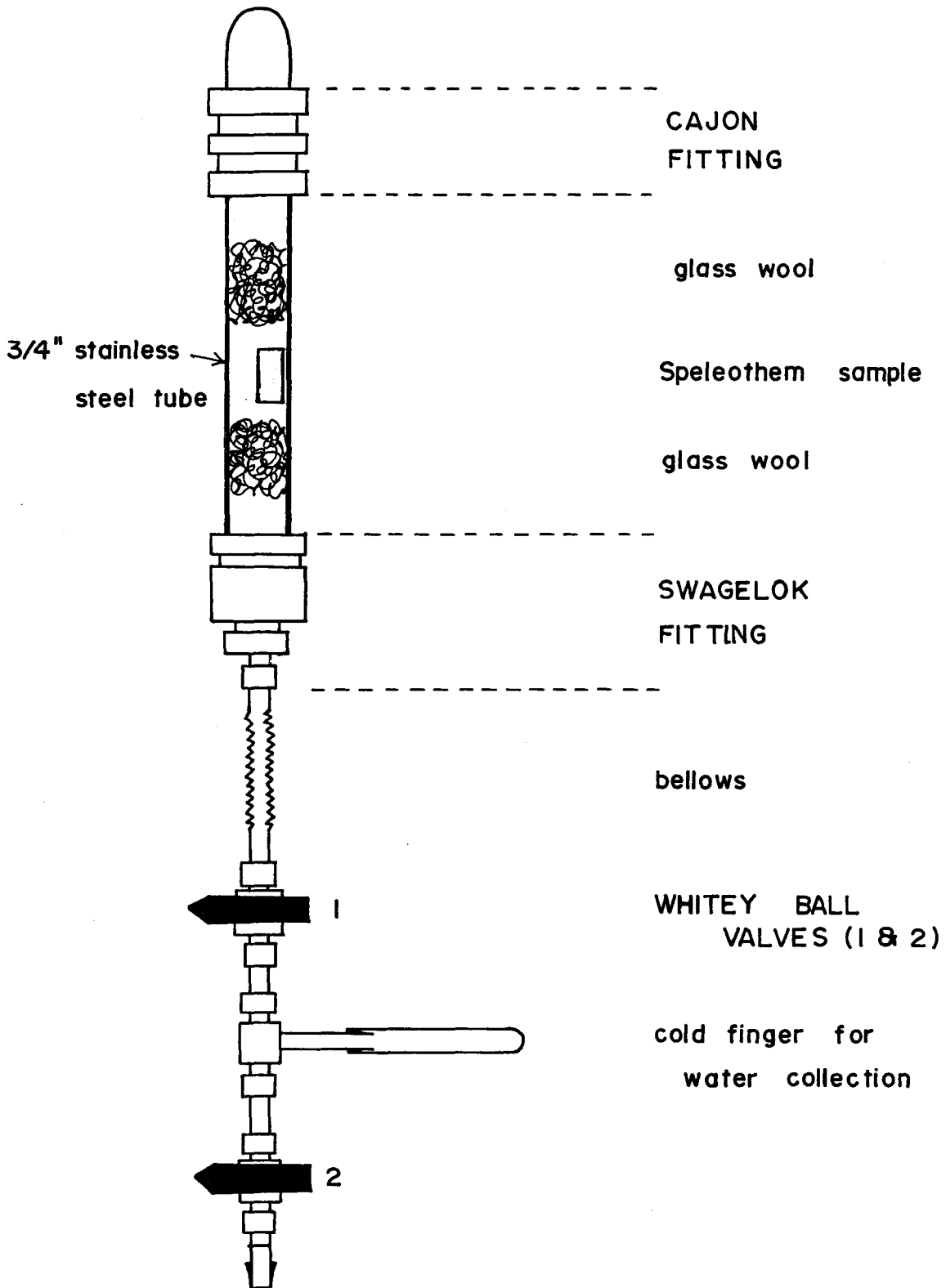
The procedure adopted in this study was slightly modified from the above methods of Epstein and Mayeda in that all the CO_2 was removed from above the (frozen) water sample and taken via a spiral trap ($\text{CCl}_4/\text{CHCl}_3$ /dry ice slush) into the mass spectrometer for analysis following 24 hours of equilibration in an agitated water bath. Such streamlining of procedure cut out the time-consuming operation of freezing all the CO_2 sample into a storage vessel from the reaction flask. Precision did not seem to be measurably affected. Agitation of the water bath speeded up the equilibration reaction but samples removed after 12 hours were found to be up to 1% lighter than those removed after 24 hours when the reaction had gone to completion. Each batch of 15 samples was checked by one standard (DTAP '78) (see section 2.4) and

conversion to VSMOW calculated according to the procedure described by Schwarcz (1971) with modifications by Knyf (1980).

2.2.3.2 Hydrogen

Water was reacted with depleted uranium in vacuo at 800°C following the method of Bigeleisen et al. (1952). Large quantities of standard reservoir hydrogen released from DTAP '78 and SWISS/DEEP '79 were generated using the design of line described by these workers. However, to improve the speed of analyses and reduce sample size, an on-line system was built (Figure 2.4). Here, a water sample is injected into the system via a microlitre syringe and frozen onto the U-tube T3 for ten minutes. The U-tube is then allowed to warm up to room temperature where it proceeds to the uranium furnace (F1). The subsequently liberated H₂ fills the system, including bulb X and is allowed to leak directly through to the mass spectrometer via VX3, VX, and N1. No attempt is made to collect the gas (normally, Toepler pumps, freezing on activated charcoal (Thompson, 1973) or forming hydrides (Friedman and Hardcastle, 1970) would be used to do this). A further advantage to the speed of analyses is that yields can be monitored on the mass spectrometer and completion of reaction observed. Water was found to be completely converted, following careful cleaning and packing of the uranium, to U₂O₄ and H₂ and no water was observed to pass into the mass spectrometer. Five minutes is generally allowed for the reaction for 1 to 2 μl samples. Note that,

Figure 2.3 Apparatus for crushing speleothem samples.



wherever water must pass through the system, V6 stopcocks are employed, and no heating of water carrying conduits is applied. Detailed operation procedures and calculation of δD is described in appendix II and section 2.4.2.3.

2.2.4 Oxygen and Hydrogen from Water Extracted from Speleothems

2.2.4.1 Extraction of Water from Speleothems

In this study, two methods have been applied to the extraction of water from speleothems. The first has been described by Harmon et al. (1979) in which the sample is crushed and heated to 180°C in an evacuated, degassed stainless steel tube. The liberated water vapour is then frozen down into a pyrex finger with liquid nitrogen (Figure 2.3).

An alternative method has been developed in which water is released by heating (Yonge, 1981 and appendix II). As yet, only hydrogen has been measured by this technique. Oxygen analyses of the water may not be possible because there may be isotopic exchange with calcite and CO_2 oxygen at the elevated temperatures used (850°C). Nevertheless, it is perhaps worth investigating because of the higher yields and precision resulting from the mode of extraction (sections 2.4 and 4.4.3).

Samples are cut from speleothems of a size such that they may contain 1 to 2 μl of water. Clearly, initial tests are required to establish this but the range extends from 0.1 to 1.0 g of sample. Water is released from them in a quartz furnace F2 in vacuo at a variety of temperatures but

usually at 850°C , such that complete calcining takes place. Both water and CO_2 are then frozen onto a spiral trap T2 at liquid nitrogen temperatures (Figure 2.4). The furnace is closed off when this is finished ($\frac{1}{2}$ hour is usually allowed) and liquid nitrogen replaced by a dry ice/methanol mixture which holds the water but releases the CO_2 to the vacuum pump R3. Eventually, the water can be transferred to the U-tube and handled in the usual way for δD analysis (section 2.2.3.2). It should be mentioned, in passing, that several other methods of decrepitation were tried with a considerable lack of success. Thus, for example, pumping the sample $\text{CO}_2/\text{H}_2\text{O}$ mixture through the spiral trap directly at dry ice temperatures results in the lighter isotopic fraction of water being carried away to the pumps by the copious quantities of CO_2 produced. Replacement of the spiral trap by a one-stage diffusion pump, in which the water is 'pumped' by freezing at dry ice temperatures and made more efficient by cooling due to adiabatic expansion of the $\text{CO}_2/\text{H}_2\text{O}$ mixture, also results in a similar loss of water. Another technique was to allow the sample mixture to pass through the uranium furnace and freezing the CO_2 down thereafter. Unfortunately, hydrogen condenses on the frozen CO_2 leaving the residual hydrogen isotopically light.

The method of total freezing of the $\text{CO}_2/\text{H}_2\text{O}$ mixture with liquid nitrogen in a spiral trap (closed to the pumps) and subsequent release of CO_2 , although taking some half an

Figure 2.4 System for extraction/collection of water from samples and its subsequent conversion to hydrogen for mass spectrometer analysis.

V = valves, V6 = 6mm bore valves,

P = pumping line, E = extraction line

X = sample line, S = standard line

T = cold trap, B = Pirani pressure gauge

N1 = stainless steel valve to mass spectrometer

D = diffusion pump, R = rotary pump

VX and VS are solenoid valves

hour longer per extraction, was found to be the only technique that consistently gave reproducible δD 's and water yields. A detailed account of the method may be found in appendix II.

2.2.4.2 Oxygen from small water samples

Since water extracted from speleothems by crushing is acquired in small quantities (0.1 to 0.01 wt%), oxygen is released with BrF_5 and subsequently converted to CO_2 by reaction with hot carbon at $1100^\circ C$ (O'Neil and Epstein, 1973). A detailed procedure has been written up by Yamamoto (1980) and the results quoted in appendix IV are taken from this contribution too.

2.3 Standards

A summary of the standards relevant to the present study is included in table 2.1. The international primary standard for reporting $\delta^{13}C$ and $\delta^{18}O$ in calcite is the Chicago Standard PDB (Epstein et al., 1951). However, since this standard is not available, a series of secondary standards has been generated. Two are in current usage at the McMaster laboratory: GCS (a marble from the Grenville Province) and NBS 20 (a sample of finely ground Solenhofen Limestone). The former has been used throughout this work.

All values for $\delta^{18}O$ and δD from water samples are quoted with respect to VSMOW. However, a number of other IAEA standards were used to determine mass spectrometer corrections and calibrate laboratory working standard

Table 2.1 Standards used for Stable Isotope Analyses

	STANDARD	$\delta^{18}\text{O}_{\text{PDB}} \pm (\text{‰})$	$\delta^{13}\text{C} \pm (\text{‰})$	ORIGIN	REFERENCE
CALCITE	PDB	0	0	Cretaceous Belemite from the Pee Dee Formation	Epstein et al., 1951
	NBS20	-4.18 ± 0.08	-1.06 ± 0.08	Solenhofen Limestone	Blattner & Hulston, 1978
	GCS	-11.768 ± 0.050	$+0.69 \pm 0.08$	Marble from the Grenville Province	Gascoyne, 1979
			$\delta\text{D} \pm (\text{‰})$		
WATER	VSMOW	0	0	IAEA; Standard Mean Ocean Water	
	NBS1	-7.89 ± 0.12	-47.1 ± 1.2	Mid-Latitude River Water	
	NBS1A	-24.29 ± 0.25	-183.2 ± 0.7	Greenland Ice	Gonfantiini, 1978
	SLAP	-55.5	-428	Southern Latitude Antarctic Precipitation	
	DTAP '77	---	-42.8 ± 1.6	McMaster distilled water	
	DTAP '78	-7.63 ± 0.20	-51.7 ± 0.8	" " "	This work, Appendix III
	SWISS/DEEP	37.05 ± 0.73	283.5 ± 1.05	Mixture of SWISS and DEEP Antarctic Ice	

hydrogen samples (see next section). These include NBS1, NBS1A, and SLAP (Gonfanti, 1978). H₂ working standards were made up from DTAP '78 and SWISS/DEEP '79. The former was used where groundwaters were being measured, and the latter as a standard for Antarctic ice. DTAP '78 and VSMOW were used as daily working standards for groundwaters whereas SLAP was used for the ice core.

2.4 Mass Spectrometry

2.4.1 602D Instrument for $\delta^{13}\text{C}$ and $\delta^{18}\text{O}$

The Micromass 602D has been specifically designed for stable isotope analysis. It is one of a family of Micromass 6 spectrometers, all of which are 90° sector, magnetic instruments of 6 cm radius. It has two thin bucket Faraday collectors coupled to a ratio recording output stage and a comparison of an unknown gas to the standard may be made via switching solenoid valves. As such, the construction is basically of the Nier-McKinney type (VG Micromass manual and McKinney et al., 1950).

The instrument can be tuned to ¹⁵N and ³⁴S although its major use is in the analysis of CO₂ where enrichment of ¹³C and ¹⁸O are measured. The 602D is designed to run in the dynamic mode where the gases for comparison are bled from capillary leaks and are alternately admitted to the mass spectrometer source. Stable gas flow is achieved by pumping the gas stream not being analysed with a phenol-ether pump. The resulting ion beams are individually

amplified and sent to a ratio integrator unit where the minor/major peak ratios are displayed and printed out. Subsequent $\delta^{13}\text{C}$ and $\delta^{18}\text{O}$ values are calculated following the procedure of Schwarcz (1971). which takes into account isotope abundance effects. Machine corrections such as tailing, discrimination, and valve mixing were found to be so small as to be considered negligible ; their correction factors being in the order of 1 part in 10^5 . Detailed procedures for calculation are from Schwarcz (1971) with modifications by Knyf (1980).

2.4.2 The D/H Mass Spectrometer

2.4.2.1 Description

Since this instrument is both 'home made' and responsible for all the δD data presented in this dissertation, it will be described in some detail. The mass spectrometer was designed by C.E. Rees of the Chemistry Dept., McMaster University in 1973 and it was partly constructed at that time. Unfortunately, it fell victim to lack of funding and remained untouched until 1977 when R. Bowins commenced design and construction of the ratio integrator unit and other components, described later, became available. At this point the author took over.

The instrument is a 90° sector type, of 6 cm radius. H_2 gas is ionized by electron bombardment and accelerated at 1845 V through a fixed magnetic field to two Faraday collectors. The collectors are spaced to collect mass 2 and

mass 3 components and repeller plates held at -90 V repel secondary electrons. The two beams are monitored by two Philbrick electrometer amplifiers. Voltages from the amplifiers are converted to frequency pulses. 10^6 of such pulses from each collector are counted on a time base. The ratio of the times (minor/major) are subsequently displayed on the DVM linked to a TI Silent 700/PDP8 system where the data are finally processed (Bowins, 1978 and Russel and Ahern, 1974). The inlet system of the instrument is a conventional Nier type (Haydon and Inghram, 1954 and Yonge, 1976) set up for dynamic gas flow. Pumping, achieving minimum pressures of 10^{-8} torr, is stabilized by an Edwards phenol-ether Diffstak pump and Sargent-Welch Directorr 50ls^{-1} rotary pump. The reliability of the former was exemplary, whilst the latter leaves much to be desired. The emission regulator and focussing unit were built following the design of Beaver (1974) and an accelerating voltage is provided by a Fluke 415B supply. Mass spectrometer pressures are monitored by a Veeco Ionization Gauge Control RGLL-7. Layout of the mass spectrometer inlet system is seen in Figure 2.4 and running characteristics in appendix II.

2.4.2.2 Operation

Hydrogen generated from the uranium furnace fills the bulb X (Figure 2.4). Similarly, the bulb S is filled with an aliquot from one of the two reservoirs (light or heavy) depending on the isotopic composition of the unknown gas. Hg from bulbs X' and S' is raised up into X and S

respectively by applying air pressure to X' and S' via a system of Fairchild regulators fed from a wall, compressed air supply. The fine tuning of the respective 2 lb/sq. ins. regulators easily brings pressures of X and S within 1% of one another thus ensuring the production of H_3^+ to be the same for both gases (Beaver, 1974). Each gas is then bled via 60 cm crimped capillaries to solenoid switches which admit each gas (standard and unknown) in turn, via a Nupro valve, into the mass spectrometer. In practice, prior knowledge of sample size meant that very little movement of the Hg was necessary to equalize pressures. Pressure equalization is achieved by monitoring the mass 2 peak, and with this done, the computer facility can be brought into play with the appropriate corrections typed in (described next) and data collection initiated. See appendix II for a more detailed account of the above.

2.4.2.3 Corrections

In the following discussion, possible corrections to the raw δD data are considered and their application explained. Possible corrections are:

- i) Solenoid Valve mixing;
- ii) Tail effects;
- iii) Fractionation of reservoir standard with time
(in bulb S);
- iv) Periodic standard reservoir corrections;
- v) H_3^+

- i) Valve mixing: this effect was examined by removal of the sample gas (D/H ratios of standard and sample were large) and checking the change in ratio of the standard and vice versa. It was found to be negligible.
- ii) Tail effects: although the mass 2 beam is typically 3.5×10^3 greater than mass 3, the resolution at these low mass numbers is so great ($\frac{\Delta m}{m}$) that mass 3 is not effected by mass 2 tailing.
- iii) Fractionation of reservoir standard with time during a run: this was determined to be $0.08\%_O/\text{min.}$ when the capillaries were crimped such that P_{H_2} dropped to 60% of diameter. More crimping would have resulted in an unacceptable loss of sensitivity; therefore, a compromise was achieved. However, aliquots of the standard gas were changed always within $\frac{1}{2}$ hour of use. The maximum correction was then $2.4\%_O$ and the residence time of the gas could be introduced into the computer program at the beginning of each run. While crimping was undertaken, null gas determinations were performed until no differences between X and S were observed.
- iv) Periodic standard reservoir corrections; DTAP'78,

VSMOW and SLAP were used on a regular basis to check the isotopic composition of the working standard and H_3^+ contributions. The δD (reservoir-VSMOW) was updated as experiments progressed although, in general, only small changes in the final δD were made (see appendix II).

v) H_3^+ correction; H_3^+ ions are generated through collisions between H_2^+ ions and neutral hydrogen molecules in the source (Friedman, 1953). Since the metastable H_3^+ ion can survive long enough to be collected at the mass 3 Faraday cup, it is a source of interference. The first step is to reduce its contribution to the $M/e = 3$ ion beam to a minimum; less than 5% is somewhat arbitrarily taken as being desirable by most workers in the field (O'Neil, 1978). As the concentration of H_3^+ is directly proportional to pressure at low pressures (Friedman, 1953), there is a trade-off between sensitivity and H_3^+ contribution. The H_3^+ contribution was initially lowered by both drilling a matrix of holes in the case to allow faster pumping away of H_2 , and applying strong source magnets so that a lowering of pressure in the case was offset by a rise in the ionization efficiency. Comparatively high accelerated voltage combined with a repeller electrode helps to draw ions out

of the source quickly thus reducing H_3^+ generating collisions.

The second step is to determine what the magnitude of the contribution of H_3^+ is and to what extent it changes with time. Although isotope ratios can be extrapolated back to zero pressure and hence the HD/HH true ratio obtained, this method is not very accurate because of non-linearity due to noise at pressures close to zero. A more desirable method involves the use of interlaboratory standards in which measured δD 's are compared to the independently calibrated values and an H_3^+ correction is obtained from this comparison. It is calculated as follows:

$$\text{The measured mass 3/ mass 2} = R_m = \frac{(HD + H_3)}{H_2} \dots\dots\dots(2.4)$$

$$\begin{aligned} \text{whereas the true ratio} &= R_t = \frac{HD}{H_2} \\ &= \frac{\{(HD + H_3) - H_3\}}{H_2} \dots\dots(2.5) \end{aligned}$$

and since the pressures are kept equal, the H_3 value remains the same in all cases.

Two interlaboratory standards were used, VSMOW and SLAP, to establish the H_3 correction because they represented the full range of δD values encountered. NBS1A was used as an intermediate to check the H_3 value.

Thus:

$$\delta D_{\text{VSMOW}}(\text{SLAP}) = \left\{ \left(\frac{R_t(\text{SLAP})}{R_t(\text{VSMOW})} \right) - 1 \right\} \cdot 10^3 = -428 \dots\dots\dots (2.6)$$

(Gonfantini, 1978)

Combining equations 2.4 and 2.5:

$$R_t = R_m - \frac{H_3}{H_2} \dots\dots\dots (2.7)$$

Equations 2.6 and 2.7 combine to give:

$$\frac{H_3}{H_2} = H = \frac{\{1000 \cdot R_m(\text{SLAP}) - 572 \cdot R_m(\text{VSMOW})\}}{428} \dots\dots\dots (2.8)$$

Since $D(\text{SLAP})$ and $D(\text{VSMOW})$, from which $R_m(\text{SLAP})$ and $R_m(\text{VSMOW})$ are taken, are determined with respect to $R_m(\text{reservoir})$ then the two values must be normalized to the single mean $R_m(\text{reservoir})$ value. H is then the value which is fed into the computer program in appendix II where it corrects ratios according to equation 2.7. The correction is normally between 4 to 5% for a running pressure of 10^{-7} Torr (measured at the diffusion pump) and a P_{H_2} equivalent to 8×10^{-9} Torr and does not seem to change significantly with time.

A further measure to reduce the effect of this correction is the use of working standards whose composition

is close to that of the samples being run. It is for this reason that H₂-standards were generated from DTAP'78 and SWISS/DEEP'79 for analysis of groundwaters and Antarctic ice respectively.

2.5 Precision and Accuracy

All δ values given in this work are related to VSMOW (δD and $\delta^{18}\text{O}$) or PDB ($\delta^{13}\text{C}$) standards (section 2.3). Table 2.2 depicts systematic errors associated with the various isotopic methods.

Errors associated with oxygen analyses on bulk water samples and hydrogen analyses on all water samples were determined during this study and are discussed in a little more detail. The error calculated for $\delta^{18}\text{O}$ of bulk water samples is based on all the DTAP'78 standards run and represents an overall error including that due to the temperature of the water equilibration bath, that due to standard GCS preparation and that due to the mass spectrometer. As previously stated, tests were made to determine the time required for CO₂-sample H₂O equilibration and the composition and volume of the CO₂ introduced taken into account. With this and determinations of DTAP'78 made on the BrF₅ line, the accuracy of the method is reasonably assured (Table 2.2).

The errors of δD analyses of water have been established with a number of interlaboratory standards (Table 2.2) and it too represents an overall error. Because standards can be

Table 2.2 Precision (at 1σ) of replicate analyses of standards and samples (data from appendices).

a) Analyses of standards (injection of water sample into an on-line uranium furnace).

Water Standards	No. $\delta^{18}\text{O}$ analyses		$\delta^{18}\text{O}_{\text{SMOW}} \pm$ (%)		$\delta\text{D}_{\text{SMOW}} \pm$ (%)		period of analysis
	$\delta^{18}\text{O}$	δD					
VSMOW	-	32	-	-	0.0	2.4	1/79-9/80
	-	42	-	-	0.0	1.1	9/80-10/81
SLAP	-	10	-	-	-429.1	2.4	9/80-10/81
NBS1A	-	11	-	-	-180.9	3.0	1/79-9/80
	-	6	-	-	-181.7	1.1	9/80-11/80
DTAP'78	34	5	-7.35	0.30	-51.7	1.1	5/81-5/81

b) Replicate analyses of the carbonate standard and waters

Sample	No. Analyses		$\pm \delta^{18}\text{O}$		Exp. Method (δD)
	$\delta^{18}\text{O}$	δD		(%)	
Carbonate std. 232 (GCS)	-	-	0.10		H_3PO_4 at 50°C
All H_2O stds.	32	64/42*	0.2**/0.3***	1.1/2.5*	H_2O injection
Fluid Inclusions - in calcite	- 23	26 19	- 0.83***	1.8 8.3	Decrepitation Crushing
Fluid Inclusions - in other minerals	-	4 pairs****	-	1.3	Decrepitation
Hydrous Minerals - in granite	-	4****	-	0.9	Decrepitation

* From 1/79-9/80

** Equilibration of sample with CO_2 at 25°C

*** Reaction of water with BrF_5

**** See Appendix V.

analysed from time to time, and used to adjust measured δD values, all errors in standards can be corrected. Waters from speleothems, on the other hand, present a problem because no two samples are known a priori to have identical δD values. Analyses of water of growth layers from equilibrium deposits give surprisingly good replication by decrepitation but not so good by crushing, as shown in Table 2.2b. The accuracy of these determinations is quite another matter, inasmuch as no standard fluid inclusions exist. Seepage waters coexisting with modern speleothems do not possess the same δD 's as the speleothems and so precision of replication and yield are the only guide. This point is discussed further in Chapter 4.

CHAPTER 3

METEORIC PRECIPITATION AND RECHARGE WATER STUDIES

3.1 Precipitation and Recharge Water at Cave Sites

3.1.1 Rationale

As alluded to in Chapter 1, a general equivalence to isotope ratios of meteoric precipitation to cave seepage water has been noted by Schwarcz et al. (1976), Harmon (1979) and Duplessy et al. (1971) for North American and Western European sites. The nature of this equivalence is that precipitation and seepage water in a given area are not only isotopically concordant with the same meteoric water line but also fall generally on the same part of the line (see Fig.1.2).

However, these studies only partly answer the question as to whether or not cave seepage water varies isotopically throughout the year in response to highly variable isotope ratios in meteoric precipitation. This is an important consideration for fluid inclusion studies because if calcite is precipitated at certain times of the year, the $\delta^{18}\text{O}$ (and δD) of fluid inclusions, and concomitantly, the $\delta^{18}\text{O}$ of calcite may record a seasonal bias, say, towards summer isotopic ratios. Should this occur, it would not affect isotopic temperatures because of the following argument:

At any given site sufficiently deep within a cave, temperatures

change by less than 1°C throughout the year (observations made in this study and White, 1977), and at any given moment, isotope partitioning is a function of temperature regardless of the source of water. It is assumed here that $\delta^{18}\text{O}$ can be inferred from δD of the inclusion water and temperature calculated from Equation 1.7.

A serious flaw in this line of reasoning could arise in assuming that inclusion water represents the solution which generated the surrounding calcite. The trapped water may have indeed exchanged with the cave drip water throughout the course of a year or more, and as such, be wholly or partly homogenized towards mean annual compositions. Should this be the case then the heavier summer isotopic ratios of calcite would lead to temperatures that were too low. Conversely, if winter calcite precipitation dominated, temperatures would be too high.

Paleoclimatic interpretation based on $\delta^{18}\text{O}$ of calcite alone (Chapter 1.2) might also be affected by seasonal variation although if seasonal biases are maintained over extended periods when secular variations occur, it would not matter. Should the seasonal periods of preferential deposition alter in length with time then the tendency towards smoothing out of secular variations would result.

δD of fluid inclusions alone, should these record the same seasonal variation, would be likewise affected. However, their use in this way would be more limited; for example, one

could envisage application to non-equilibrium deposits in which hydrogen isotope ratios are less affected by kinetic fractionation. In fact, where rapid outgassing of CO_2 in a cave atmosphere of 100% humidity is the mechanism of deposition, hydrogen isotope ratios would not be affected at all. This point is taken further in Chapter 5.

Fluid inclusion data from four modern deposits and limited accompanying summer and winter seepage measurements from Bone-Norman cave, West Virginia, hint at a summer bias towards calcite precipitation (Thompson et al., 1976). Based on the Craig-Dansgaard meteoric water line (with $d_o = 10$), they give inferred values of $\delta^{18}\text{O}$ for fluid inclusions as $-8.9 \pm 0.2\%$, while summer meteoric precipitation averages to $-9.1 \pm 1.0\%$. A criticism of their conclusion can be made because winter precipitation lies to the left of the meteoric water line (Fig. 1.2) leading to the possibility of the line shifting during the winter period. In this case, new oxygen values can be inferred from the δD data which would compare favourably with the average winter precipitation values of $-10.3 \pm 1.0\%$. If the modern cave temperature is used with the oxygen isotope data from calcite to calculate seepage water oxygen values from Equation 1.7 and plotting these with δD from the fluid inclusions, the Craig-Dansgaard line is implied. However, using this line, isotopic temperatures range from 5.4 to 14.1 $^{\circ}\text{C}$ which does not make the argument for summer calcite precipitation very compelling. Nevertheless,

two fluid inclusion analyses of modern calcite from Cold Water Cave, Iowa, gave $\delta D = -55.6\%$ against summer seepage values of -52.2% . (Harmon and Schwarcz, 1981). Temperatures calculated based on the fluid inclusion-calcite pairs and the meteoric water line ($d_o = 10$) are 9.0°C against 8.8°C for measured cave temperatures. Furthermore, in excess of forty soda straw calcite-summer seepage oxygen isotope pairs from five North American sites, including Bermuda, yielded reasonable cave temperatures. It should be stressed that oxygen isotope ratios from seepage water were measured directly. Whilst the work of Harmon and Schwarcz (1981) does not contradict the supposition of preferential summer calcite deposition, no winter collections of seepage water were made and it is therefore not known whether the seepage water in all these cases changes its isotopic signature during the winter or not.

Ambiguity exists as to the presence of seasonal isotopic variations in drip waters and since knowledge of this is important, as argued in the beginning of this section, three cave areas in the Eastern U.S.A. were chosen for detailed water studies. Description of this work follows.

3.1.2 Field Program

Three sites were studied in detail: Tumbling Creek Cave, Missouri (soil samples were taken in addition to meteoric precipitation), Indian Echo Caverns, Pennsylvania, and Shenandoah Caverns, Virginia. To add perspective, other sites were sampled too but not on an annual basis. These included

Friar's Hole System, W. Va., Bone-Norman Cave, W. Va., Marengo Caverns, Indiana, Wind Cave, South Dakota, McFail's Cave, New York, various caves in Alabama, Cumberland Caverns, Tennessee, various caves on Vancouver Island and a cave in South Georgia (appendix III).

In all cases, except for some samples from Alabama and Vancouver Island, glass bottles were used to collect and store samples. Although plastic bottles are more convenient, glass was favoured because when two samples of the same water, one contained in a plastic bottle and the other in glass, were left for eight months on a window sill, the plastic bottle water changed its hydrogen isotopic composition by -30‰ whereas the glass bottle water remained the same. This is the opposite of what might be expected from membrane diffusion through the plastic container wall. An alternative explanation could be that sunlight, in tending to depolymerize the plastic, had allowed isotopic exchange to occur between the walls of the container and the water. Hydrogen in manufactured goods might be expected to be light due to kinetic fractionation taking place as the material is processed. Although the above depicts the worst possible storage situation, glass was used as a cautionary measure, and in addition, bottles were stored in the cave after sealing until final collection. After arrival in the laboratory they were stored in the refrigerator.

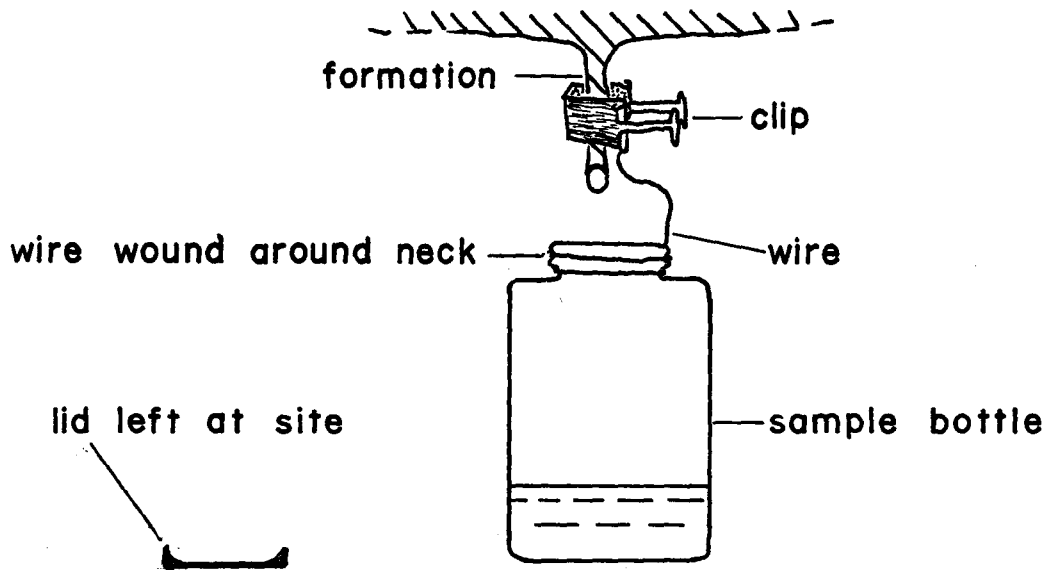
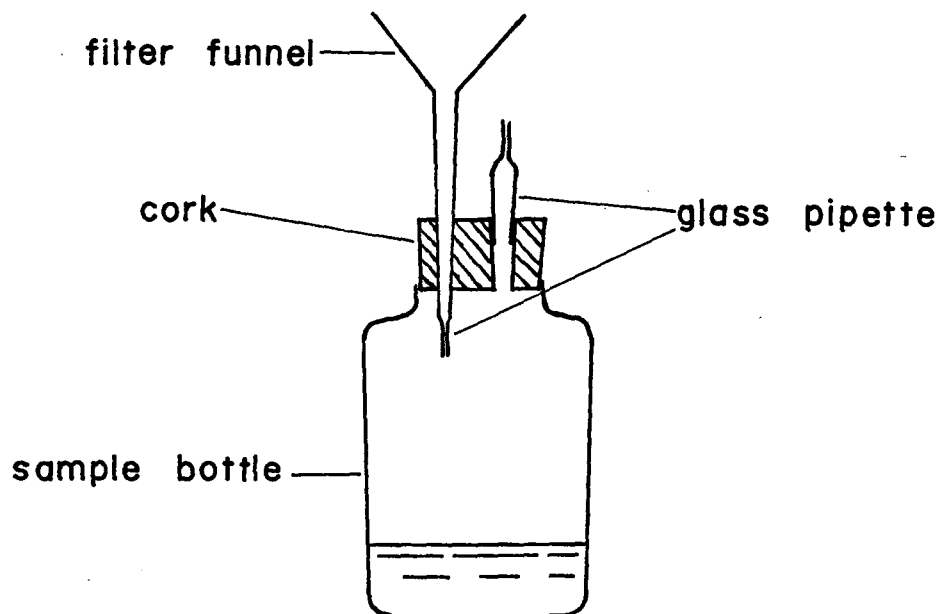
Water from the three principal caves of this study was

collected from a number of drip stations within each cave, whereas other seepage water was obtained from milking clusters of soda straws (in preference to taking fast drips from a single straw). In the latter case, bottles were attached carefully to straws as shown in Fig. 3.1a and collected at intervals ranging from two weeks to two months (see appendix III and Figures 3.2, 3.3, and 3.4). When sufficient sample had been collected, bottle caps were sealed doubly with electricians tape. Meteoric precipitation was collected in the same kind of glass bottles but some attempt was made to prevent evaporation during the period of collection (see Fig. 3.1b): Rain water passes through the funnel and pipette into the bottle, a further pipette allows air to pass out. This somewhat perfunctory system worked well enough except the funnel pipette tended to become blocked and frosts were unkind to the apparatus. Fresh snow was simply scooped into the bottle and sealed on the spot.

Unfortunately, to obtain a complete record of meteoric precipitation over the period June 1978 to August 1979 would have entailed more sophisticated apparatus or zealous surveillance of the researcher, neither of which was possible. However, a number of studies involving total precipitation have been undertaken by other workers and these are discussed later on in this Chapter.

Soil water was taken from a depth of about 1 m adjacent to the entrance shaft of Tumbling Creek Cave by

Figure 3.1 Cave seepage and rain water collection apparatus.

a) DRIP WATER COLLECTION**b) RAIN GAUGE**

tunneling the soil laterally and placing the bottle beneath drips in the roof of the tunnel.

3.1.3 Meteoric precipitation, soil and seepage water at Tumbling Creek Cave, Mo.

Tumbling Creek Cave has been set up for scientific pursuit and designated the Ozark Underground Laboratory by its director Tom Aley. The cave is in the highly dissected, rolling hills of the Western Ozarks just south of the Springfield Plateau. Topographic relief ranges between 150 and 300 m. Genetically, the area is in late youth to early mature stage of fluvial development; original plateau remaining at the higher elevations. The hillsides immediately above Tumbling Creek Cave are forested.

The host rock in the cave is the Ordovician Jefferson City formation, a light brown to brown, medium to finely crystalline dolomite and argillaceous dolomite. Exposed outcrops show vertical solutional enlargement of fractures and joints. Regional bedding is essentially horizontal. Within the cave 19 lithologic sub-units have been identified; dolomite, chert, shale and sandstone, comprising a thickness of around 15m (Thomson and Aley, 1971). Seepage sites were situated at about 10m below surface.

Some 10 drip sites were sampled, 6 of them on a regular basis. Because of the uniformity of the data, (appendix III) no attempt was made to discriminate between sites. Instead, an average of all the drip sites sampled

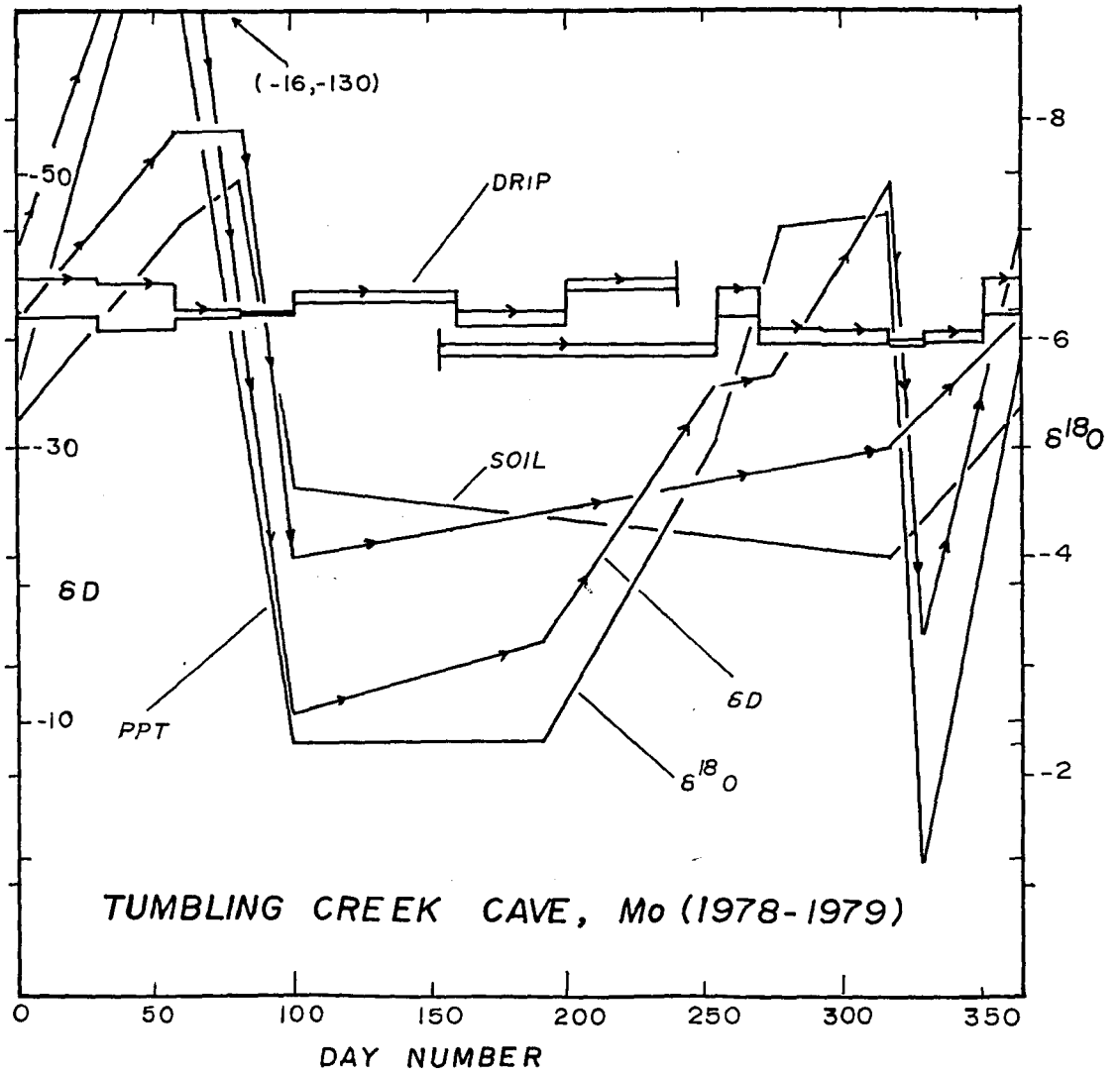
has been used to represent average recharge water. In figure 3.2, the points marked "drip" depict the average data of periods from day 154, 1978 to day 257, 1979. Soil and precipitation points are based on single analyses. The ordinate of the graph is scaled so that δD and $\delta^{18}O$ profiles represent departures from the meteoric water line (equation 1.8, $d_o = 10$).

Figure 3.2 exhibits isotopic fluctuations in groundwater and soil moisture as a response to seasonal variations in meteoric precipitation. Meteoric precipitation is quite variable and Dansgaard (1964) describes several factors which influence this isotopic variation:

- i) Degree of evaporation from falling raindrops, a function of temperature and humidity, (δ 's rise with increased evaporation).
- ii) Condensation temperature (δ 's fall with falling temperature).
- iii) Amount of precipitation formed (δ 's fall with increased rainfall).
- iv) Seasonal shift of precipitation source area.

The above factors appear to be responsible for the precipitation profile of figure 3.2 but to varying degrees. The condensation temperature is almost certainly responsible for the January/February minimum (snow sample) and the general swing to heavier values in the summer months. The summer values may also be influenced by fronts derived from

Figure 3.2 Yearly isotopic profiles for soil and cave seepage water and meteoric precipitation from Tumbling Creek Cave, Mo.



the Gulf of Mexico as well as from evaporation of falling raindrops occurring preferentially in the warmer period. The light pulse around October may reflect the "amount effect" following a heavy thunderstorm. April and May have the heaviest rainfall (Thomson and Aley, 1971), but the amount effect is not seen due to insufficient collection. Harmon (1979) and Sears (1976) however, report large negative pulses for these months but do not observe an amount effect. If isotopically heavy summer samples had been affected by evaporation then departures to the right of the meteoric water line should be seen. The scatter of precipitation data about the meteoric water line (Figure 3.5) is suggestive of evaporation but this could be due to collection procedures (fresh snow lies close to the line). It should be noted, for the moment, that soil values are less scattered and are close to the line characterized by $d_o = 7.8 \pm 1.5$ and mean seepage data, with very little scatter, defines this line. The fact that mean seepage data also lies to the right of the meteoric water line may be due to a net evaporation effect. This point will be returned to. Both Sauzey (1974) and Dansgaard (1964) also report scatter of precipitation data about the meteoric water line.

The soil data is scarce due to the budgetary constraints on the use of Lysimeters. However, the results are interesting and require some discussion. The soil

profiles in figure 3.2 seem generally to follow those of precipitation insofar as the data permit interpretation, but considerable damping of the signals has taken place. Most importantly, damping seems to be complete at the drip sites within the cave.

Zimmerman et al. (1967) have shown that isotopic mixing through diffusion is very rapid and fast enough to produce equilibrium at any one point in the soil. Re-equilibration of soil water takes place very quickly compared to downward flow rates. For example, they found the top few cms of soil labelled with HTO remained as a distinct layer for up to six months after application, reflecting extremely slow downward infiltration. Foster (1975) proposed a similar mechanism for recharge in chalk in which high levels of thermonuclear tritium were not reflected in the groundwater. Loss of tritium was attributed to diffusion to stationary water in smaller pores whilst infiltrating water moves downward to the water table. Sears (1976), working on soils in Pennsylvania, found recharge water to represent less than 1% of the total water present. He further reports that only a small proportion of total precipitation reaches the water table (in this case a dolomite aquifer) by supposing that groundwater represents a weighted average of all precipitation reaching the aquifer. If complete mixing in the soil zone takes place, then the groundwater will be constant and

equal to the weighted average. However, a total of 106 cm precipitation for the year 1973/74 gave a weighted average heavier than that for groundwater by 1.6% in oxygen and 10% in hydrogen. Sauzey (1974) reports the same effect in Illinois and suggests the dominance of autumn and winter recharge. Sears (1976) finds that 65-70% of precipitation is lost by evapotranspiration. Of the remaining 30-35% getting to the aquifer, most is during the cooler months where such effects are minimal and even complete loss of summer precipitation may occur on occasions. The latter is difficult to accept although, for if ground waters do lie on the meteoric water line, then partial evaporation effects cannot be severe. Drip sites are observed to dry up completely at the height of summer. Alternatively, transpiration may be a non-kinetically fractionating mechanism. All cave seepage waters in general lie to the right of the meteoric water line (Figure 3.6) defining a line corresponding to $d_o = 7.8$, and as mentioned, may be due to a net summer evaporation effect. Again an alternative may be that such a line more closely resembles continental conditions in general. For example, Taylor (1974) chooses an intercept $d_o = 5$ as being representative of Western U.S.A. groundwaters.

The observation that drip waters in this study were seen to increase in flow rate almost concurrently with the onset of heavy precipitation but with no isotope effect

observable requires some explanation. Reeves (1979) working on chalk aquifers proposes a piston flow mechanism in which hydraulic conductivity increases with increased saturation of the aquifer. This mechanism could be operating in karst terrains too. Thus, saturation of increasingly large microfissures may occur until the vertical unsaturated hydraulic conductivity is sufficient to match the rate of inflow. As explained, inflow water will constantly exchange with pore water maintaining a composition almost identical to adjacent pores. This process is known as piston displacement through pores and further explains the coincidence of observed tritium migration rates and pore piston rates (Zimmerman et al., 1967). However, pure piston flow cannot be operating and must be combined with some vertical mixing in order to smooth the isotope record observed. As cave drip rates were seen to increase with increased infiltration, so copious amounts of calcite were precipitated around sample containers, suggestive of resident saturated groundwater moving in response to surface water injection.

3.1.4. Meteoric Precipitation and Seepage Water from Two Other North American Sites

Two other sites were studied on an annual basis; these were: Indian Echo Caverns, Hummelstown, Pa, and Shenandoah Caverns, Shenandoah Valley, Va. Indian Echo Caverns are formed in the Conococheague limestone, subgroup

of the Conestoga formation of Cambro-Ordovician age, situated on the eastern side of the Valley and Ridge structural unit. Shenandoah Caverns are formed in the Newmarket limestone within the Appalachian Basin and are of Lower to Middle Ordovician in age (Fisher et al., 1975 and Eardley, 1962).

The isotopic records from both areas (Figures 3.3 and 3.4) appear very similar to that of Tumbling Creek Cave (Figure 3.2). The essential difference is that both sites tend to be isotopically lighter than Missouri which is not surprising as they are further north and experience lower mean annual temperatures (See factor (ii) in 3.1.3). The altitude of all the caves is similar at about 200m. Again, lack of precipitation data does not allow a very close comparison to be made between the three sites. Worth mentioning, is that higher snowfalls at the more northerly caves may dominate their ultimate groundwater values to a greater extent than at Tumbling Creek Cave.

All three drip water isotopic profiles (Figures 3.2, 3.3. and 3.4) indicate a lack of seasonal variation. None of the records appears to respond to, for example, the very light isotopic input in winter. Indeed, from the preceding arguments in section 3.1.3, it seems unlikely that a seasonal variation is likely to occur. It would be highly speculative to ascribe even a year to year variation. However, the Missouri data hint at this possibility with a

Figure 3.3 Yearly isotopic profiles for cave seepage water and meteoric precipitation from Indian Echo Caverns, Pa.

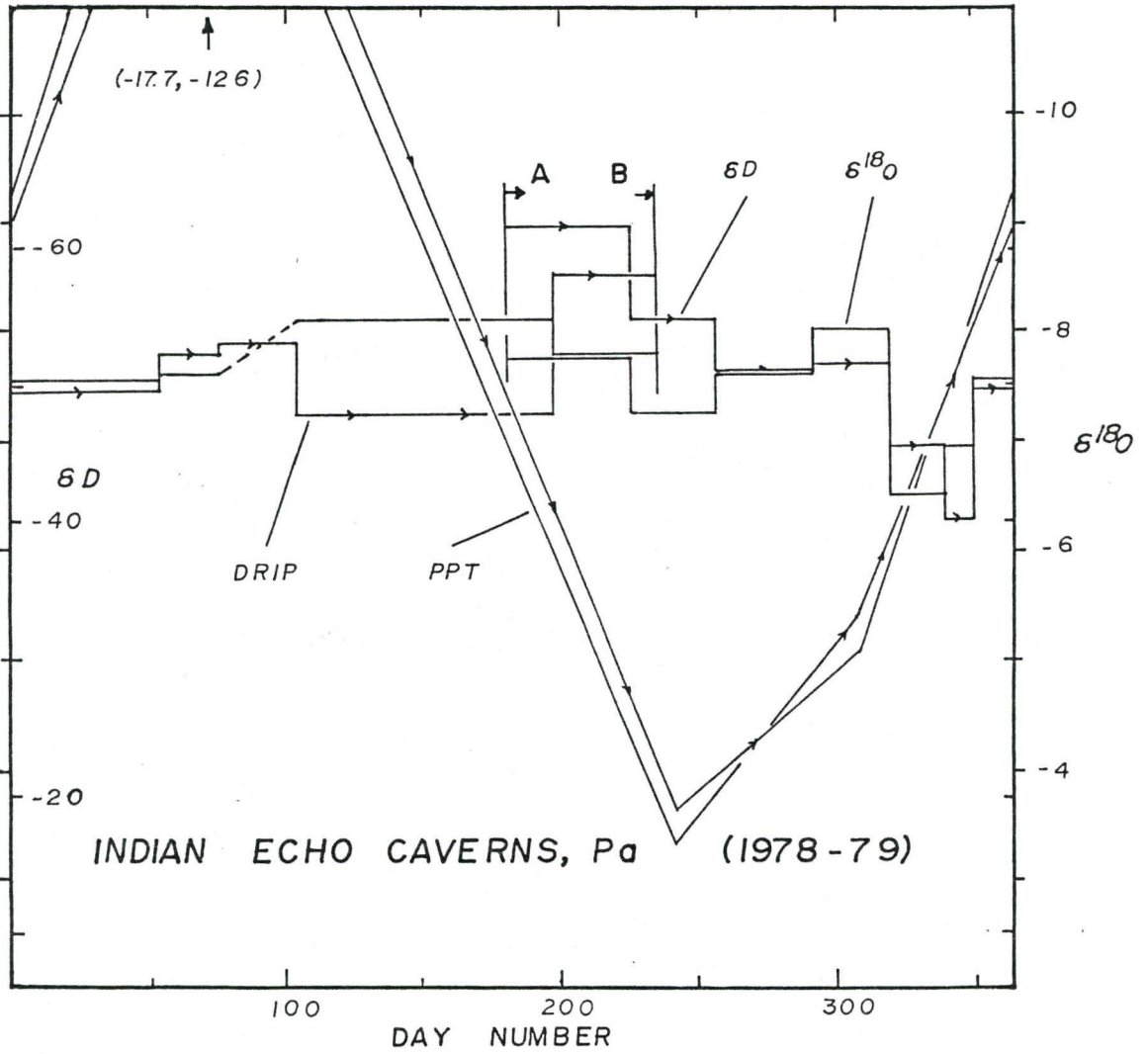
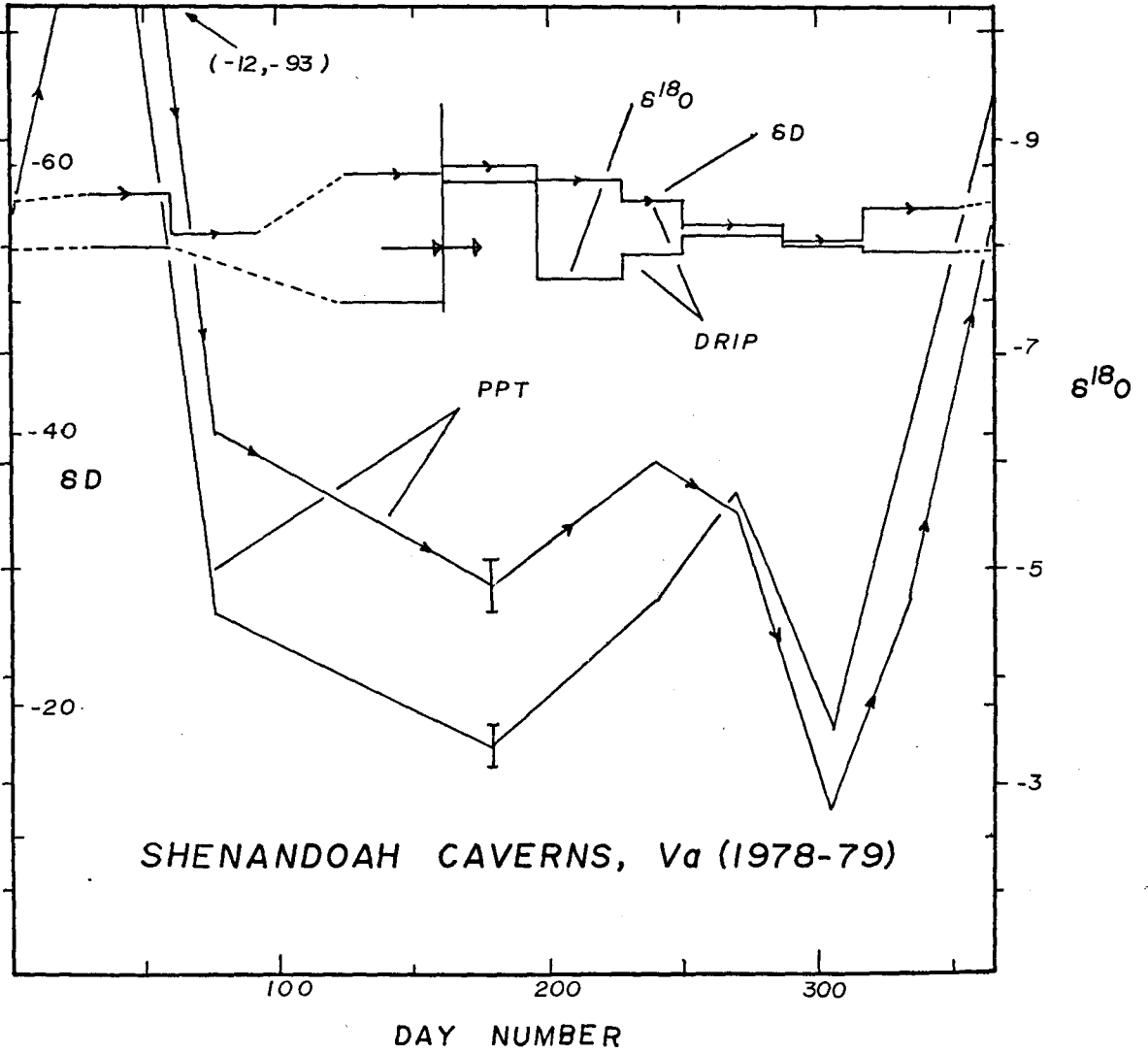


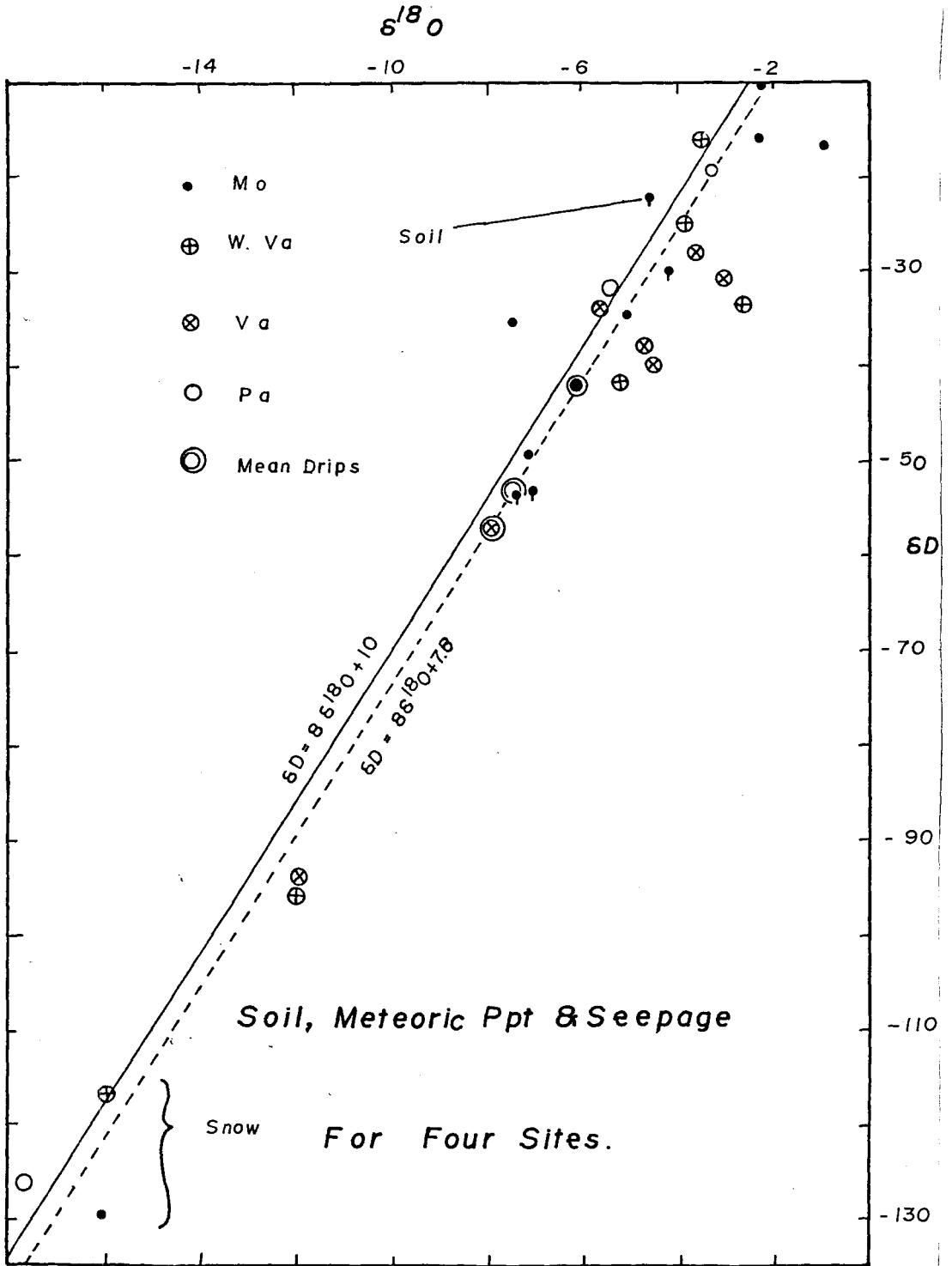
Figure 3.4 Yearly isotopic profiles for cave seepage water
and meteoric precipitation from Shenandoah Caverns, Va.



0.5‰ and 5‰ difference in $\delta^{18}\text{O}$ and δD respectively for the summer data of 1978 and 1979. These are reasonable values for yearly mean variations in precipitation at many sites (IAEA, 1979). It is also worth remembering that 1977 was an unusually cold winter and that the record may be responding to this. Such differences are not seen at the other two sites whose drip sites were situated at around the same depth (about 10m), but without the tortuosity of groundwater flow that Tumbling Creek Cave must experience from several thin aquitards within the cave's lithology. Indian Echo lies within flat lying, massively bedded limestone whereas Shenandoah Caverns are formed on steeply dipping beds; both should allow a relatively more direct passage of water. Perhaps these latter caves had already responded to the lighter 1977 water.

The extensive isotopic data (appendix III) that lead to the conclusion that the isotopic composition recharge water is constant and essentially equal to the weighted mean annual precipitation, stands in contrast to the findings of Harmon (1979). The Kentucky cave seepage data from this study are variable and suggest a two week isotopic response to meteoric precipitation ($\delta^{18}\text{O}$ measured only). One criticism of this work is that this conclusion rests on three or four of the nineteen points plotted. The drip sites in Great Onyx Cave were 20m below a surface that admittedly has a "thin veneer of soil" but these sites are

Figure 3.5 $\delta^{18}\text{O}$ versus δD for soil and seepage water and meteoric precipitation for four Eastern U.S. cave sites. Single or filled circles are precipitation and double circles are mean seepage water values (see Appendix III).

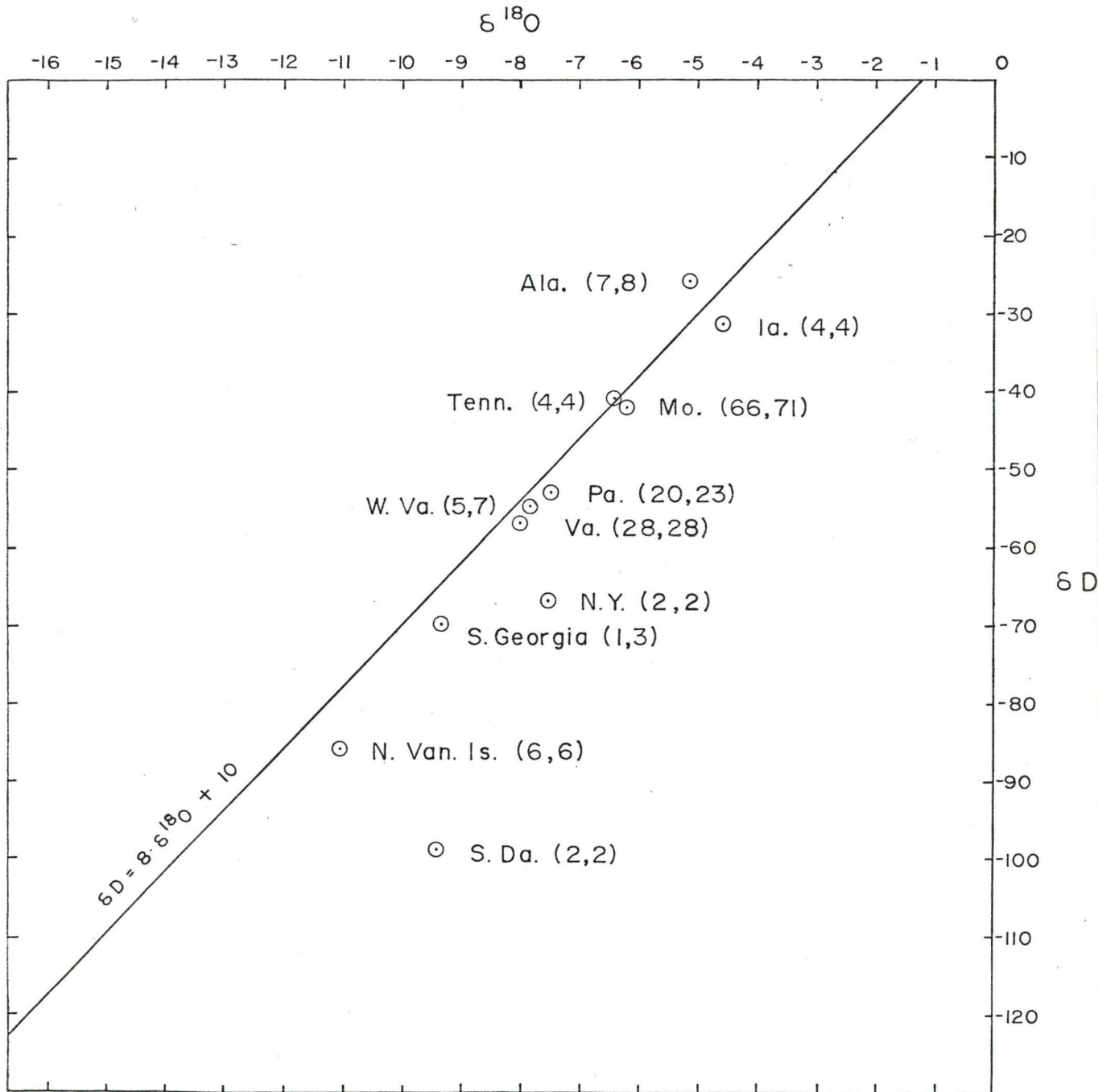


at twice the depth of the three caves reported in this study. It is tempting to conclude that further measurements might have smeared out isotopic troughs that perhaps appeared fortuitously after pulses of isotopically light rainfall.

3.1.5 Seepage Water from Caves in Other Areas

If one accepts the tenet of 3.1.3' that the constancy of isotopic ratio in cave drip waters reflects weighted mean precipitation over a period of at least one year, then it would be generally applicable to all cave sites. Figure 3.6 is a plot of all drip water data (the mean for each area; see also appendix III) including the three locales already discussed. All data lies to the right of the line defined by the intercept $d_o = 10$ with the exception of various data from Alabama. The line defined by $d_o = 7.8$ calculated for the three closely studied caves, does not change significantly if all (weighted) data is taken into account except values for Wind Cave and McFail's cave. The $\delta^{18}O$ values for these latter sites are difficult to interpret. The hydrogen values seem to compare favourably with expected meteoric precipitation but the oxygen values do not (Friedman et al., 1964). Failure to fully equilibrate the CO_2 for analysis generates more negative values (see Chapter 2). Evaporation leads to heavier values but along a slope of about 5 rather than 0. The (Ja) Marengo Cave water, on the other hand, is displaced along a

Figure 3.6 $\delta^{18}\text{O}$ and δD for mean cave seepage of eleven North American sites and one site from South Georgia. (x, y) represents the number of analyses of $\delta^{18}\text{O}_s$ and δD_s respectively.



line of slope 4.7 which is probably due to evaporation resulting from enhanced air circulation due to the construction of a second entrance to the cave.

The general trend of seepage water being slightly heavier isotopically than meteoric precipitation is suggested for the majority of sites studied and the reasons for this have been discussed in section 3.1.3. There is also geographical consistency in the data, particularly with regard to hydrogen measurement which plot conformably on the hydrogen isotope contour map of Taylor (1974).

The seepage water data also permits the calculation of $d\delta^{18}O/dt$ (factor (ii) in section 3.1.3) for regions of North America (See Figure 3.7). Discounting the results from Belize, the value obtained for the remaining drip water is $0.58 \pm 0.07 \text{ ‰}/^{\circ}\text{C}$. If data from six North American IAEA precipitation sites is included this figure changes by only a small amount to $0.57 \pm 0.05 \text{ ‰}/^{\circ}\text{C}$ (Veracruz data excluded). These values are quite different from those published by a number of workers (See Tables 3.1 and 3.2) who cite values of around $0.3 \text{ ‰}/^{\circ}\text{C}$ for continental U.S.A. However, it is important to realize that these latter values have been obtained quite differently from the method adopted by Dansgaard (1964) for middle to high latitude, essentially marine, environments. In this case, mean annual rainfall is plotted against mean annual temperature for a number of sites, for which the value

Figure 3.7 $\delta^{18}\text{O}$ versus temperature of cave seepage water and meteoric precipitation for 20 North American sites. Data is weighted least squares fitted (see also Table 3.2).

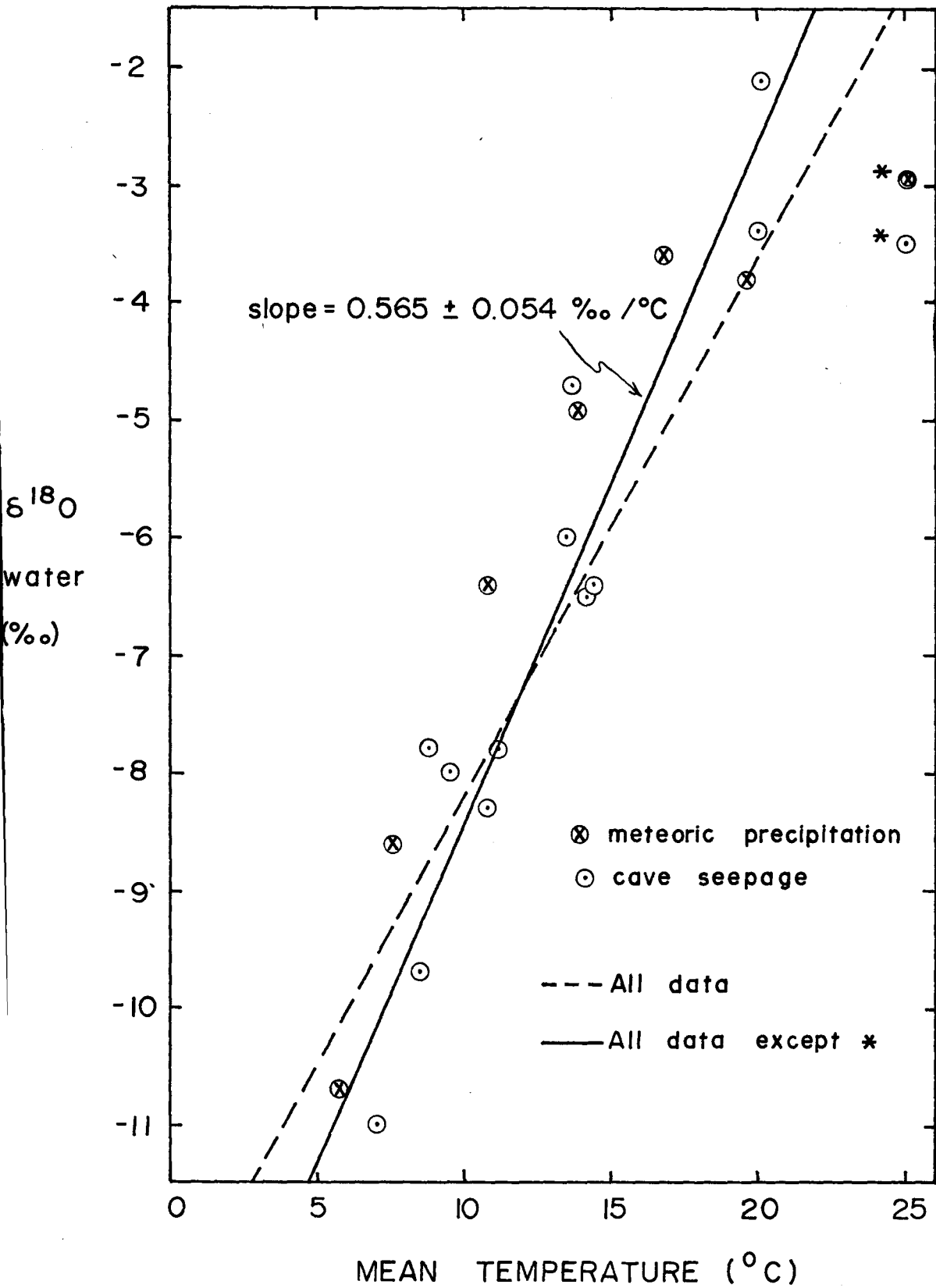


Table 3.1 Measurements of the Temperature Dependence of $\delta^{18}\text{O}$ of Precipitation

AREA STUDIED	$d\delta^{18}\text{O}/dT$ (‰/°C)	REFERENCE
Antarctic snow	0.9	Picciotto et al. (1960)
N. Atlantic precipitation and Greenland ice	0.70	Dansgaard (1964)
Seasonal Chicago precipitation	0.30	Stuiver (1968)
Seasonal West Virginia pptn.	0.28	Thompson (1973a)
Chicago and Edmonton pptn.	0.39	Harmon et al.* (1978a)
Arizona, Texas & Mexico pptn.	0.30 - 0.33	Harmon et al.* (1978a)
Yukon and N.W.T. Canada pptn.	0.17 - 0.18	Harmon et al.* (1978a)
Bermuda pptn.	0.01	Harmon et al.* (1978a)
Kentucky pptn.	0.38	Harmon et al.* (1978a)
Maritime Europe pptn.	0.22 - 0.23	Evans et al. (1978)

* using IAEA World Precipitation Survey data for 1969 - 1970

Table 3.2 a) $\delta^{18}\text{O}$ of Seepage Water and Mean Annual Meteoric Precipitation for 20 N. American Sites

AREA STUDIED	$\delta^{18}\text{O}(\%)$	MEAN TEMP($^{\circ}\text{C}$)	REFERENCE	
Texas	- 3.4	20.0	Harmon et al., 1978	Cave Seepage Water
West Va.	- 8.0	9.5	Harmon et al., 1978	
Iowa	- 7.8	8.8	Harmon et al., 1978	
Bermuda	- 2.1	21.0	Harmon et al., 1978	
Kentucky	- 6.0	13.5	Harmon et al., 1979	
Vancouver Is.	-11.0	7.0	This study	
New York	- 9.7	8.5	This study	
Pennsylvania	- 7.8	11.1	This study	
Virginia	- 8.3	10.8	This study	
Missouri	- 6.4	14.4	This study	
Tennessee	- 6.5	14.2	This study	
Alabama	- 4.7	13.7	This study	
Belize*	- 3.5	25.0	This study	
Chicago	- 6.4	10.5	IAEA, 1979	Meteoric Pptn.
Waco	- 3.8	19.7	IAEA, 1979	
Hatteras	- 3.6	16.8	IAEA, 1979	
Santa Maria	- 4.9	13.9	IAEA, 1979	
Ottawa	-10.7	5.8	IAEA, 1979	
Flagstaff	- 8.6	7.6	IAEA, 1979	
Veracruz*	- 2.7	25.1	IAEA, 1979	

* Influenced by the "Amount Effect" (Dansgaard, 1964)

b) Weighted Least Squares Fitting of Data From a)

DATA SET	$d\delta^{18}\text{O}/dT \pm (\%./^{\circ}\text{C})$	CORRELATION COEFFICIENT(R)
All except *s	0.565 \pm 0.054	0.93
All	0.448 \pm 0.051	0.90
Cave Seepage	0.578 \pm 0.068	0.94
Meteoric Pptn.	0.500 \pm 0.082	0.95

obtained is $0.695\% / ^\circ\text{C}$ whereas the workers cited in Table 3.1. take spot measurements of $\delta^{18}\text{O}$ (precipitation) and temperature over a given period, usually of one year, for a single station. Plotting cave seepage water versus cave temperature for a number of sites is analogous to the Dansgaard (1964) approach and considerably higher figures are obtained than those seen in Table 3.1 for continental North America. This has important implications with regard to previously interpreted records from speleothem. Why this discrepancy occurs, may be due to the fact that the Dansgaard (1964) approach, in taking means, incorporates a weighting factor (amount of precipitation) which the other method, by taking spot measurement of temperature and precipitation does not. In fact, it would be difficult to accomplish this, particularly say, during an intense storm where both temperature and $\delta^{18}\text{O}$ are likely to vary considerably (Friedman et al., 1964). The justification for the exclusion of Veracruz meteoric and Belize seepage data stems from the observation of Dansgaard (1964) that high temperature low latitude regimes are subject to the amount effect (factor (iii), section 3.1.3) yielding isotopically lighter values than expected.

The lower gradient of $d\delta^{18}\text{O}/dt$ for continental environments is mainly due to participation of light re-evaporated fresh water from the land surface. However, how much lower is the gradient than the gradient of

0.70 ‰/°C published for the middle to high latitude marine environments? Which approach should be taken to calculate it? Gray and Thompson (1974) report intersite correlation of $\delta^{18}\text{O}$ (cellulose) and mean annual temperature for tree rings of 0.5 ‰/°C for the Western Cordillera from the Yukon to California. Gray (1979) reports similar correlations for peat and aquatic plants of 0.52 ‰/°C from widely distributed sites in North America. However, five-year growth rings from single trees from Edmonton and Fort Vermillion give $d\delta^{18}\text{O}/dT$ of 1.2 and 1.0 ‰/°C which he attributes to local environmental factors or even microclimatic effects. Epstein et al. (1977) question this conclusion stating that kinetic isotope effects associated with evapotranspiration from leaves play a dominant role in determining $\delta^{18}\text{O}$ of cellulose. It is true that these values are higher than any reported elsewhere (Table 3.1). Nevertheless, the intersite gradients are very similar to the value of 0.56 ‰/°C obtained for cave seepage water and precipitation (Figure 3.7 and Table 3.2).

Finally, it should be noted that Gray (1979) finds that $d\delta/dT$ at a site is always $\leq d\delta^{18}\text{O}/dT$ (determined between sites) and other data, for example (see Table 3.1), tend to confirm it.

The question remains whether $\delta^{18}\text{O}/dT$ changes at a site, as it passes into periods of distinctly different climate in response to changes in the local environment, or a shift in geographical position? The latter possibility is more consistent with the previous arguments but recourse to measurement of water in

speleothems, assuming it to be representative of past seepage water, should provide a convincing answer. This is discussed further in Chapter 5.

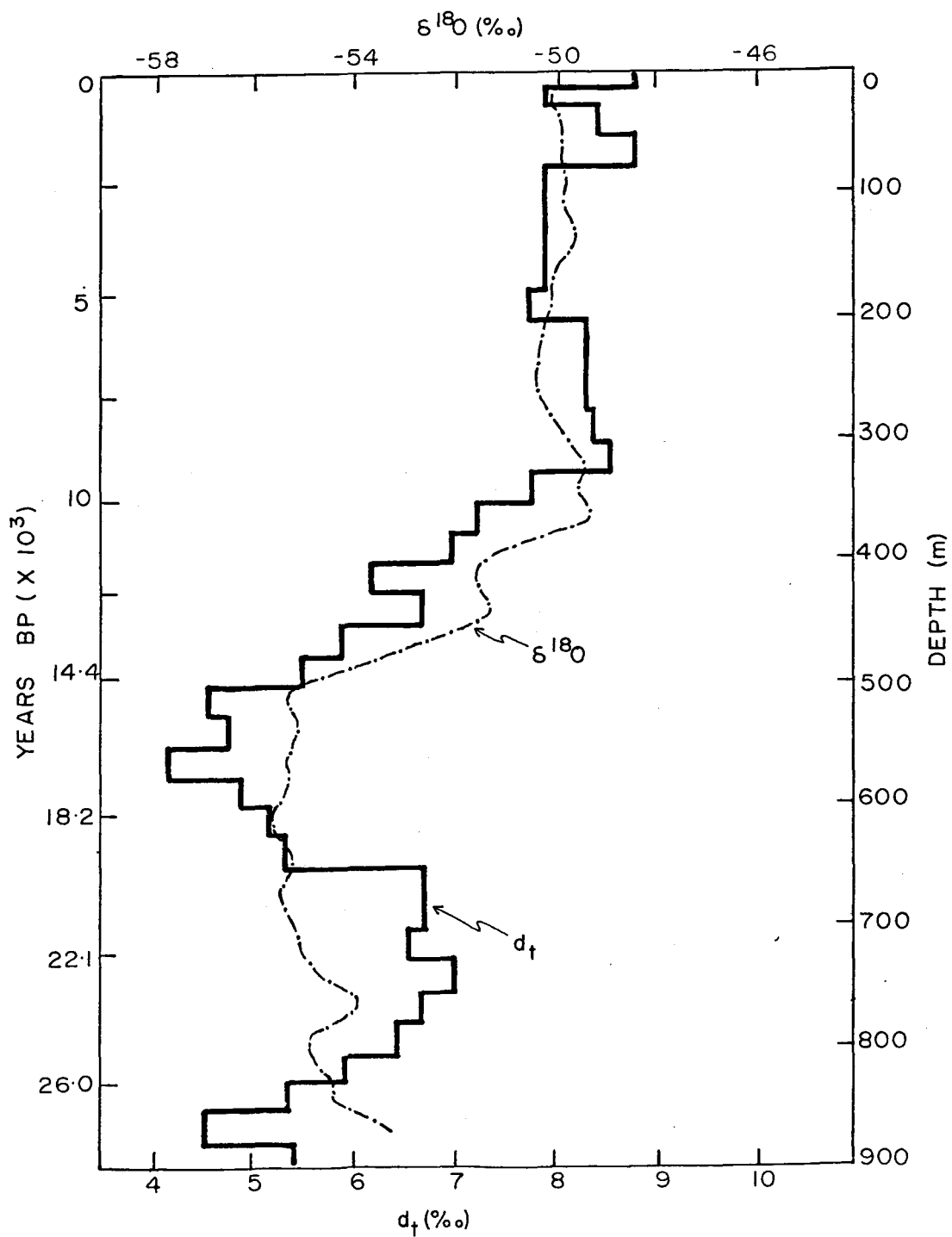
3.2 Antarctic Ice Study

In Chapter 1, the work of Harmon and Schwarcz (1981) was reviewed. In their study, 38 out of 49 paleotemperatures from fluid inclusions were unacceptably low, sometimes below zero. Inasmuch as oxygen isotope ratios had been inferred from the measurement of δD values using a meteoric water line with $d_o=10$, it is suggested that the value of d_o may have been different in the past. By reducing d_t to zero they found that "sensible" temperatures resulted. The zero intercept was taken to be a maximum change. This parallel shift of the meteoric water line with time is supported by the work of others. Epstein et al. (1970), working on Wisconsin ice from the Byrd Core, Antarctica, published the following line:

$$D = 7.9 \cdot \delta^{18}O + 0 \quad \dots\dots\dots(3.1)$$

forcing their data to lie on a line of slope 8, yield a d_t (see Equation 1.8) value of about 4.0 ‰. Merlivat and Jouzel (1979) derive a theoretical model which relates d_o to humidity over the oceans. A moisture deficit of the

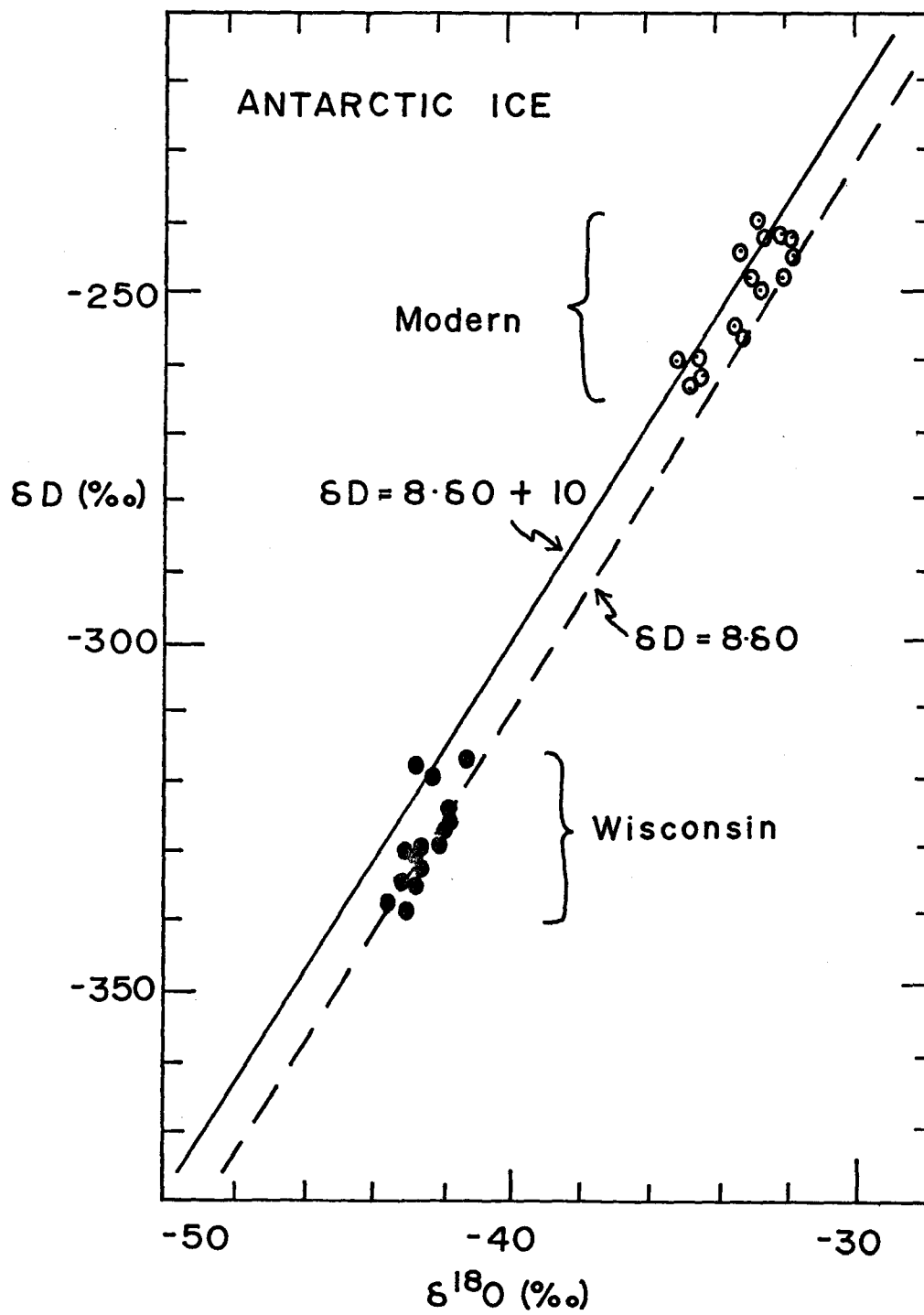
Figure 3.8 $\delta^{18}\text{O}$ and d_t versus depth/age of the Dome C Antarctic
Ice core (after Lorius et al., 1980).



air over the ocean, equal to 10%, in comparison to 20% for modern conditions was deduced from Saharan groundwaters older than 20ka (data of Sonntag et al., 1979). d_t was found from the Dome C Core in East Antarctica; a record of more than 30ka (Figure 3.8). d_t is clearly seen to change as $\delta^{18}O$ decreases from 10ka back to 30ka and varies from present day values of around 9‰ to minimum values of about 4‰.

Prior to the work of Lorius et al. (1980) and without the raw data of Epstein et al. (1970) a plot of d_t versus time could not be made. Thus a study of the Antarctic Ice Core, stored at SUNY, Buffalo was initiated and is in progress at the time of writing. Results obtained so far are presented in Figure 3.9 and appendix IIIc. A distinct change in d_o from a value of about 8‰ for modern ice to a value (d_t) of about 1‰ for Wisconsin ice is observed. The latter value is somewhat lower than those of Lorius et al. (1980). It is worth noting that d_t might vary globally more smoothly than δD or $\delta^{18}O$ of ice alone since it doesn't depend on temperature at the site of precipitation, only at the source and that will be essentially uniform whether water falls in Arctic or Antarctic. Therefore, d_t might allow more precise correlation between ice cores. Further measurements along the core should generate an interesting comparison of these two records.

Figure 3.9 $\delta^{18}\text{O}$ versus δD for Wisconsin and Modern ice from the SWISS/DEEP Antarctic Ice core. Lines are not fitted through the points but represent the range of d_t indicated by Harmon and Schwarcz (1981).



3.3 Concluding Remarks

From the preceding discussion, the following observations can be made:

1. $\delta^{18}\text{O}$ values from modern calcite-seepage water pairs yield temperatures close to cave temperatures.
2. Variations in the isotopic composition of meteoric precipitation is explainable in terms of factors proposed by Dansgaard (1964) although no "amount" effect is observable (except for samples from Belize).
3. The isotopic variability of soil water is less than that of precipitation and is intermediate between those of meteoric and cave seepage water.
4. Cave seepage water does not vary significantly on a seasonal or annual basis and its constancy is explained by extremely slow downward infiltration compared to lateral equilibration rates. Water may take more than one year to reach drip water sites.
5. Seepage water from the eastern United States conforms to a line described by $\delta\text{D} = 8 \delta^{18}\text{O} + 7.8$. This departure from $d_0 = 10$ may be due to local evaporation during summer months.
6. Seepage water flow is highly variable but the flow rate does not correlate with isotopic composition. This can be explained by a piston flow mechanism operating in the vadose zone.

7. The isotopic ratio in cave seepage waters reflects the mean annual weighted average of meteoric precipitation over a period of at least one year, making them very useful for determining intersite dependence of $\delta^{18}\text{O}$ on mean annual temperature.
8. The dependence of $\delta^{18}\text{O}$ of seepage water on temperature from site to site is around $0.56\text{‰}/^{\circ}\text{C}$ and does not differ significantly from the value for IAEA North American precipitation data. This gradient is close to those obtained by other workers for tree rings, peat and aquatic plants but is different from the middle to high latitude value of $0.695\text{‰}/^{\circ}\text{C}$ for marine stations obtained by Dansgaard (1964).
9. $d\delta^{18}\text{O}/dT$ values for single sites are quite different from the intersite dependence and may have important repercussions on previous interpretations $\delta^{18}\text{O}$ (calcite) records from speleothems.
10. Most seepage water conforms to the isotopic contour map published by Taylor (1974), particularly for δD values.
11. Previously observed low fluid inclusion isotopic temperatures can be explained by a shift in the meteoric water line in the past to lower intercepts (d_t values) during glacial periods. Results from the Antarctic ice core support the experimental and theoretical work of others that the line was subject

to such a shift during the Wisconsinan Glaciation.

12. d_t , being independent of temperature may allow a more precise correlation between ice cores than δD or $\delta^{18}O$ of ice from both the Arctic and Antarctic.

CHAPTER 4

STUDY OF WATER IN SPELEOTHEMS

4.1 Introduction

In Chapter 1 it was argued that depositional temperatures can, in principle, be determined from isotopic measurements of oxygen in both calcite and the water from which the calcite formed. Portions of this water are trapped within speleothems as fluid inclusions. Schwarcz et al. (1976) measured hydrogen isotope ratios of the fluid inclusions because it was suspected that the oxygen in them could exchange with the comparatively large calcite reservoir. Hydrogen isotope ratios of the fluid inclusions can be used to infer the original oxygen composition providing that the inclusion water is identical to the seepage water that was originally trapped. This and the equivalence of seepage water to precipitation is discussed in Chapter 3.

What follows is a presentation and discussion of results obtained on water extracted from speleothems by the two methods, crushing and decrepitation, discussed in Chapter 2. The water samples obtained by both are generally isotopically too light in oxygen and hydrogen, when compared to accompanying seepage water or with respect to the paleotemperatures

which they yield. This, and other characteristics, suggest that not all the water is present as trapped droplets of seepage water.

Possible sites of hydrogen in speleothems are considered to be:

- i) in fluid inclusions; both macro- (tear-drop shaped) and micro (linear, spindle-shaped),
- ii) within growth layers,
- iii) at crystal terminations (as fluid inclusions),
- iv) in anastomosing channels,
- v) adsorbed,
- vi) coordinated within the calcite crystal lattice,
- vii) from hydroxyl groups,
- viii) associated with organic or inorganic impurities trapped in speleothems.

Mobility of water in sources (i) to (iv) and mechanisms associated with the formation of sources (v) to (viii) all could lead to isotope effects. The following sections attempt to investigate these possible sources.

4.2 Petrology of Speleothems

4.2.1. Speleothem Morphology

A substantial and informative study has recently been made of the fabrics of stalactites, in which 174 thin sections

were examined (Kendall and Broughton, 1978). Prior to this, only perfunctory studies have been undertaken with little thought given to the fabrics observed (Moore and Sullivan, 1978). More recent work has focussed on unattached deposits such as cave pearls (Hahne et al., 1968) and popcorn (Thrailkill, 1976). One Holocene stalagmite has been studied in some detail by Folk and Assereto (1976). All these more recent studies of carbonate rock fabrics aim at seeking explanations based on complex diagenetic processes; for example, histories which encompass marine and freshwater environments. In contrast, speleothems are supposedly simple and subject to relatively unchanging conditions.

Speleothems are almost always composed of calcite, which has precipitated from groundwater solutions derived from the soil zone with P_{CO_2} values some 10-100 times that of the cave air. The resulting outgassing of CO_2 provides the mechanism for deposition (Picknett et al., 1976). Many morphologies can result depending on physical conditions but four major types will be considered here:

i) Soda-straws are an initial tubular form resulting from deposition at the upper surface of drips where they are in contact with the cave roof or previously deposited calcite. Later, water may flow down the outside due to some blockage and,

ii) stalactites of a carrot shape are formed (continuous lateral migration of the drip leads to "curtain" formations).

As the drip leaves the roof pendant it is still saturated because outgassing of CO_2 is too slow for the drip to attain equilibrium with the cave air (Rocques, 1969). As the drip splashes against the floor, subsequent deposition may form stalagmites or flowstone.

iii) stalagmites; ideally, flat-topped, cylindrical formations. The shape is indicative of the constancy of the growth rate, different shapes can arise under conditions of varying growth rate (White, 1976).

iv) Flowstone may result if lateral growth from thin water films takes place. Growth layers accumulate sub-horizontally or as inclined sheets and appear to be unrestricted in lateral extent.

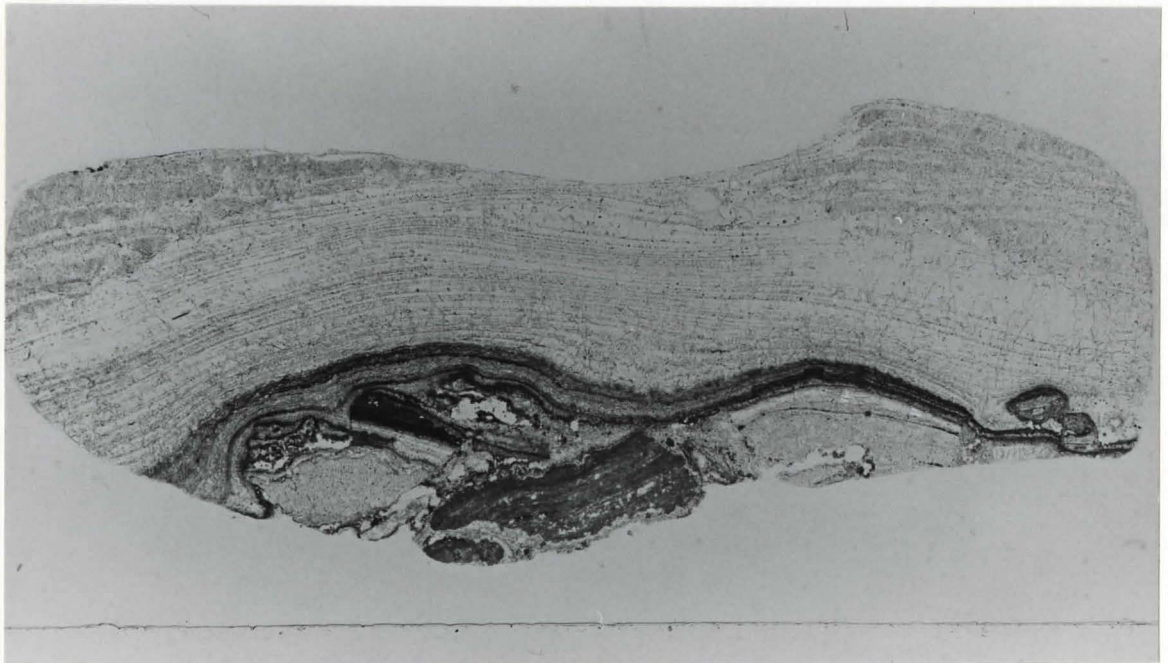
Stalagmites and flowstones lend themselves well to paleoclimate studies and it is their petrology that will be considered here in some detail.

4.2.2. Crystal Morphology

Speleothems increase in size by the accretion of successive growth layers. Elongate crystals of calcite within speleothems propagate parallel to the growth direction (Plate 4.1). Growth layering is discernible by zones containing impurities or, as discussed later, abundant fluid inclusions which record periods of slower, or cessations of, carbonate precipitation (Plate 4.2).

The elongate crystals of calcite that radiate normally

Plates 4.1 and 4.2 Mirror Lake #1 under crossed Nicols and in plain light respectively. Three distinct sections are seen: the base, fragments of limestone (gravel) in a dirty calcite matrix is separated from upper, more massive, unit by radially oriented columnar crystals that extend, in some cases, fully across the unit as well as transcending easily observable growth layers. The uppermost portion (restricted to the left and right flanks of the specimen) is composed of a somewhat randomly oriented microcrystalline mosaic. This fabric may be a function of a splash effect following the collision of drips with the middle unit. Growth layers appear to be sets of linear inclusions. Field is 2 x 4 cm.



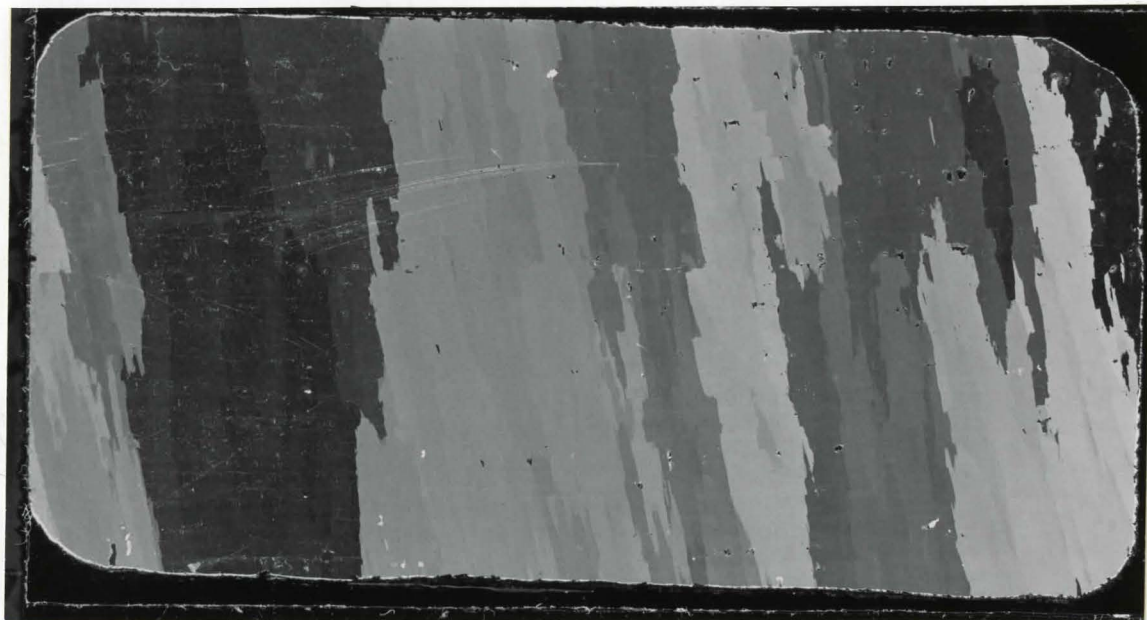
from growth layers form the massive fabric of speleothems. Their size ranges from a few microns to a few cm in length. Crystals with widths less than $5\mu\text{m}$ that are markedly elongate and pointed are referred to as acicular whereas those with widths greater than $5\mu\text{m}$ are described as columnar or palisade after Kendall and Broughton (1978). Columnar crystals are marked by jagged boundaries with complex and irregular re-entrants (Plate 4.3). Crystals often widen at the expense of neighbours along parts of their length but are elsewhere encroached on by these same neighbours. Crystal size is to some extent dependent on the distance from marked growth bands in the direction of growth advance.

Breaks in growth seem to afford seeding sites for subsequent calcite precipitation and this leads to the deposition of innumerable tiny crystallites on the speleothem's growing surface.

Subsequently, a range of columnar crystal sizes typically of the dimension already given, build up a calcite mosaic that is dominated by elongate, palisade crystals having their C-axis oriented normal to the growing surface (Plate 4.1). Small changes in crystal orientation give rise to a systematic and uniform brush extinction within colonies of approximately homoaxial orientation. This, with an apparent curvature of cleavage, testifies to the lattice deformation that cannot be due to external stress. Cleavage traces can readily be seen at

Plate 4.3 View of flowstone 73107 under crossed Nicols. Columnar crystals are seen to be large (>2 cm long by 0.2 to 1 cm wide) displaying characteristic jagged boundaries and complex reentrants. Abundant fluid inclusions, oriented parallel to the C-axis, linear to bulbous-shaped, less than 100 μ m long, are seen throughout the fabric. Some porosity is apparent too but randomly distributed and generally of a larger size than the bulbous inclusions.

Plate 4.4 View of flowstone 76010 under crossed Nicols. Rhombohedral cleavage traces with slight curvature are noted here. More detail is given opposite Plate 4.11 with the enlarged view.
Fields are 2 x 4 cm.



rhombohedral angles to the growth bands (Plate 4.4).

SEM micrographs (Plate 4.5) indicate that so-called single columnar crystals are, in fact, crystal aggregates of numerous parallel crystallites of shape depicted in Figure 4.1. These are discussed next with respect to the origin of speleothem fabrics. One further fabric should be mentioned, that of the randomly oriented calcite mosaic observed by Folk and Assereto (1976). In thin section, this is seen as an inclusion-rich, length-slow calcite mosaic. These authors ascribe its origin to aggrading neomorphism of an earlier acicular aragonite. Only one sample of this texture, 75350 from Jamaica (Plate 4.6), was encountered.

4.2.3. Fluid Inclusions

Fluid inclusions occur in speleothems in a variety of shapes and sizes and are inhomogeneously distributed through them. They are gradational in form between elipsoidal, sausage or tear-drop shapes and linear, spindle shapes. The former variety are the largest being between 5 and 50 μ m long and are readily observable in the light microscope (Plate 4.7). Often they display growth anisotropism (as previously shown) being tapered towards the growth direction and may occasionally be partially filled with water. Although they are inhomogeneously distributed, zones occur where they can make up as much as 5% of the rock. These zones tend to parallel the growth surface and hence delineate growth bands. As mentioned, shape and,

Figure 4.1 (After Kendall and Broughton, 1978)

- a) Diagram illustrating the effect of lateral crystallite growth culminating in imperfect coalescence which allows entrapment of water between crystallites. This mode of entrapment gives rise to linear inclusions.
- b) Interpretation of the regular inclusion array seen in Plate 4.5 by a process in which crystallites progressively merge to form columnar crystals. Former positions of crystallite terminations on earlier growth surfaces are shown as dashed lines. Intercrystallite spaces (linear inclusions) are shown as solid lines.

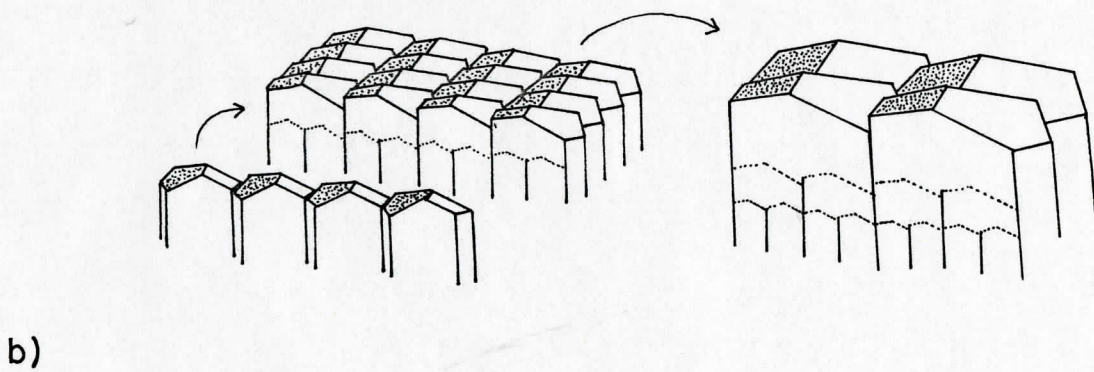
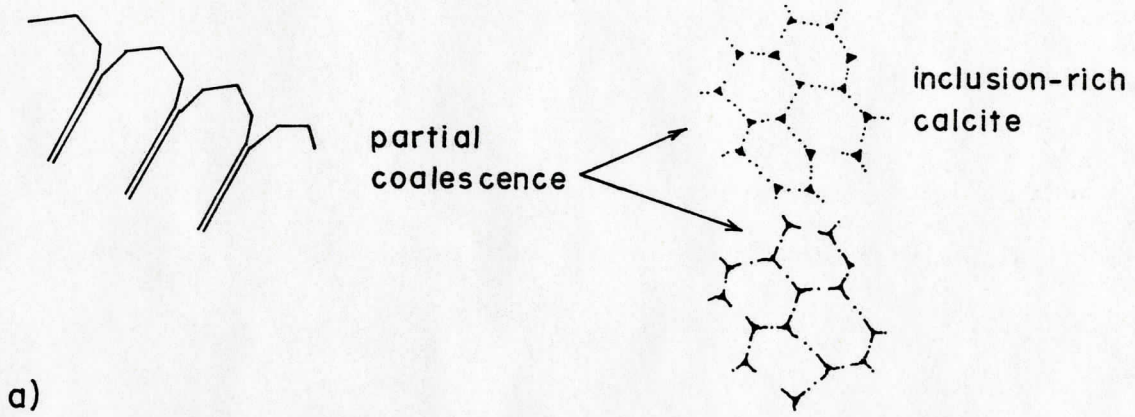


Plate 4.5 (also Plate 1.3) Fracture surfaces of columnar calcite crystals in Stalactites.

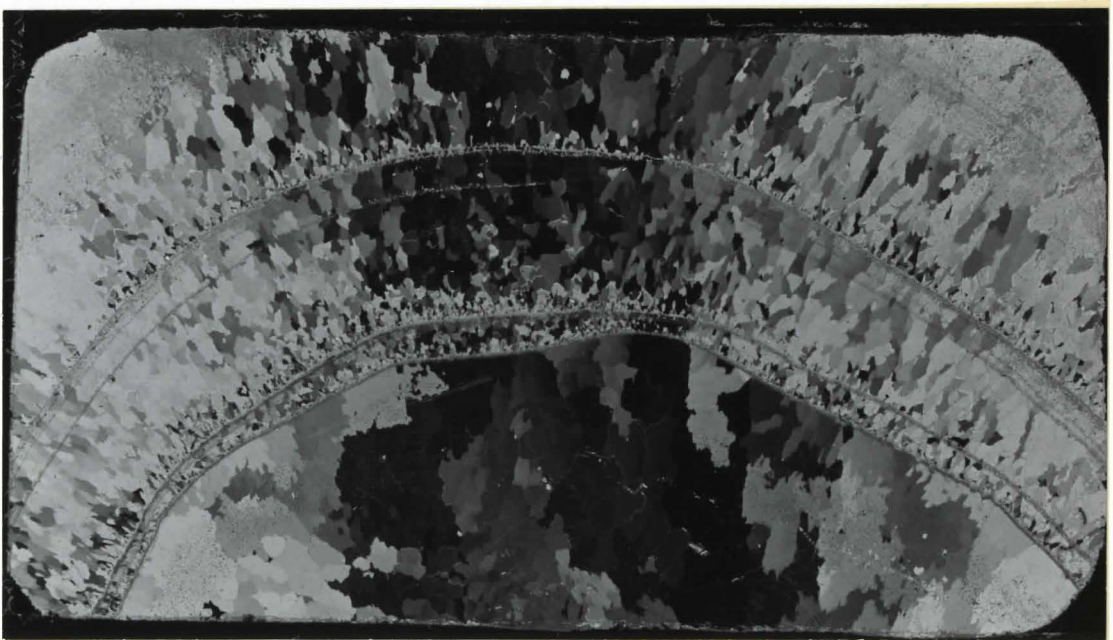
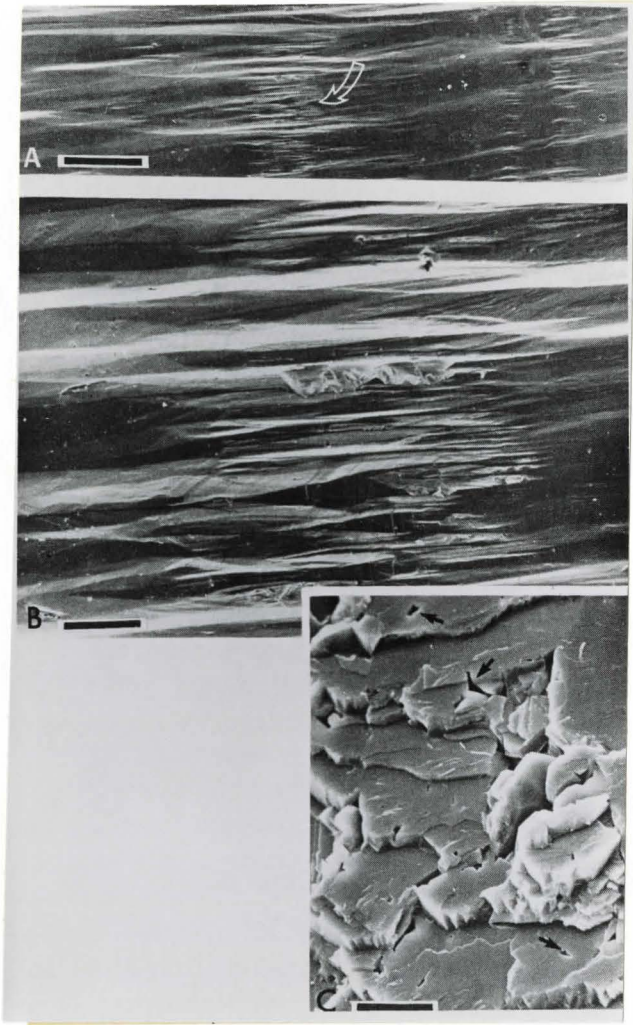
A: General S.E.M. view to show inclusion-rich layers (scale = 20 μ m).

B: Detail of A (arrowed). Inclusion appears as spindle-shaped depressions and are interpreted as parts of elongate cavities that lie between close-packed, partially coalesced crystallites (scale = 100 μ m).

C: S.E.M. view of fracture surface oriented normal to that in A and B, and approximately parallel to a former growth-surface. Triangular pores (arrowed) are interpreted as remnants of former inter-crystallite spaces (scale = 10 μ m).

Plate 4.6 View of stalagmite 75350 reveals a length-slow mosaic of the type described by Folk and Assereto (1976). These authors ascribe such an origin to aggrading neomorphism of an earlier acicular aragonite.

Field is 2 x 4 cm.

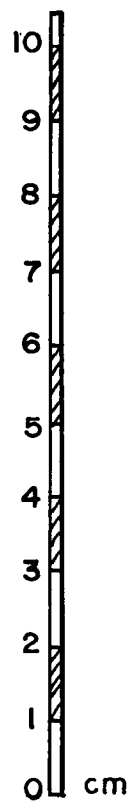
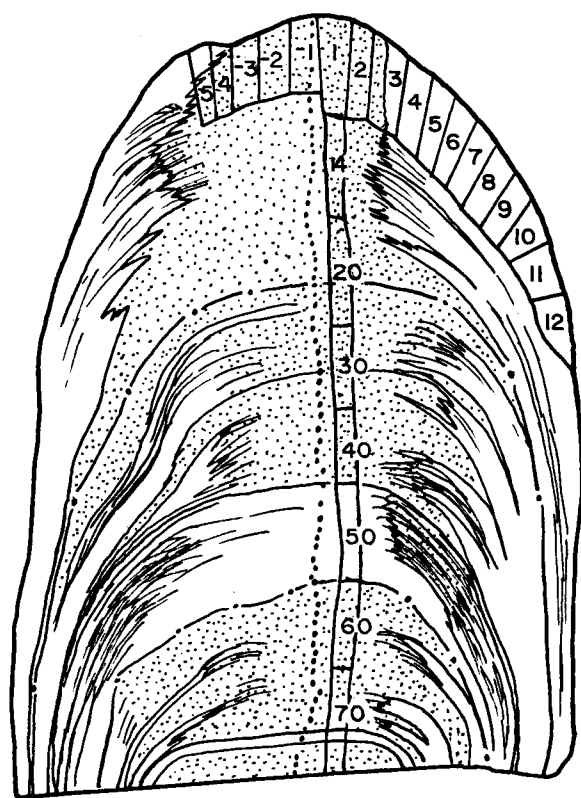


to some extent size, of fluid inclusions are gradational between the bulbous and the linear types. The linear variety are negative crystals, with their boundaries defining crystal faces. The size range extends from a few mm in length to around $10\mu\text{m}$ or less and around $10\mu\text{m}$ down to $1\mu\text{m}$ or less in width. This type of inclusion can be seen in the SEM micrograph (Plate 4.5) and thin section (Plate 4.7). The lower limit of linear inclusion size is not distinguishable with the SEM but, in thin section in some zones where inclusions are not seen to be present, the calcite displays a pseudo-pleochroism (light-brown to colourless) interpreted as being due to microinclusions (Kendall and Broughton, 1979). Linear inclusions very markedly delineate growth bands (Plate 4.4) and are otherwise seen as a series of mutually interfering, spindle-shaped depressions in the SEM (Plate 4.5). The pores are roughly triangular in cross-section with concave sides and are aligned in the direction of the crystal's c-axis. Fluid inclusion density tends to correlate with the intensity of "miliness" seen in hand specimens and this is often most marked on the outer parts of stalagmites (Figure 4.2). The tendency for linear inclusions to mark out growth bands provides clues as to the mode of formation of speleothem calcite and the fluid inclusions themselves. This is considered next.

4.2.4. The Origin of Fluid Inclusions

Fluid inclusions occur by entrapment of water as spel-

Figure 4.2 A cross-section through a stalagmite (797MP1) from McFail's Cave, N.Y. Numbered areas indicate where samples were removed for isotopic analysis. Clear regions indicate the presence of milky-white calcite due to dense populations of fluid inclusions. Speckled regions are areas of clear calcite. The distribution of milky and clear calcite is typical of many stalagmites.

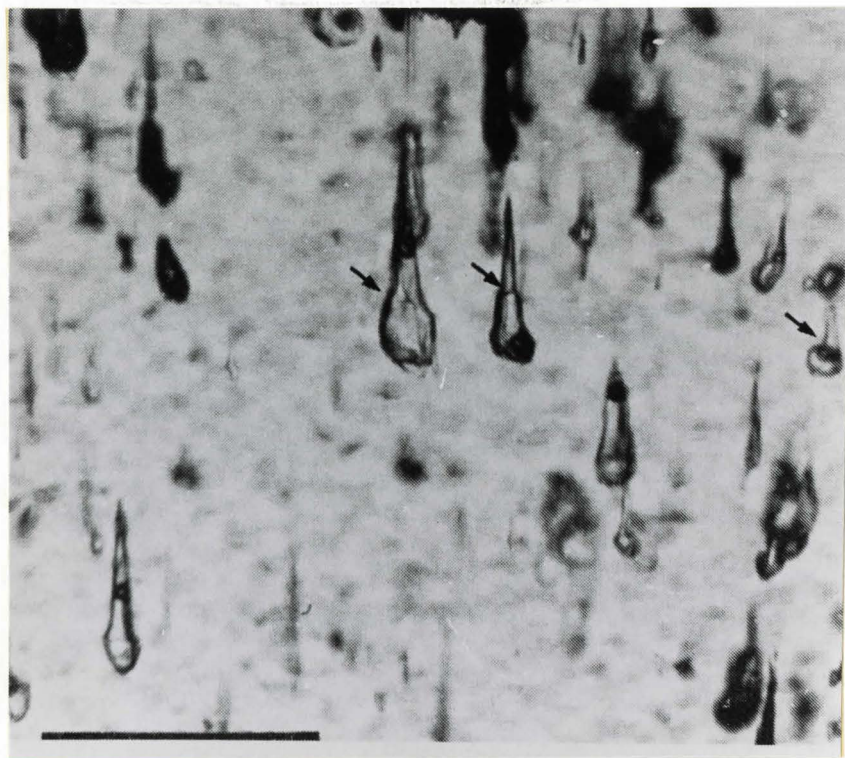


797MP1

Plate 4.7 (also Plate 1.1) Detail of large thorn-shaped inclusions showing marked growth anisotropism and constrictions (arrowed). Host calcite grew towards the top of the photograph (After Kendall and Broughton, 1978).

Plate 4.8 View of stalagmite (top) 807CH1 under crossed Nicols. Columnar crystals are highly elongate (3.4 mm x 0.2 mm) and formed in a stellate array exhibiting brush extinction. Growth bands are observable in the centre of the section characterised by smaller, less well oriented, crystals. In plain light, there is a marked graininess that corresponds to crystal boundaries. Such observations indicate that these boundaries may contain water although no sets of individual inclusions can be seen. Some porosity is seen to the right of the section corresponding to the junction with another adjacent stalagmite.

Field is 2 x 4 cm.



eothem growth advances. However, entrapment seems to be greatest following times when according to Kendall and Broughton (1978), the rate of water supply changes or ceases altogether or when impurity absorption impedes the growth of prior columnar crystals. These authors, as a result of the observations described above, propose a model for the origin of columnar crystals and hence fluid inclusions contained within them. This model is outlined below. Firstly, they argue that previous interpretation of fabrics being largely as a result of an acicular precursor recrystallizing to form columnar calcite crystals is not correct. Columnar crystals are primary and develop as a result of numerous small syntaxial overgrowth crystallites accumulating on the growing surfaces. During growth, partial coalescence takes place and the resulting inter-crystallite spaces trap water forming linear inclusions (see Figure 4.1). The strongest argument for the primary nature of the fabrics is the observation that columnar crystals extend all the way to the surface of actively growing speleothems (Plate 4.1) and that this growing surface is rough to the touch due to the presence of a multitude of (crystallite) projections. The density of linear inclusions at growth horizons may be due to interruptions in the degree of perfection of crystallite growth and hence the reduced tendency for coalescence. Subsequently, lateral growth of crystallites behind the growing surface, as it advances further, would cause re-

generation of columnar crystals. However, complete coalescence does not occur here as evidenced by the presence of fluid inclusions and shown by the SEM view (Plate 4.5). The triangular cross-section of the inclusions indicate the arrangement of crystallites as they grew. Linear inclusion size is a function of crystallite size which, in turn, may be determined by the thickness of water films. Large projections would disturb the water flow, diverting it around them, thus inhibiting their growth. Bulbous-shaped inclusions are of a different origin as evidenced by the tendency of some of them to be only partially filled (linear inclusions appear to be completely filled in thin section). Almost complete or complete cessations of water supply and hence episodic growth is implied. Revitalization of the water flow would then seal over rugosities and air bubbles adhering to the growing surface by the growing together of adjacent columnar crystals of slightly different orientation. The latter mechanism would also explain the narrowing of the type of fluid inclusion towards the growth direction.

One further observation of Kendall and Broughton (1978), which is worthy of note, is the surprising lack of impurities in the deposits they studied. This lends weight to the supposition that visible growth layers are usually generated by changes in the rate of water supply rather than more catastrophic occurrences which bring in detrital or organic material. Furthermore, complete dissolution of calcite from speleothems

in HCl results in very little insoluble material. Thrailkill (1976) argues against the presence of living bacterial matter and further remarks on the lack of organic material in most samples studied. However, the role of humic and fulvic acids may be important in determining crystal fabrics as suggested by Schwarcz (1981) and the colour of speleothems may be due to organics (Gascoyne, 1977). This subject remains to be investigated more fully.

Of importance to fluid inclusion stable isotope studies is the relative proportion of inclusion types. The observations of Kendall and Broughton (1978) suggest that liquid water is both dispersed throughout the columnar crystal fabric, predominantly in microinclusions, and within marked growth horizons.

4.2.5. Description of Speleothems Analysed in This Study

4.2.5.1. Modern, Active Deposits

Bone-Norman (SS1): A 5 cm x 0.5 cm soda-straw taken with accompanying drip water from Bone-Norman Cave, W. Va. (Thompson, 1973). As implied, the deposit was actively growing at the time of collection generating a clear, colourless calcite.

Friar's Hole (SS1): A 4 cm x 0.4 cm soda-straw taken with accompanying drip water from Friar's Hole, W. Va. (Yonge, 1979). This actively growing deposit is clear and translucent.

Mirror Lake 1: Nubbin of calcite actively growing on gravel in Indian Echo Caverns, Hummelstown, Pa., 7 cm across

the base and 1.5 cm in height. The samples taken for stable isotope analysis are from the 0.5 cm thick milky-white top layer. The basal layers composed of limestone gravel in a dirty calcite matrix were avoided.

In thin section taken at right-angles to the growth layers (Plates 4.1 and 4.2), 3 distinct sections are seen. The base, fragments of limestone in a dirty calcite matrix is separated from the upper, more massive unit by an impurity layer. The central portion is characterized by radially oriented columnar crystals that very often extend fully across the unit as well as transending easily observable growth layers. The uppermost portion (restricted to the left and right ends of the specimen) is composed of a somewhat randomly oriented microcrystalline mosaic. This fabric may be a function of a splash effect following the collision of drips with the middle unit (seen to extend to the top of the deposit along its axis). Growth layers appear to be sets of linear inclusions.

807CW3: Actively growing nubbin from Cold Water Cave, Iowa, (Harmon 1975), 4 cm across by 1 cm deep. The sample, cut from the centre, was of a clear to brown translucent calcite devoid of visible growth layers.

Wind Cave 1: 5 cm long by 0.8 wide soda-straw taken from Wind Cave, S. Da. (White, 1976). This deposit is coated in chalk-white porcellanous rind but the inner layers are milky white concentrically alternating with clear calcite.

Alternate layers are about 0.3 mm thick. The sample was found dry and broken, close to other similar looking deposits that were actively growing.

807CH1-1: Two actively growing amalgamated stalagmites 15.5 and 8 cm high with a basal diameter of 14 cm from Canadian Hole, W. Va. (Yonge, 1979). This deposit is characterized by an unusual purity and is thus completely white save for a 1 cm thick brown layer at the base. Both stalagmite portions are typical in that interior calcite is clear whereas the outside assumes a milky-white texture. The sample (1) was taken from the axial top of the smaller stalagmite. The junction between the two stalagmites is marked by a porous region.

The thin-section (Plate 4.8) is taken normal to the growth layers from the smaller deposit. Columnar crystals are highly elongate (3.4 mm x 0.2 mm) and formed in a stellate array exhibiting brush extinction (The former observation is consistent with the fibrous debris seen after the sample has been calcined). Growth bands are observable in the centre of the section, characterized by smaller less-well oriented crystals. In plain light, there is a marked graininess that corresponds to crystal boundaries. Such observations indicate that these boundaries may contain water although no sets of individual inclusions can be seen. Some porosity is seen to the right (towards the junction of the two stalagmites) of the section.

Llano Chiquito 1: Calcite was found coating a number of rotting trees in Sumidero del Llano Chiquito, SLP district, Mexico (Fish, 1978). The source of water responsible for these precipitates appeared to be an inlet in the roof of the cave. The cave is liberally decorated. The deposit is layered, up to a few cm thick and deeply buff-coloured leaving the sample barely translucent.

Bugaboo 1: While this is not a speleothem, it has been included in this study because it was formed below ice at 0°C giving it a good temperature control. It is an impure calcite, coating a glaciated rise of granodiorite over an area of several square metres in the Bugaboo Mountains, B.C. Since the margin of an ice field was located a few metres from the deposit it was taken to be sub-glacially precipitated. The formation of these interesting deposits has been described by Hanshaw and Hallett (1978). Growth layers are marked by detritus and intervening calcite is buff-coloured and translucent.

4.2.5.2. Ancient, Inactive Deposits (See Table 4.1)

73107: Part of a massive flowstone from Government Quarry Cave, Bermuda (Harmon, 1975) topped by 0.5 cm buff-coloured translucent rind. Below the rind, unvarying in appearance, the speleothem is composed of a creamy to milky-white calcite with prominent sets of growth layers. Samples were cut from a 1 cm band immediately below the rind. In thin

section (Plate 4.3), columnar crystals are seen to be large (2 cm long by 0.2 to 1 cm wide) displaying characteristic jagged boundaries and complex reentrants. Abundant fluid inclusions, oriented parallel to the c -axis, linear to bulbous-shaped, up to 100 μ m long, are seen throughout the fabric. Some porosity is apparent too but randomly distributed and of a larger size than the bulbous inclusions or greater than 50 μ m.

75350: A 12 cm long stalagmite (in situ) from Coffee River Cave, Jamaica (Gascoyne, 1979). The deposit is almost pure white in appearance when cut axially. Three very notable growth horizons contain buff-coloured detrital grains of fine sand size and are probably hiatuses. Intervening calcite is clear-translucent to slightly milky except in the second from top layer (0.5 to 1 cm wide) where it is milky-white and opaque. The outermost layer is composed of a 1-2 mm, light brown coloured, translucent rind. A sample was taken from the second layer on the growth axis. The thin sections (Plate 4.6) reveal a length-slow mosaic of the type described by Folk and Assereto (1976). Individual growth layers grade upward in crystal size from 10 μ m up to 0.3 x 0.3 cm sized crystal domains. The growth layers contain linear inclusions.

77151B: The central part of a large flowstone block from Victoria Cave, England (Gascoyne, 1978). Within the flowstone massif is a stalagmite about 8 cm high and conical, tapering to a 1 cm diameter point composed of visibly layered milky-

white calcite. Samples were taken from the top layer of this stalagmite 5 cm to the right of the axis.

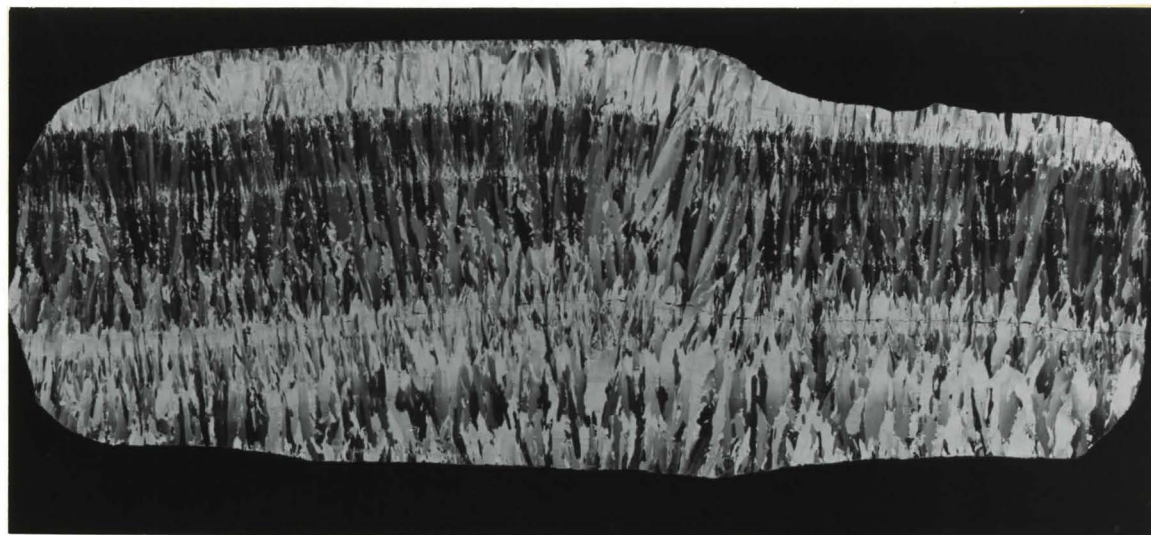
The thin section (Plate 4.9) is taken from the position described above. Highly elongate columnar crystals exhibiting brush extinction extend fairly regularly across ~ 0.5 cm growth bands. The sample is quite fissile at these terminations as shown by a crack in the lower part of the photograph. (It is, in fact, possible to cleave portions of this sample along these prominent growth horizons.) Ends of columnar crystals, where they coincide with growth bands, tend to form rhombohedral terminations. Pseudo-pleochroism associated with these terminations **may be** due to microinclusions.

South Georgia 1: From South Georgia, Grid Reference: 53S, 36W, this pure milky-white 15 cm long stalactite was growing in a cleft cave, formed in greywacke. The deposit tapered from a base 2 cm in diameter to a tip 0.5 cm in diameter, the latter reminiscent of a soda-straw. The upper part of the stalactite was partially covered by popcorn of the same texture as itself. A sample was removed from the tip for analysis.

797MP1: Actively growing stalagmite, 12 cm long by 7 cm wide, from McFails' Cave, N.Y. It is quite cylindrical and flat-topped making it ideal for study. As depicted in Figure 4.2, the axial portion is essentially composed of clear, slightly brown calcite except where it is transected by quite detritally-rich narrow growth bands or wide (0.5 cm) zones of milky-

Plate 4.9 View of Flowstone 77151B under crossed Nicols (see text). Highly elongate columnar crystals exhibiting brush extinction extend regularly across 0.5 cm growth bands. Crystals tend to form rhombohedral terminations. Pseudo-pleocroism associated with the terminations may be due to microinclusions.

Plate 4.10 View of stalagmite 797MP1 (near base) under crossed Nicols. Well defined growth layers give rise to nucleation of randomly oriented crystals, sometimes microcrystalline. These resolve upwards into highly elongate columnar crystals exhibiting brush extinction due to slight changes in orientation. Linear inclusions are rich in layers towards the top of the plate. Some cavities are filled with sparry calcite. Field is 2 x 4 cm.



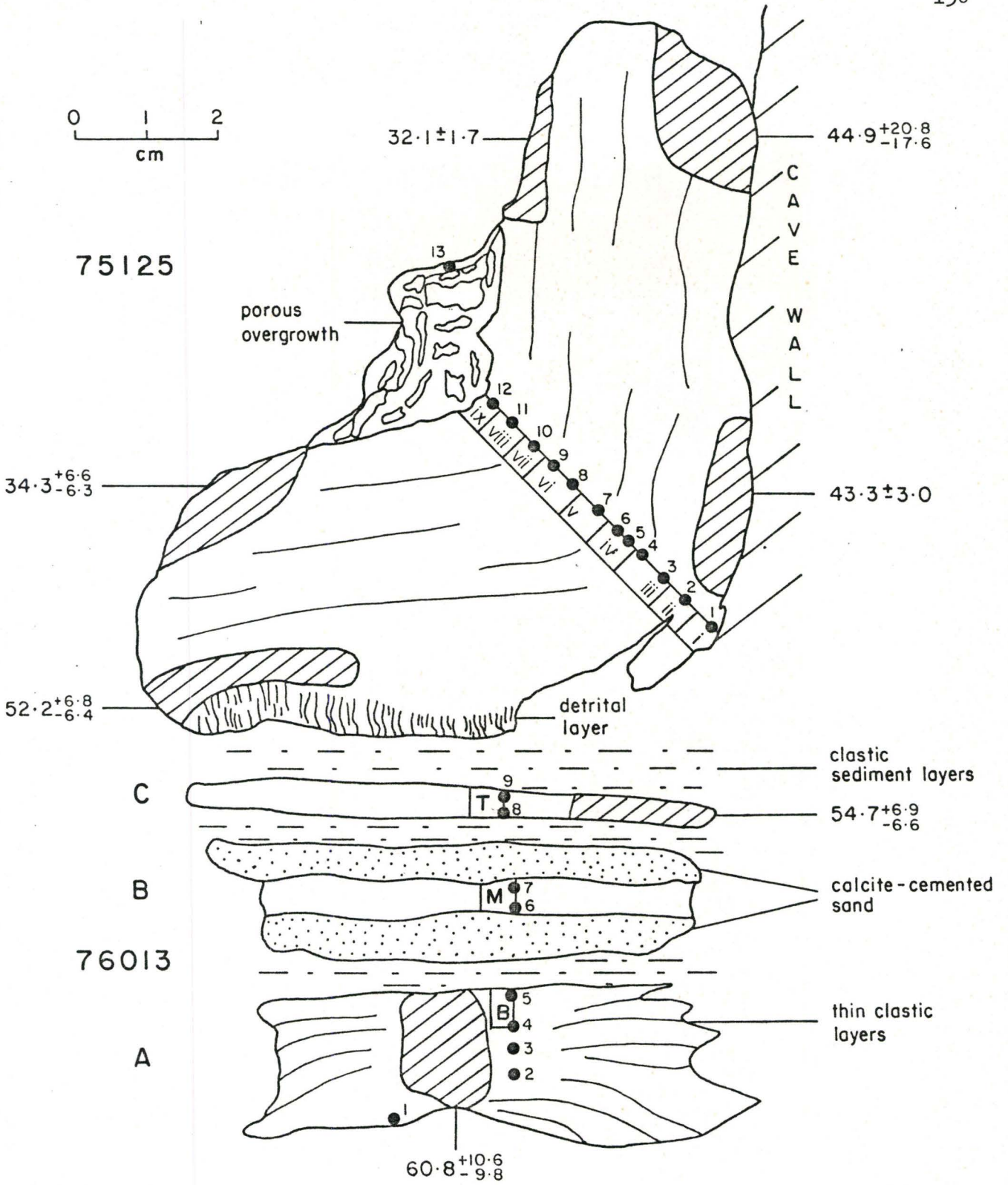
white calcite. One growth band at 3.5 cm from the top is quite dirty, 1 mm thick, and may represent an hiatus. As typical of many stalagmites the axial core is composed of relatively clear calcite while the flanks of the stalagmite are composed of more milky calcite that grades into clear calcite where growth layers turn downward (Figure 4.2).

A thin section was taken from close to the base of the deposit (Plate 4.10). Well defined growth layers give rise to nucleation of randomly oriented crystals, sometimes microcrystalline. These resolve upwards into columnar crystals highly elongate (3-4 mm x 0.2 mm), and exhibiting brush extinction due to slight changes in orientation as crystals build up on a curved surface. Some triangular to tear-drop shaped inclusions (0.03 mm) are apparent in some layers whereas linear inclusions are rich in others. Detrital grain can be seen toward the base of the section.

75125: In situ stalagmite/flowstone forming remnants of a fake floor from Cascade Cave, Vancouver Island (Figure 4.3). Massive white calcite alternating between slightly milky to transparent in a 0.5 cm periodicity is sandwiched between a porous overgrowth layer on top and a detrital layer beneath.

In thin section columnar crystals extend through growth bands themselves defined by concentrations of 10-50 μ m linear inclusions. Columnar crystals can be quite large (1 cm long by 0.5 cm wide or larger). Growth layers exhibit small depressions

Figure 4.3 A schematic showing the relationship between the samples 75125 and 76013 from Cascade Cave, Vancouver Island. Roman numerals and letters refer to samples taken for deuterium isotope analysis, otherwise integers refer to samples removed by drilling and analysed for oxygen and carbon isotope analysis.



("dips") (0.1 mm deep) that propagate up through 1-2 mm of deposit (Plate 4.11).

76013 (A, B and C): Three layers of granular calcite underlying 75125, separated from it and from each other by layers of sand to silt size detritus up to 1 cm thick. (C is the youngest layer, followed by B then A). Textures identical to 75125.

75123: In situ yellow stalagmite, 7 cm high from Cascade Cave, Vancouver Island. Somewhat like 75125, layers alternate on a 0.3 cm periodicity between milky to clear calcite. The base is marked by a compacted sandy horizon and flanks are milky.

The thin section reveals columnar crystals 2 cm long by 0.3 cm wide. Bands of fine layering (20 μ m spacing) resemble a wood-grain texture. Very fine striations cross layers at right-angles. The junctions of striations and layers are marked by dips as described in 76010. Margins of columnar crystals often define edges of these dips. (Also seen in 76010; see Plate 4.11)

76010: Although no data is presented for this deposit due to some early problems with experimental method, it has features referred to in the thin sections of samples 75125 and 75123 and general features relevant to others. 76010 is also a flowstone deposit from Cascade Cave, Vancouver Island (Plate 4.11).

Plate 4.11 (as in Plate 4.4) Enlarged view of 76010 under crossed Nicols. Large columnar crystals transcend finely resolved growth layers. Rhombohedral cleavage with some curvature is evident forming 60° and 30° angles with the layering. Dips are seen in growth bands and these often correspond to crystal margins. Dips occasionally penetrate downwards via lineations to cavities containing detrital grains. Growth bands are made up of dense linear inclusions oriented parallel to columnar crystals.

Field is 2 x 4 cm.

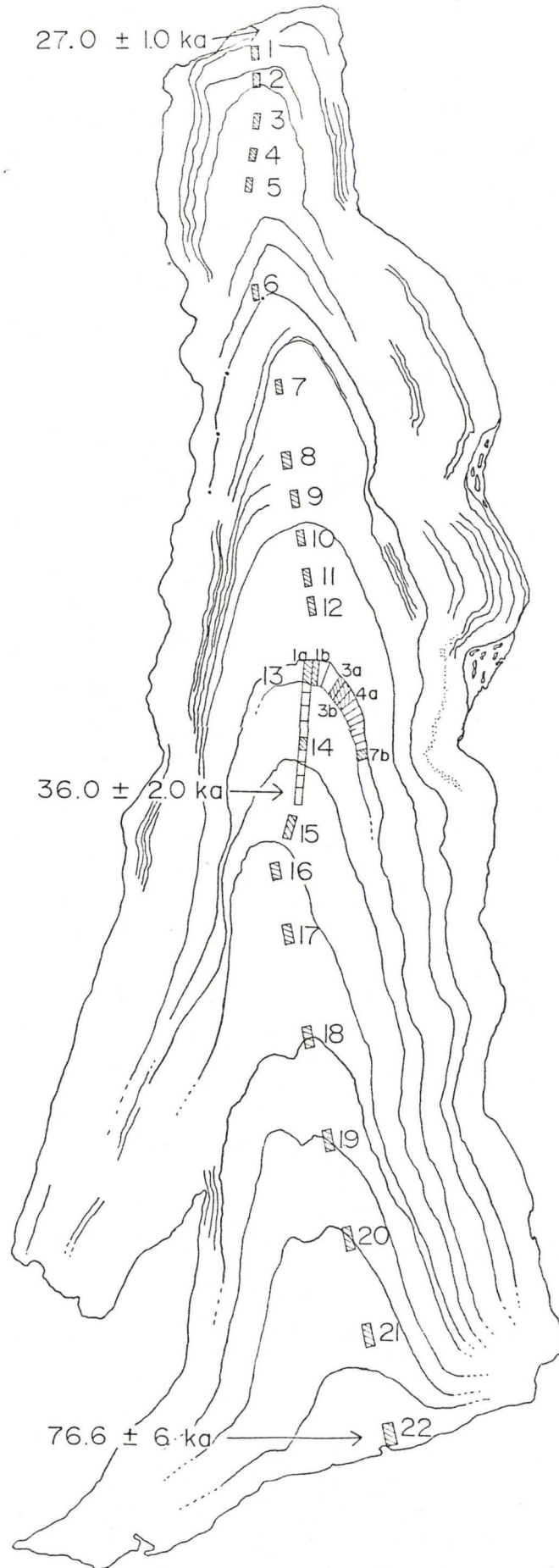


Slight curvature of cleavage is evident as described by Kendall and Broughton (1978) and forms rhombohedral angles (roughly 30° and 60°) with growth layers. Dips are seen in growth bands and these correspond to crystal edges. Also noted are occasional detrital grains as thin cavities joined by lineations to these dips (top 1/3 of photograph in the middle). Some dips in growth bands appear to be relict rhombohedral (perhaps scalenohedral in some cases) tops to columnar crystals as they were building upwards. Most, however, appear to be rounded in appearance. Dense linear inclusions mark these regions and delineate growth horizons.

74017: Strongly tapered, irregular stalagmite, 54 cm long from Coldwater Cave, Iowa (Figure 4.4 and Harmon et al., 1979). It is massively crystalline and non-porous, well laminated with thin alternating translucent-brown to opaque whitish-brown layers. Major growth layers are 1 to 5 cm thick at base becoming less distinct towards the top. Minor growth layers are 1-3 mm thick. The deposit was in situ when collected but covered by breakdown slabs and the base was covered by 7 to 8 cm of sediment.

77162: Flowstone, 16 cm thick from Lost John's Cave, U.K. (Waltham, 1974). Massively crystalline and porous. Darker growth bands are more porous, up to 0.5 cm thick occurring at 2 cm intervals. Texture is milky-white to buff coloured with no clear calcite visible. Porosity is of the form of

Figure 4.4 Schematic of the 54 cm long stalagmite 74017 from Coldwater Cave, Iowa. Samples taken for stable isotope analysis are shown as hatched rectangles and lines indicate prominent growth layering.



negative crystals on a millimetre scale.

76501: Stalagmite, 83 cm long and 7 cm in diameter from Tumbling Creek Cave, MO (see Chapter 3.1.3 for cave location). First 22 cm of the deposit is dark brown in colour, whereas upper portions are white. The outside 3-5 mm is defined by a calcite porcellanous rind. The remaining interior is massively crystalline (domains are 1 to 2 cm in length) with almost all calcite being transparent. Large cavities are noted in the axial portion particularly in the top 6 to 8 cm.

4.2.5.3. Age Data

Tables 4.1 and 5.5 show age data for all the samples described in the previous two sections. Where appropriate, reference to the date is given or, in the case where (modern) dates have not been determined radiometrically, justification for considering them to be modern is given.

4.3 Water Content of Speleothems

4.3.1 Review of Previous Work

The first attempt to extract H_2O from speleothems was undertaken by Thompson (1973). Unfortunately, water content for only some of the samples, which were further analysed for isotopic composition, are described. He does indicate, however, that 5g was considered a minimum weight for D/H analysis and explores the way in which water is lost from 10 cube-shaped pieces of calcite of side 1.2 cm from Grapevine Cave, Va.

Table 4.1 Age Data of Samples Studied

SAMPLE NAME WITH PORTION OF DATED ALIQUOT	AGE (Ka) B.P.	ERROR IN AGE +/-	REFERENCE/REMARKS
Bone-Norman (SS1)	M*	-	-actively growing soda-straw
Friar's Hole (SS1)	M	-	-actively growing soda-straw
Mirror Lake 1	M	none	-growing on gravel laid 1946
807CW3	M?	-	-actively growing nubbin grow- ing on post-Wisconsin sediment
Wind Cave 1	M?	-	-similar to actively growing soda-straws growing close to it
807CH1	M?	-	-both (amalgamated) stalagmite actively growing
Llano Chiquito 1	M	none	-actively growing on rotting wood
Bugaboo 1	M	-	-found close to retreated ice margin
73047	MC	10	-Harmon (1975)
75350 Top	8.7	15.0/15.1	-Gascoyne (1979)
Base	38.9	6.8/6.7	-
77151B Top	264.5	29.1/23.1	-Gascoyne (1979)
Base	250.4	28.9/23.0	-
South Georgia 1	M?	-	-actively growing stalactite
797MP1 Top	M	-	-actively growing stalagmite
Base	4.6	1.4	-Gascoyne (1981)
75125 Top (0.5 cm)	34.3	6.6/6.3	-Gascoyne (1980)
Top (1.5 cm)	32.1	1.7	-
upper middle	44.9	20.8/17.6	-
Base (1.5 cm)	43.3	3.0	-
Base	52.7	6.8/6.4	-
75013 C	48.7	8.5/8.2	-Gascoyne (1980)
A	60.8	10.6/9.8	-
75123 Top	50.5	6.9/6.5	-Gascoyne (1980)
Base	56.1	3.8/3.7	-
76010	55.5	8.2/7.7	-Gascoyne (1979)
74017 Top	27.0	1.0	-Gascoyne (1981)
Middle	36.0	2.0	-
Base	76.6	6.0	-
77162 Base	101.2	3.1/3.0	-Gascoyne (1981)
76501 (6-9)	74.3	16.9	-Gascoyne (1981)

*Modern

These 4.7g aliquots were taken from successive layers in a stalagmite and placed in a vacuum oven and taken to various temperatures up to 110°C. After each temperature step, the cubes were reweighed and the experiment was terminated at 110°C after 116 hours when the water was assumed to have been totally removed. An important question arises here; was the included water completely removed during the extended heating period? It is unfortunate that the samples were taken from vertical locations along the axis rather than attempting replicate runs with cuts adjacent to one another along the same set of growth layers. Nevertheless, average cumulative weight losses are 0.251 ± 0.056 or 0.053 ± 0.012 wt%. This figure falls within the range published for crushing extraction experiments of 0.01 to 0.10 wt% (Schwarcz et al., 1976) but falls well below that for decrepitation as will be seen later. Thompson, in light of these investigations recommends dropping or severely reducing the initial heating step, which is intended to remove absorbed water from the sample, prior to crushing and subsequent analysis. Above 60°C, serious loss of water results ($25.4 \pm 9.0\%$ of the water ultimately collected at 110°C). Finally he concludes that anomalous results (described later) are probably due to extraction procedures.

Beyond the heating experiment of Thompson (1973), little has been written with respect to the systematics of water extraction from speleothems although much apparently has been

done. Harmon (1975) alludes to 31 fluid inclusion analyses but does not give water yields or aliquot size for individual samples. However, based on the samples of Thompson (1973) and Harmon (1975) the range of water contents is stated by Schwarcz et al. (1976) to be between 0.01 to 0.10 wt%, as already mentioned. In contrast to Thompson (1973), their sample size is given to be from 1 to 4g. Presumably, Thompson's conclusion as to the minimum sample size of about 5g was subsequently found to be excessive. With some additional data on deposits from Iowa and Missouri, Harmon et al. (1979) publish yields from crushed calcite of between 0.003 and 0.099%. This range of water contents is consistent with their use of sample weights of between 1 and 20g to obtain enough water for analysis. Water was assumed to come from fluid inclusions and the apparent water loss encountered by the heating experiments lends weight to this assumption. The question of impurities, detrital or organic, was touched on briefly by Schwarcz et al. (1976) because of its possible contribution to the water content of speleothems but it was not investigated beyond cursory observation of the hand specimens and thin sections.

Harmon (1979) noted an order of magnitude increase in water production from speleothems when heated to 700°C over an initial heating at 200°C. He further noticed a depletion in deuterium content of the water in the higher temperature fractions over the lower temperature fractions by as much as 20%..

4.3.2. A Comparison of Water Content of Speleothems by Crushing and Decrepitation

The results of these two modes of water extraction are given in Table 4.2. The range of water contents obtained by crushing is between 0.009 and 0.412 wt%. With the exception of 73107 from Bermuda, the range is within that published by Schwarcz et al. (1976). Decrepitation (undertaken at calcining temperatures of $\sim 850^{\circ}\text{C}$; see Chapter 2) increases yields to between 0.237 and 1.010 wt%, 3 to 7 times those obtained by crushing. However, there are notable exceptions, such as individual samples of 807CH1 and 77151B (δD analysis only) where crushing yields were very low. Since 77151B gave larger yields during independent preparation for $\delta^{18}\text{O}$ analyses, it may be that in the cases where yields were very low, crushing of a given set of inclusions and their subsequent extraction were not being effectively carried out. An important question arises here: are the waters obtained from each method of extraction of the same origin or does decrepitation release water from other sites in addition to trapped liquid water, such as coordinated water or hydroxyl groups? Alternatively, crushing releases water from only the larger inclusions and not smaller ones, depending upon the fineness to which the sample is crushed. Also, when the sectioned sample is evacuated at room temperature, the larger inclusions connected to the surface or to incipient fractures, may partially release their water (see see

Table 4.2 A Comparison of Water Yields from Speleothems Using Crushing and Decrepitating Modes of Extraction

SAMPLE	NO. of ANAL.	AVERAGE SAMPLE WT (mg)	M.Y.	YIELD WT. (%)		YIELD RATIO D/C
				CRUSHING (THIS	DECREPITATION WORK)	
77151B	1	750	-	-	0.358	-
	1	1,071	-	0.009	-	-
	3	8,022	0.053 ± 0.016	-	-	39.78
73017	2	295	-	-	1.010	-
	15	377 ± 69	-	0.412 ± 0.083	-	-
	18	1,527 ± 243	0.359 ± 0.015	-	-	2.45
797MP1	6	478 ± 93	-	-	0.361 ± 0.011	-
	2	2,200	-	0.059 ± 0.027	-	-
	2	5,720	0.060 ± 0.015	-	-	6.12
807CH1	2	790	-	-	0.237	-
	2	2,980	-	0.018 ± 0.005	-	13.17
Llano	1	439	-	-	0.336 ± 0.047	-
Chiquito 1	1	637	-	0.047	-	7.12
Mirror	3	402	-	-	0.555 ± 0.304	-
Lake 1	2	848	-	0.026 ± 0.50	-	4.40

D = Decrepitation; C = Crushing

M.Y. = Water extracted for $\delta^{18}O_i$ analyses (after M. Yamamoto, 1980)

tion 4.2), leaving smaller, isolated inclusions intact. Crushing would then liberate water from some of the remaining smaller inclusions where they are intercepted by resultant cleavage planes but others might be untouched and a considerable reservoir of water could still remain. Data is presented later in section 4.3.6. in which calcite, ground and sieved to 80 mesh, is shown to contain quantities of water in excess of 50% of that of the original sample. Whatever the mode of storage of water in the sample, complete calcining should release all the available water. Water release as a function of temperature is described next.

4.3.3. Water Yields from Partial Extraction by Decrepitation

Partial extractions of replicate aliquots of 77151B were undertaken to try to ascertain the kinetics of water release from calcite and determine whether more retentive sites are compositionally different. The object of the experiment was to remove water from populations of fluid inclusions of a given size range. At successively higher temperatures, it was expected that progressively smaller fluid inclusions would be released since the stress acting on the enclosing calcite should be proportional to the pressure and volume of the water vapour in the inclusions. The experiment was performed so that yields were the result of cumulative fractions. After a sample had been taken to a given temperature and sufficient time had passed to permit liberation of the water, it was discarded. Samples

were heated for 1 hour, although in practice, the water release seems to occur very quickly, in a few minutes. However, after the initial pulse, it is possible to collect small quantities for up to 24 hours afterwards. The results of the experiment are shown in Table 4.3 and Figure 4.5 where yield is plotted against temperature. The release of water is somewhat linear up to 650°C. Above this, calcining takes place and the yield is increased by a factor of 2.4. The approximate linearity of the low temperature end of the curve perhaps suggests the rupturing of increasingly smaller inclusions yielding the same volume of water from each successive population. The sudden increase in water content associated with the high temperature datum suggests that a good deal of the total water is associated with very small inclusions or a distinct, more tightly bound water site. The yield is not seen to tail off at lower temperatures but this decline probably does not occur until below 50°C as already described from the work of Thompson (1973).

One further experiment was conducted to study water release from speleothems. The apparatus employed was a gravimetric and differential thermal analysis (DTA) instrument. Unfortunately, weight loss at lower temperatures is masked by sample buoyancy as surrounding air heats up. The facility to do the experiment in vacuum was not **available** at the time. At higher temperatures, calcining takes place resulting in a 40% loss in sample weight, swamping any signal associated with loss

Figure 4.5 A graph of δD_i versus water yield ($\delta D_i, Y$) and temperature ($\delta D_i, T$) and temperature versus water yield (T, Y) for cumulative fractions of water extracted from 77151B by decrepitation.

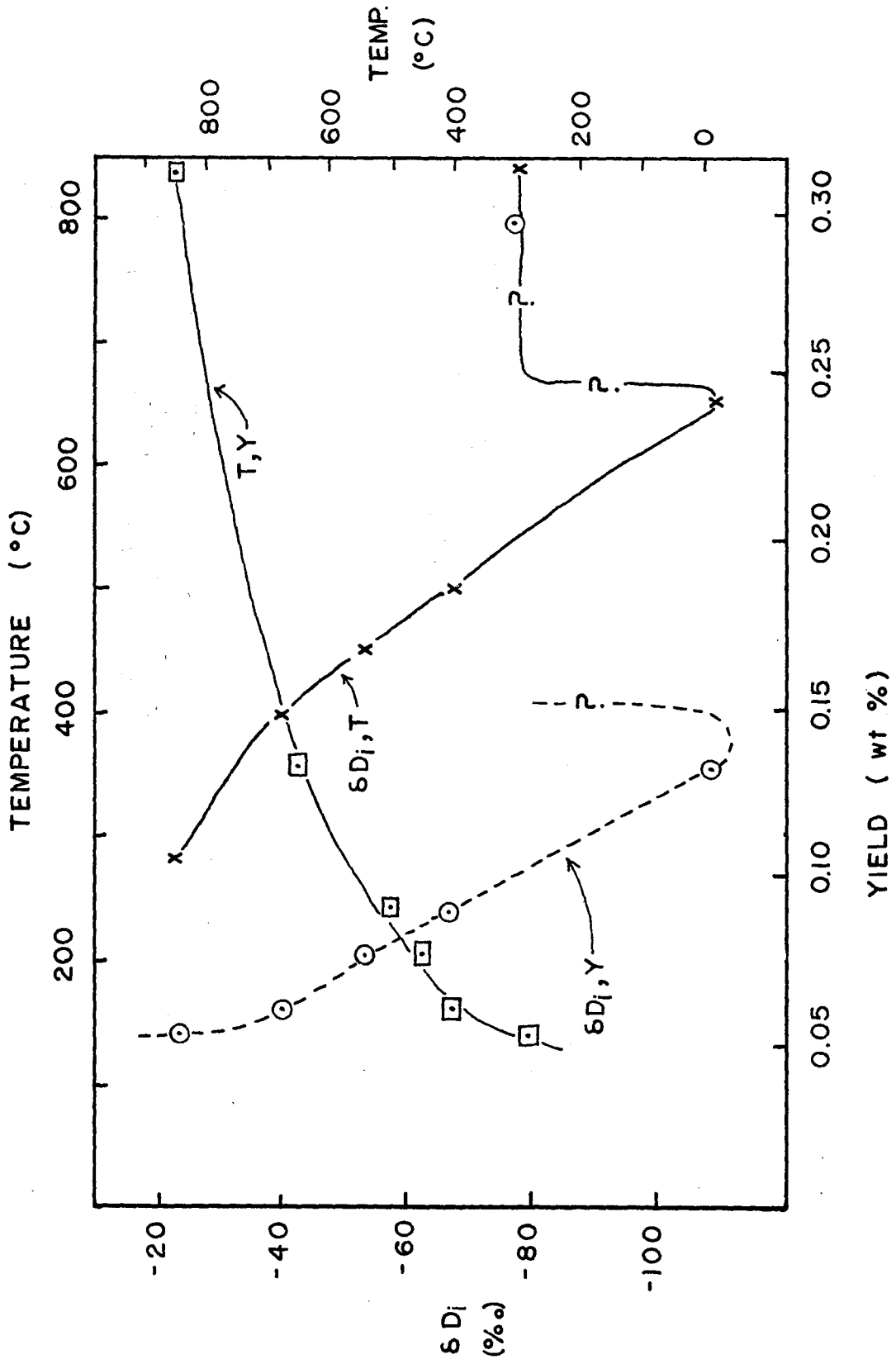


Table 4.3 Isotope Data for Partial Extractions of 77151B by Decrepitation

SAMPLE	SAMPLE WT. (mg)	Y (wt.%)	δD_i (‰)	EXTRACTION TEMP (°C)	$\delta D'_i$ (‰)	Y' (wt.%)
77151B(ix)	987	0.054	- 23.2	280	- 23.2	0.054
(x)	1070	0.061	- 40.2	400	-171.3	0.007
(xi)	1327	0.076	- 52.6	450	-103.0	0.015
(xii)	1170	0.085	- 67.0	500	-188.6	0.009
(xiii)	1092	0.131	-109.5	650	-188.0	0.046
#1	750	0.314	- 76.9	850	- 53.6	0.183

of water. The DTA signal shows only the phase change due to CaCO_3 being converted to CaO and CO_2 .

4.3.4. Variations of Water Yield Within Speleothems in relation to Textural Milkiness

The degree to which calcite takes on a milky-white appearance in hand specimens is considered here because of its possible relation to the presence of fluid inclusions. Schwarcz et al. (1976) report that where fluid inclusions are extremely abundant, the speleothem appears milky in aspect. This is especially noticeable in coarsely crystalline varieties of speleothem. Those regions containing no observable fluid inclusions under the light microscope, were transparent. As described previously, milky white calcite tends to be restricted to the periphery of stalagmites whilst interiors are composed of clear calcite domains.

The first question that arises is as to whether or not water is restricted solely to the observable fluid inclusions associated with milky regions of the speleothem. A second question arises if water is found in all parts of the deposit regardless of appearance. If it is, the question is how water is stored within the calcite; i.e. is milkiness a function of fluid inclusion density of those fluid inclusions over a given size (say, those that are observable under the microscope) or is water in the clearer regions stored in sites other than fluid inclusions?

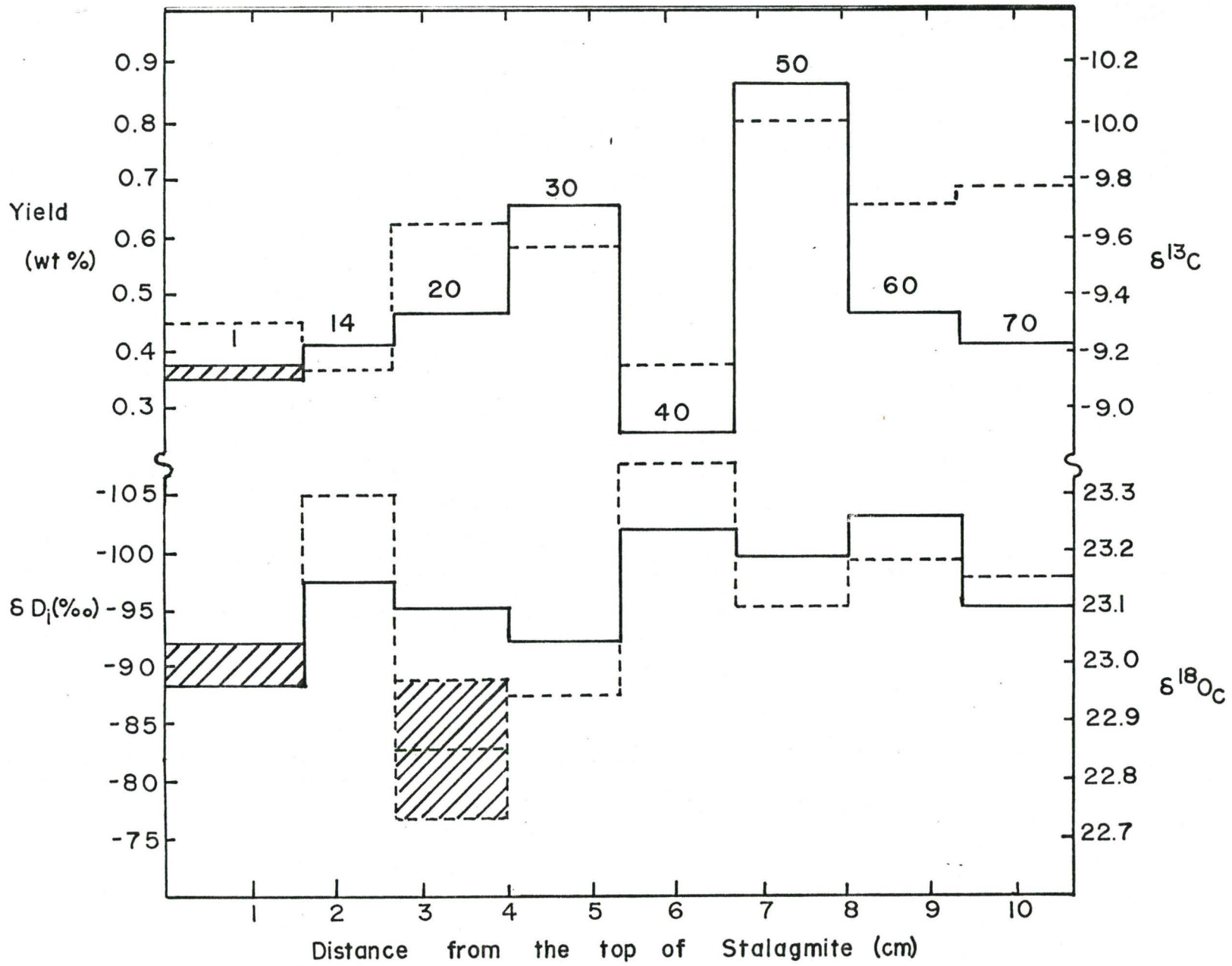
The following observations address these questions.

Stalagmite 797MP1 is useful for investigation of the above questions because it exemplifies well the association of peripheral milky-white calcite and axially clear calcite, although some milky areas extend completely across growth bands. Milky-white domains and a water yield profile can be seen in Figure 4.2, 4.6 and Appendix IV (bii). Samples taken from the growth layer were cut such that the sample volume was the same in each aliquot with the shape varying because growth bands thin towards the outside. Water yields from samples along the growth layer are very constant (0.36 ± 0.03 wt%), with the exception of #8, yet samples taken from clear calcite #-2 and #-5 do not appear to contain less quantities of water. These observations stand in contrast to the axial data (Figure 4.6). Large yields here correspond with regions that are milky-white; a yield of one of these aliquots, #50, being higher by almost a factor of two than the average value. The regions of milky-whiteness at the axis, however, are not as continuous as those on the flanks of the deposit and are often interstratified with clear calcite. As described earlier, few or no fluid inclusions are observed in these clear regions.

These observations suggest that regions of milky whiteness are not necessarily areas which contain greater quantities of water but are perhaps indicative of the presence of visible fluid inclusions which give rise to this textural property.

Figure 4.6 Plot showing water yield, δD_i , $\delta^{13}C$ and $\delta^{18}O_c$ along the axis of stalagmite 797MP1 from McFail's Cave, N.Y. Solid curves refer to the left hand and dashed line to the right hand axes.

Shading refers to the precision of isotopic determination at 1 σ .



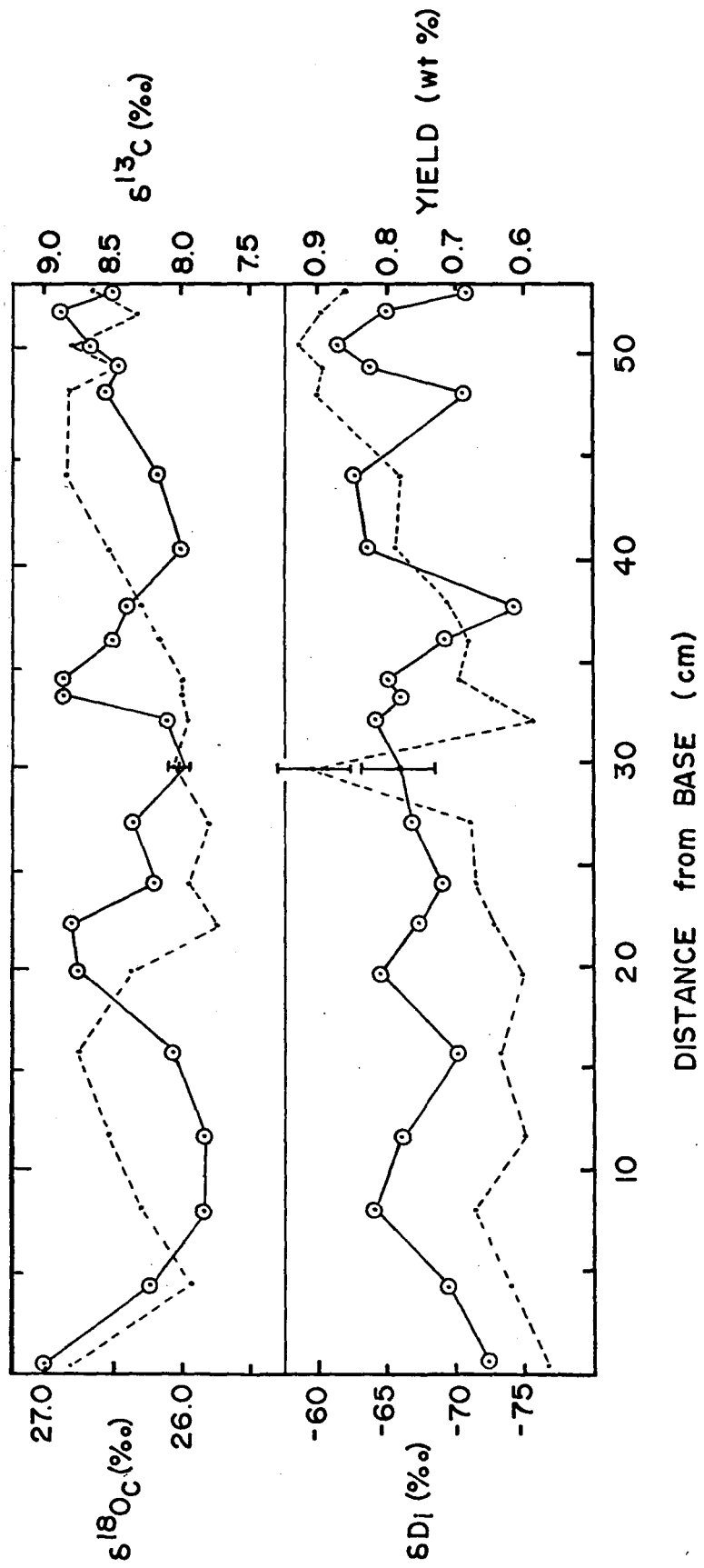
If microinclusions exist within the areas of clear calcite then their presence was not revealed in this study. Pseudopleochroism thought to be due to microinclusions, observed by Kendall and Broughton (1978), was not encountered. A further attempt to observe microinclusions involved the immersion of the sample sieved to 80 mesh in oil of the appropriate refractive index ($n = 1.662$) such that microinclusions would be observable as relief forms under the microscope. However, none were observed yet the sample powder retained in excess of 58% of its original water (see section 4.3.6.).

Speleothems 75123 and 75125 (from Cascade Cave, Vancouver Island) are milky white and quite similar in appearance. 75125 is nevertheless slightly more transparent than 75123 and does indeed contain less water by a factor of 2.3. 75125 and 75132 contain on average 0.4000 ± 0.075 and 0.178 ± 0.014 wt% of water respectively.

74017 (from Coldwater Cave, Iowa) is translucent but its colours are brown to red-brown rather than milky-white. Some of the axial portions tend towards a clear calcite; in particular, samples 8 to 12 are of this type but the yield profile (Figure 4.7) gives no indication of lower water content when these samples are encountered. Rather, the yield seems to decrease steadily downwards from 0.86 to 0.59 wt%.

In summary, there appears to be little correlation between milkiness and water content, even though microscopical-

Figure 4.7 Plot showing $\delta^{18}\text{O}_c$, δD_i , $\delta^{13}\text{C}$ and water yields for stalagmite 74017 from Coldwater Cave, Iowa. Solid curves refer to the left hand and dashed curves to the right hand axes.



ly milkiness is associated with the presence of abundant fluid inclusions. The conclusion therefore, is that not much of the total water bound in speleothems is in the form of microscopically resolvable fluid inclusions.

4.3.5. Variations in Water Content of Speleothems and Relation to Growth Rates

A histogram of water contents shows a tendency for the majority of samples to group around the 0.3 to 0.4 wt% interval (Figure 4.8). The single sample plotted at the 1.4 wt% (cross-hatched) interval is the sub-glacially precipitated calcite referred to earlier in the sample descriptions. However, the mechanism of deposition is quite different from that of cave deposits (Hanshaw and Hallet, 1978).

Water content displays a weak correlation with growth rate of stalagmites (Table 4.4 and Figure 4.9). Water content appears to increase with growth rate extrapolating to zero at zero growth rates. Faster growth may be associated with thicker water films allowing individual crystallite growth to continue unobstructed to larger proportions. The effect of this would be to generate larger negative crystals which in turn could carry increased quantities of trapped water. An alternative and more logical explanation would be that an increase in degree of supersaturation in the water leads to a greater seeding of crystallites and a concomitant rise in the number of intercrystallite spaces. The outcome would be faster growth

Figure 4.8 Histogram of water contents for the samples studied.
The double cross-hatching refers to the sub-glacially precipitated sample (Bugaboo #1).

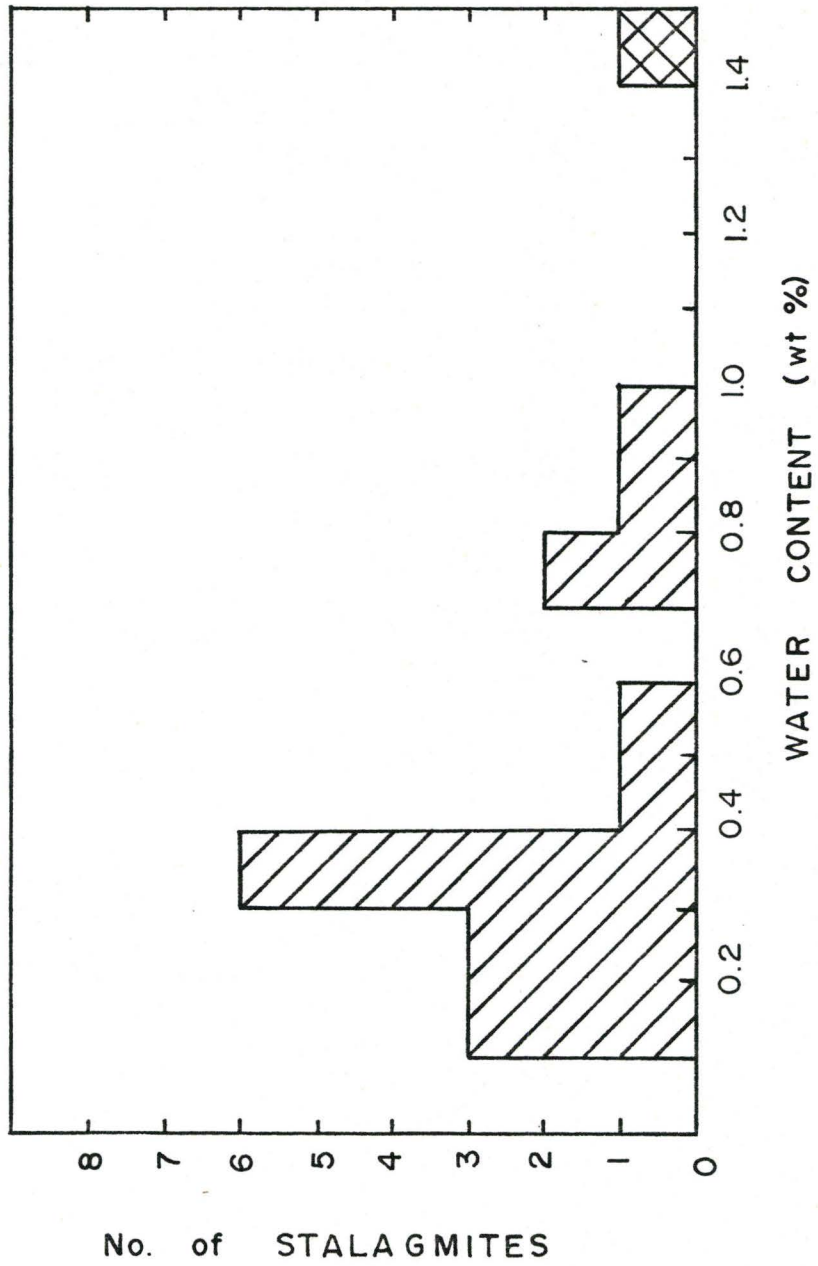


Figure 4.9 Plot of water content versus growth rate of stalagmites for which δD_i analyses were made.

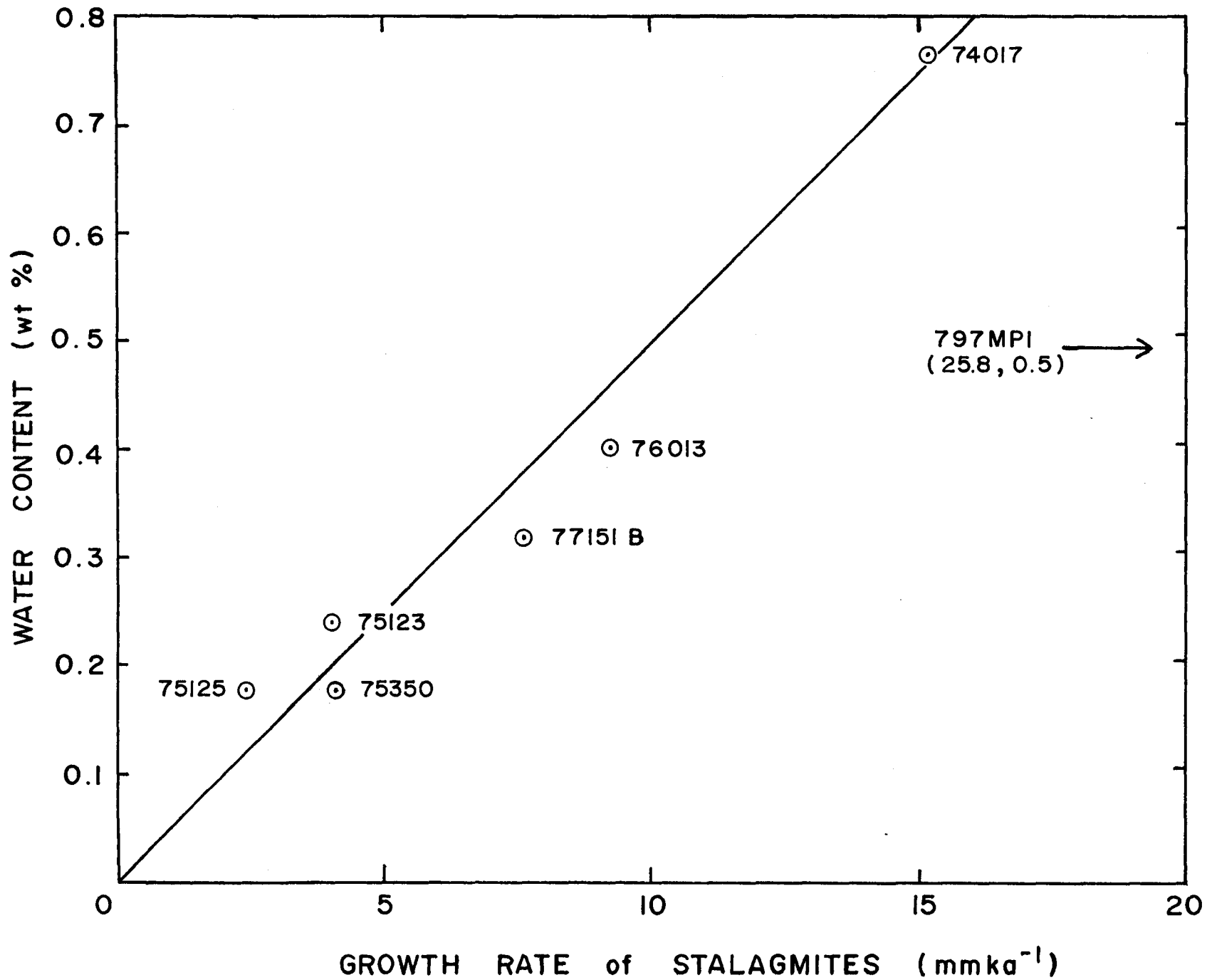


Table 4.4 Growth Rates and Water Contents for Various Samples

SAMPLE	WATER YIELD (wt.%)	TIME DIFFERENCE BE- TWEEN BASE & TOP (Ka)	LENGTH OF DEPOSIT (mm)	GROWTH RATE (mm/Ka)
75125	0.178	25.0	60	2.4
75123	0.400	6.0	55	9.2
797MP1	0.859	4.6	120	15.7
76013	0.243	6.0	30	5.0
77151B	0.314	14.1	107	7.6
74017	0.830	42.0	540	15.2
75350	0.178	30.2	120	4.0

due to greater calcite precipitation and an increased storage of water within the greater number of pores. This idea would be in accord with the weak or apparent lack of correlation between milkiness and water content in that increased growth rate does not necessarily lead to the production of microscopically resolvable fluid inclusions. Since the larger inclusions tend to be formed on the flanks of stalagmites, their development may be a function of increased or laminar water flow away from the drip source at the stalagmite's axis.

4.3.6. Characterization and Quantification of O and H in Speleothems by IR and Neutron Diffraction Spectroscopy

So far, this chapter has concentrated on the water obtained from speleothems with the general assumption that the water liberated from them resides as liquid water within the deposit. The possibility that oxygen and hydrogen could originate from lattice or coordinated water, or hydroxyl components, in addition to fluid inclusions, was investigated using neutron diffraction and infrared spectroscopy. Clearly, if water is bound up in the calcite structure it will have important bearing on the observations previously described. An attempt was made to correlate the water absorption peak, observed in the IR spectra, with the water content of various calcite powders. Whilst such a correlation does not prove that water is in lattice sites but rather that liberated water from extraction experiments can be identified from the spectra, a lack of correl-

ation would indicate, that sites other than liquid water are not being revealed by IR.

4.3.6.1. Neutron Diffraction Spectroscopy

Neutrons are strongly diffracted from ordered hydrogen, so it was felt that small quantities of bonded hydrogen would be revealed in this way. Three samples were chosen for study: 73107 (0.893 wt% water), 797MP1#2L (0.361 wt% water) and GCS (0.080 wt% water). These samples were ground to less than 64 mesh. The resultant spectra were generated from a triple axis system situated in the McMaster reactor building by Mr. J. Cooper.

In no cases could any of the peaks generated be ascribed to ordered hydrogen although a slight shift in the baseline was probably due to a background of water. All spectra were gathered quite quickly, but all appeared essentially identical. The above interpretations were made by Professor M.F. Collins of the physics department and the spectra are retained by him.

4.3.6.2. Infrared Spectroscopy

Infrared spectra were run on several samples of differing water content. Raman spectroscopy was attempted on 797MP1 #2 (64 mesh, 0.211wt% H₂O) but no peaks due to water were observed. In fact, only the ν_1 and ν_4 carbonate vibration modes at 1087 and 714cm⁻¹, and not the ν_3 at 1432 cm⁻¹, were observed in addition to librational modes below 600cm⁻¹. The rationale

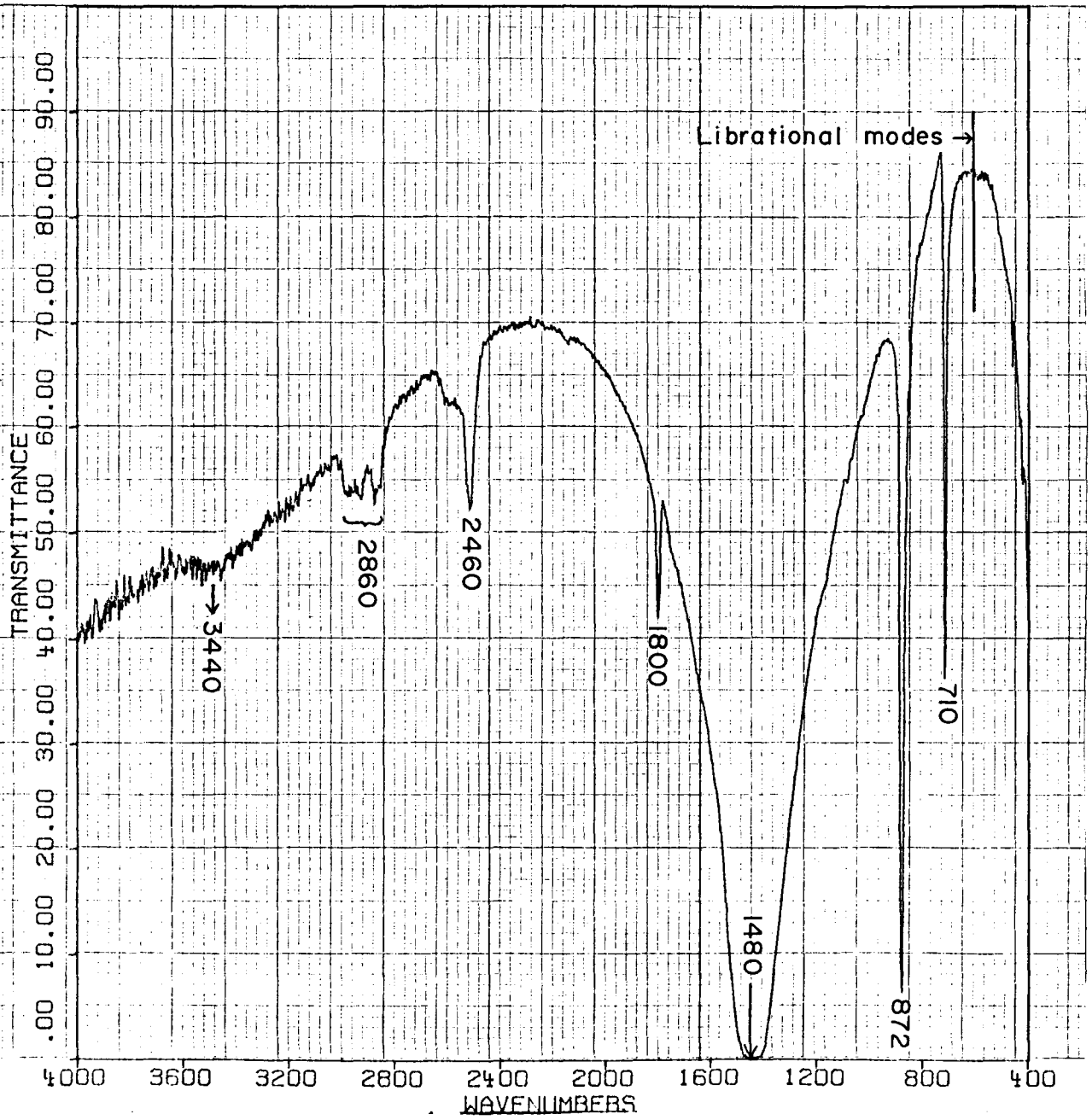
behind using Raman stems from the possibility of its use in reflected light. In this way it was hoped to compare finely ground powders to cut slices of the sample so that the difference between trapped and bound water might be observed. As it was, the cut slice gave a poor spectrum in which smaller peaks were swamped by intrinsic noise.

Conventional and Fourier Transform IR (designated IR and FTIR respectively) utilize transmitted radiation. This necessitated using around 1% sample to 99% matrix (KBr was used in this case because the water backgrounds were found to be low) finely ground and pressed into a clear pill at about 5 tons/sq. ins.. A significant portion of the spectrum between 4000 and 1000cm^{-1} was also observed when a cleavage slice of iceland spar about 0.5 mm was placed in the beam but unfortunately, speleothem calcite is too cloudy and results in nearly complete absorption of the IR beam and was thus subsequently not used.

In using the KBr technique considerable care was taken to remove absorbed water. As recommended by J. Delderfield (1978), the KBr and sample were dried overnight at 110°C before manufacture of the pill. The resulting pill was then dried again under the same conditions and placed in an atmosphere of dry nitrogen during the experiment.

Although the spectrum for calcite shown in Figure 4.10 is that generated from FTIR, very little difference is observed using IR; therefore the latter, being cheaper, was used

Figure 4.10 FTIR spectrum for calcite. Absorption peaks (numbered) are described in Table 4.5 and text.



subsequently. The spectrum is typical of calcite (White and Scheetz, 1977) with the exception of the broad peak at 3445cm^{-1} . The calcite peaks are described in Table 4.5. The peak at 3445cm^{-1} is thought to be unstructured water since pure water absorbs at this wave number (Nakamoto, 1963). Unfortunately, the bending mode at 1630cm^{-1} which should be present, is completely masked by the broad CO_3 asymmetric stretch. Should the water be coordinated, then rocking, wagging and metal-oxygen stretching vibrations should appear at 900, 768 and 673cm^{-1} . These are not apparent or they are masked by the ν_2 and ν_4 CO_3 vibrational modes. Coordinated water should also show a downward shift from the pure water peak to as low as 3000cm^{-1} (Jones, 1953). This is seen, for example, in water of hydration of gypsum. The presence of hydroxyl groups should also be marked by a sharp absorption peak above 3600cm^{-1} . OH peaks are in similar positions for $\text{LiOH}\cdot\text{H}_2\text{O}$ (Jones, 1953) and clays (Roy and Roy, 1956) (see for example, figure 4.11).

Since evidence was shown for the presence of hydrogen other than the 3445cm^{-1} peak of liquid H_2O , it was considered important to try and correlate this broad absorption peak for water with the water content of the samples. Various samples of different water contents were run in the quantitative absorption mode between 4000 and 2000cm^{-1} (Figure 4.12). A working curve (after Schwarcz and Speelman, 1965) was generated from three different weights of 797MP1 (Figure 4.13 and

Table 4.5 Vibrational Modes for Calcite

WAVE NUMBER	VIBRATION	VIBRATIONAL MODE	REFERENCE
600		Librational	White and Scheetz (1977)
710	ν_4	Planar bending of $\text{CO}_3^{=}$	Adler and Kerr (1963)
872	ν_2	Out of plane bending of $\text{CO}_3^{=}$	Adler and Kerr (1963)
1480	ν_3	Main $\text{CO}_3^{=}$ assymmetric stretch	Adler and Kerr (1963)
1800	Other complex $\text{CO}_3^{=}$ vibrational mode		White (1979)
2460			
2860			

Figure 4.11 Partial IR spectrum of slightly calcined calcite which has been allowed to absorb water. The sharp OH^- absorption is superimposed on one side of the broad absorption peak for water.

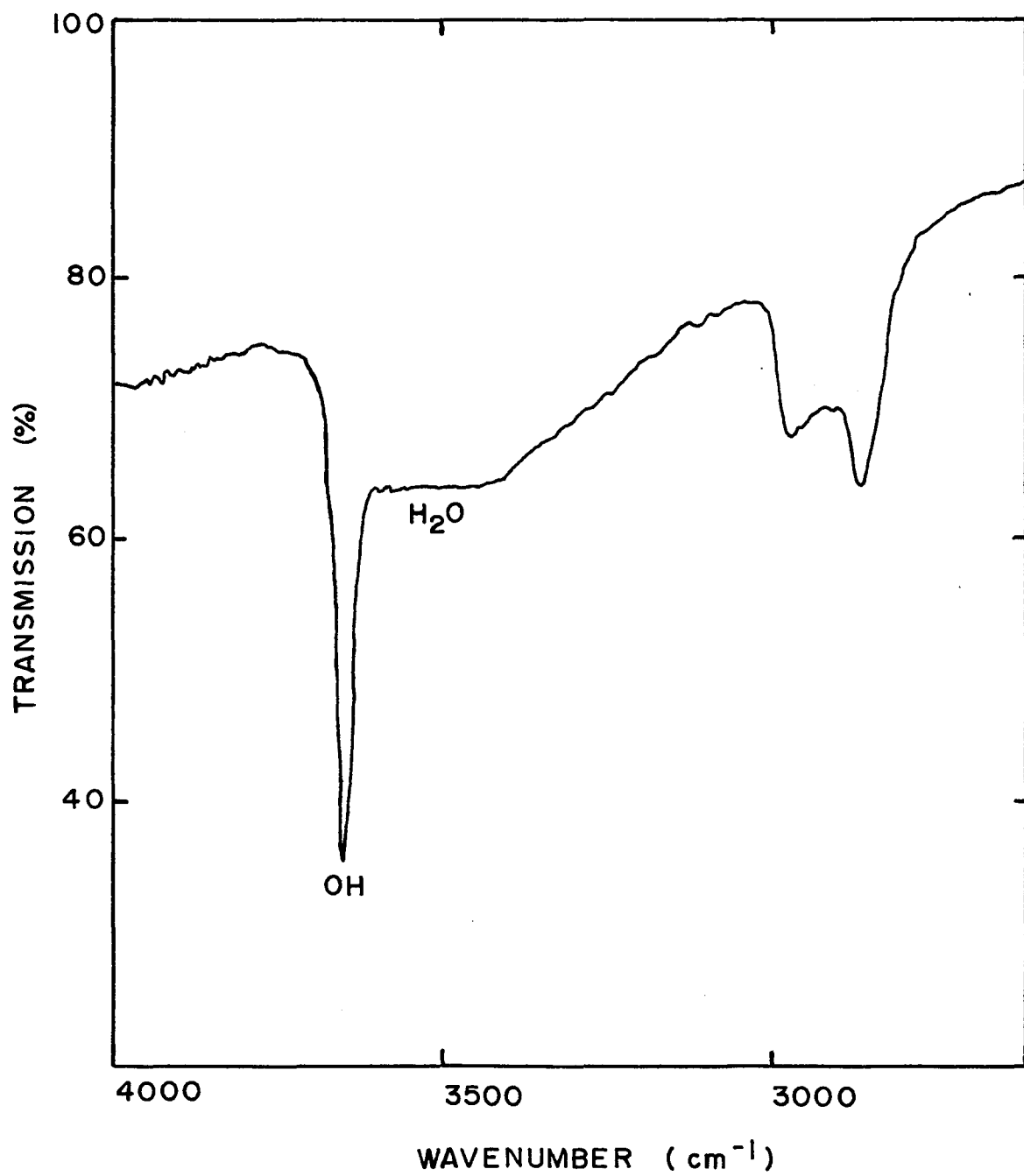


Figure 4.12 IR absorption spectra for various speleothem samples and varying sample quantities. KBr blank spectrum is also included.

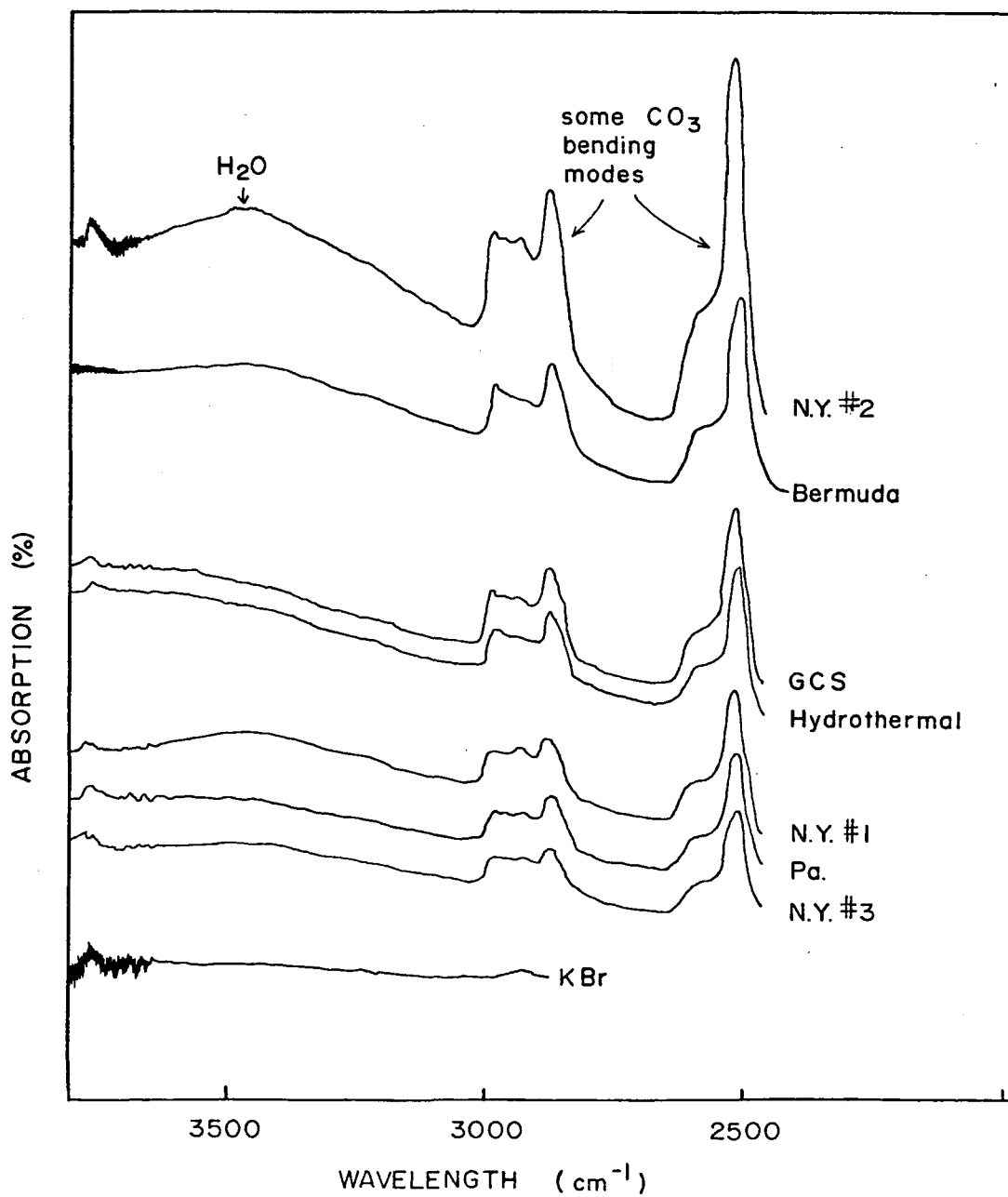


Figure 4.13 Absorption peak heights for water (centred at 3445 cm^{-1}) per sample weight versus water content for various (powdered) calcite materials.

See Table 4.6 for data.

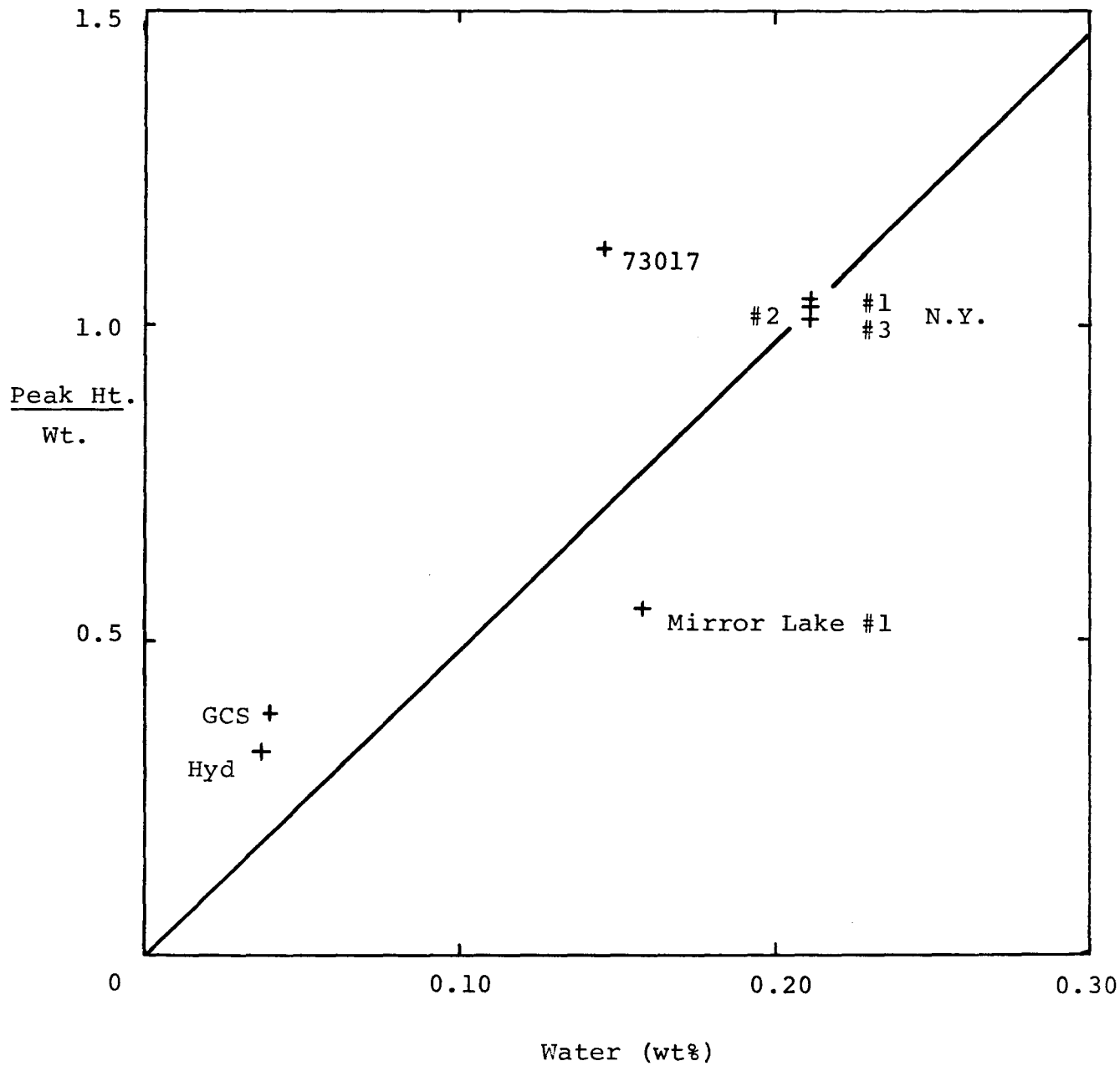


Table 4.6 Compilation of Water Yield Data from Calcite Powders by Decrepitation and Their IR Absorption Spectra (see Figure 4.13)

SAMPLE	WT. KBr (mg)	WT. SAMPLE (mg)	H O CONTENT (wt%)	ABSORPTION PEAK HEIGHT AT 3445 cm^{-1} (arbitrary units) corrected for KBr blank **	<u>Peak height</u> Sample weight
N.Y. #1*	365	3.43	0.211	3.6	1.04
#2	500	8.31	0.211	8.6	1.03
#3	236	1.98	0.211	2.0	1.01
Mirror Lake#1	280	2.90	0.158	1.3	0.45
73017	260	3.76	0.146	4.2	1.12
G.C.S.	250	3.46	0.040	1.3	0.38
Hyd.	235	3.86	0.037	1.3	0.34
KBr(Blank)	320	0	-	0.9	--

*N.Y. = 797MP1

Pa = Mirror Lake

Bermuda = 73107

G.C.S. = Grenville Calcite Standard

Hyd. = Hydrothermal calcite (iceland spar)

** zero base line drawn from 3710 to 3000 cm^{-1} (see Figure 4.12)

Table 4.6). It is important to note that the water being observed is that from a crushed residue and is therefore either bonded or contained in micro-inclusions.

As can be seen from figure 4.13 there seems to be a considerable difference in the proportionality between absorption and water content between different samples. Thus it does not appear that a single mode of entrapment as, for example, liquid water inclusions, can account for all the water observed in these calcites. However, such a conclusion must be viewed cautiously since it assumes that the water content determined on other crushed aliquots of each sample are equivalent to the water content of the sample included in the KBr disc. The constancy of water content of these powdered samples has not as yet been established and hence possible errors in wt. % H₂O cannot be ascribed. Furthermore, there is some uncertainty in the amplitude of the water absorption peak with respect to both how the baseline should be drawn and how the blank correction is to be applied.

Observations made using polarized IR on one speleothem at Caltech by G. Rossman (1981) indicate that water in the calcite is unoriented.

4.3.7 The Size and Size Distribution of Fluid Inclusions

Based on Observations of Water Yields

Petrographic microscope and SEM observations indicate a range of fluid inclusion size from around 10 μ m down to sub-micron sizes. There seems no reason why, with varying degrees of crystallite coalescence, the intercrystallite pores should not extend down to Angstrom dimensions.

Each subsection of 4.3

is examined for its contribution to ascertaining the dimensions of these pores.

Thompson (1973) suggests that a good deal of the water is released in vacuo at temperatures around 100°C from aliquots of speleothems. However, he did not proceed to higher temperatures, especially to those where calcining would occur and it seems likely that he was unaware of the presence of remaining water. Yields, in particular, are commensurate with those obtained for crushing. It appears therefore possible, that water was released only from the larger inclusions without much hint of a contribution from the smaller sites. Alternately, perhaps water is released along prominent lineations, such as those seen in Plate 4.11, from inclusions distributed locally around them.

Comparing water yields from crushed samples to decrepitated samples, from 2.5 to 13.2 times as much water is collected by the latter method (Table 4.2). 71.4% or more of the water is thus coming from these higher temperature sites, or, if structural water is assumed to be absent, the smaller inclusions. Partial release experiments by stepwise heating with temperatures higher than those used by Thompson might suggest a multi-site disposition of the water in populations of different sized inclusions. However, a simpler explanation for the yield data alone would be a gradual increase in release of water with temperature as water is mobilised along pores

rather than the progressive rupturing of sets of fluid inclusions of a given size. More data would substantiate the fine structure of the temperature versus yield correlation. What is noted nonetheless, is the marked increase in yield (2.4 times) above calcining temperature indicating a surprising reluctance of the water to move. Again if this water is not chemically bound to the calcite lattice then it is probably trapped in the smallest pores.

Unfortunately, textural studies are inconclusive. One generalization that appears from these studies is that, for a given speleothem, the water content is surprisingly constant, even crossing textural domains. Given high yield ratios (as defined in Table 4.2) and that crushing liberates water from visible inclusions seen as a cloudy fabric in hand sample, then a possible explanation is that because most of the water is coming from microinclusions, it may be difficult to discern the contribution from large inclusions. For example, variation in yield of the 797MP1 samples (Table 4.2) of ± 0.027 wt% is quite similar to the total amount of water contributed by crushing, that is, 0.059 wt%. Even given that crushing only liberates water from large inclusions, which is most unlikely, the "crush" component could easily be masked by the microinclusion component. Complementary to this last remark, is the fact that the same speleothem gave 58% of its average water content when water was extracted from it by decrepitation after it had

been ground and sieved to 80 mesh (180 μ m opening). Clearly, this is a lower limit to the water contained in microinclusions since some of that component is also lost during crushing. Nevertheless, we can inquire what size of microinclusion could be present inside a grain that is less than 180 μ m in diameter to provide this water content.

The upper limit of fluid inclusion size can be calculated approximately, assuming that the average grain is a 100 μ m-sided cube containing one fluid inclusion. The cube will weigh approximately 3×10^{-6} g. We can take the water content of this cube to be approximately 0.2 wt%. From Plate 4.5, a very crude estimate can be made of linear inclusion proportions of 10 to 100 units of length to one square unit of cross-sectional area. The length of the inclusion comes out to be between 100 and 400 μ m which means that it is longer (or nearly longer) than the dimension of the enclosing calcite. However, it should be re-emphasized that these values are based on an upper limit controlled by the unlikely assumption that each grain contains one fluid inclusion. However, even if each grain contained 100 fluid inclusions, which at 100:1 length to width ratio, could easily be accommodated, such inclusions would, nevertheless, be observed under the light microscope. It may be recalled from section 4.3.4 that the oil immersion experiment revealed none.

Considering the resolving power of the microscope to be about 3 μ m then, at the dimensions stated above, the minimum number of fluid inclusions to remain visible must be

between 10^7 and 10^9 .

In section 4.4 we shall consider the implications of the size of fluid inclusions to the interpretation of isotope data.

4.4 $\delta^{18}\text{O}$ and δD of Water Extracted from Speleothems

4.4.1 Introduction

Chapter 1 reviews the isotopic studies of fluid inclusions to date. Two important points arise from the review: firstly, that isotopic paleotemperatures, when calculated assuming the present day deuterium excess ($d_o = 10\%$), are a little too low and secondly, that few analyses of modern deposits have been made. The paper of Harmon and Schwarcz (1981) essentially utilizes most of the data generated from past work (all are measurements of δD_i) and attempts to reconcile it by invoking the change in d_t to lower values than 10% in the past to recalculate isotopic temperatures. Paleotemperatures re-determined in this way yield reasonable values. The fluid inclusion data from 5 modern deposits, although somewhat sparse,

suggest that isotopic temperatures are recoverable from fluid inclusion water and host calcite because they agree in general with thermometrically measured temperatures. However, the variability of these isotopic temperatures, as mentioned, is quite large being $\pm 4.0^{\circ}\text{C}$ for the 4 West Virginia deposits analysed (Schwarcz et al., 1975). This leaves some doubt as to the validity of the remaining 47 paleotemperatures although large temperature changes should be discernable. Their correction of these paleotemperatures is justified since it has been shown by other sources that the meteoric relationships have changed in the past (see Chapter 1). Nevertheless, despite the variability of the data from modern deposits, the isotopic paleotemperature data looks surprisingly convincing when the deuterium excess is reduced to zero.

A critical appraisal of the past fluid inclusion data is extremely important because neither the fluid inclusion data for $\delta^{18}\text{O}$ (Yamamoto, 1980) nor δD (this study) agree with these findings. In fact, the precision of replicate δD_i analyses given by Harmon and Schwarcz (1981) and Harmon (1981) as $\pm 3\%$ and ± 3 to 4% , respectively was found to be greater by more than a factor of 2 than that achieved during this study or Yamamoto (1980) for crushing extractions. Admittedly, the latter precision was inferred from $\delta^{18}\text{O}_i$ analyses. The present work is described in the following sections.

4.4.2. Isotopic Testing of the Samples for Equilibrium Deposition

Where possible, the criteria of Hendy (1971) have been followed to determine isotopic equilibrium fractionation of the samples. That is, $\delta^{18}\text{O}$ and $\delta^{13}\text{C}$ have been measured along growth bands. This data has been compiled for the samples in Tables 4.2, 4.9 and 4.10 and is included in Appendix IV. Where complete axial isotopic profiles are presented, the growth layers are included in tables accompanying the text, as in Figure 5.1 for example.

Where equilibrium deposition has not been determined unambiguously is in the soda-straw samples, in which growth layers are not very extensive. These samples comprise Bone Norman #1, Friar's Hole #1 and Wind Cave #1. **Justifying use** of the former two samples, is replicate δD_i analyses and the fact that accompanying seepage water lies close to the meteoric water line. Such evidence, of course, does not guarantee that δO_c is in equilibrium but lends assurance that at least the calcite-forming water is not fractionated. Thus evaporation effects can be ruled out but not necessarily kinetic fractionation effects produced by rapid outgassing of CO_2 during deposition. The soda-straw from Bone Norman Cave was collected from well within the cave in a draught free zone (as indeed were all the deposits with the exception of two to be mentioned **below**), in the same area from which modern equilibrium calcite had been

collected previously (Thompson, 1973) and is therefore likely to be in equilibrium. The stalactite from a short greywacke cave from South Georgia (#1) has been shown to be out of equilibrium (Knyf, 1980) but is included because it nevertheless gave reasonable results. The sub-glacial precipitate from the Bugaboo Mountains, B.C. has not been tested for equilibrium and its somewhat high isotopic temperature may be a function of this.

With the exception of the samples described above, equilibrium deposition has been encountered for the samples used in this study. It is therefore expected the seepage, hence deposition, water is unfractionated and isotopically equivalent to corresponding meteoric precipitation. The isotopic correspondence of seepage water and average meteoric water has also been demonstrated in Chapter 3.

4.4.3. Comparison of Isotope Ratios of Water from Crushing and Decrepitation Extraction Methods

Whilst water yields from the two modes of extraction are distinctly different, with much higher yields coming from decrepitation, isotope ratios are not significantly different by contrast.

Firstly, the precision of the two methods is considered. Samples were assumed to be replicate having been cut from the same set of growth layers (section 4.2 and Appendix IV). The

precision of analyses from all the crushing data are $\pm 0.83\%$ for $\delta^{18}\text{O}_i$ and $\pm 8.3\%$ for δD_i whereas for decrepitation, δD_i precision is $\pm 1.8\%$. Given that the McMaster apparatus for crushing extraction may be more problematic than those used in the published work and given that the published values of $\pm 3\%$ are more representative, the precision for decrepitation is still greater by a factor of 1.7 to 2.2. The lower precision encountered for analysis by crushing may stem from the fact that not all the water is liberated and partial rupturing of remaining inclusions could result in a diffusive loss of water with a concomitant kinetic fractionation effect. If decrepitation can be shown to give the same results then the method is more appropriate to the study of paleotemperatures; it is faster, uses smaller samples and is more precise.

Now let us consider the comparison of δD 's. Table 4.7 illustrates that for 3 of the 6 samples water liberated by crushing is identical to that from decrepitation within error. Of the remaining 3, 77151B, as already mentioned, was suspect because of an abnormally low yield associated with the δD_i analysis by crushing. It seems likely some of the sample was lost during extraction since the crushing yields for $\delta^{18}\text{O}$ analysis were considerably higher. Two values from Llano Chiquito #1 are different by 30.7% but no explanation can be offered for this discrepancy. 807CH1 has already been noted in the petrology section (4.2) as being somewhat unusual in appearance and

Table 4.7 A Comparison of δD_i and $\delta^{18}O_i$ in Water Extracted from Speleothems by Crushing and Decrepitation

SAMPLE	EXTRAC. MODE	ANAL. NO.	$\delta^{18}O_i$ %*	$\delta^{18}O_c$ %	δD_i %	$(\delta^{18}O_i)$ %	$T_{\delta D}$ °C	$T_{\delta^{18}O}$ °C	METEORIC RELATIONSHIP
77151B	D	1			-76.9	-11.19	-12.6		
Victoria Cave, U.K.	C	1	{	-14.10 ±0.77	-41.8	- 6.10	+ 4.9	-21.0	$\delta D = 6.9\delta^{18}O + 0.3$ (Evans et al., 1978)
	C	3							
73017	D	2			-41.1±0.1	- 7.55	+ 3.3		
Bermuda	C	15	{	- 5.34 ± 0.79	-43.2±9.2	- 7.90	+ 3.7	+ 5.8	$\delta D = 6.0\delta^{18}O + 4.2$ (Harmon et al., 1978)
	C	18							
797MP1	D	6			-89.9±1.6	-12.49	- 5.3		
N.Y.	C	2	{	-10.71 ± 1.32	-90.8±3.8	-12.60	- 5.7	+ 2.1	$\delta D = 8\delta^{18}O + 10$ (Dansgaard, 1964)
	C	2							
807CH1	D	2		+25.16	-109.6±0.1	-14.95	-18.8		$\delta D = 8\delta^{18}O + 10$ (Dansgaard, 1964)
	C	2			-70.1±7.3	-10.01	- 2.7		
Llano Chiquito#1	D	1		+24.05	-59.2	- 8.65	+ 6.5		$\delta D = 8\delta^{18}O + 10$ (Dansgaard, 1964)
	C	1			-89.9	-12.49	- 7.5		
Mirror Lake #1	D	3		+24.06	-72.4±1.8	-10.30	+ 0.2		$\delta D = 8\delta^{18}O + 10$ (Dansgaard, 1964)
	C	2			-71.0±6.9	-10.13	+ 0.8		

D = Extraction by decrepitation

C = Extraction by crushing

$\delta D_i, \delta^{18}O_i$ = Isotope ratios from included water

$(\delta^{18}O_i)$ = $\delta^{18}O$ inferred from δD_i by the given meteoric water line

$T_{\delta D, \delta^{18}O}$ = Temperatures determined from δD_i and $\delta^{18}O_i$ respectively

*data after Yamamoto (1980)

± = 1σ for 6 or more points otherwise the range is given

$\delta^{18}O_c$ = $\delta^{18}O$ of host calcite

gives rise to very light δD_i values compared to other samples in the vicinity such as, for example, Bone Norman S.S.1 seen in Table 4.8. The results of isotopic comparison between crushing and decrepitation can be seen in Table 4.7. Thus, while isotopic equivalence between crushing and decrepitation yields is well established for half the samples studied, the results for the remainder contradict this conclusion. However, these latter data should be viewed with caution. The difficulty of achieving replication for the crushing method both in this study and that of Yamamoto (1980) has been mentioned. Therefore, for those samples, in which isotopic equivalence appears not to occur, more extractions need to be undertaken as in two of the three cases only one crushing extraction has been performed and in the remaining case only two replicate extractions were carried out. The crushing extraction associated with 77151B, as mentioned above, lacks precision because of the apparently small proportion of sample collected. Nevertheless, the above data do suggest some inconsistency that requires further investigation.

Of the remaining three samples, replicate data are more numerous and isotopic equivalence between the two extraction methods seems convincing.

From the above discussion, it is not possible to say unequivocally that δD_i from crushing equals that from decrepitation but the evidence for this isotopic equivalence seems more for than that against it. Further support for this view is provided in the next section where water extracted from

Table 4.8 Comparison Between Isotopic Composition of Seepage Waters and Calcite-Bound Water in Modern and Interglacial Deposits

SAMPLE	δD (‰)	δD_i (‰)		$\Delta\delta D_{s-i}$ (‰)	$\delta^{18}O_c$ (‰)	ISOTOPIIC TEMP (°C)			CAVE TEMP °C	AGE (Ka)	METEORIC RELATIONSHIP	
		CR	US			A	B	C			SLOPE	$d_{o,t}$
Bone-Norman(SS1)	- 55.0	-	- 78.3	25.0	24.41	3.2	6.5	7.8	10.0	M	8	10 ¹
Friar's Hole(SS1)	- 55.1	-	- 69.7	15.6	23.81	4.6	13.3	14.6	9.5	M	8	10
Mirror Lake #1	- 52.0	- 71.7	- 72.4	21.8	24.06	0.2	9.7	11.0	11.1	M	8	10
797MP1	- 67.0	- 95.6	- 89.9	24.9	23.13	- 5.3	5.5	6.8	8.0	M	8	10
807CW3	- 59.0	- 83.1	- 80.7	23.3	24.58	- 5.4	4.5	5.8	7.8	(M?)	8	10
Wind Cave #1	-102.0	-	-127.1	28.2	20.22	-10.2	- 0.9	0.4	~ 5.0	(M?)	8	10
807CH1	- 55.1	-109.6	-109.7	59.5	25.16	-18.8	- 8.3	- 7.0	9.5	(M)	8	10
Llano Chiquito #1	- 25.3 ⁵	-	- 54.2	30.1	24.05	6.5	20.4	21.7	~19.0	(M)	8	10
75350	- 4.3 ³	-	- 30.7	26.9	26.30	10.9	24.3	-	24.0	(M)	6	4.2 ²
Bugaboo #1	-106.0 ³	-	-160.7	0.7	12.26	3.0	13.8	-	0.0	(M)	8	10
South Georgia #1	- 70.0	-	- 77.0	7.6	26.00	- 4.3	5.5	-	3.8	(M)	8	0 ³
73107	- 18.0	- 41.0	- 41.1	23.8	27.54	3.3	11.0	-	>10.0 ⁶	162.0	6	4.2
77151B	- 52.0	-	- 76.9	26.6	26.22	-12.6	0.3	-	~ 0.0 ⁷	257.4	6.9	0.3 ⁴

M = Modern

(M) = Samples not used to determine $\Delta\delta D_{s-i}$

(M?) = Questionably modern

CR = Crushed residue

US = Uncrushed sample

$\Delta\delta D_{s-i} = 10^3 \ln \alpha_{s-i}^D$ where $\alpha_{s-i}^D = (\delta D_s + 10^3) / (\delta D_i + 10^3) = 22.1 \pm 3.9$

$$\approx \delta D_s - \delta D_i$$

A = Determined using equations 1.3 and 1.8

B = Determined applying $\Delta\delta D_{s-i}$ to recover δD_i and equations 1.3 and 1.8

C = Determined as in B but using $d_{o,t} = 7.8$ as^Sdetermined for cave seepage in the Eastern U.S. (Chapter 3)

¹Dansgaard (1964)

²Harmon et al. (1978)

³IAEA (1979)

⁴Evans et al. (1978)

⁵Harmon (1975)

⁶McIntyre (1967)

⁷Gascoyne (1979)

speleothem powders is shown to be isotopically the same as water extracted by decrepitation and hence, in some cases, crushing.

If isotopic equivalence exists between the two methods then this would be evidence that water liberated by decrepitation does not contain structural components chemically bound to the calcite lattice but is being released entirely from fluid inclusions. In other words, crushing and decrepitation would be releasing water from isotopically equivalent sites. However, it will be shown subsequently that this water is isotopically fractionated with respect to parent seepage water from which the calcite grew.

4.4.4. Isotopic Composition of Water Extracted by Decrepitation of Crushed Samples

Because comparisons of two methods of extraction seem largely to yield water whose δD is the same, a complementary experiment was undertaken to see if calcite powders would also give the same results. Of the 6 samples chosen for the study (Table 4.8 and Appendix IV,b(ii)) only 797MP1#-5LD seems to fall outside the range of experimental error but even then it is only 3.2‰ heavier than the mean of the growth layer value from which it was taken (Figure 4.2). The discrepancy is explainable perhaps because calcite powders are difficult to handle in the furnace. Powders generally need to be dried overnight at temperatures usually close to 100°C and with the findings of

Thompson (1973) such temperatures would involve considerable loss of water. At high temperatures the powders are particularly difficult to handle because CO_2 released during calcining causes the grains to go into frenetic activity with some escaping the glass wool cover and coming to rest in the spiral trap. This situation has to be avoided because the CaO grains could react with water when the trap warms up to room temperature. Sample 797MP1#1 has previously been noted to yield isotopically equal water whether crushing or decrepitation extraction have been undertaken. The decrepitation of the crushed residue also gives the same δD value as crushing.

In summary, water extracted by decrepitation from calcite powder was found to yield the same results as that extracted from cut samples.

4.4.5. Decrepitation of Hydrothermal Minerals as a Test of the Method of Extraction

Coexisting hydrothermal minerals from the Taulin Ore Deposit, China were decrepitated according to the procedure described in Chapter 2 and Appendix II and δD_i was analysed. The reason that this experiment was undertaken, apart from the interest in a geochemical study of the ore body (Ding et al., 1981), was to see if different coexisting minerals, including calcite and quartz, were isotopically equivalent.

Although the equivalence of crushing and decrepitation methods of extraction is suspected, some concern was felt

that δD_i from decrepitation of calcite might be an experimental artifact. The reason for this suspicion is that during decrepitation, copious quantities of CO_2 must be separated from relatively small amounts of water, and this might result in small quantities of water being carried away with CO_2 as CO_2 is removed by the wastepump. Since quartz does not break down during decrepitation and if coexisting quartz and calcite are found to be isotopically equivalent, then concerns that water was being lost in this way would be unfounded.

The coexisting quartz (004) and calcite (004) gave δD_i values as -46.1 and -47.6% respectively (Appendix V). Although somewhat limited, this experiment lends some assurance to the fact that the isotopic fractionation of water extracted from speleothems with respect to their parent solutions is probably due to some natural process and is not an artifact of the experiment.

4.4.6. Decrepitation Temperature Versus δD_i

The experiment done on 77151B to study this relationship is described in section 4.3.3. and the results are shown in Figures 4.5 and 4.14 and Table 4.3. In Figure 4.5, the points represent δD_i of cumulative fractions as the temperature (or yield) is increased. In Figure 4.14, the data is re-plotted such that the δD_i of each fraction is correlated with yield. The correlation is somewhat surprising as isotopically heavy water is being released at the lowest temperature step

Figure 4.14 δD_1 versus fractional water yields from 77151B
at various decrepitation temperatures. Data is from
Table 4.3

(280°C). At the next step, very light water is released and thereafter, subsequent fractions are light, although not as light as this, until 650°C when calcining starts and the remaining 58% of water returns to an isotopically heavier value. This latter value (-50.9%) is in fact heavier than the total decrepitation value of -77%. The justification for the curve shape in Figure 4.6 stems from the observation that once calcining commences, complete release of water takes place. The calcining temperature of 850°C is used merely to improve the rate of analysis and is normally employed for all decrepitation extractions.

The low temperature portion of the curve is hard to explain because a straightforward diffusive process would result in the loss of light isotopes preferentially. One possibility is that the low temperature fraction is due to contamination such as absorbed water but steps are taken (Chapter 2) to remove this possible component. Apart from this, absorbed water might be expected to be present in variable amounts and yet generally the consistency of replication argues against this. Another explanation that might account for the low temperature end of the curve could be that water is being liberated from isotopically distinct sites accounting for at least 42% of the water. Suppose, for the moment, that at low temperatures the larger fluid inclusions are being released and that progressively smaller ones are released subsequently until

finally lattice water is released at high temperatures. How plausible is this model? The fact that supposed 'lattice' water is heavier in isotopic composition than the high temperature inclusions is the reverse of that expected since deuterium does not concentrate in the mineral phase (Hoefs, 1980). It is perhaps consistent with the low temperature extractions. This multi-site model is unlikely because of the evidence presented for the isotopic equivalence of crushing and decrepitation methods of extraction. Furthermore the occupation of the many sites would have to be repeatable from calcite aliquot to calcite aliquot, sample to sample and geographical locality to geographical locality in order to demonstrate the interval consistency of δD and $\delta^{18}O$ results depicted in Tables 4.7 and 4.8 and Figures 4.6 and 4.7.

Without further evidence, a simpler way out of the dilemma is to accept that water is liberated from many fluid inclusion sites of different sizes that are isotopically equivalent. The curve in Figure 4.14 can then be explained as follows: The low temperature end of the curve (up to 280°C) represents the release of larger inclusions although if this is a diffusive process then at lower temperatures one might expect to see light fractions appearing. In the second fraction the water might be being released diffusively from a new, tighter set of fluid inclusions. Subsequent fractions then get progressively lighter from the third step because of further diffusive loss of

water from still lighter sets of inclusions. Once the sample starts to calcine at 650°C, then the remaining water is released which is heavier than the total decrepitation water because of the earlier diffusive losses.

Whilst the above model is itself somewhat speculative and simplistic, in the absence of a number of definitive and careful experiments, it is presumptuous to seek more complex explanations even though it is acknowledged that the system is unlikely to be a simple one.

4.4.7. A Comparison of Isotopic Ratios in Cave Drip Water (δD_s) and Decrepitation Water from Modern Speleothems (δD_i)

As described in Chapter 1, earlier studies suggested that δD_i was equal to δD_s although reconsideration of some of this data reveals an important exception which will be discussed in Chapter 5. Nevertheless this study was undertaken because of the importance of examining and establishing the relationship between δD_i and δD_s . Furthermore, it should be reemphasized that results presented in Chapter 3 indicate that δD_s and $\delta^{18}O_s$ are constant throughout a period of at least a year and represent the mean annual precipitation. Thus any differences between δD_i and δD_s cannot be attributed to short-term fluctuations of δD_s . All the deposits considered in the section designated 'modern' are, in fact, Holocene and appear to represent no more than 1 to 2Ka based on average growth rates and some are demonstrably younger (see Table 4.1). An

assumption, which can be substantiated from ice cores (for example; Dansgaard et al., 1969) is that there has been no great change in the isotopic composition of mean annual precipitation.

A comparison between δD of waters extracted from modern deposits is given on Table 4.8. Calcite-bound waters are lighter than accompanying seepage by an average of $22.1 \pm 3.9\%$ in δD (the fractionation is designated $\Delta\delta D_{s-i}$ and the fractionation factor α_{s-i}^D (see Table 4.8)). Tentatively, a similar observation can be made for $\delta^{18}O$ too but with only the data from 797MP1 to go on. The value obtained is 3.14% (Table 4.9); the notation is likewise $\Delta\delta^{18}O_{s-i}$ and α_{s-i}^O . Clearly, the seepage water is modified isotopically during or after entrapment. Since neomorphic effects are not observed (see section 4.2), isotopic fractionation of the water does not appear to be a result of recrystallization. Isotopic data from 6 samples in Table 4.8 have not been used to calculate $\Delta\delta D_{s-i}$. These follow: Wind Cave #1, which is a soda-straw, was found on the ground and was dry. Seepage water was obtained from similar soda-straws growing in the proximity. Unfortunately, but understandably, the Park authority forbade removal of these growing deposits. The age of the Llano Chiquito #1 sample is not in question since it was actively growing or wood washed into the cave but coeval water was not collected. δD_s is an average of 3 determinations from another cave (Del Arroyo, see Harmon,

1975) that is situated some 700 m lower. $\Delta\delta D_{s-i}$ in this case could be lower than the 30.1‰ calculated as lighter average precipitation would be expected at the higher site. 807CH1#1 does not conform to the general pattern ($\Delta\delta D_{s-i} = 59.5‰$). The age of the deposit is in doubt, because although it appeared to be actively growing, $\delta^{18}O_c$ does not seem to reflect present day values in the area. The trapped water may reflect periods of lighter precipitation although it is even too light to be explained completely by this. It is anticipated that more work will be undertaken to resolve the problem of this interesting stalagmite. 75350#1 was not used because there is uncertainty as to δD_s at the cave. The value given, -4.3‰, is that for mean meteoric precipitation for San Juan, Puerto Rico (IAEA, 1979). Finally, the last two samples: Bugaboo #1 and South Georgia #1 are not strictly Karstic cave deposits. The former formed under ice and the latter in a cleft cave composed of greywacke. Bugaboo #1 contains a great deal of water and, as mentioned in 4.3, results from a different mode of formation. It appears, and rather interestingly so, that ice or regelation water is being preserved without modification within this, and perhaps other, sub-glacial precipitates. δD of coeval ice was estimated from Hislop (1979). The deposit from South Georgia was not included because it was found not to be an equilibrium deposit. Nevertheless, it has been **presented** because its isotopic temperature resembles the summer cave temperature. However,

the δD_s is different from that expected at that latitude. The IAEA (1979) data for Stanley Island, close to the South Georgia latitude suggest that the mean annual precipitation of this site should be closer to -58% rather than -70%.

Two other speleothems, 73107 and 77151B which have been included in Table 4.8 are interglacial deposits and if $\Delta\delta D_{s-i}$ is calculated for them, both values fall within the $22.1 \pm 3.9\%$ value determined for modern deposits. An important consideration is whether or not $\Delta\delta D_{s-i}$ is temperature dependent, but no correlation is noted. The data used to determine $\Delta\delta D_{s-i}$ are mostly too close in temperature to permit a sensible correlation. Before $\Delta\delta D_{s-i}$ can be considered further as a possible means of recovering temperatures from fossil deposits some discussion of the depleted nature of δD_i is required and now follows.

4.4.8. Some Speculation on Isotopic Composition of Fluid Inclusions

This study and the work of Yamamoto (1980) has shown that water in speleothems is isotopically lighter than seepage water from which it was deposited. Because this anomalous isotopic depletion was found in some modern, actively growing speleothems, changes in past meteorological regimes cannot be sought as a means of explaining the phenomenon. The possibility that experimental artifacts could affect all the fluid inclusion data is constrained by the observation of similar findings using different techniques of extraction, preparation

and analysis. Infrared and Neutron diffraction methods fail to reveal the presence of structural or oriented water, although their presence remains a possibility. Isotopic comparison of water extracted by crushing versus decrepitation further argues against the presence of structural water components.

Therefore, we must now ask how water can be unstructured and unoriented and yet fractionated? One possible mechanism is that water is fractionated by adsorption onto crystal surfaces. Unfortunately, very little has been written about isotope effects during adsorption of liquids. However, Stewart (1974) found adsorbed water in clays to be strongly depleted in deuterium, occasionally by as much as 130%. The effect in calcite may appear to be weaker because of the adsorption of only some of the water within the fluid inclusions. Thus the electrostatic or Van de Waals forces may be strong enough to produce an isotope effect between the hydration layers and the bulk solution. The isotope effect should fall off in magnitude away from the crystal surface. This, the Stern double layer, is known to extend outwards for around 10^2 Angstroms thus placing some limitation on the cross-sectional dimensions of the intercrystallite pores for the isotope effect to be measurable.

In section 4.3.7 a very crude calculation was made as to the upper limit of intercrystallite pore diameter of between 1 and $10\mu\text{m}$. These were based on 10:1 and 100:1 length to

width ratios of pores respectively and the condition that they just fit inside the (100 μ m) grains. However, it seems hardly likely that fluid inclusions could remain intact when their dimensions are equal to that of the grain containing them. Microscopic observations of grains in immersion oil should reveal inclusions down to a few microns in length, yet none have been seen. Inclusions of 1 μ m in length will have diameters of 10^2 to 10^3 angstroms which is within the range of the Stern Double Layer. If the inclusions are generally of this size, each 100 μ m grain would contain 10^6 to 10^8 of them; a density of 10^{12} to 10^{14} per cm^3 .

Assuming that the Stern Double Layer is containing isotopically fractionated water then a problem arises because in order to produce the same fractionation in all samples regardless of age and locality, the same size and range distribution of fluid inclusions would have to occur. Be that as it may, in the absence of a more plausible explanation, the mechanism of adsorption is proposed for the isotope depletion noted in water extracted from speleothems.

In summary, it appears that the possibility exists for using $\Delta\delta_{s-i}^D$, and, possibly even $\Delta\delta_{s-i}^{18O}$, to calibrate fossil speleothems such that isotopic temperatures can be recovered from them. Application of the fractionations to accomplish this is examined hereinafter.

4.4.9. A Comparison of Isotopic Temperatures Using δD_i and Cave Temperatures

Isotopic temperatures calculated using equations 1.5 and 1.8 are too low to be acceptable, many falling below zero. Changing δD_i by application of $\Delta\delta D_{s-i}$ brings almost all temperatures to more acceptable values (Table 2.4 and Figures 4.6 and 4.7). Even then, some of the temperatures appear still too low. Of the isotopic temperatures calculated for the 5 modern samples used to determine $\Delta\delta D_{s-i}$, 4 out of the 5 are low by up to 3.3°C whereas the fifth, Friar's Hole (SS1), is too high by 4.4°C. The inconsistency of the latter is due to its low $\Delta\delta D_{s-i}$ of 15.6% which, at the moment remains unexplained, but may be analytical. The other 4 temperatures are low for perhaps two reasons: firstly, that the $\Delta\delta D_{s-i}$ used may be too small because of the inclusion of the lower value of $\Delta\delta D_{s-i}$ Friar's Hole (SS1) in the data set used for the calculation of $\Delta\delta D_{s-i}$; secondly, the meteoric water line determined for a number of cave sites in the Eastern U.S. has a lower intercept ($d_o = 7.8 \pm 1.5$) than that published ($d_o = 10.0 \pm 1.0$ (Chapter 3)). Applying the former value ($d_o = 7.8$) raises all the isotopic temperatures by about 1.3°C and, ignoring Friar's Hole (SS1) in the determination of $\Delta\delta D_{s-i}$, the temperature is raised by a further 0.5°C. 4 out of the 5 modern isotopic temperatures are then much more acceptable. Of the 5 paleotemperature profiles (Figures 4.6, 4.7 and 5.5), perhaps only 797MP1, the

Holocene stalagmite from N.Y., can be subjected to the 1.3°C change because of the meteoric water line determined from cave drip waters. The other profiles might also be subject to change but it is not known what the meteoric water line at these sites would have been during the Pleistocene. At this point, a reminder should be made that most cave seepage isotope ratios lie to the right of the meteoric water line (see Figure 3.6 and Chapter 3.1.3.) and it may be that all paleotemperatures should be subject to small changes as a result of this. This is discussed further in the next chapter when the significance of paleoclimatic profiles in speleothems is considered.

The inclusion or exclusion of the Friar's Hole (SS1) data clearly affects the precision, if not the absolute value, of temperature determinations. Since there is no a priori reason for dropping this value of $\Delta\delta\text{D}_{\text{s-i}}$ of 15.6‰, the average $\Delta\delta\text{D}_{\text{s-i}}$ is retained. It should be added though that most of the remaining (tentative) data in Table 4.8 and all the paleotemperature profiles argue against the validity of this result.

The errors considered in the calculation of precision of isotopic paleotemperature are:

- i) Errors in slope (± 0.2) and intercept (± 1.5) of the meteoric water line;
- ii) Error in $\Delta\delta\text{D}_{\text{s-i}}$ ($\pm 3.9\%$) based on the 5 modern speleothems;
- iii) Analytical errors in δD_i ($\pm 1.8\%$) and $\delta^{18}\text{O}_c$ ($\pm 0.1\%$).

(Appendix IV). If $\Delta\delta D_{s-i}$ with an error of $\pm 3.9\%$ is used then precision of temperature determinations is $\pm 4.3^\circ\text{C}$. Clearly, these values, if valid, will allow meaningful interpretation of paleotemperature records, like those presented in Figures 4.6, 4.7 and 5.5, whose temperature range is around 8°C . Errors in relative temperatures may not be as large if the value of $\Delta\delta D_{s-i}$ is at least constant at a given site for a single speleothem. Thus error bars presented in the profiles are calculated without the addition of this error and are $\pm 2.9^\circ\text{C}$.

4.4.10. A Comparison of Isotopic Temperature Using $\delta^{18}\text{O}_i$ and Cave Temperatures

The possibility of applying $\Delta\delta^{18}\text{O}_{s-i}$ in the determination of isotopic temperatures is considered here, *although* albeit tentatively. These results must be considered as preliminary because only one modern deposit was analysed (797MP1) and because of the possibility of post-depositional oxygen isotopic exchange already mentioned. Post-depositional exchange would be expected to make $\delta^{18}\text{O}_i$ heavier as temperature over most of the past 250,000 ka B.P. was probably lower than now (Harmon et al., 1979; see also Chapter 1). Surprisingly, the $\delta^{18}\text{O}_i$ data indicates the reverse; like δD_i fluid inclusions tend to be depleted in ^{18}O with respect to meteoric water of the same δD . If $\Delta\delta^{18}\text{O}_{s-i}$ is also constant (or temperature dependent), then the possibility of isotopic temperature recovery presents itself without the need to resort to meteoric relationships for its

Table 4.9 Isotope Ratios and Isotopic Temperatures of Speleothems for which $\delta^{18}\text{O}_i$ was measured

SAMPLE	NO. of ANAL. of $\delta^{18}\text{O}_i$	$\delta^{18}\text{O}_s$ (‰) ^S	$\delta^{18}\text{O}_i^*$ (‰) ⁱ	$\delta^{18}\text{O}_c^*$ (‰) ^c	T_i (°C)	T_{icorr} (°C)	T_M (°C)	MEAN SAMPLE AGE (Ka)**
77151B	3		-14.10 ± 0.77	27.00	-21.0	-11.3	7.5	257.4
73017	18	-2.34 ¹	- 5.34 ± 0.79	27.54	+ 5.8	+18.7	19.0	110.0
797MP1	2	-7.60 ²	-10.71 ± 1.132	23.13	+ 2.1	+14.6	8.0	0
76501(6-9)	4		- 6.69 ± 0.69	26.17	+ 8.5	+18.4	15.6	74.3
77162	4		-10.45 ± 1.06	26.92	-10.1	+ 0.6	7.5	110.0

$$\Delta\delta^{18}\text{O}_{s-i} = 10^3 \ln \alpha_{s-i}; \alpha_{s-i} = (\delta^{18}\text{O}_s + 10^3) / (\delta^{18}\text{O}_i + 10^3)$$

*Data after Yamamoto (1980)

1. Harmon (1975) (for modern data)

2. Appendix III

T_{icorr} = Temperature corrected by $\Delta\delta^{18}\text{O}_{s-i} = 3.11$ ‰

T_M = Modern cave temperature

**See Table 4.1

determination.

From the $\delta^{18}\text{O}_i$ data of 797MP1 (Table 4.9) and the drip water data (Appendix III), $\Delta\delta^{18}\text{O}_{s-i}$ gives a value of 3.14‰. $\delta^{18}\text{O}_i$ data of the interglacial Bermuda flowstone (73107 in Table 4.2) and modern $\delta^{18}\text{O}_s$ (Harmon, 1975) give $\Delta\delta^{18}\text{O}_{s-i}$ at 3.01‰. The value for McFails Cave may be too large because the drip water data lie far to the right of the meteoric water line (Figure 3.6) and this may be due to an incorrect determination of $\delta^{18}\text{O}_s$. δD_s is about the value expected for that region (Taylor, 1974). On the basis of $\Delta\delta^{18}\text{O}_{s-i}$ from the modern deposit, isotopic temperatures have been corrected in Table 4.10. Because of the ages of samples, it is a little difficult to evaluate the temperatures. -11.3°C for 77151B is obviously too low but 0.6°C for 77162 from Lost John's Cave, U.K. at 101 Ka B.P. may be reasonable because a number of U.K. speleothems dated by Gascoyne (1976) stopped growing at this point although this time is generally considered to be during the last interglacial. Other temperatures calculated are perhaps more promising but perhaps tend to be a little too high. 73107 from Bermuda is interglacial and yields a reasonable temperature. Without further results, it is difficult to evaluate the promise of this approach to isotopic temperature determinations. However, the point is reemphasized that included waters are depleted in ^{18}O rather than enriched as expected from post depositional oxygen isotopic exchange with the host calcite.

CHAPTER FIVE

THE POTENTIAL OF THE METHOD FOR PALEOTEMPERATURE AND PALEOCLIMATIC DETERMINATION

5.1 Application to Pleistocene Climatology

5.1.1 Introduction

Stable isotope profiles were generated from 5 speleothems in an attempt to recover meaningful isotopic paleotemperatures using the method outlined in Chapter 4. These temperatures were calculated following three steps:

(i) δD_i is modified by $\Delta\delta D_{s-i}$ to infer δD_s , assuming no variation in $\Delta\delta D_{s-i}$,

(ii) δO_s is determined from δD_s by application of a given meteoric water line of the form given in Equation 1.8,

(iii) $\delta^{18}O$ of the host calcite is determined and depositional temperatures are calculated using Equation 1.5.

Unfortunately, none of the records extend over a full glacial to interglacial period for reasons given later. All are interglacial or interstadial deposits from latitudes between 45 and 55°N where speleothem growth seems to have stopped at times of glacial maxima. Nevertheless, variations of δD_i and $\delta^{18}O_c$ with time and site temperature are further examined

in light of their contribution to paleoclimatology.

5.1.2 Speleothems From the Holocene and Sangamon Interglacial Periods

5.1.2.1 Holocene Stalagmite from McFail's Cave, N.Y.

797MP1 grew from 4.6 Ka to the present when it was found actively growing. It was shown to be growing in isotopic equilibrium according to the criteria of Hendy (1971), correlation coefficients between $\delta^{13}\text{C}$ and $\delta^{18}\text{O}$ along three growth horizons, A, B and C, being 0.187, 0.526 and 0.175 respectively. Furthermore $\delta^{18}\text{O}_c$ does not show a linear correlation with distance along any of the three growth horizons measured (Figures 4.2 and 5.1).

Stable isotope data, associated isotopic temperatures and ages are presented in Table 5.1 and Figure 5.2. One of the problems with the decrepitation method for extracting water from speleothem aliquots is that the sample is completely calcined. This results in the loss of CO_2 from the sample and hence the inability to make simultaneous δD_i , $\delta^{18}\text{O}_c$ and $\delta^{13}\text{C}$ analyses. Aliquots of calcite for δD_i analysis are thus taken immediately adjacent to drill holes along growth layers. In the case of 797MP1, where axial $\delta^{18}\text{O}_c$ and $\delta^{13}\text{C}$ profiles were very detailed, the calcite aliquot for one δD_i analysis may have in excess of ten counterpart analyses of $\delta^{18}\text{O}_c$ and $\delta^{13}\text{C}$ (see Appendix IV). Table 5.1 reports only the mean values of $\delta^{18}\text{O}_c$ and $\delta^{13}\text{C}$ associated with single δD_i values.

Figure 5.1 $\delta^{18}\text{O}_c$ and $\delta^{13}\text{C}$ of points along growth bands of 797MP1 and 74017. Solid and dotted lines relate to left and right hand axes respectively. Precision of $\delta^{18}\text{O}_i$ analyses are ± 0.15 ‰ at 1 σ .

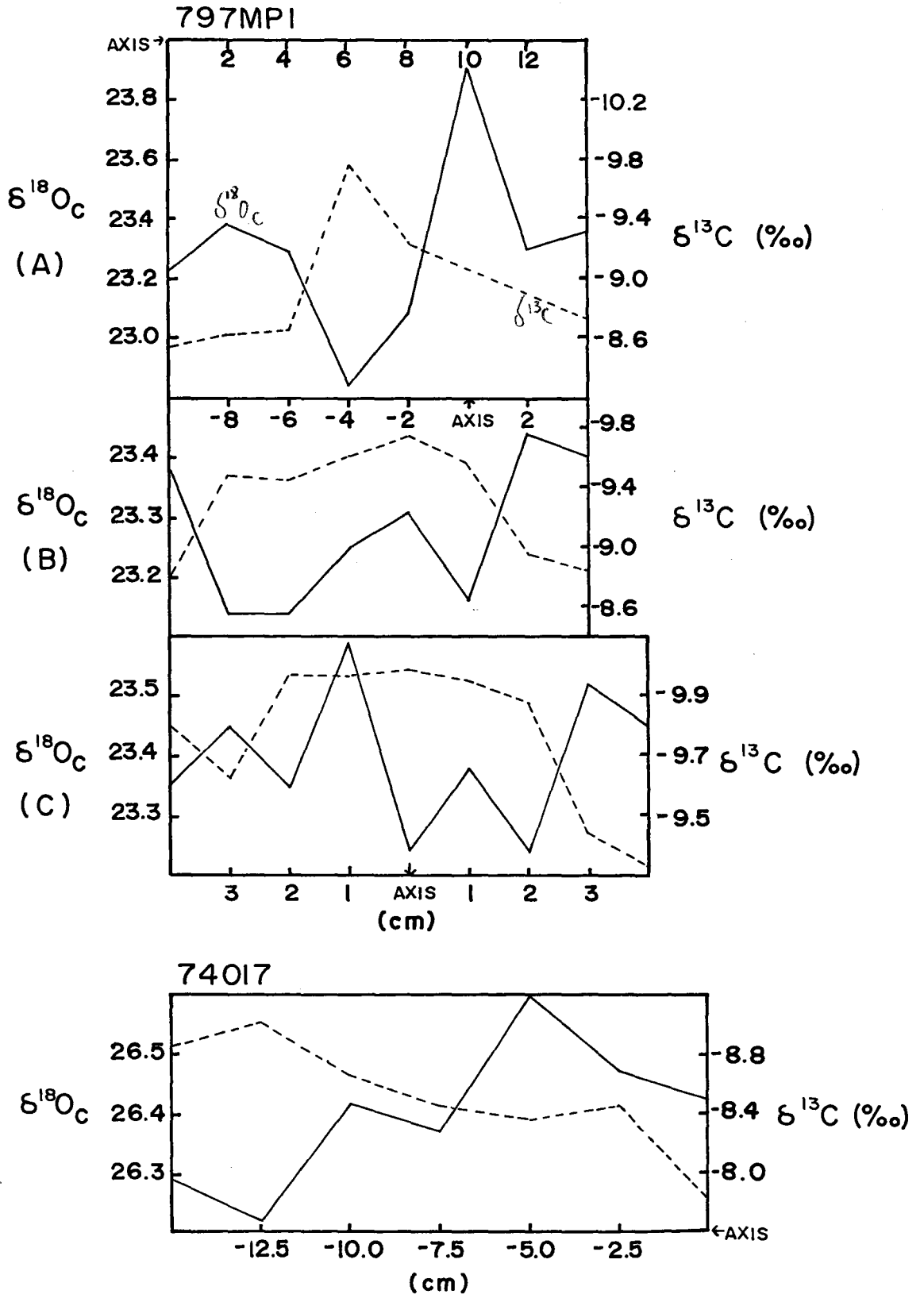


Table 5.1 Isotopic Compositions, U/Th* Ages and Calculated Depositional Temperatures** for Stalagmite 797MP1, McFail's Cave, N.Y.

SAMPLE NO.	HEIGHT ABOVE BASE	H ₂ O(wt%)	$\delta^{18}O_c$ (‰)	δD_i (‰)	TEMP °C	AGE (Ka)
797MP1 #	Top	-				Modern
1	10.0	0.361	23.01	- 89.9	5.1	
14	8.4	0.411	23.30	- 97.3	1.0	
20	7.0	0.458	22.85	- 95.1	3.7	
30	5.8	0.650	22.94	- 91.9	6.9	
40	4.5	0.252	23.35	-101.8	-1.2	
50	3.3	0.859	23.10	- 99.3	0.8	
60	2.1	0.454	23.18	-102.8	-1.1	
70	0.8	0.405	23.15	- 95.1	3.6	
	Basal 2 cm	-				4.6±1.4

*After Gascoyne (1981) see also table 5.5

**Calculated following the procedure outlined in Section 5.1.1

The isotopic temperatures listed in Table 5.1 and seen as a profile in Figure 5.2 may be subject to a positive temperature shift of 1.3°C if a slightly different meteoric water line, $d_{\text{O}} = 7.8$, rather than 10 derived from cave waters in the Eastern U.S. (Chapter 3), is applied. In so doing, no temperatures fall below zero, with the present day temperature being raised to 6.8°C , close to the thermometrically determined cave temperature of 8.0°C . As mentioned in Chapter 4, it is only to seepage waters in caves (and modern isotopic temperature records) in the Eastern U.S. that the $d_{\text{O}} = 7.8$ line is applied, although the tendency of cave drip waters in many areas to fall to the right of the Craig-Dansgaard meteoric water line and thus yield $d_{\text{O}} < 10$ is noted. Such trends, however, do not significantly affect the discussion hereafter.

5.1.2.2 Holocene Stalagmite from Cold Water Cave, Iowa

74014 has been described extensively (Harmon et al., 1979 and 1979a and Harmon and Schwarcz, 1981) because earlier age data, comprising four dates, suggested that it had grown over the period 25 Ka to 6 Ka, covering the Wisconsin Glacial Maximum at 17 Ka. δD_1 and isotopic temperature profiles constructed from the record somewhat fortuitously revealed both a significant depletion in deuterium and low temperatures at the time of the Glacial Maximum. Reevaluation of the four dates from the original raw data by Gascoyne (1981) suggests that 74014 grew from about 12 Ka to 2 Ka. Therefore the depletion

Table 5.2 Isotopic Compositions*, U/Th Ages**, and Calculated Depositional Temperature*** for Stalagmite 74014, Coldwater Cave, Iowa

SAMPLE NO.	HEIGHT ABOVE BASE	H ₂ O(wt%)	$\delta^{18}O_c$ (‰)	δD_i (‰)	TEMP °C	AGE (Ka)
-	Top					
74014:5	77	0.26	24.47	-67.1	11.9	20±1.1
:10 _x	65	0.12	24.20	-72.8	10.1	
:10 _y	65	0.12	24.28	-72.0	10.1	
: 9	56	0.10	24.77	-72.0	8.2	
: 8	51	0.17	24.74	-74.9	6.9	
-	48					12.0±0.6
: 7	38	0.09	24.25	-79.4	6.6	
: 4	23	0.07	24.10	-76.9	8.4	
-	18					10.0±2.0
:12	13	0.08	24.13	-72.3	10.6	

*From Harmon et al. (1979a)

**After Gascoyne (1981) and Table 5.5

***Calculated following the procedure outlined in Section 5.1.1

in δD_i and low calculated temperatures cannot be attributed to extreme late Wisconsin climatic change but was more likely an early Holocene event. As with the other samples described here, 74014 is treated as if fractionation towards lighter isotopic values took place as seepage waters were incorporated in the deposit. The recalculated temperatures (Table 5.2) seem a little high but the mean value of $9.0 \pm 2.0^\circ\text{C}$ is well within the $8.8 \pm 0.5^\circ\text{C}$ range for the modern cave temperature. At any rate, the 'youngest' temperature determined, 11.9°C , agrees with the modern temperature to within the $\pm 2.9^\circ\text{C}$ precision for the method.

Data pertaining to paleoclimatic interpretation is presented in Table 5.2 and depicted in Figure 5.8.

5.1.2.3 Three Mid-Wisconsin Speleothems from Cascade Cave, Vancouver Island

75125, 75123 and 76013 grew successively from 64 Ka to 28 Ka (see Figures 4.3 and 5.5; Figures are not in order of citation because of more detailed discussion of them later). They have been shown to be equilibrium deposits by Gascoyne (1979). Figure 5.6, modified with the addition of δD_i and isotopic temperature data from this study, is from Gascoyne (1980) and comprises all the stable isotope and age measurements. These are also presented in Table 5.3. Figure 4.3 indicates the relationship between the $\delta^{18}\text{O}_c$ data of Gascoyne (1980) and δD_i data of this study. Isotopic temperatures are

Table 5.3 Isotopic Composition, U/Th Ages and Calculated Depositional Temperatures* for Speleothems, 75123, 75125, and 76013, Cascade Cave, Vancouver Island

SAMPLE NO.	WATER CONTENT (wt%)	$\delta^{18}\text{O}$ (‰) ^c	δD_i (‰)	ISOTOPIC TEMP °C	AGE (Ka)
75125 Top 1cm	-	-	-	-	32.1±1.7
" " "	-	-	-	-	34.3±6.5
(ix)	0.170	19.17	-116.0	7.9	
(viii)	-	18.88	-	-	
(vii)	0.196	19.10	-129.4	1.7	
(vi)	0.159	19.41	-124.8	2.7	
(v)	0.185	19.17	-129.7	1.3	
(iv)	0.191	19.24	-124.6	3.4	
(iii)	0.170	19.49	-119.7	4.8	
1cm above base	-	-	-	-	52.2±6.6
(ii)	0.157	19.63	-123.6	2.4	
Basal 1cm	-	-	-	-	44.9±19.2
" " "	-	-	-	-	43.3±3.0
76013 C	0.266	20.09	-117.5	3.6	54.7±6.8
A	0.155	20.22	-106.0	8.7	60.8±10.2
75123 Top, 1AD	0.298	19.82	-123.7	1.7	45.3±9.8
2	0.291	19.94	-120.0	3.0	
5	0.301	20.13	-117.6	3.4	
6	0.433	20.06	-116.8	4.0	
7	0.408	19.94	-118.5	3.7	
Base, 2AD	0.266	20.37	-115.4	3.5	56.1±3.8

For locations of samples see 4.3
 $\delta^{18}\text{O}$ and ages from Gascoyne (1979); see also Figure 4.3 for
 sample relationships and table 5.5 for age data.

*Calculated following the procedure outlined in Section 5.1.1

calculated from the combination of these data sets.

5.1.2.4 Mid-Wisconsin Stalacmite from Cold Water Cave, Iowa

74017 was thought originally to have grown over the Wisconsinan Glacial Maximum from 35 to 9 Ka based on two dates (Harmon, 1975). Latterly, these dates have been shown to be in error. Based on three new dates (Gascoyne, 1981) 74017 appears to have grown from 74 to 27 Ka. This is unfortunate, because as yet no speleothems from this cave appear to have grown over the Wisconsinan Glacial Maximum when the greatest possible temperature range would have been encountered.

Stable Isotope and temperature data are presented in Figures 5.1 and 5.7 and Table 5.4. Figure 5.1 indicates that the deposit probably grew in isotopic equilibrium with the correlation between $\delta^{18}\text{O}_c$ and $\delta^{13}\text{C}$ along a growth layer yielding a correlation coefficient of 0.377. This is consistent with the observation that the only natural access to the cave is via a siphon and the cave is, therefore, essentially a draught-free site with relative humidity in excess of 95%. Presently the cave's temperature is constant at $8.8 \pm 0.5^\circ\text{C}$. Figure 4.4 shows the relationship between the samples for δD_i and $\delta^{18}\text{O}_c$ and $\delta^{13}\text{C}$ analysis. These values are shown as functions of age on Figure 5.7 and presented in Table 5.4.

Table 5.4 Isotopic Composition, U/Th Ages* and Calculated Depositional Temperatures** for Stalagmite 74017, Cold Water Cave, Iowa

SAMPLE NO.	HEIGHT ABOVE BASE	H ₂ O(wt%)	$\delta^{18}\text{O}$ (‰) C	δD_i (‰)	TEMP °C	AGE (Ka)
- 2	Top 2cm					27.0±1.1
1	53.0	0.860	26.48	-70.8	1.5	
2	52.0	0.896	26.88	-64.8	3.8	
3	50.5	0.930	26.66	-61.8	5.1	
4	49.3	0.890	26.45	-63.7	5.0	
5	48.1	0.901	26.54	-70.4	1.4	
6	44.0	0.778	26.15	-62.7	6.6	
7	40.5	0.790	25.97	-63.5	6.9	
8	37.7	0.710	26.39	-74.1	0.3	
9	36.2	0.682	26.50	-69.1	3.2	
10	34.2	0.696	26.86	-64.9	2.8	
11	33.2	0.648	26.85	-65.9	2.4	
12	32.1	0.572	26.11	-64.2	6.1	
13	29.7	0.911	25.99	-66.5	5.4	
14	27.0	0.680	26.34	-66.8	3.9	
- 1	25.0					36.0±2.0
15	24.0	0.674	26.19	-69.0	3.4	
16	21.9	0.644	26.80	-67.2	2.0	
17	19.5	0.600	26.75	-64.6	3.4	
18	15.7	0.634	26.06	-70.2	3.3	
19	11.7	0.600	26.75	-65.9	6.3	
20	8.0	0.672	25.84	-64.0	7.0	
21	4.2	0.640	26.24	-69.4	3.0	
22	0.5	0.564	26.97	-72.2	-1.0	
- 3	Basal 3cm					73.8±5.5

*After Gascoyne, 1981. see also table 5.5

**Calculated following the procedure outlined in Section 5.1.1

Table 5.5 Age Data and Radio-Isotope Ratios of Fossil Speleothems Used for Paleoclimate Study

CAVE NAME	SAMPLE NO.	ANALYSIS NO.	LOCATION	[U] ppm	$\left(\frac{^{234}\text{U}}{^{238}\text{U}}\right)_t$	$\left(\frac{^{234}\text{U}}{^{238}\text{U}}\right)_o$	$\left(\frac{^{230}\text{Th}}{^{232}\text{Th}}\right)$	$\left(\frac{^{230}\text{Th}}{^{234}\text{U}}\right)$	AGE (Ka)	$\pm 1\sigma$
McFail's ¹ Cold Water ²	797MP1	-1	Basal 1cm	0.58	2.991	3.017	9.800	0.049	4.60*	0.60
	74014	:12	84cm above base	1.64	1.320	1.322	>1000	0.018	1.9	1.1
		:14	43	3.81	1.287	1.297	29.8	0.104	11.8	0.6
		:11	17	2.52	1.251	1.258	>1000	0.090	10.2	2.3
Cascade Cave ³	74017	- 3	middle 2cm	0.29	1.346	1.378	8.7	0.288	36.0	2.0
		- 2	top 3cm	0.68	1.336	1.363	93.8	0.225	27.4	1.1
		- 1	basal 3cm	0.28	1.099	1.121	38.4	0.498	73.8	5.6/5.4
	75123	- 1	basal 0.5	0.13	1.505	1.592	29	0.414	56.1	3.8/3.7
		-2A	top 1cm	0.07	1.765	1.882	12	0.383	45.3*	9.9/916
	75125	- 3	top 1cm	0.20	1.932	2.026	3.6	0.277	21.4*	13.4/13.1
		-4A	upper middle	0.31	1.192	1.217	1.3	0.342	-7.2*	46.0/51.9
		- 6	basal 0.5	0.13	1.775	1.897	21	0.394	52.7	6.8/6.4
		- 7	basal 1.5	0.14	1.758	1.856	24	0.338	43.3	3.0
		- 8	top 0.5cm	0.20	1.941	2.030	73	0.261	32.1	1.7
	76013	C-1	upper layer	0.11	1.603	1.703	73	0.407	48.7*	8.5/8.2
Victoria Cave		A-2	basal 1cm	0.09	1.695	1.825	>1000	0.443	60.8	10.6/9.8
	77151B	C4	1cm below hiatus	0.41	1.057	1.114	128	0.914	250.4	28.9/23.0

$\left(\frac{\text{U}}{\text{U}}\right)_t$ = ratio after time t

$\left(\frac{\text{U}}{\text{U}}\right)_o$ = initial ratio

[U] = concentration of U

* = corrected for detrital ^{230}Th

¹ = Gascoyne (1981)

² = Gascoyne (1981) and Harmon (1975)

³ = Gascoyne (1979)

5.1.3 Paleoclimatic Interpretation

5.1.3.1 Holocene Records

1. Temperature versus Time

797MP1 (N.Y.) and 74014 (Iowa) extend from 12 Ka to the present and these can be considered in reference to what is known of the geographically associated paleoclimatology of this period.

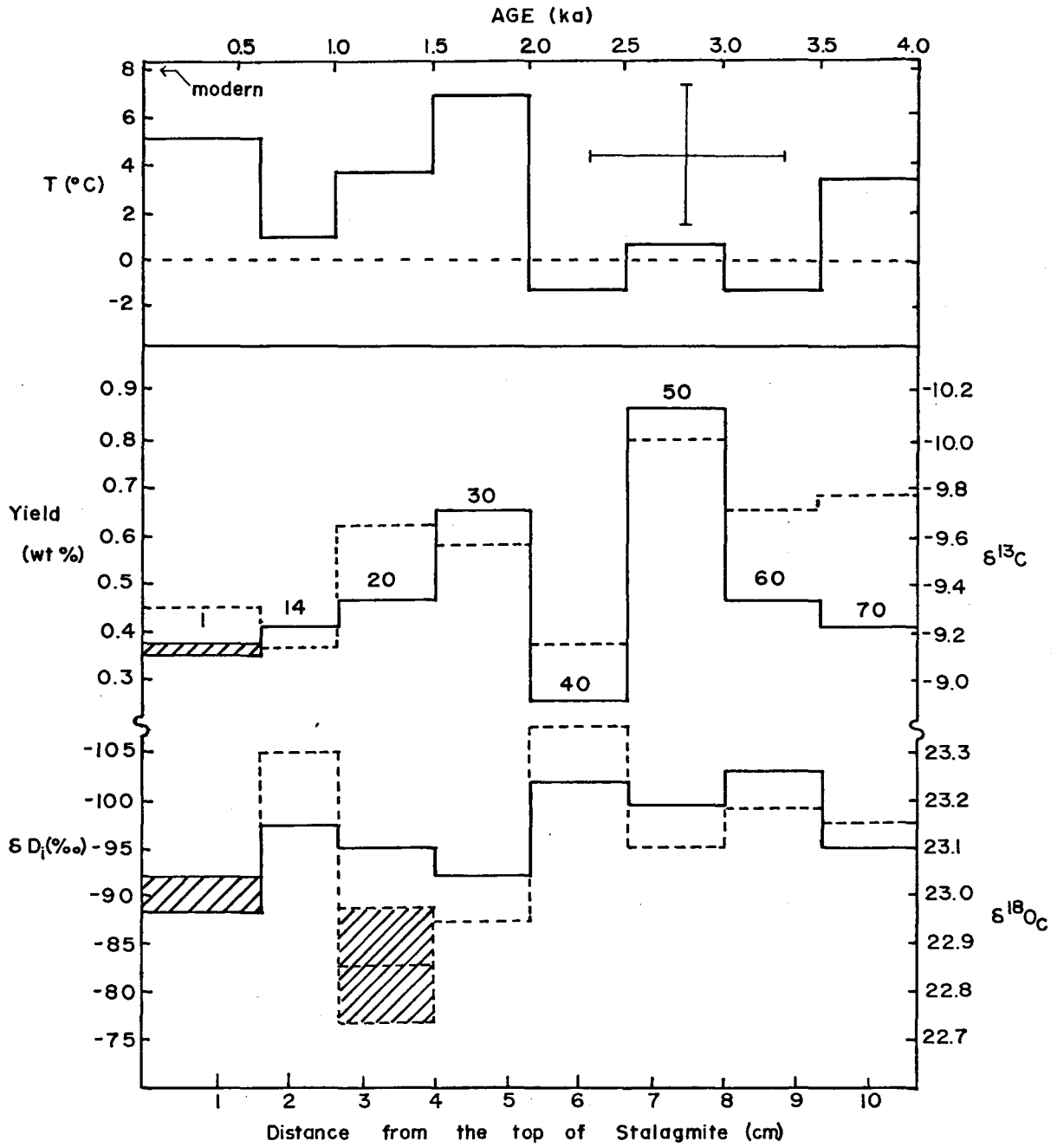
Gribben and Lamb (1978), in a general review of climatic change in historical times, divide the last 7,000 into four epochs following the last major glaciation.

- (i) 7 to 5 Ka; post-glacial Climatic Optimum,
- (ii) 2.9 to 2.3 Ka; Iron Age Cold,
- (iii) 1.0 to 0.8 Ka; Secondary Climatic Optimum,
- (iv) 0.55 to 0.13 Ka; Little Ice Age.

With the systematic error in isotopic temperature determinations (2.9°C), the temperature records can be only broadly interpreted. 797MP1 will be considered first (Figure 5.2).

From 3.5 to 2.0 Ka, a cooler period than today is observed, perhaps corresponding to the Iron Age Cold dating from 2.9 to 2.3 Ka as cited above. The later warming period from 2.0 to 1.0 Ka may then be aligned with the Secondary Climatic Optimum (1.0 to 0.8 Ka). The cooling from 1.0 to 0.6 Ka, which would then be correlated with the Little Ice Age (0.55 to 0.13 Ka), is more difficult to accept but may be reasonable when the

Figure 5.2 Plot showing water yields, δD_i , $\delta^{13}C$, $\delta^{18}O_c$ and Isotopic Temperature along the axis of stalagmite 797MP1 from McFail's Cave, N.Y. Solid and dotted lines refer to left and right hand axes respectively. Shaded areas represent 1σ errors.



precision of the dating is taken into account. The chronology is fixed by a base date of 4.6 ± 1.4 Ka, an assumed constant growth rate and the assumption that the top is modern because it was actively growing. In summary, with the dating precision in mind, it is possible to conclude that epochs (i) to (iv) are represented in the profile of 797MP1. What is further noted is that the amplitude of this temperature profile (7.8°C) is larger than that expected. 2 to 3°C was thought to be the maximum temperature range encountered during the four epochs, but our larger offset is probably due to the uncertainty ($\pm 2.9^{\circ}\text{C}$) in the method of obtaining isotopic temperatures.

The temperature profile for 74014(Fig. 5.8) does not show the detail exhibited by 797MP1 and hence cannot be related to the epoch system described above. However, it must be noted that only 5 temperatures (2 replicate) have been determined between the dates 12.0 and 2.0 Ka and such detail may have been missed. Between these dates, temperatures increased to modern values up to the cessation of growth, the latter possibly corresponding to the Secondary Climatic Optimum. The temperature minimum at around 12 Ka may correspond to the small glacial advance seen at the Twocreekian/Valderan boundary of the Illinois Glacial Record (Figure 5.8). Higher temperatures just prior to this advance may represent a brief amelioration of climate during the Twocreekian.

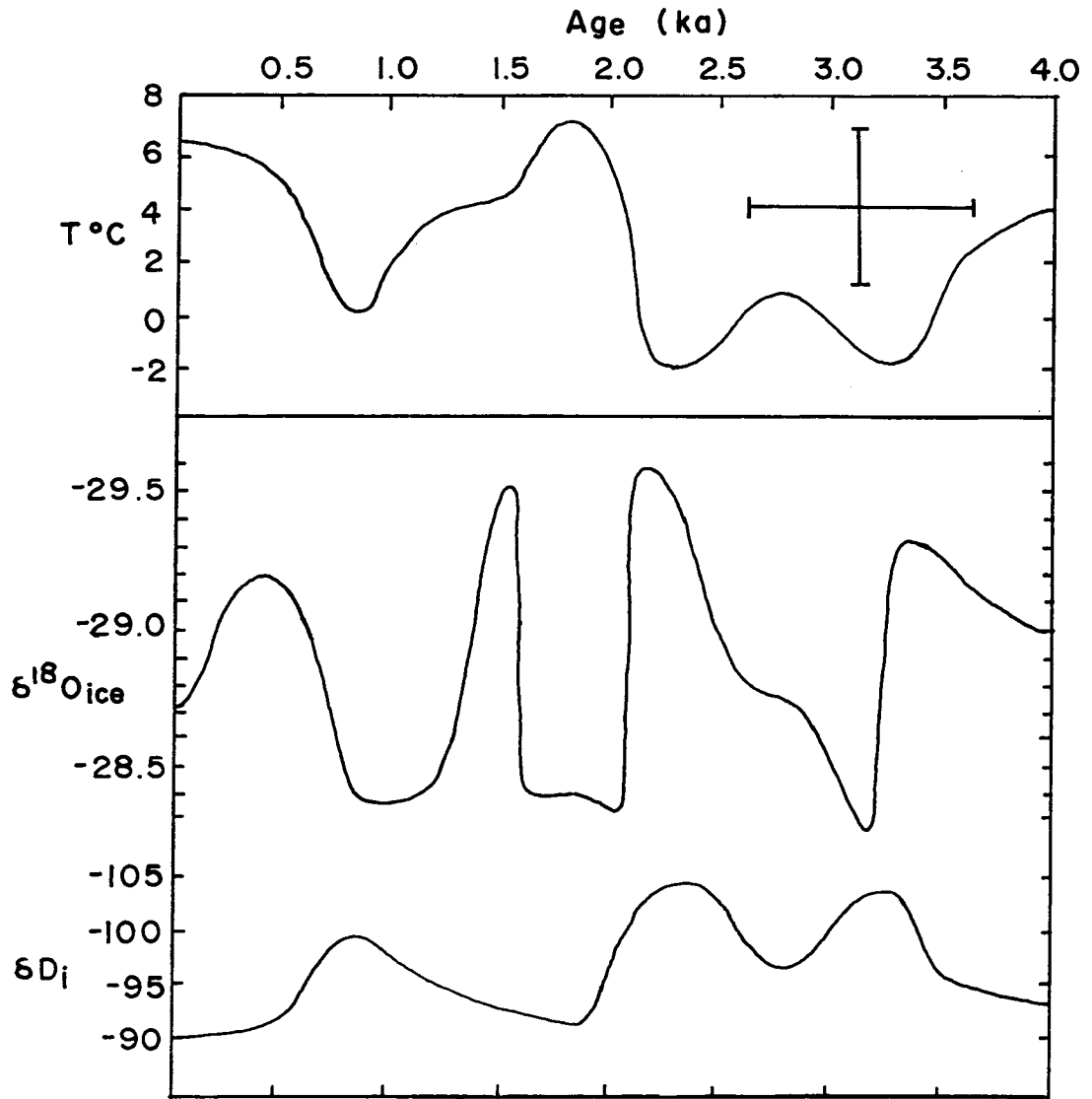
In conclusion, the temperature profiles for both 797MP1

and 74014 seem generally to be in accord with the other, independent, records presented here and no marked disagreements are noted. Stable isotope profiles are considered next.

2. δD_i and $\delta^{18}O_c$ versus Time

When δD_i for 797MP1 is compared to δD of the ice core record from Camp Century, Greenland (Dansgaard et al., 1969) which can be matched to the general climatic record presented by Gribben and Lamb (1978), some similarities are observed (Figure 5.3). The records appear to conform between 4.0 and 2.0 Ka and the discontinuity at around 2.0 Ka is seen in all records presented so far (i.e. both the speleothems and the ice core records). Two peaks are observed in the ice core record where δD_i records only a single peak at about 0.8 Ka. One explanation is that the first peak at 0.4 Ka in the ice core record has not been recorded in the speleothem due to temporary cessation in growth. However, careful perusal of the growth layers in the upper part of the deposit does not suggest that this occurred. The lack of correspondence of the records in the top section of the speleothem thus remains open to question. δD_i from 74014 (Figure 5.8) shows a general decrease to a minimum around 12 Ka. Thereafter values increase fairly steadily up until the deposit ceased to grow at 2 Ka. In this way, the profile closely resembles that of temperature. Again, the early part of the record, before δD_i reaches the minimum value, may correspond to a very brief warming period, assigned to the Allerød

Figure 5.3 A comparison of Isotopic Temperatures and δD_i from 797MP1 (N.Y.) with $\delta^{18}O$ of ice from the Camp Century Ice Core, Greenland (Dansgaard et al., 1969).



interstadial at 11.7 Ka in the Camp Century ice core record.

After the minimum δD_i , the increase in δD_i probably reflects the general warming period from the final cold pulse at 11.0 Ka which has continued to the present.

The $13.0 \pm 1.8\%$ and $12.3 \pm 3.0\%$ range in δD_i for 797MP1 and 74014 are somewhat larger than expected. The possibility that $\Delta\delta D_{s-i}$ is temperature dependent and generates a wider range of δD_i than expected has already been raised. Nevertheless, it should be pointed out that some continental sites do experience large ranges in δD , up to 30% in the Sinai and Negev deserts over, admittedly, glacial to interglacial periods (Gat and Carmi, 1970, and Gat and Issar, 1974), whilst some experience no change at all, as in the London Basin for example (Evans et al., 1978). Harmon et al. (1979), for a number of North American cave sites, report an average range of δD_i of 12% for maximum temperature changes. However, in all the cases mentioned so far, including the speleothems discussed here, δD is increasingly depleted at progressively lower temperatures within a given record.

In summary, although there are some reasons to suspect that the range of δD_i in 797MP1 (and 74014) are rather too great, they fall within the range published by other workers.

Of interest is the possibility of using the stable isotope data from speleothems to investigate changes in the isotopic composition of sea water, and changes in the d_t inter-

cept. Unfortunately, the two Holocene records presented do not really extend far back enough for these changes to be noted. Ninkovitch and Shackleton (1975) and Lorius et al. (1980) report little change in the composition of seawater and d_t respectively, over the last 10 Ka. These factors are considered in the next section when interstadial speleothems are discussed.

Finally, Figures 5.4 and 5.5 plot δD_i and $\delta^{18}O_c$ versus isotopic temperature. (The slope values reported for $d\delta D_i/dT$ have been converted to $d\delta^{18}O_i/dT$ by dividing by 8.) $d\delta^{18}O_i/dT$ for 797MP1 and 74014 are +0.20 and +0.21‰/°C respectively whereas $d\delta^{18}O_c/dT$ are -0.08 and -0.04‰/°C respectively. The slopes may reflect a dependence of δD_i on temperature, which almost equals the opposite dependence of α_{cw} on site temperature of about -0.24‰/°C, hence the low slopes of $d\delta^{18}O_c/dT$. These values are reasonable for continental sites (Table 3.1).

5.1.3.2 Interglacial/Interstadial Records

1. Temperature versus Time

The four interstadial speleothems, whose data is presented here, extend from 74 Ka to 27 Ka. The three speleothems from Vancouver Island together form a continuous record extending from 60 Ka to 28 Ka and the one stalagmite from Iowa covers a similar period from 74 Ka to 27 Ka. The records from the two areas can thus be compared.

The temperature profile of the Vancouver Island record, derived from δD_i and $\delta^{18}O_c$, is compared to that inferred by

Figure 5.4 Correlations of $\delta^{18}\text{O}_c$ (+) and δD_i with Isotopic Temperature for 74014, Iowa.

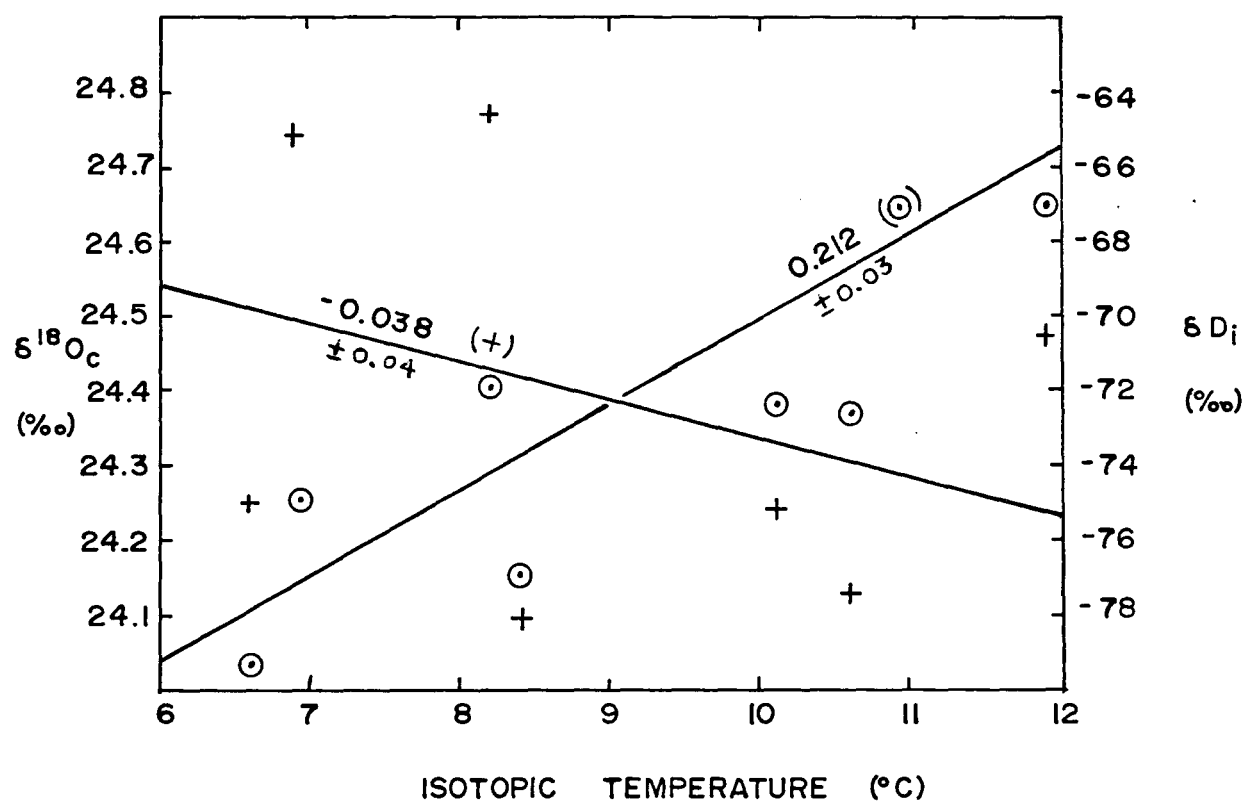
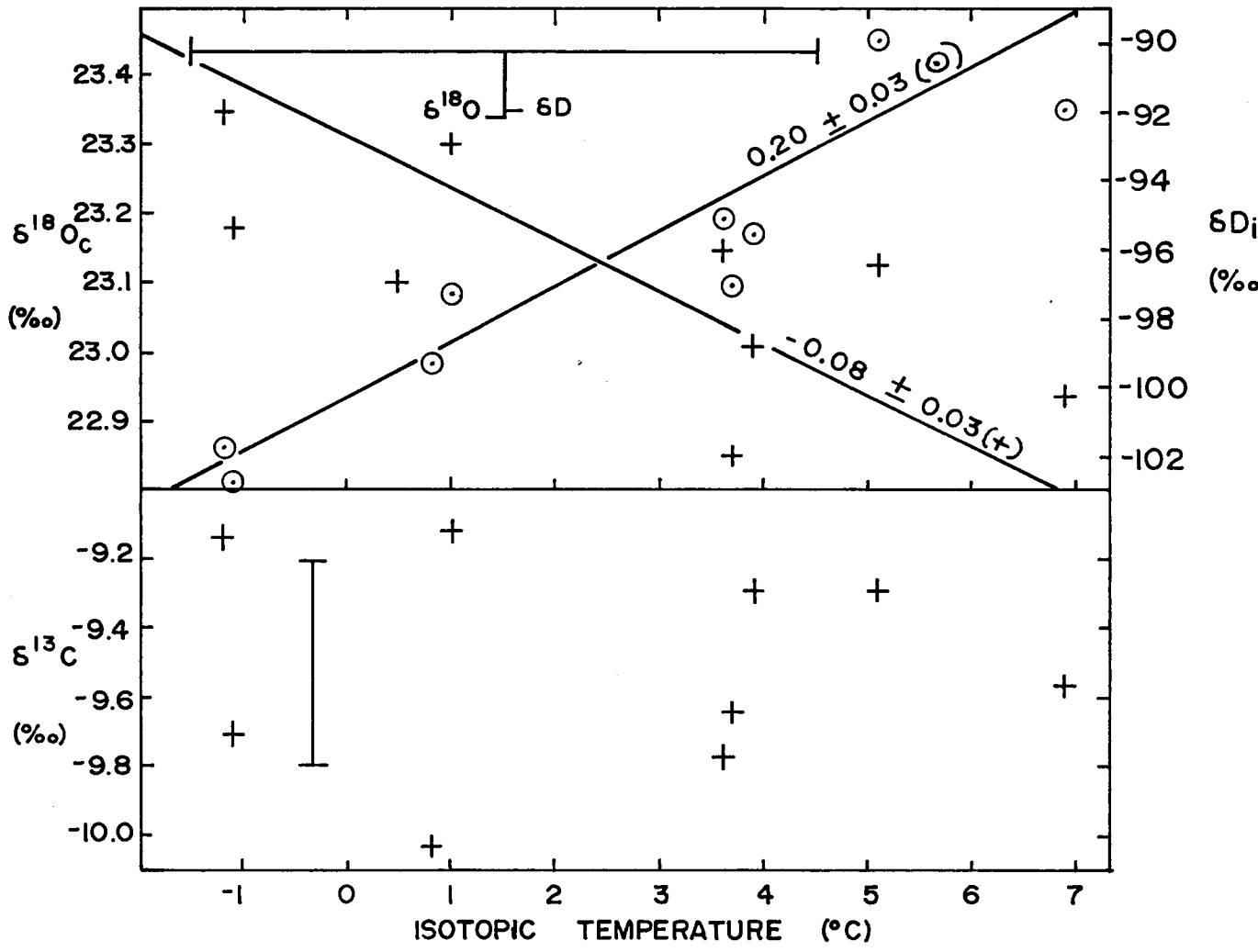


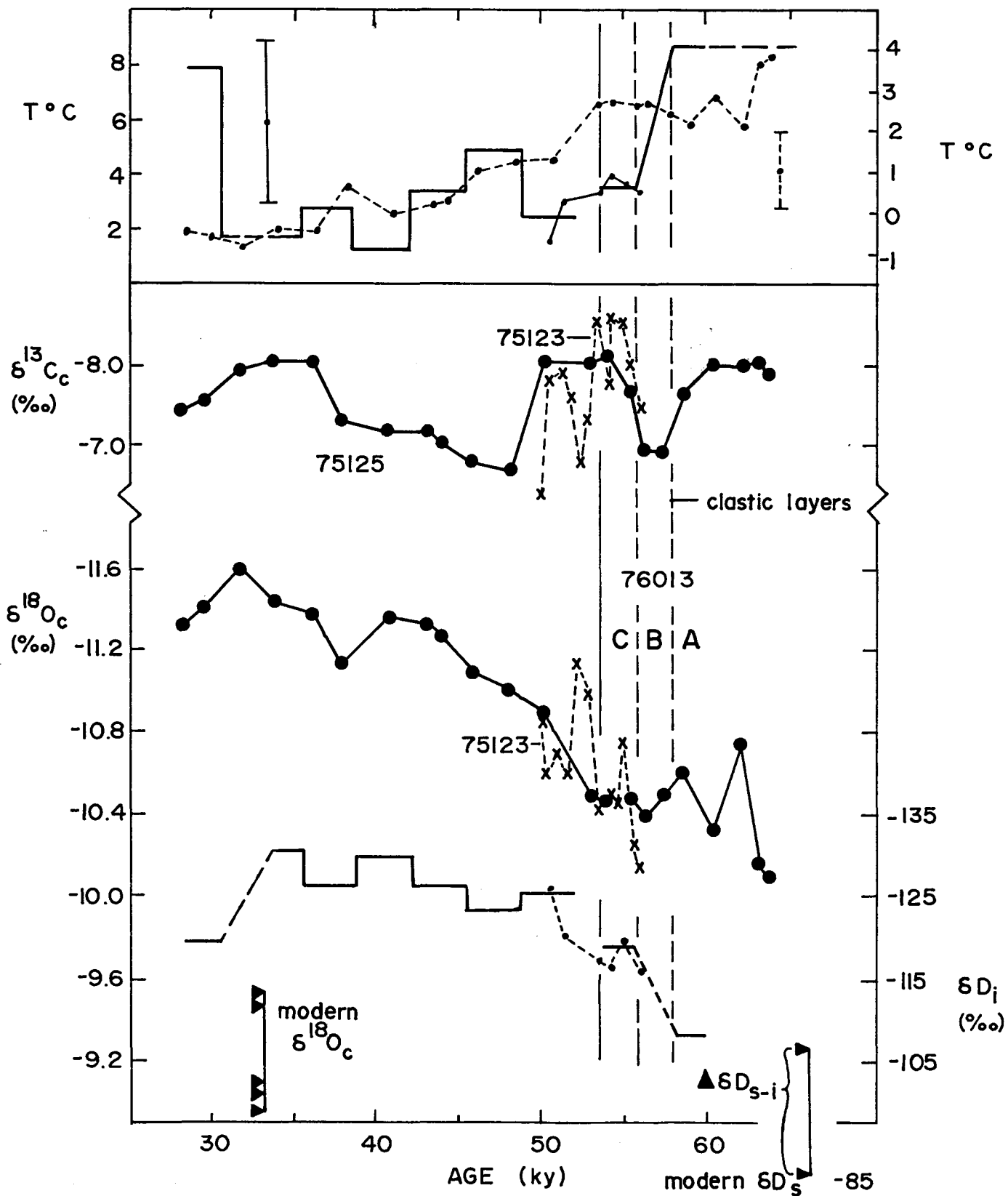
Figure 5.5 Correlations of $\delta^{18}\text{O}_c(+)$, $\delta^{13}\text{C}$ and δD_i with
Isotopic Temperature for 797MP1, N.Y. Errors
are at 1σ .



Gascoyne et al. (1980) (Figure 5.6). These workers determined site temperature by making estimates of the past $\delta^{18}\text{O}_p$ (p = precipitation). Since Vancouver Island is a marine site, $d\delta^{18}\text{O}_p/dT$ was assumed to be that determined by Dansgaard (1964) for a wide range of present day marine environments, namely $0.7\text{‰}/^\circ\text{C}$. Allowance was then made for the change of isotopic composition of seawater for that period (0.65‰) based on the deep sea foraminiferal record of Ninkovitch and Shackleton (1975). Interestingly, Gascoyne et al. (1980) found that $d\delta^{18}\text{O}_p/dT$ had to be greater than or equal to Dansgaard's estimate of $0.7\text{‰}/^\circ\text{C}$, as lower values generate sub-zero temperatures. Use of $0.7\text{‰}/^\circ\text{C}$ just yields positive temperatures within experimental error (see top of Figure 5.6). Their temperature record, falling from 60 Ka to 32 Ka, agrees with the palynological and sedimentological observations of others for the region (see Gascoyne (1979) for review).

In general, there is agreement in the trends of the two temperature records presented in Figure 5.6; temperatures fall from maximum values at about 60 Ka to a minimum around 32 Ka. The sudden fall in temperature at 56 Ka to a trough between 56 Ka and 50 Ka and the sudden rise in temperature after 32 Ka obtained in this study are not seen in the record of Gascoyne et al. (1980). Furthermore, the former record appears to be offset from the latter by about $+2^\circ\text{C}$. It is difficult to evaluate these differences because even if only the systematic

Figure 5.6 Plots showing $\delta^{18}\text{O}_c$, δD_i , $\delta^{13}\text{C}$ and Isotopic Temperatures of three speleothems; 75125, 75123 and 76013, from Cascade Cave, Vancouver Island. Also shown are the temperatures determined by Gascoyne et al. (1980) and $\delta^{18}\text{O}_c$ and $\delta^{13}\text{C}$ values are from these authors too. Solid and dotted lines (temperature scales) refer to left and right hand axes respectively.



errors in temperature are taken into account, the temperature differences become barely significant. If one then goes on to consider the errors involved in the estimate of $d\delta^{18}\text{O}_p/dT$, namely the assumption of 0.7‰/°C for modern marine environments being valid in the past (values up to 0.9‰/°C have been encountered, see Table 3.1) and the precision of deep sea core dating, then perhaps only very broad comparisons can be made.

The isotopic temperature record for 74017 is presented in Figure 5.7. Again, relatively large systematic errors in temperature determinations permit only broad interpretations to be made.

This profile, along with $\delta^{18}\text{O}_c$ and δD_i , has been placed in context with other records of the Wisconsinan Glacial Stage as given by a number of workers (Figure 5.8). The Illinois Glacial Record (Frye and Willman, 1973) is also accompanied by a relative temperature curve based on a number of glacial and periglacial observations. The Iowa Glacial Record (Leighton, 1957) is included with that of the Eastern Great Lakes (Dreimanis and Goldthwait, 1973).

At around 65 Ka, the speleothem yields temperatures higher than at any other time along its record. This event corresponds in time to a period of glacial retreat seen in the Eastern Great Lakes Glacial Record but is perhaps a little prior to the estimated date of a period of warmer conditions observed in the more proximal Illinois Glacial Record at around

Figure 5.7 Plot showing $\delta^{18}\text{O}_c$, δD_i , $\delta^{13}\text{C}$, water yields and Isotopic Temperatures from Coldwater Cave, Iowa. Solid and dotted lines refer to left and right hand axes respectively. Note change in time scale.

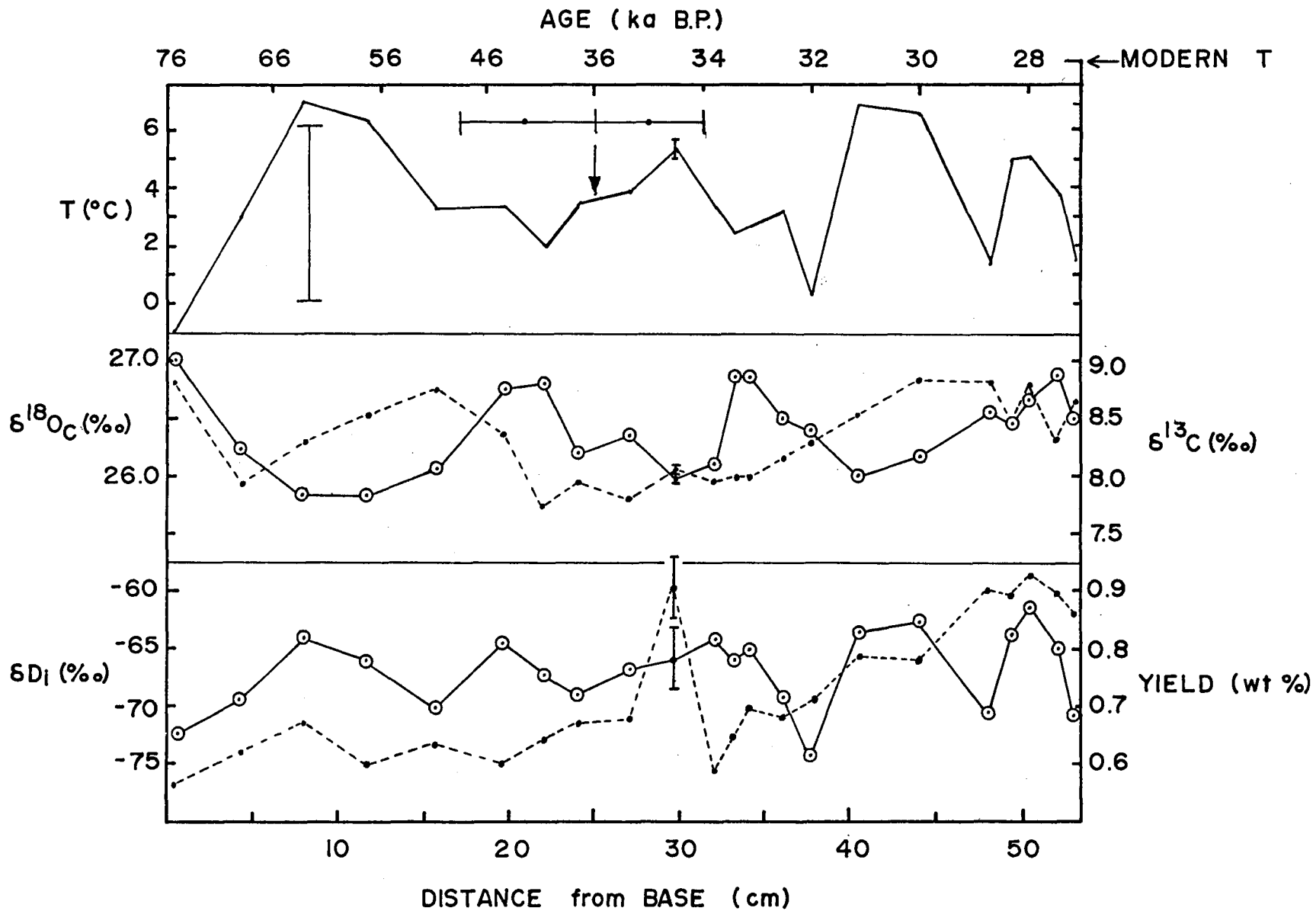
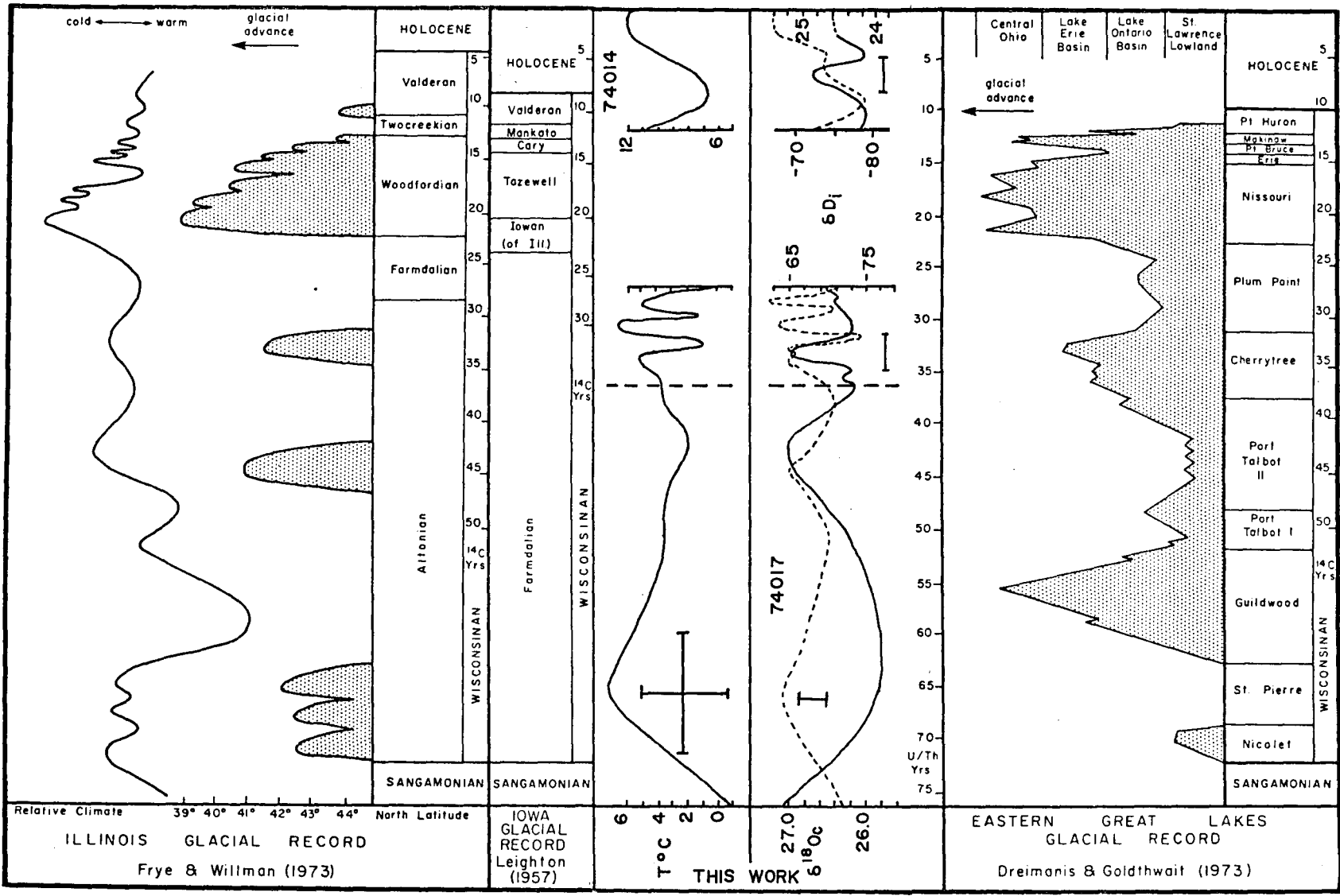


Figure 5.8 Comparison of the glacial stratigraphic records of the Eastern Great Lakes, Illinois, and Iowa with the Iowa speleothem isotopic paleoclimate record. The time scale for the glacial stratigraphic records is based upon ^{14}C ages and that of the speleothem record from $^{230}\text{Th}/^{234}\text{U}$ ages. Compilation of data other than that from speleothems 74017 and 74014 is that of Harmon (1975).

TIME (10³ Years B.P.)



60 Ka. Given the relative precision of the U/Th and ^{14}C methods used to date these events, they could be coeval, especially as the Altonian warm stage is at or beyond the limit of ^{14}C dating. The cooler period observed at the beginning of the Illinois Glacial Record at the Sangamon/Wisconsinan boundary is matched by that of 74017 and may be correlated with the Nicolet Glacial Advance at 70 Ka seen in the Eastern Great Lakes Glacial Record. All records, including 74017, from 65 Ka onwards, hint at a general episodic cooling of climate ending at 17 Ka, the Wisconsinan Glacial Maximum. Of note, are the minima seen in the record of 74017 at 42 Ka and 32 Ka matched by a glacial advance and cooling in the Illinois Glacial Record at 44 Ka and 34 Ka, the latter corresponding to the Cherrytree Glacial Advance observed in the Eastern Great Lakes Glacial Record. A final warm peak seen in the record of 74017 is reflected in the Farmdalian and Plum Point glacial retreats in the Illinois and Eastern Great Lakes records respectively. Abrupt cooling in both glacial records at around 23 Ka, corresponding to the onset of the Wisconsinan Glacial Maximum, coincided in time with the cessation of growth of 74017 and may have been caused by the development of permafrost.

In summary, it is noted that there is considerable agreement between the relative climatic record of Frye and Willman (1973) and the temperature record of 74017 which would have been expected in view of their geographic proximity.

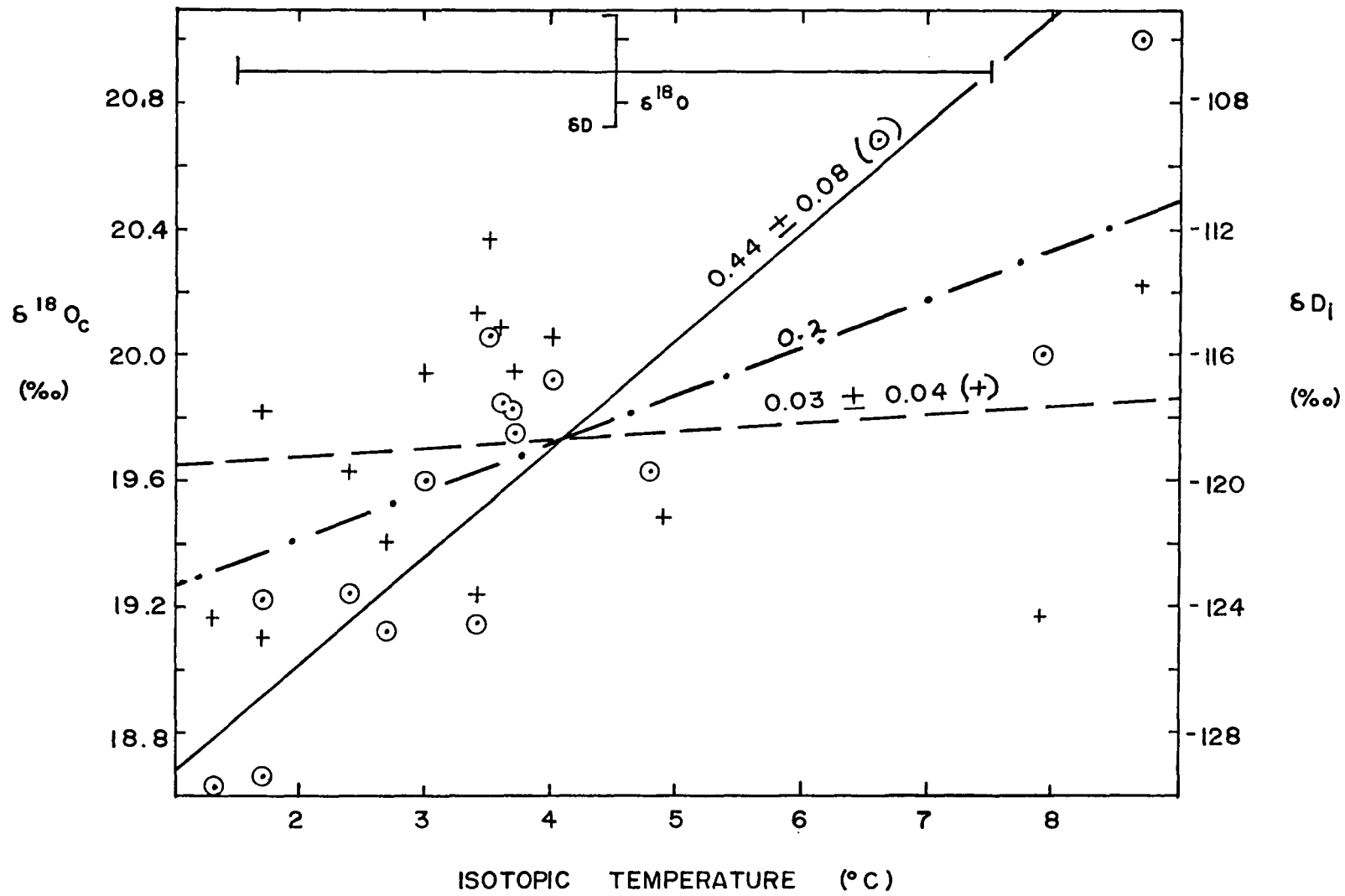
2. δD_i and $\delta^{18}O_c$ versus Time

The δD_i profiles for all three Vancouver Island speleothems are similar in shape to those of $\delta^{18}O_c$ and like them, the records from all three deposits link up over common periods of deposition, lending some assurance to the validity of the results.

The total range of δD_i in the records is 24‰. Given that the temperature range is between 7°C (this work) and 5°C (Gascoyne et al., 1980), the present day $d\delta^{18}O_p/dT = 0.7 \text{ ‰/°C}$ (5.6‰/°C for deuterium) and the change in $\delta^{18}O$ of seawater over that period equals 0.65‰/°C (5.2‰/°C in deuterium), the total range of δD_i expected is between 34.0‰ and 22.8‰ respectively. The latter figure derived from the temperature range of Gascoyne et al. (1980) is the same as the measured range. Again the error in isotopic temperatures ($\pm 2.9^\circ\text{C}$) is emphasized with respect to these comparisons and the use of a 7°C range in temperature has, likewise, a large error associated with it.

The similarity of the shape of the $\delta^{18}O_c$ profile to the δD_i profile is also indicative of the strong dependence of δD_p on temperature. The value of 0.44‰/°C for $d\delta^{18}O_i/dT$ ($= 1/8 (d\delta D_i/dT)$) in Figure 5.9 can be compared with Gascoyne et al.'s estimate of 0.57‰/°C which takes into account the changing isotopic composition of seawater. The presence of the two high temperature points has the effect of reducing the $d\delta D_i/dT$ value. Likewise, the two

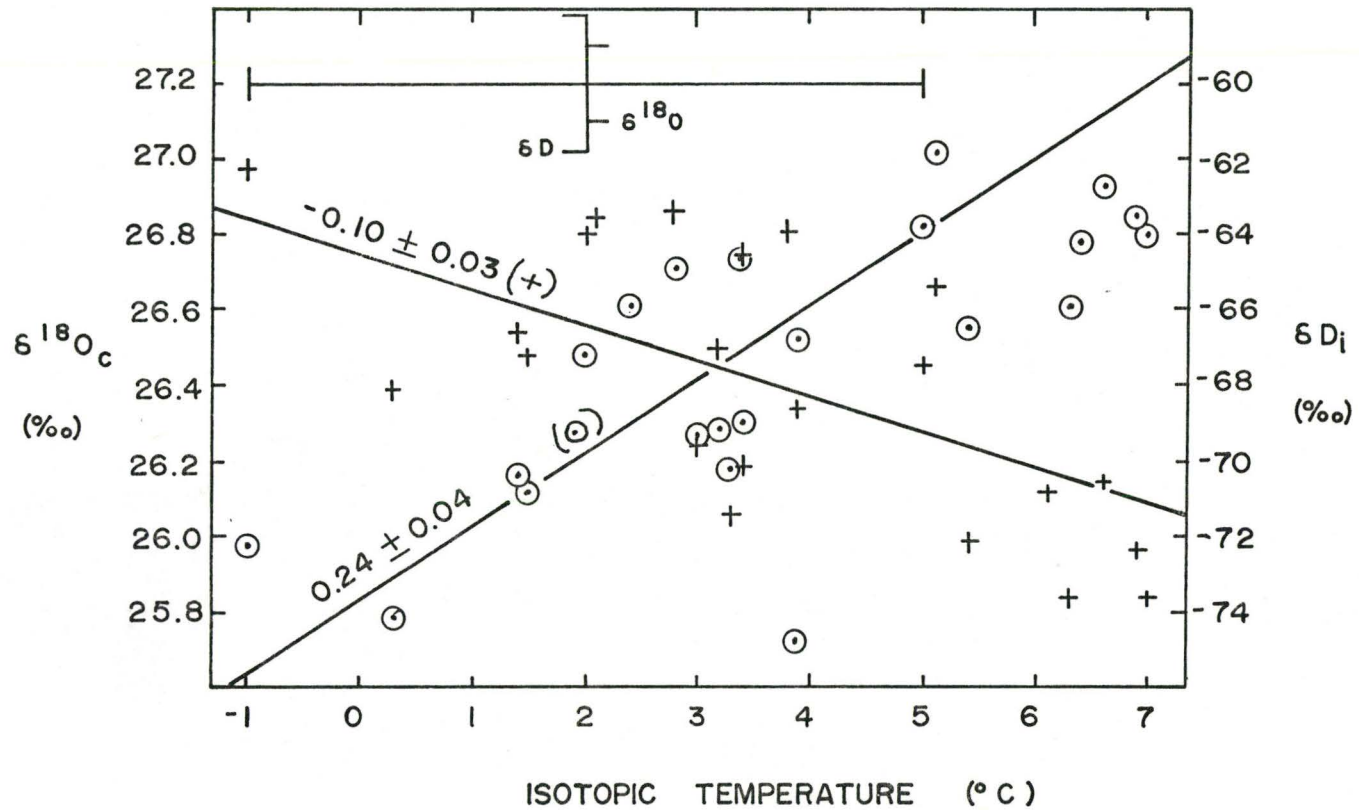
Figure 5.9 Correlations of $\delta^{18}\text{O}_c$ (+) and δD_i with Isotopic Temperatures for speleothems 75125, 75123, and 76013, Vancouver Island. Errors are at 1σ .
---. Slope of $0.2\text{‰}/^\circ\text{C}$ shown for comparison (see page 242).



high temperature points reduce $d\delta^{18}O_c/dT$ to a low value of $0.03\%/^{\circ}C$ but the important point to make at Vancouver Island is that $d\delta^{18}O/dT > 0$, as Gascoyne et al. suggest, and in distinct contrast with its behaviour elsewhere. With a magnitude of $d\delta D_i/dT$ of $0.44\%/^{\circ}C$, one would expect $d\delta^{18}O_c/dT$ to be around $0.20\%/^{\circ}C$ (as shown in figure 5.9) due to the effect of α_{cw} . Thus, in summary, the results of Figure 5.9 are viewed cautiously with the speculation that the two highest temperatures determined are suspect.

The δD_i record for 74017 may be compared to the various glacial records mentioned earlier. A tentative comparison could go as follows: At around 74 Ka δD_i is relatively light corresponding to the Nicolet advance in the Eastern Great Lakes and a greater, triple advance in the Illinois record. At 66 Ka δD_i is heavy reflecting the St. Pierre retreat (Eastern Great Lakes) and the largest retreat in the Altonian (Illinois). δD_i is lighter again at 50 Ka recording the Guildwood advance (Eastern Great Lakes) and the greatest advance in the Altonian. The δD_i peak at 45 Ka may be related to either the Port Talbot I or II retreat leaving a trough at 38 Ka to be ascribed to the Cherrytree and final Altonian advances. The generally high values of δD_i from 34 Ka to 27 Ka may correspond to the Plum Point and Farmdalian retreats. The final descent of δD_i at 27 Ka would be due to the onset of full glacial conditions as reflected in the Missouri and Woodfordian major advances. Because of the errors in U/Th and ^{14}C dating (particularly earlier

Figure 5.10 Correlations of $\delta^{18}\text{O}_c$ (+) and δD_i with Isotopic Temperature for 74017, Iowa. Errors are at 1σ .



than 50 Ka for ^{14}C dating), these comparisons are merely suggestive rather than being definitive. However, the general tendency for δD_i to become lighter between 66 and 36 Ka does seem to agree with the progressively cooling conditions depicted in Frye and Willman's relative climate (Figure 5.8).

The range in δD_i for 74017 is around 12‰, the same as that measured for the two Holocene (continental) records but smaller than that of Vancouver Island. The similarity of the range of δD_i in 74017 to the Holocene records is somewhat surprising because the ice volume effect (0.65‰ in $\delta^{18}\text{O} \cong 5.2\%$ in δD for this period) should have been observed. With similar temperature ranges in each speleothem, one would have expected the range of δD_i in 74017 to be about 7‰. However, the effect of changing weather regimes such as the change in length of storm trajectories cannot be taken into account. Increase in the length of storm tracks during cooler periods, for example, could account for the discrepancy, and Vancouver Island, receiving unvarying westerly weather, would not encounter it.

Plotting $\delta^{18}\text{O}_c$ and δD_i versus isotopic temperature for 74017 yields essentially similar slopes as the continental Holocene records $d\delta^{18}\text{O}_i/dT (=1/8(d\delta D_i/dT)) = +0.24\%/^{\circ}\text{C}$ and $d\delta^{18}\text{O}_c/dT = -0.10\%/^{\circ}\text{C}$. Again the continental $d\delta^{18}\text{O}_p/dT$ effect tends to override the effect of temperature on α_{cw} (figure 5.10).

5.1.4 General Discussion

The $\delta^{18}\text{O}_c$, δD_i and temperature data presented in the

previous sections allow some general comments about past climates and the usefulness of speleothems as paleoclimate indicators to be made.

The viability of $\delta^{18}\text{O}_c$ records alone as relative paleotemperature indicators is in some doubt. The three $d\delta^{18}\text{O}_c/dT$ values determined from continental deposits (797MP1, 74014 and 74017), although negative, are close to zero. This means that the dependence of $\delta^{18}\text{O}_c$ on site temperature (α_{cw}) barely exceeds the countervailing effect of $d\delta^{18}\text{O}_p/dT$. In these cases, it would be unreasonable to ascribe troughs and peaks in the $\delta^{18}\text{O}_c$ profiles to warming and cooling events respectively. The profile for 74017 (Figure 5.8) illustrates the dilemma quite well. At 65 Ka, for example, the trough corresponds to a warming event but peaks at 43 Ka and 33 Ka also appear to reflect warming events. The shape of the temperature profile for 74014 is not reflected in the $\delta^{18}\text{O}_c$ record either. The problem of interpretation, however, in the Holocene record of 797MP1 is less severe and peaks appear to relate to cooler periods. The one δD_i value for 77151B from England permitted the calculation of an isotopic temperature point equal to zero (see Table 4.9). This corresponds to a distinct peak in $\delta^{18}\text{O}_c$ at 254 Ka which had been taken to be a cooling event based on comparison with modern calcite (Gascoyne, 1979). The value of $d\delta^{18}\text{O}_p/dT$ for the U.K. is generally low, varying with locality, and averaging about $0.15\%/^{\circ}\text{C}$ (Evans et al., 1978) and if it had the same value in

the past, the use of a negative dependence of $d\delta^{18}\text{O}_c/dT$ is probably a valid application to the interpretation of $\delta^{18}\text{O}_c$ profiles. A general conclusion that can be drawn from these data is that unless $d\delta^{18}\text{O}_p/dT$ is significantly less than the temperature dependence of $\delta^{18}\text{O}_c$ on α_{cw} , then $\delta^{18}\text{O}_c$ profiles cannot be interpreted unambiguously.

In the case of the three speleothems from Vancouver Island (a maritime site) there seems less of a problem (Figure 5.6); $d\delta^{18}\text{O}_c/dT$ is dominated by $d\delta^{18}\text{O}_p/dT$ and therefore a lightening of $\delta^{18}\text{O}_c$ corresponds to a fall in temperature. The similarity of the δD_i profile to that of $\delta^{18}\text{O}_c$ helps to confirm the dominance of the precipitation effect over the α_{cw} effect and, indeed, that due to the changing isotopic composition of seawater.

In all the calculations of isotopic temperatures, d_t and d_o in the meteoric water line equation have been assumed to be close to or equal to 10‰. The justification for the use of this value stems from the fact that no fully glacial deposits have been studied. Deuterium deficiency during interstadial periods was probably not very different from that of today. Lorius et al. (1980) determine a shift of around 4‰ for the Wisconsin Glacial Maximum. A 4‰ change in the meteoric water line to a lower intercept raises temperatures by 2.3°C. In both the Vancouver Island and Iowa records raising the temperature by this amount seems, in part, unreasonable. Isotopic temperatures from

the former depart even further from those calculated by Gascoyne et al. (1980) but temperatures from the Iowa site could be raised by 2.3°C and still not exceed the present day cave temperature. However, since both records are interstadial, temperature changes due to changes in d_t should be smaller. In any case, changing of temperatures using the maximum value of d_t does not change the trend of the arguments presented earlier.

Assuming that δD_i records are an accurate reflection of past precipitation, then it should be possible to observe changes in δD_p from one type of climate to another, from glacial to interglacial. The problem reduces to comparing Mid-Wisconsin δD_i values to modern values. The approach is the same as that of Harmon et al. (1979) who compared average δD_i from fossil deposits and subtracted from this δD of modern meteoric water giving rise to the quantity $\Delta\delta D(t)$. They found that the average glacial to interglacial shift to be -12% and for interglacial to interstadial, -7% , as discussed in Chapter 1. However, it should be noted that if fluid inclusions are compared to modern precipitation, fossil precipitation would always appear to be depleted by $\geq 22.1\%$ (see 4.4.7). When this is done for Iowa and Vancouver Island, the results are contradictory.

The average δD_i value for 74017 (Iowa) is $-67.1(-45.0\%)$ whereas modern fluid inclusions give $-67.0(-44.9\%)$ and $-78.1(-56.0\%)$ for the top of 74017 and 807CH3 (Table 4.10) respectively (Figures in brackets are corrected for $\Delta\delta D_{s-i}$). These data are confusing because modern drip water for the cave is around -54% , consistent with 807CH3 but not the (2,000 year-

old) top of 74014. Nonetheless, using the mean δD_i values for 74017 and modern drip water $\Delta\delta D(t)$ gives +9‰ ; the reverse of that expected. Mean δD_i for the Vancouver Island deposits is -120.4 (-98.3)‰ whereas modern drips are -88‰ (Chapter 3), yielding a $\Delta\delta D(t)$ value of -10.3‰.

The enrichment in fossil δD_i at the Iowa site is somewhat puzzling. One explanation may be that the determination of δD_p is in error although the data of 807CH3 would not support this. Perhaps a more likely explanation is that during the Wisconsinan interstadial, the cave was dominated by heavier summer recharge water. Estimates made of C-H bound hydrogen in ancient and modern wood cellulose suggest that during the Wisconsinan Glacial period precipitation was enriched in deuterium by +19‰ (Yapp and Epstein, 1977). Harmon et al. (1979) suggest that a seasonal bias towards heavy summer precipitation might explain the 19‰ enrichment in hydrogen. At this stage, explanations of the enrichment of δD_i in the Iowa deposit remain speculative.

The $\Delta\delta D(t)$ of -10.3‰ for interstadial Vancouver Island is, however, consistent with the idea of an increased ocean-continent temperature gradient during cooler times which more than compensated for the increase in deuterium content of the world's oceans.

Summary

From the preceding sections of this chapter in which

stable isotope and isotopic temperature profiles of six speleothems were presented and discussed, the following general points can be made.

1. Errors in isotopic temperatures ($\pm 2.9^{\circ}\text{C}$) permit only broad interpretations of temperature profiles whose range is typically 7 to 8°C .

2. Temperature profiles broadly parallel the relative climatic records, such as glacial advances, presented in the literature. However, lack of dating precision, particularly in the ^{14}C dates, beyond 50 Ka make some of these comparisons dubious.

3. The two Holocene stalagmite records from Iowa and N.Y. show some agreement both in δD_i and temperature.

4. The two Holocene stalagmite records show some agreement with a Greenland ice core when the timing of δD peaks is compared.

5. δD_i decreases with falling (isotopic) temperature within a given record but when comparisons are made with mean interstadial δD_i and modern δD_i , there is disagreement. The Vancouver Island record yields an isotopic depletion of -10% from interglacial to interstadial climate whereas the Iowa record suggests the reverse at $+9\%$. The discrepancy is not understood.

6. In the three continental deposits, $d\delta^{18}\text{O}_p/dT$ almost exactly counteracts the change in $\delta^{18}\text{O}_c$ due to the temperature

dependency of α_{cw} . Therefore, caution is advised in using $\delta^{18}O_c$ alone to interpret relative warming and cooling episodes except where $d\delta^{18}O_p/dT$ is significantly different from the α_{cw} effect as in the U.K. or on Vancouver Island. In the latter case $d\delta^{18}O_p/dT$ was found to be $\geq 0.44\%/^{\circ}C$, dominating both the ice volume and α_{cw} effects.

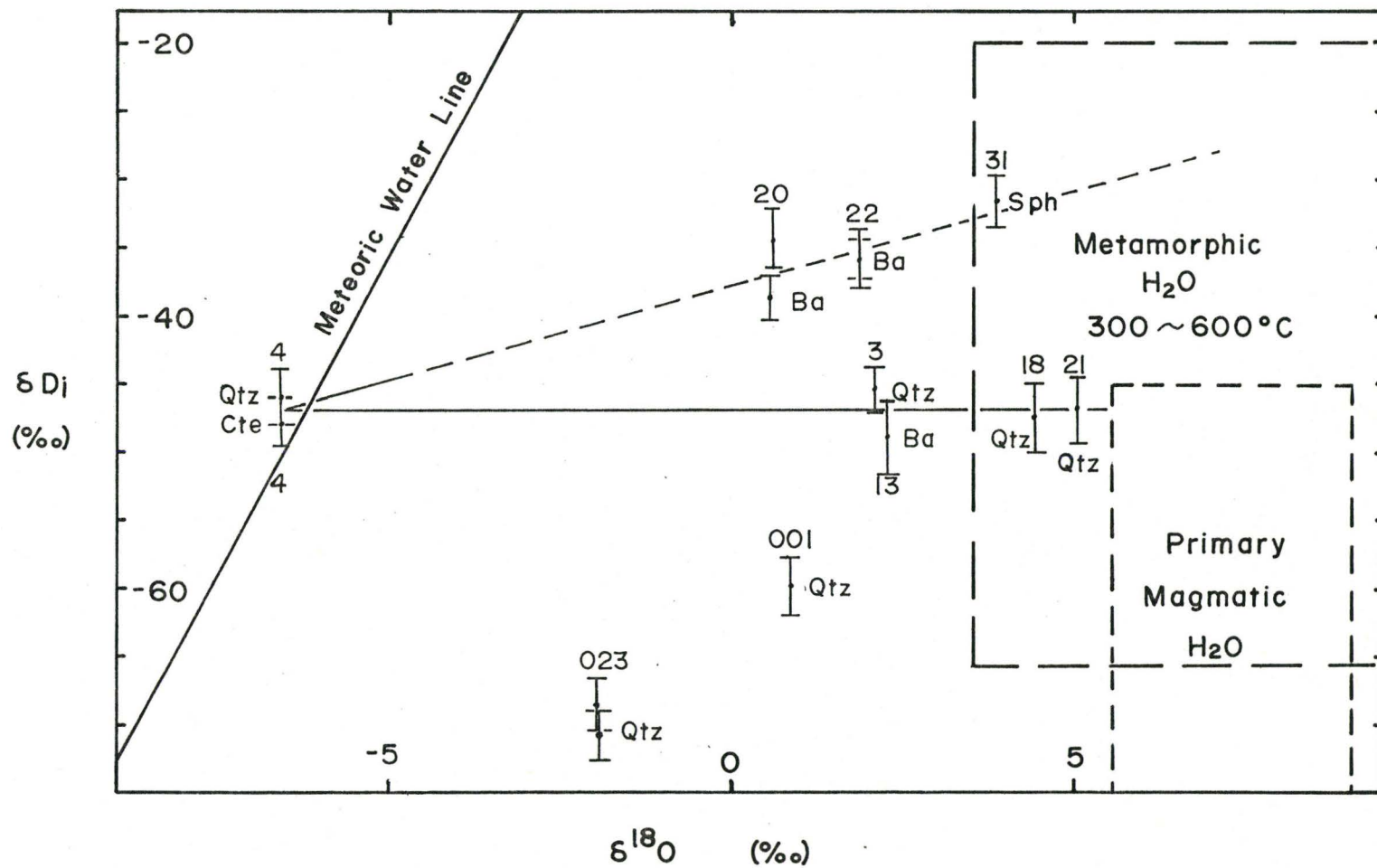
7. The change in δD of seawater during the Mid-Wisconsin Interstadial is observed in the Vancouver Island record and may be just discernable in the Iowa record.

8. d_t changes from interglacial to interstadial periods are probably less than half that of interglacial to full glacial periods during which the change is 4%. Temperatures will be raised due to this effect by around $1^{\circ}C$ only, therefore, not significantly affecting the temperatures determined in which d_t was given the modern global value of 10 (unless otherwise stated).

5.2 Application of the Decrepitation Method to Hydrothermal Minerals

A number of minerals were collected from the Taulin hydrothermal ore body, China. These minerals included calcite, quartz, barite and sphalerite and all contained fluid inclusions to varying degrees. Water from these minerals was extracted following exactly the technique for calcites described in Chapter 2. The replication of the method for three pairs and a coexisting calcite and quartz (described in Chapter 4) is $\pm 1.3\%$, (Appendix V and Figure 5.11). All results are plotted

Figure 5.11 δD_i versus $\delta^{18}O$ for various hydrothermal minerals from the Taulin Ore Deposit, China. $\delta^{18}O$ values for the included water were inferred from sulphur isotope temperatures (Ding et al., 1982).
Qtz = quartz, Ba = Barite, Sph = Sphalerite and
Cte = Calcite.



on Figure 5.11 with $\delta^{18}\text{O}$ having been inferred from sulphur isotope temperatures and the oxygen in the quartz phases. The coexisting quartz and calcite (#4) plot close to the meteoric water line and, perhaps with exception of quartz sample #001 and 023, all other waters appear to have evolved from this starting composition. The horizontal and inclined lines are consistent with meteoric/magmatic or metamorphic water interaction. The horizontal line indicates exchange of oxygen only, possibly from the wall rock (Sheppard et al., 1971), whereas the inclined line suggests participation of hydrogen as well as oxygen similar to waters evolved from acid hot spring environments (Craig, 1963). However, the details of the work are provided by Ding et al., (1982) for further discussion. The above description as with that of the Tynong granites is merely to introduce the further applicability of the decrepitation method.(see also appendix V).

5.3 The Future

Because the developmental aspect of the work and its associated problems consumed a considerable portion of the time allotted to the thesis, the study can only be regarded as preliminary with feasibility being its aim. Regarded as such, there are clear pointers for future research. Of greatest importance, is the need to establish $\Delta\delta\text{D}_{\text{s-i}}$ and its possible temperature dependence with modern deposits and coeval seepage. Active soda-straws might be ideal for this

because they generally are fast growing and therefore (if active) young. They are very widely ranging even growing in caves where larger deposits are absent, thus allowing caves of widely varying temperature regimes to be sampled. To aid investigation of the systematics of the $\Delta\delta D_{s-i}$ effect, environmentally controlled laboratory experiments to grow calcite should be attempted.

If $\Delta\delta D_{s-i}$ can be better established then a huge number of continental sites are potentially available for paleoclimatic study. The recovery of depositional temperatures from speleothems is advantageous over relative climatic records as deduced, for example, from ice or marine foraminiferal cores. The relative accessibility of speleothems, with their intrinsically more reliable dating, adds to their importance as Pleistocene climate recorders.

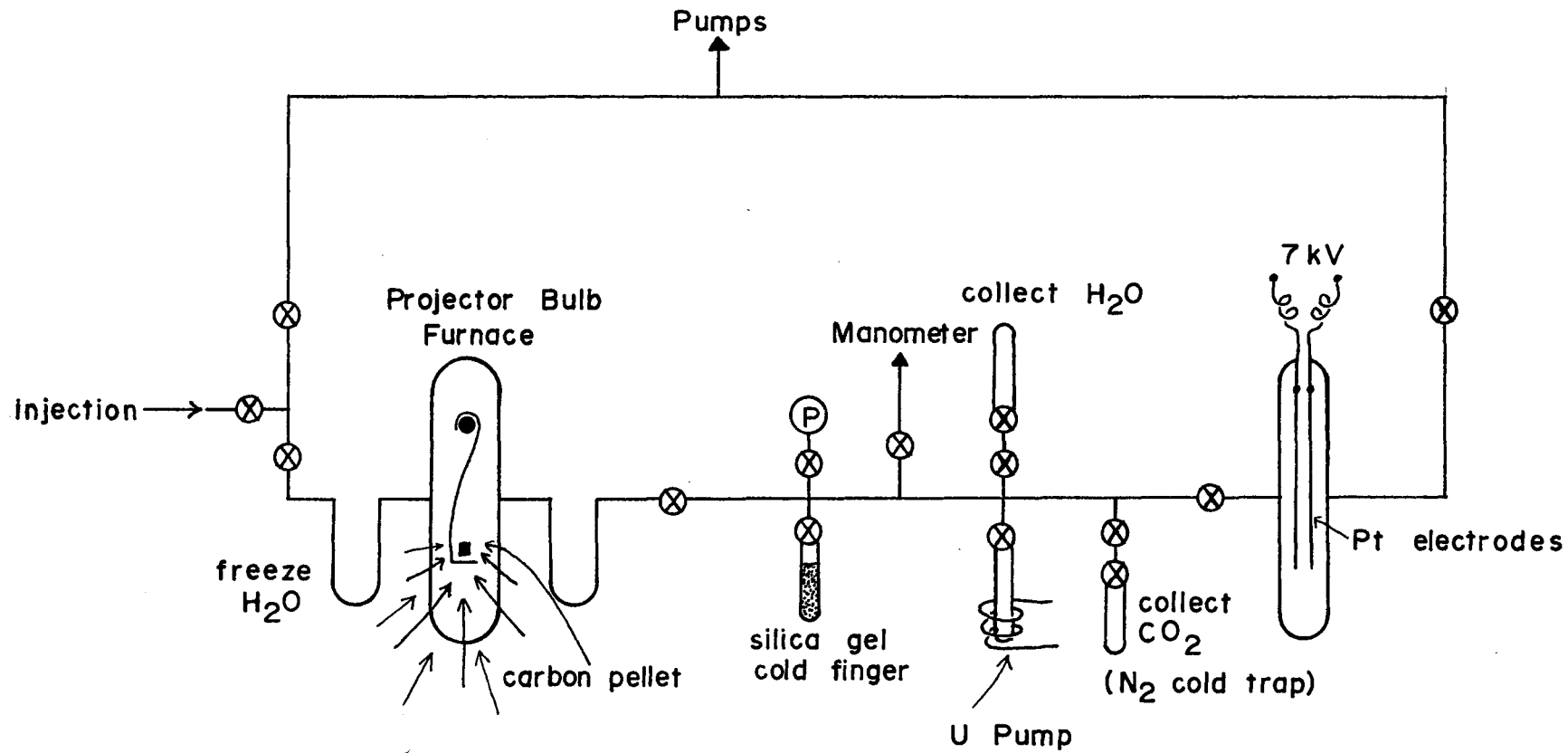
Immediately beyond the need to tighten up the calibration $\Delta\delta D_{s-i}$, is the need to test the geothermometer across the largest possible temperature range, but temporally rather than geographically, as suggested earlier. The difficulty of finding a deposit whose growth spans a glacial/interglacial period where a maximum temperature range should be encountered has been alluded to. Cave sites should be sought as far north as possible where speleothem growth persists during glacial maximum periods. The Wisconsinan Glacial Maximum is the best choice of time because it is the most recent and one of the

most intense glacial events recorded. An excellent complementary study to Late Wisconsinan climatology could be further work on sub-glacial precipitates. This is all the more pertinent because fluid inclusions from one sub-glacial precipitate, at least, appears to preserve the δD of the ice from which it was formed.

A few δD_i determinations on speleothems for which a record of $\delta^{18}O_c$ has been acquired allows a relative climatic scale to be established with some degree of certainty and δD_i can be used as a record itself. The latter would be useful (as mentioned in Chapter 1) for non-equilibrium deposits where disequilibrium has been induced by the rapid outgassing of CO_2 rather than by evaporation.

Finally, the appearance of a $\Delta\delta^{18}O_{s-i}$, in which $\delta^{18}O_i$ is depleted with respect to $\delta^{18}O_s$, requires further investigation. Success in this area, although indications are somewhat unpromising, would mean that paleotemperatures could be recovered without resort to estimates of meteoric water lines. Furthermore, in addition to ice cores, fluid inclusions could be used to determine past meteoric water lines too, and d_t determined as a function of both space and time. The measurement of δD and $\delta^{18}O$ simultaneously from a given group of fluid inclusions would remove the problem of sample inhomogeneity when measuring δD and $\delta^{18}O$ on separate aliquots and the need for large samples. An extraction line to do this was, in fact,

Figure 5.12 Apparatus for simultaneous production of H₂ and CO₂ from μ mole quantities of water.



constructed but lack of time meant that it was never tested but it is described nevertheless (see Figure 5.12). The line would utilize the water-gas reaction and is somewhat similar to, but simpler than, that used by Gray and Thompson (1979) in which water is passed several times over a carbon pellet. The water is converted to H_2 , CO_2 and CO . H_2 is collected as uranium hydride, CO_2 and CO are frozen down with liquid nitrogen, the latter on silica gel. The CO is converted to CO_2 with a cold electric discharge at 7 Kv between Pt electrodes. The resulting CO_2 and H_2 are finally removed for mass spectrometric analysis. This technique, if able to be combined with decrepitation methods described earlier, is potentially very powerful because of the relative rapidity of analyses, the quantity of information collected per extraction and its application to a wide selection of water carrying minerals.

Again it is emphasized that stable isotope analyses on fluid inclusions in minerals generally are somewhat few and as interest in such information increases, as appears to be happening at present, then methods like the above should gain importance. Although it is beyond the scope of the thesis to go into the multitude of applications that can be visualized, a general feature of all fluid inclusions is that they represent the "missing" phase necessary to isotope geothermometry and to the interpretation of environments in such systems. For example, the possibility of extracting water

from limestone lends itself to the study of diagenetic conditions of the limestone. The controversy of the origin of dolomite; whether it be a groundwater or marine (or both) based origin, might well be studied from the analysis of stable isotopes in the water it contains.

The presence of water in minerals appears to be extremely widespread and yet their isotopic study seems particularly in its infancy. Although the horizon looms large with possibility, the importance of unravelling Pleistocene climatology from speleothems **must** be underscored. Hopefully, the present study sheds further light on the complex systematics of these deposits such that this end might be achieved.

REFERENCES

- ADLER, H.H. and P.F. KERR, 1963. IR absorption frequency trends for anhydrous normal carbonates. *Am. Min.* 48, 124-137.
- AMBACH, W., H. EISNER, M. ELSÄSSER, U. LÖSCHHORN, H. MOSER, W. RAUERT and W. STICHLER, 1976. D, T and Gross-Beta-Activity Investigations on Alpine Glaciers. *J. Glaciol.*, 17, 77, 383-400.
- BACK, W. and B.B. HANSHAW, 1979. Major Geochemical Processes in the Evolution of Carbonate-aquifer Systems. *J. Hydrol.*, 43, 287-312.
- BATHURST, R.G.C., 1964. *Developments in Sedimentology: 12 Carbonate Sediments and Their Diagenesis*. Elsevier 658 pp.
- BEAVER, E., 1974. An improved electron impact ion source power supply. *Mass Spec. Orig. Papers*, 22, 3, 203-207.
- BIGELEISEN, J., M.L. PERLMAN and H.C. PROSSER, 1952. Conversion of hydrogenic materials to hydrogen for isotopic analysis. *Anal. Chem.* 24, 1356-1357.
- BLATTNER, P. and J.R. HULSTON, 1978. Proportional variations of geochemical $\delta^{18}\text{O}$ scales - an interlaboratory comparison. *Geochim. Cosmochim. Acta*, 42, 59-62.
- BLOOM, A.L., W.S. BROECKER, J.M.A. CHAPPELL, R.K. MATTHEWS and K.J. MESOLELIA, 1974. Quaternary sea level fluctuations on a tectonic coast: new $^{230}\text{Th}/^{234}\text{U}$ dates from the Huon Peninsula, New Guinea. *Quat. Res.*, 4, 185-204
- BOTTINGA, Y., 1968. Calculation of fractionation factors for carbon and oxygen isotopic exchange in the system calcite - carbon dioxide water. *J. Phys. Chem.*, 72, 800-807.
- BOTTINGA, Y. and H. CRAIG, 1969. Oxygen isotope fractionation between CO_2 and water and the isotopic composition of marine atmospheric CO_2 . *Earth Plan. Sci. Lett.*, 20, 250-256.
- BOWINS, R., 1978. Personal Communication.
- BROECKER, W.S. and E.A. OLSON, 1960. Radiocarbon measurements and annual rings in cave formations. *Nature*, 185, 93-94.

- BROECKER, W.S. and J. VAN DONK, 1970. Insolation changes, ice volumes, and the ^{18}O record in deep-sea cores. *Rev. Geophys. Space Phys.*, 8, 169-198.
- CRAIG, H., 1957. Isotopic standards for carbon and oxygen and correction factors for mass spectrometric analysis of carbon dioxide. *Geochim. Cosmochim. Acta*, 12, 133-149.
- CRAIG, H., 1961. Isotopic variations in meteoric waters. *Science*, 133, 1702-1703.
- CRAIG, H., 1963. Isotopic geochemistry of water and carbon in geothermal areas. *Proc. Spoleto Conf. on Nuclear Geol.*, Ed.: E. Tongiorgi, Spoleto 1963.
- CRAIG, H., 1965. The measurement of oxygen isotope paleotemperatures. *Proc. Spoleto Conf. on Stable Isotopes in Oceanographic Studies and Paleotemperatures*, 3, 3-24.
- CRAMER, J.J., G.P. BEAKHOUSE, I. McDOUGALL, Y.N. SHIEH and C.J. YONGE, 1982. Radiometric and Stable Isotopes in the Differentiated Tynong Monzogranite, Australia. In preparation.
- CULLINGORD, C.H.D., 1962. *British Caving: -An introduction to speleology*, Routledge and Kegan Paul Ltd., 592 pp.
- DANSGAARD, W., 1964. Stable isotopes in precipitation. *Tellus*, 16, 436-468.
- DANSGAARD, W., S.J. JOHNSEN, J. MØLLER and C.C. LANGWAY Jr., 1971. Climatic record revealed by the Camp Century ice core, *in* Late Cenozoic Glacial Ages, K.K. Turekian ed. Yale Univ. Press, New Haven, 1971, 37-56.
- DAVIS, G.H., G.L. NEYER and C.K. YEN, 1968. Isotope hydrology of the artesian aquifers of the Styrian Basin, Austria, *Steirische Beitr, Hydrologeol.*, 51.
- DELDERFIELD, J., 1978. Personal Communication.
- DING, T., H.P. SCHWARCZ and C.J. YONGE, 1981. Oxygen and Hydrogen Isotope Studies of the Taulin Ore Deposits, China. In preparation.
- DREIMANIS, A. and R.P. GOLDTHWAIT, 1973. Wisconsin glaciation in the Huron, Erie and Ontario Lobes. *Geol. Soc. Amer. Mem.*, 136, 71-105.

- DUPLESSY, J.C., J. LABEYRIE, C. LALOU and H.V. NGUYEN, 1971. Continental climatic variations between 130,000 and 90,000 years B.P. *Nature*, 226, 631-633.
- EARDLEY, A.J., 1962. *Structural Geology of N. America* (2nd ed.) Harper & Row, 743 pp.
- EPSTEIN, S., R. BUCHSBAUM, H. LOWENSTAM and H.C. UREY, 1951. Carbonate-water isotopic temperature scale. *Geol. Soc. Amer. Bull.*, 62, 417-426.
- EPSTEIN, S. and T.K. MAYEDA, 1953. Variations of ^{18}O of waters from natural sources. *Geochim. Cosmochim. Acta*, 4, 2.3-224.
- EPSTEIN, S., R.P. SHARP and A.J. GOW, 1970. Antarctic Ice Sheet: Stable isotope analyses of Byrd Station cores and interhemispheric climatic implications. *Science*, 168, 1570-1572.
- EVANS, G.V., R.L. OTLET, R.A. DOWNING, R.A. MONKHOUSE and G. RAE, 1978. Some problems in the interpretation of isotope measurements in British aquifers. IAEA Int. Symp. on Hydrol. Neuberberg. F.R.G.
- FISH, J.E., 1979. Xilitia Plateau. *Can. Caves*, Vol. 11, 1, 5-10.
- FISHER, H., P. PETTIJOHN, W. READ and J. WEAVER, 1960. *Studies of Appalachian Geology*. J. Wiley & Sons, 460 pp.
- FOLK, R.L. and R. ASSERETO, 1976. Comparative fabrics of length-slow calcite and calcitized aragonite in a Holocene speleothem, Carlsbad Cave, N. Mex. *J. Sed. Pet.*, Vol 46, 486-496.
- FOSTER, S.S.D., 1975. The chalk groundwater tritium anomaly - a possible explanation. *J. Hydrol.*, 25, 159-165.
- FRIEDMAN, I., 1953. D content of natural waters and other substances. *Geochim. Cosmochim. Acta*, 4, 49-103.
- FRIEDMAN, I. and K. HARDCASTLE, 1970. A new technique for pumping hydrogen gas. *Geochim. Cosmochim. Acta*, 34, 125-126.
- FRIEDMAN, I., A.C. REDFIELD, B. SCHOEN and J. HARRIS, 1964. Variation of the D content of Natural Waters in the Hydrologic cycle. *Rev. Geophys.*, 2, 177-224.

- GASCOYNE, M., 1977. Trace element geochemistry of speleothems. Proc. 7th Int. Speleo. Cong. Sheffield, England, Sept/1977, 205-208.
- GASCOYNE, M., 1979. Isotope and Geochronologic Studies of Speleothem. Ph.D. Thesis, McMaster Univ., Hamilton, Ontario.
- GASCOYNE, M., 1980. Personal Communication.
- GASCOYNE, M., H.P. SCHWARCZ and D.C. FORD, 1978. Uranium Series Dating and Isotope Studies of Speleothems: Part I; Theory and Techniques, BCRA Trans., V 5, No 2, pp 91-111.
- GASCOYNE, M., H.P. SCHWARCZ and D.C. FORD., 1980. Mid-Wisconsin Paleotemperatures from a Vancouver Island Stalagmite. Nature, 285, 474-476.
- GAT, J.R. and I. CARMI, 1970. Evolution of the isotopic composition of atmospheric waters in the Mediterranean Sea area. J. Geophys. Res., 75, 3039.
- GAT, J.R. and A. ISSAR, 1974. Desert isotope hydrology; water sources of the Sinai Desert. Geochim. Cosmochim. Acta, 42, 1117.
- GATES, W.L., 1976. Modeling the Ice-Age climate. Science, 191, 1138-1144.
- GONFANTINI, R., 1978. Standards for stable isotope measurement in natural compounds. Nature, 271, 534-536.
- GRAY, J., 1979. The Use of Stable-Isotope Data in Climate Reconstruction. Unpublished manuscript, 50 pp.
- GRAY, J. and P. THOMPSON, 1977. Climatic information from $^{18}\text{O}/^{16}\text{O}$ analysis of cellulose, lignin and whole wood from tree rings. Nature, 270, 708-709.
- GRAY, J. and P. THOMPSON, 1979. Personal Communication.
- GRIBBIN, J. and H.H. LAMB, 1978. Climatic change in Historical Times. In Climatic Change (ed) Gribbin, Cambridge Univ. Press, 280 pp.
- HAHNE, C., M. KIRCHMAYER and J. OTTENMENN, 1968. "Höhlenperlen" Besonders aus Bergwerken des Ruhrgebietes Modellfalle zum Studium diagenetischer Vorgänge an Einzeloiden. Neues Jahrb. Geol. Paläontol., A bhandl., 130, 1-46.

- HANSHAW, B.B. and B. HALLETT, 1978. Oxygen isotopic composition of sub-glacially ppt. calcite: Possible paleoclimatic significance. *Sci.*, V. 200, 16 June, 1978, 1267-1270.
- HARMON, R.S., 1975. Late Pleistocene paleoclimates in North America as inferred from isotopic variations in speleothems. Ph.D. Thesis, McMaster Univ., Hamilton, Ontario.
- HARMON, R.S. and H.P. SCHWARCZ, 1981. Changes of ^2H and ^{18}O enrichment to meteoric water and Pleistocene Glaciation. *Nature*, 290, 125-128.
- HARMON, R.S., D.C. FORD and H.P. SCHWARCZ, 1977. Interglacial chronology of the Rocky and MacKenzie Mountains based on $^{230}\text{Th}/^{234}\text{U}$ dating of calcite speleothems. *Can. J. Earth Sci.*, 14, 2543-2552.
- HARMON, R.S., P. THOMPSON, H.P. SCHWARCZ and D.C. FORD, 1978a. Late Pleistocene paleoclimates of North America as inferred from stable isotope studies of speleothems. *Quat. Res.*, 9, 54-70.
- HARMON, R.S., 1979. An isotopic study of groundwater seepage in the central Kentucky Karst, *Water Res.*, 15, 2, 476-480.
- HARMON, R.S., 1981. Personal Communication.
- HARMON, R.S., H.P. SCHWARCZ and D.C. FORD, 1978b. Late Pleistocene sea level history of Bermuda. *Quat. Res.*, 9, 205-218.
- HARMON, R.S., H.P. SCHWARCZ, P. THOMPSON and D.C. FORD, 1978c. Critical comment on 'Uranium-series dating of stalagmites from Blanchard Springs Cavern, Arkansas, USA'. *Geochim. Cosmochim. Acta*, 42, 433-439.
- HARMON, R.S., H.P. SCHWARCZ and J.R. O'NEIL, 1979. D/H ratios in speleothem fluid inclusions: A guide to variations in the isotopic composition of meteoric precipitation. *EPSL*, 42, 254-266.
- HARMON, R.S., H.P. SCHWARCZ, D.C. FORD and D.L. KOCH, 1979a. An isotopic paleotemperature record for late Wisconsin time in northeast Iowa. *Geology*, 7, 430-433.
- INGHRAM, M.G. and R.T. HAYDON, 1954. A Handbook on Mass Spectroscopy. Nuclear Sci. Ser. Rep. 14 Nat. Ac. Sci-Nat. Res. Council Pub., 311, 51 pp.

- HENDY, C.H., 1969. The isotopic geochemistry of speleothems and its application to the study of past climates. Ph.D. Dissertation, Victoria Univ., Wellington, New Zealand.
- HENDY, C.H., 1971. The isotopic geochemistry of speleothems I. The calculation of the effects of different modes of formation on the isotopic composition of speleothems and their applicability as paleoclimatic indicators. *Geochim. Cosmochim. Acta*, 35, 801-824.
- HENDY, C.H. and A.T. WILSON, 1968. Paleoclimatic data from speleothems. *Nature*, 216, 48-51.
- HOEFS, J., 1980. Stable Isotope Geochemistry. Springer-Verlag N.Y., Heidelberg, Berlin. pp.
- HISLOP, R.W.P., 1974. Stable Isotopes for Identifying Accumulation and ablation processes on the Wapta Idefield. M.Sc. Thesis, Univ. of Calgary. 88 pp.
- INTERNATIONAL ATOMIC ENERGY AGENCY, 1981. Statistical Treatment of Environmental Isotope Data in Precipitation, 253 p. Tech. Prp. No. 206, IAEA Vienna.
- JONES, L., 1953. IR spectra of LiOH, LiOH-H²O and D species. Remarks on fundamental frequency of DH⁻. *J. Chem. Phys.*, V. 22, 2, 217-219.
- KARAKASTONOGLU, J., 1981. E.S.R. dating of speleothems. M.Sc. Thesis, McMaster Univ., Hamilton, Ontario.
- KENDALL, A.C. and P.L. BROUGHTON, 1978. Origin of fabrics in speleothems composed of columnar calcite crystals. *J. Sed. Petr.*, 48, 519-538.
- KNYF, M., 1980. Personal Communication.
- KU, T.-L., 1976. The uranium-series methods of age determination. *Ann. Rev. Earth Plan. Sci.*, 4, 347-380.
- LATHAM, A.G., 1981. Paleomagnetism, Rock Magnetism and Dating of Speleothem Deposits. Ph.D. Thesis, McMaster Univ., Hamilton, Ontario, 509 pp.
- LATHAM, A.G., H.P. SCHWARCZ, D.C. FORD and G.W. PEARCE, 1979. Paleomagnetism of Stalagmite Deposits. *Nature*, 280, 383-385.

- LEIGHTON, M.M., 1960. Classification of the Wisconsin glacial stage of the north-central U.S. *J. Geol.*, 68, 529-552.
- LORIUS, C., L. MERLIVAT, J. JOUZE and M. POURCHET, 1980. A 30,000 year isotope climatic record from Antarctic Ice. Abstract submitted to IAEA, 1980.
- MCCREA, J.M., 1950. On the isotopic chemistry of carbonates and a paleotemperature scale. *J. Chem. Phys.*, 18, 849-857.
- MCINTYRE, A., 1967. Coccoliths as Paleoclimatic Indicators of Pleistocene Glaciation. *Science*, 158, 1314-1317.
- McKINNEY, C.R., J.M. MCCREA, S. EPSTEIN, H.A. ALLEN and H.C. UREY, 1950. Improvements in mass spectrometers for the measurement of small differences in isotopic abundance ratios. *Rev. Sci. Inst.*, 21, 724.
- MERLIVAT, L and J. JOUZEL, 1979. Global climatic interpretation of the D-¹⁸O relationship for precipitation. *J. Geophys. Res.*, 84, C.8, 5029-5033.
- MOLINARI, J., 1977. Quelques remarques pratiques et une représentation commode facilitant l'exploitation des variations naturelles en D et en ¹⁸O dans les eaux. *J. Hydrol.*, 32, 383-392.
- MOORE, G.W. and G. NICHOLAS-SULLIVAN, 1978. *Speleology*, Zephyrus Press, 150 pp.
- NAKAMOTO, K., 1963. *Infrared spectra of inorganic and coordination compounds*. J. Wiley & Sons, N.Y. & London, 328 pp.
- NINKOVITCH, D. and N.J. SHACKLETON, 1975. Distribution, stratigraphic position and age of ash layer 'L' in the Panama Basin. *Earth Plan. Sci. Lett.*, 27, 20-34.
- O'NEIL, J.R., 1978. Personal Communication.
- O'NEIL, J.R., R.N. CLAYTON and T. MAYEDA, 1969. Oxygen isotope fractionation in divalent metal carbonates. *J. Chem. Phys.* 51, 5547-5558.
- O'NEIL, J.R., L.H. ADAMI and S. EPSTEIN, 1975. Revised value for the ¹⁸O fractionation factor between CO₂ and H₂O at 25°C. *U.S. Geol. Surv. J. Res.*, 3, 623-624.
- PICCIOTTO, E., X. de MAERE and I. FRIEDMAN, 1960. Isotopic composition and temperature of formation of Antarctic snows. *Nature*, 187, 857-859.

- PICKNETT, R.G., L.G. BRAY and R.D. STENNER, 1976. The chemistry of cave waters, Part II: Advance Discussion, in The Science of Speleology, T.D. Ford and C.H.D. Cullingford eds. Academic Press, London, 225-248.
- RAISBECK, G and F. YIOU, 1979. Possible use of ^{41}Ca for radioactive dating. Nature, 277, 42-43.
- REEVES, M.J., 1978. Recharge and Pollution of the English Chalk. Some Possible Mechanisms. Eng. Geol., 14, 231-240.
- ROQUES, H., 1969. A review of present-day problems in the physical chemistry of carbonates in solution. Cave Res. Gp. Gt. Brit., Trans., VII, 3, p. 139.
- ROSSMAN, G., 1981. Personal Communication.
- TOY, D.M. and R. ROY, 1957. H-D exchange in clays and the problems in assigning IR in the OH^- region. Geochim. Cosmochim. Acta, 11, 72-85.
- RUSSEL, R.D. and T. AHERN, 19⁷⁴. Economical Mass Spectrometer Ion Current Measurement with a Commercial Parametric Amplifier. Rev. Sci. Inst., 45, 11, 1467-1468.
- SAUZEY, G., 1974. Interpretation of Lysimeter Data. IAEA Report #160, 90 pp.
- SCHWARCZ, H.P., 1971. Conversion of mass spectrometric data for C, O, S. Tech. Memo. 71-7, Dept. of Geology, McMaster Univ., Hamilton, Ontario.
- SCHWARCZ, H.P., 1976. Personal Communication.
- SCHWARCZ, H.P., 1980. Absolute age determination of archeological sites by uranium series dating of travertines. Archeometry, 22, 1, 3-24.
- SCHWARCZ, H.P., 1981. Personal Communication.
- SCHWARCZ, H.P., R.S. HARMON, P. THOMPSON and D.C. FORD, 1976. Stable isotope studies of fluid inclusions in speleothems and their paleoclimatic significance. Geochim. Cosmochim. Acta, 40, 657-665.
- SCHWARCZ, H.P. and E.L. SPEELMAN, 1965. Determination of S and C coordination in scapolite by IR absorption spectrophotometry. Am. Min., 50, 656-666.

- SEARS, S., 1976. Inorganic and Isotopic Geochemistry of the Unsaturated Zone in a Carbonate Terrane. Ph.D. Thesis, Penn. State Univ., 236 pp.
- SHACKLETON, N.J., 1979. Personal Communication.
- SHACKLETON, N.J. and N.D. OPDYKE, 1976. Oxygen isotope and paleomagnetic stratigraphy of Pacific core V28-239, Late Pliocene to latest Pleistocene, *in* Investigation of Late Quaternary Paleoceanography and Pleaeoclimatology, R.M. Cline and J.D. Hays eds. Geol. Soc. Amer. Mem., 145, 449-464.
- SHEPPARD, S.M.F., R.L. NEILSEN and H.P. TAYLOR Jr., 1971. H and O in minerals from porphyry Cu deposits. *Econ. Geol.*, 66, 515.
- SMITH, D.B., R.L. OTLET, R.A. DOWNING, R.A. MONKHOUSE and F.J. PEARSON, 1975. Age of groundwater in the chalk of the London Basin. *Water Res. Res.*, 12, 3, 394-402.
- SONNTAG, C., E. KLIZCH, E.P. LÖHNHERT, E.M. EL-SHAZLY, K.O. MUNNICH, C. JUNGHANS, U. THORWEIKE, K. WEISTROFFER and F.M. SWAILEM, 1979. Paleoclimatic Information from D and O in ^{14}C dated N. Saharan Groundwaters. *Iso. Hydrol., Proc. Int. Symp.*, 2, 569-581.
- STEWART, G.L., 1974. Clay-water interaction, the behaviour of ^3H and ^2H in adsorbed water and the isotope effect. *Soil Sci. Am. Proc.*, 36, 421-426.
- STUIVER, M., 1968. Oxygen-18 content of atmospheric precipitation during last 11,000 yrs. in the Great Lakes region. *Science*, 162, 994-997.
- TAYLOR, H.P. Jr., 1974. The application of oxygen and hydrogen isotope studies to problems of hydrothermal alteration and ore deposition. *Econ. Geol.*, 69, 843-883.
- THOMPSON, P., 1973a. Speleochronology and Late Pleistocene climates inferred from O, C, H, U and Th isotopic abundances in speleothems. Ph.D. Thesis, McMaster Univ., Hamilton, Ontario.
- THOMPSON, P., D.C. FORD and H.P. SCHWARCZ, 1975a. $^{234}\text{U}/^{238}\text{U}$ ratios in limestone cave seepage waters and speleothems from West Virginia. *Geochim. Cosmochim. Acta*, 39, 661-669.

- THOMPSON, P., H.P. SCHWARCZ, and D.C. FORD, 1976. Stable isotope geochemistry, geothermometry and geochronology of speleothems from West Virginia. *Geol. Soc. Amer. Bull.*, 87, 1730-1738.
- THOMSON, C.K and T. ALEY, 1971. Ozark Underground Laboratory. *Ozark Caver*, 3, 5 & 6, 19 pp.
- THRAILKILL, J., 1976. Speleothems: In Walter, M.R. (Ed) *Stromatolites (Devel. in Sed. 20)*. Elsevier, Amsterdam, pp. 73-86.
- TRUSCOTT, M. and H.P. SCHWARCZ, 1978. Personal Communication.
- UREY, H.C., 1947. The thermodynamic properties of isotopic substances. *J. Chem. Soc.*, 562-581.
- UREY, H.C., H.A. LOWENSTAM, S. EPSTEIN and C.R. MCKINNEY, 1951. Measurement of paleotemperatures and temperatures of the Upper Cretaceous of England, Denmark and the south-east U.S.A. *Geol. Soc. Amer. Bull.*, 62, 399-416.
- WALTHAM, A.C., 1970. Cave development in the limestone of the Ingleborough District. 136, 574-585.
- WALTHAM, A.C., 1974. Geology and geomorphology of the caves of N.W. England, in *Limestones and Caves of North-West England*, A.C. Waltham ed., David and Charles, Newton Abbot, 25-45, 79-105, 273-309.
- WHITE, W., 1976. Cave Minerals and Speleothems, in *The Science of Spel.*, T.D. Ford and C.H.D. Cullingford (eds.). Academic Press, London, 267-327.
- WHITE, W., 1977. *In Speleology*, G.W. Moore and G. Nicholas-Sullivan (eds.). Zephyrus Press, 150 pp.
- WHITE, W., 1979. Personal Communication.
- WIGLEY, T.M.L., 1975. Personal Communication.
- WIGLEY, T.M.L. and M.C. BROWN, 1976. The physics of caves, in *The Science of Speleology*, T.D. Ford and C.H.D. Cullingford eds. Academic Press, 329-358.
- WHITE, W. and B.E. SCHEETZ, 1977. Vibrational Spectra of the Alkaline Earth Double Carbonates. *Am. Min.*, V. 62, 36-50.
- YAMAMOTO, M., 1980. Instructions for the operation of the BrF

line for H₂O. Tech. Memo, 80-3. Dept. of Geology, McMaster Univ., Hamilton, Ontario.

- YAPP, C.J. and S. EPSTEIN, 1977. Climatic implications of D/H ratios of meteoric water over North America (9500 - 22000 B.P.) as inferred from ancient wood cellulose C-H hydrogen. *Earth Plan. Sci. Lett.*, 34, 333-350.
- YONGE, C.J., 1976. Application of Neutron Activation to the Dating of Young Terrestrial Rocks. M.Phil., Surrey Univ., U.K., 80 pp.
- YONGE, C.J., 1979. Canadian Hole Keeps Growing. *Can. Caver*, V. 11, 2, 6-14.
- YONGE, C.J., 1981. Fluid Inclusions in Speleothems as Paleoclimate Indicators. *Proc. 8th Int. Cong. of Spel. VI*, 301-304.
- YONGE, C.J., 1982. Operation of the D/H mass spectrometer. Tech. Memo. 81. Dept. of Geology, McMaster Univ., Hamilton, Ontario.
- ZIMMERMAN, U., K.O. MUNMOH and W. ROETHER, 1967. Downward movement of soil movement traced by means of hydrogen isotopes. *In*, *Isotope Techniques in the Hydrologic Cycle*, Geophys. Monog. No. 11, AGU, pp 28-36.

APPENDIX IIsotopic Relationships

Abbreviations used:

- c = pertaining to calcite
- i = pertaining to water included in speleothems
- s = pertaining to cave seepage water
- w = pertaining to water generally
- x = unknown sample
- s = standard
- $\bar{\Delta\delta}$ = average shift in delta values
- $\Delta\delta$ = delta shift based on one example
- ‰ = permil
- t = time at which the intercept d is recorded; o is present day

(i) Delta Notation

$$\delta D = \left\{ \frac{(D/H)_x}{(D/H)_s} - 1 \right\} 10^3 \text{‰} \dots\dots\dots 1$$

$$\delta^{18}O = \left\{ \frac{(^{18}O/^{16}O)_x}{(^{18}O/^{16}O)_s} - 1 \right\} 10^3 \text{‰} \dots\dots\dots 2$$

$$\delta^{13}C = \left\{ \frac{(^{13}C/^{12}C)_x}{(^{13}C/^{12}C)_s} - 1 \right\} 10^3 \text{‰} \dots\dots\dots 3$$

(ii) Isotopic Shifts

$$\Delta\delta_{s-i}^D = 1000 \ln \alpha_{s-i}^D \dots\dots\dots 4$$

$$\Delta\delta_{s-i}^{18}O = 1000 \ln \alpha_{s-i}^{18}O \dots\dots\dots 5$$

(iii) General Meteoric Relationship

$$\delta D = 8 \delta^{18}O + d_t \dots\dots\dots 6$$

(iv) Isotopic Temperature Equation (in °K)

$$10^3 \ln K_{cw} = 2.78 (10^6 T^{-2}) - 2.89 \dots\dots\dots 7$$

$$\approx \delta^{18}O_c - \delta^{18}O_w \dots\dots\dots 8$$

where $1000 \ln K$ is less than 10.

APPENDIX II

- a) D/H Mass Spectrometer: Operational characteristics
and procedure.

- b) Calculation of δD and computer program

Operation of Deuterium Mass Spectrometer

- a) Water Samples Only:
1. Set or check variac setting for the Hg diffusion pumps at 55V and fill traps with liquid nitrogen. Set the Uranium furnace to 750°C and when pumps are operating fully, open N1 to mass spectrometer slowly.
 2. Fill T1 with dry ice and methanol. (Prepare T2 trap with the same, if rock samples are to be analysed later).
 3. Check V6E2, if open, close very carefully. Check that U-furnace is being pumped by DR1.
 4. Pump out volume behind syringe stopper; V6E3, V6E4, VE5 open; VP5 closed. Set P2 switch to 2. Dial should fall to about 5.
 5. Check that volumes X and S are being pumped by DR1, they should be, but if not, close U-furnace at VP2 and VX1 and open them up. When P1 (set switch to 1) registers < 10 (≈ 35) μmHg open up furnace again.
 6. Close V6E4 and open V6E2 (very carefully). This order is very important and put liquid nitrogen on T3.
 7. Inject about 1.4 μl of water sample with microlitre syringe. Leaving syringe in situ allow 10 minutes for freezing sample over. Meanwhile, if in run cycle, close VP2 and pump out previous gas from X via VX2, then open furnace to pump.
 8. Check and adjust major and minor (mass 2 and 3) peaks to "zero" (under 1000 (~ 500) but never zero, is good). Call OLDDELD at terminal.
 9. After 10 minutes, close V6E2 (very carefully), VP2 and VX2, remove trap (T3) and open V6E4, pull out plunger, replace after a few seconds and pull out syringe.
 10. Standard, close VR2 (or VR4 if light sample has been introduced) and open VR1 (or VR3).
 11. Close VP4, VP1 (or VP3) and open VR2 (or VR4). After a few seconds, close VS2 (VS1 should be open) and close vent to compressed air on the S side. Record the time. Major peak readings should be 8×10^{-9} , use fine adjustment compressed air regulator (S-side) to achieve this.
 12. Check peak positions (change decade dial on HV supply). They can change if the room (normally at 69°F) changes temperature.

13. Allowing around 5 - 10 minutes for reduction of water sample (Watch major peak X-setting until it stops rising), adjust mercury on X-side so that it also reads $8 \times 10^{-9} \text{A}$. In practice 1.4 ml of water will yield about this signal and subsequent adjustments will be small. If too much gas is generated then close V6P1 and open VX2. Close VX2 and open V6P1 do this until the required signal is achieved. Record yield on X-side (pH₂ column).
 14. Close VX1 and start run: Type in time, set knob to R, set switch to auto on ratio integrator, set red button at terminal and press run.
 15. Open VP2 and V6E2 to pump both ends of the U-furnance.
 16. Close V6E2, go back to instruction 6.
- b) Water from rock samples: (Water from crushed rock samples is treated initially in the same way as water samples, see Chapter 2 for prior extraction, start as for water samples).

Instruction 4 is the same except pumping of rock furnace takes place. If the sample is a powder, open V6E3 very slowly. Pumping is normally accompanied by low heating for varying amounts of time up to 24 hours.

Instruction 6 will read: Close V6E4, put liquid nitrogen on spiral trap T2, raise furnace F2 to required temperature and heat for an appropriate time (normally $\frac{1}{2}$ to 1 hour). When this is completed, close V6E3 and open V6E4 and pump out non-condensable gas. Exchange liquid nitrogen on T2 for methanol and dry ice and place liquid nitrogen on T3 top it up). The remaining gases, mainly CO₂, will be retained (P2 just below 20). Then close V6E4 open V6E2 (very carefully) and freeze over for 10 minutes. Go to instruction 8 and continue.

- c) Closing down: V6E2 should be closed. Bulbs X and S and the Uranium furnace should be pumped by DR1. T2 should be pumped by R3. Turn U-furnance down to 200°C and type BYE (return) into the terminal before switching off. Close N1.

Calculation of δD

The program DDELD is called and four initial values must be checked and changed as the need arises. These values are H, T, W, and Z (See program).

H is the H_3 correction and T, is the time factor for fractionation of the standard gas in bulb S, both are explained in Chapter 2.4.2.3. W is the VSMOW value for δD with respect to the reservoir gas. Z pertains to T and is the time (in minutes) for which the aliquot of reservoir gas has been residing in S.

Of the 24 data values read in, 20 are used in the subsequent calculation amounting to 5 separate determinations of raw δD . Each block of H data points (2X's and 2S's) is averaged such that ratios are taken at five particular times during the run. Variations in ratio with time are therefore removed.

The average of 5 δD 's is then processed with H_3^+ and reservoir fractionation being taken into account (lines 150 and 250) and is printed as corrected δD 's both with respect to the reservoir and VSMOW (lines 260 and 280), also see output.

The program (following) DDELD is stored on the PDP8 tape file and can be accessed by Silent 700 T.I. teletype.

```

10 H=12000
20 T=0.08
30 W=110.3
40 INP"TIME IN MINS"Z
50 FOR N=0T02\N=4*M
60 INP X(N+1),X(N+2),S(N+1),S(N+2),X(N+3),X(N+4),S(N+3),S(N+4)
70 NEXM
80 N=1\M=0
90 IF X(N)<100000 THEN 450
100 IF S(N)<100000 THEN 500
110 N=N+1\IF N<13 THEN 90
120 M=1
130 U(N)=(X(2*N+1)+X(2*N+2))/2
140 V(N)=(S(2*N)+S(2*N+1))/2
145 V=V+V(N)\U=U+U(N)
150 P(N)=U(N)/V(N)\R(N)=(U(N)-H)/(V(N)-H)
160 L=L+P(N)\M=M+R(N)
170 GOTO 200
180 N=N+1\IF N<6 THEN 130
183 PRI"MEAN X ="U/5\PRI"MEAN S ="V/5
185 U=((U/V)-1)*1000\PRI"TOTAL DEL D ="U
190 L=L/5\M=M/5
195 PRI"UNCORR MEAN ="L\PRI"CORR FOR H3 MEAN ="M
197 GOTO 240
200 R(N)=(R(N)-1)*1000
210 R(N)=(R(N)-((M/5)-1)*1000)^2
220 R=0\R=R+R(N)
230 GOTO 180
240 R=SDR(R/4)
250 M=(M-1)*1000+T*2
260 PRI"DEL D CORR. FOR H3 & TIME WRT REF ="M\PRI"+-"R
270 M=(M-W)/(1+(W*0.001))
280 PRI"DEL D WRT SMOV ="M
285 PRI\PRI
300 END
450 X(N)=X(N+1)
460 GOTO 110
500 S(N)=S(N+1)
510 GOTO 110

```

TIME IN MINS? 10

? 0283686, 0251467, 0272821, 0272811, 0262342, 0262004, 0274202, 0273463

? 0261560, 0261943, 0273076, 0274056, 0262297, 0262185, 0273241, 0271181

? 0263046, 0262730, 0273188, 0273499, 0261062, 0259599, 0271351, 0272275

MEAN X = 261876.8

MEAN S = 273006.8

TOTAL DEL D =-40.76822

UNCORR MEAN = .9592352

CORR FOR H3 MEAN = .9573611

DEL D CORR. FOR H3 & TIME WRT REF =-41.83888

+ - 1.901254

DEL D WRT SMOV =-131.3136

APPENDIX IIIBulk Water Isotopic Analyses

a) Standards

b) Samples

a(i) Replicate δD Determinations for VSMOW, SLAP, NBSIA,
DTAP 77 and 78, T1 ANTEI and T2 BEIJUNG

Standard	Date Span	No. of Samples	Sensitivity to 1 μl H_2O ($pH_2 \times 10^{-1} A$)	δD wrt SMOW \pm (%)	Machine ** duplication (%)
VSMOW	§ 1/79- 6/80	15	--	0.0 \pm 2.0	0.6
	8/80- 9/80	4	4.5 \pm 0.1	-2.1 \pm 2.8	0.6
	9/80- 9/80*	13	4.9 \pm 0.3	0.0 \pm 2.5	---
mean				\pm 2.4	
	9/80-10/80*	4	5.3 \pm 0.1	0.0 \pm 1.2	----
	10/80-11/80	5	4.6 \pm 0.2	-0.2 \pm 1.2	0.9
	§ 11/80- 3/81*	11	4.8 \pm 0.4	0.0 \pm 1.1	0.4
	3/81- 4/81	4	4.6 \pm 0.2	+0.3 \pm 1.0	---
	4/81- 5/81*	5	4.8 \pm 0.1	0.0 \pm 1.2	0.2
	6/81- 8/81	4	4.8 \pm 0.2	-2.0 \pm 0.3	0.2
	9/81-10/81	4	5.5 \pm 0.2	-3.6 \pm 0.8	0.6
	10/81-10/81*	5	4.9 \pm 0.1	0.0 \pm 1.4	0.5
mean				\pm 1.05	
SLAP	§ 11/80- 3/81*	7	4.5 \pm 0.1	-428 \pm 2.4	---
	4/81- 4/81	1	5.1	-432.4	----
	5/81- 6/81*	2	5.1	-431.2	---
NBSIA	§ 1/79- 6/80*	7		-183.3 \pm 3.0	
	8/80- 9/80	4	4.3 \pm 0.2	-176.7 \pm 1.0	0.4
	9/80-10/80*	4	4.9 \pm 0.1	-167.8 \pm 1.1	---
	§ 11/80-11/80	2		-181.7	---
DTAP'77	1/79- 6/80	6		- 42.8 \pm 1.6	1.1
DTAP'78	5/81- 5/81	5	4.6 \pm 0.3	- 51.7 \pm 1.1	0.5
T1 ANTEI	6/81	3	5.1 \pm 0.0	- 58.0 \pm 0.8	---
T2 BEIJUNG	6/81	2	5.1	- 62.3	0.4

* Reservoir gas was changed on these occasions.

**Change in δD value following a successive run of the same gas in the machine.

§ Standards run to check H_3^+ correction and internal consistency of measured δD values.

a(ii) Replicate $\delta^{18}\text{O}$ determinations for DTAP'78, VSMOW, SLAP, NBSIA, NBSI, and GISP

Standard	Date Span	No. of Samples	$\delta^{18}\text{O}$ (VSMOW) + (%)	Machine Duplication
DTAP'78	9/79 - 10/79	6	-7.42 ± 0.18	0.03
	10/79 - 11/79	5	-7.37 ± 0.12	0.06
	11/79 - 1/80	3	-7.65	0.05
	1/80 - 2/80	8	7.7 ± 0.11	0.04
	2/80 - 3/80	4	7.77 ± 0.05	0.05
	3/80 - 5/80	8	7.74 ± 0.18	0.02
mean	-----	-	7.63 ± 0.20	----
VSMOW	17/80	1	+ 0.11	----
SLAP	17/80	1	-55.85	----
NBSIA	7/80	1	-24.90	----
NBSI	6/79	1	- 8.48	----
GISP	17/80	1	-21.29	----

b (1) Cave Drip Water, Soil Water and Precipitation for
Three East United States Caves

Total Mean drip water:
 $\delta^{18}\text{O} = 5.98 \pm 0.56$
 $\delta\text{D} = 41.4 \pm 1.9$

OUT.No	154 - 255	255 - 273	274 - 304	305 - 330	331 - 357	358 - 30	31 - 58	59 - 82	83 - 101	102 - 169	170 - 193	194 - 243	243 - 257
SITE													
A		-6.00 -45.9			-5.89 -41.1	-3.56 -39.3	-6.53 -43.5		-39.5 -6.03 -40.3		-6.61 -43.3	-6.17 -43.3	
B		-5.82 -41.1			-5.84 -32.5	-6.08 -35.5	-6.36 -43.4		-43.6 -6.51 -43.1		-6.21 -42.6		
C						-3.69 -36.6			-44.2 -6.28 -37.1				
1	-4.62 -36.9												-6.65 -44.6
2		-6.05 -45.0	-5.95 -43.7	-5.95 -43.7	-5.61 -44.8	-4.54 -38.1	-6.14 -43.5	-5.99 -43.9	-6.05 -40.0	-6.44 -40.0		-5.77 -39.9	
3	-5.55 -39.1	-6.02 -42.8	-6.31 -43.8	-5.06 -40.5	-5.10 -41.9	-4.77 -39.2	-6.03 -44.2	-6.45 -42.8	-6.35 -48.4				-5.93 -46.1
4		-6.08 -41.7	-6.22 -44.6	-3.43 -35.2	-6.21 -46.0	-3.48 -35.9	-4.77 -43.7	-5.98 -47.1	-5.89 -40.3	-5.71 -45.3	-6.41 -41.9	-5.81 -41.8	-6.30 -40.3
5	-6.13 -46.0			-4.83 -4.05									-6.27 -43.2
6	-4.69 -41.6	-6.17 -42.3	-6.34 -42.9		-6.20 -32.9	-6.10 -43.2	-5.84 -43.3	-6.01 -43.6	-6.23 -36.9	-6.66 -36.5	-6.49 -41.0	-6.31 -44.0	
7		-36.6											
8													
9	-3.97 -32.8												
10	-4.12 -38.3												
mean	-4.85 -38.8	-6.02 -43.1	-6.21 -43.1	-5.85 -40.0	-5.99 -39.9	-4.60 -38.3	-6.18 -43.6		-6.12 -43.5	-6.19 -40.9	-6.27 -40.6	-6.43 -42.2	-6.12 -41.3
soil					-4.24 -30.0				-7.04 -53.2	-7.38 -52.9	-4.63 -22.0		
ppt		-5.08 -34.6	-7.31 -35.3	-0.96 -16.8	-7.16 -49.4				-16.09 -129.6		-2.26 -10.3	-2.34 -15.9	

Total Mean Drip Water:
 $\delta^{18}\text{O} = -7.72 \pm 0.67$
 $\delta\text{D} = -57.6 \pm 2.4$

SHEVANDOAH CAVERNS, Va

1978 - 1979

SITE	30 - 59	60 - 90	122 - 162	163 - 196	197 - 228	229 - 250	251 - 287	288 - 317	317 - 356
1	-7.76 -55.8		-7.43 -57.3	-8.76 -62.3	-7.69 -64.4	-7.73 -54.2	-8.35 -53.6	-7.53 -52.4	-8.56 -58.4
2	-8.20 -58.7	-61.8 -55.3		-8.42 -57.0	-6.61 -58.9				
3	-7.97 -56.7		-7.71 -62.0	-8.50 -58.5	-7.89 -58.1	-7.75 -57.0	-8.7 -51.1	-7.86 -52.8	-7.44 -56.3
4	-7.97 -60.8		-7.31 -66.0	-8.73 -61.5	-7.55 -55.1	-8.01 -61.5	-8.24 -62.0	-8.59 -57.1	-7.61 -57.3
mean	-7.98 -58.0	-61.8 -55.3	-7.48 -61.8	-8.60 -59.8	-7.44 -59.1	-7.83 -57.6	-8.15 -55.6	-7.99 -54.1	-7.87 -57.3
ppt	-12.00 -93.9	-4.52 -39.8				-4.72 -37.8	-5.71 -33.8	-3.47 -16.3	-10.72 -28.2

Total Mean Drip Water:
 $\delta^{18}\text{O} = -7.77 \pm 0.78$
 $\delta\text{D} = -52.1 \pm 4.5$

INDIAN ECHO CAVERNS, Pa.

SITE	162 - 226	227 - 257	258 - 292	293 - 320	321 - 340	341 - 350	351 - 54	55 - 76	77 - 105	106 - 198	199 - 235
1	-7.20 -51.4		-7.31 -54.1		-6.75 -45.5	-6.89 -41.5	-7.65 -49.3	-9.22 -60.6	-62.9	-39.5	
2	-7.94 -55.3	-7.09 -52.0	-7.31 -54.0	-8.05 -54.9	-7.14 -52.5		-7.62 -52.9	-7.66 -52.8	-45.5	-8.12 -60.9	-7.62 -58.8
3		-7.45 -53.8	-7.50 -48.7	-7.92 -50.6						-47.1	-7.02 -55.6
mean	-7.57 -53.3	-7.27 -55.5	-7.61 -52.3	-7.98 -52.8	-6.95 -49.0	-6.89 -41.5	-7.63 -51.1	-8.44 -56.7	-9.65 -54.2	-8.12 -49.1	-7.32 -57.2
ppt				-5.41 -31.7							-3.30 -19.9

b(ii) Cave drip water and precipitation from other areas:

Cave	Location	$\delta^{18}O$	δD	Date Collected	Water Type*
Friar's Hole	W. Va. #1	-16.01	-116.7	2/79	S
	F1	- 7.76	- 57.8		D
	F2	- 8.20	- 60.7		D
	2	-12.00	- 95.9		R
	3	- 5.44	- 31.6	5/79	R
	F3	- 7.57	- 52.7	6/79	D
	F4	- 7.90	- 51.8		D
	4	- 2.60	- 4.9		R
	5	- 2.63	- 33.5		R
	CH1		- 55.6		D
	6	- 3.85	- 24.8	7/79	R
	7	- 5.18	- 40.7	8/79	R
	NB1		- 51.3	4/81	D
	F5		- 55.1	4/81	D
Mean D		- 7.86	- 55.5		
Various Sites	Van.Is.V1B	-12.31	- 87.2	6/75	D
	V5A	-11.11	- 84.4		D
	V3B	-11.03	- 88.2		D
	V6B	-10.59	- 82.8		D
	V3A	-10.52	- 87.1		D
	VCZ	-10.82	- 85.0		D
Mean		11.06	- 85.8		
#310	Ala. 1	- 5.03	- 26.7	6/78	D
	2	- 5.14	- 29.6		D
	3	- 5.14	- 29.1		D
	1R	- 3.97	- 37.3		R
Hughes Spring	#2	- 5.55	- 22.1		D
Wendy's Cave	#1		- 24.8	3/78	D
	2	- 5.52	- 26.0		D
Key Cave	#1	- 5.02	- 32.0		D
	2	- 4.87	- 18.5		D
McFail's ,	N.Y. #1	- 7.10	- 67.4	7/80	D
	2	- 7.30	- 67.0		D
Cumberland Caverns ,	TENN. #1	- 6.33	- 32.1	6/78	D
	2	- 5.82	- 44.5		D
	3	- 7.52	- 38.4		D
	4	- 6.26	- 49.4		D
	1R	- 2.11	- 85.7		R
Mean D		- 6.48	- 41.1		

* D = Drip; S = Snow; R = Rain

Cave	Location	$\delta^{18}O$	δD	Date Collected	Water Type*
Wind Cave,	S, Da. #1	- 9.32	-107.2	8/78	D
	2		- 98.0		D
	3	- 9.61	- 94.5		D
	Mean	- 9.47	- 99.9		
Marengo Cave,	Ia. 1	- 4.25	- 28.1	8/78	D
	2	- 4.58	- 35.9		D
	1	- 4.33	- 29.8	9/78	D
	2	- 5.24	- 32.5		D
Mean	- 4.60	- 31.6			
South Georgia	#1		- 73.2	6/80	D
		- 9.32	- 68.2		D
			- 68.7		D
Mean	- 9.32	- 70.0			
Belize	#1	- 3.69	- 16.8	14/81	D
	5	- 3.14	- 13.9		D
	12	- 4.37	- 24.3		D
	15	- 3.12	- 16.6		D
	19	- 3.60	- 18.3		D
	31	- 2.89	- 16.5		D
	34	- 3.91	- 22.3		D
	45	- 3.24	- 12.6		D
	53	- 3.82	- 30.1		D
	56	- 3.98	- 17.0		D
	71	- 3.56	- 16.0		D
	72	- 3.91	- 22.3		D
	73	- 3.81	- 20.8		D
	90	- 0.28	- 18.3		D
	93	- 3.82	- 25.7		D
99	- 1.16	- 19.1	D		
Mean	-3.63 \pm 0.41	- 19.5 \pm 4.9			

* D = Drip; S = Snow; R = Rain

b(iii) δD and $\delta^{18}O$ data from the SWISS/DEEP Antarctic Ice Core

Sample	Number	$\delta^{18}O$	δD	Age
DEEP	# 1	-41.39	-319.6	WISCONSIN
Run 8/10/80	2	-40.31	-324.7	
	3	-41.71	-317.5	
	4	-42.14	-334.9	
	5	-42.05	-330.0	
	6	-42.45	-337.9	
	7	-41.77	-334.7	
	8	-41.75	-328.7	
	9	-42.32	-339.1	
	10	-42.60	-332.7	
	11	-41.08	-327.0	
	12	-40.94	-324.7	
	13	-41.63	-331.0	
	14	-41.84	-327.6	
	15	-41.29	-334.0	
Mean		-41.68 \pm 0.61	-329.6 \pm 6.3	
SWISS	# 1	-32.37	-247.4	PRESENT
	2	-32.60	-244.0	
	3	-32.17	-246.8	
	4	-32.52	-248.3	
	5	-32.26	-239.6	
	6	-31.58	-248.1	
	7	-31.24	-243.2	
	8	-31.41	-244.7	
	9	-31.49	-241.2	
	10	-32.00	-241.8	
	11	-32.64	-255.8	
	12	-32.82	-255.3	
	13	-33.70	-262.4	
	14	-33.18	-259.2	
end run 15/10/80	15	-34.29	-263.3	
Mean		-32.42 \pm 0.85	-249.4 \pm 7.8	

APPENDIX IVIsotope data of water from speleothems
and co-existing calcite

- a) Extraction by crushing

- b) Extraction by Decrepitation (δD only)

a (i) Oxygen *

Sample	Sample Weight(g)	H ₂ O Content Weight (%)	$\delta^{13}\text{C}(\text{‰})$	$\delta^{18}\text{O}_c(\text{‰})$	$\delta^{18}\text{O}_c(\text{‰})$ PDB	Isotopic Temp. ($^{\circ}\text{C}$)	Age (ka)
73017 Bermuda							
1-7-2	2.109	0.415	- 9.87	-5.56	-2.49	3.3	~150
1-7-3	1.857	0.446	-10.03	-5.85	-2.62	2.7	
1-14-1	1.810	0.461	- 9.71	-5.67	-2.41	2.6	
1-15-1	1.731	0.447	- 9.68	-5.45	-2.55	3.9	
2-0-1	1.327	0.285	-10.14	-4.45	-2.67	8.4	
2-0-3	1.607	0.300	-10.07	-3.99	-2.55	9.8	
3-0-1	1.226	0.282	- 9.63	-6.28	-2.59	1.0	
3-0-2	1.210	0.342	- 9.67	-5.66	-2.87	4.4	
4-0-1	1.393	0.365	-10.97	-6.06	-3.07	3.6	
5-0-1	1.635	0.507	-10.45	-5.68	-3.00	4.8	
6-0-1	1.675	0.322	-10.24	-6.04	-3.19	4.2	
7-0-1	1.295	0.242	- 9.74	-6.51	-3.00	1.7	
8-0-1	1.640	0.367	- 9.99	-4.06	-3.32	12.7	
9-0-1	1.408	0.312	- 9.68	-4.85	-3.19	8.9	
10-0-1	1.348	0.334	- 8.35	-4.83	-2.75	7.2	
10-0-2	1.460	0.316	- 8.77	-4.55	-3.04	9.5	
MEAN		0.359 \pm 0.076		-5.343 \pm 0.787	-2.832 \pm 0.288	5.54 \pm 3.41	
76501 Missouri							
#1	6.042	0.149	-10.66	-6.71	-3.62	3.2	236
#2	8.134	0.023	-10.64	-8.05	-4.68	2.1	215
#3	7.971	0.027	-10.21	-16.31	-4.24	-25.9	202
#6	7.231	0.083	- 6.98	-6.88	-4.42	5.7	96
#7	8.424	0.046	- 8.25	-6.47	-4.88	9.2	77
#8	8.597	0.013	- 8.66	-6.03	-4.56	9.6	68
#9	9.596	0.140	- 9.95	-5.98	-4.47	9.5	56

a (i) Oxygen* ... cont'd

Sample	Sample Weight (g)	H ₂ O Content Weight (%)	$\delta^{13}\text{C}$ (‰)	$\delta^{18}\text{O}_i$ (‰)	$\delta^{18}\text{O}_c$ (‰) PDB	Isotopic Temp. (°C)	Age (ka)
77162 Lost Johns							
1-3-1	1.173	0.276	- 3.45	-11.87	-3.24	-15.0	150
1-3-2	1.441	0.225	- 3.41	-10.44	-3.16	-11.5	
1-2-4	1.639	0.198	- 6.24	-10.16	-3.97	- 7.9	
1-2-5	2.097	0.215	- 6.24	- 9.31	-3.97	- 5.0	
MEAN		0.229 ± 0.034		-10.45 ± 1.06	-3.59 ± 0.45	- 9.9 ± 4.3	
77151 Victoria Cave							
B-1-1	5.925	0.44	- 7.55	-14.98	-4.04	-22.7	~250
B-2-1	9.095	0.44	- 5.35	-13.75	-3.59	-20.5	
B-3-1	9.048	0.71	- 5.60	-13.57	-3.61	-19.8	
MEAN		0.53 ± 0.16		-14.10 ± 0.77	-3.75 ± 0.25	-21.0 ± 1.5	
807MF1							
NY-1-1	6.583	0.45	- 9.50	-12.03	-7.4	-2.5	Modern
NY-1-3	4.857	0.74	- 9.47	- 9.39	-7.33	7.2	

* =After M. Yamamoto (pers comm.)

a (ii) Hydrogen

Sample	Number	H ₂ O Content (%)	δ ¹⁸ Oc (‰)	δDi (‰)	Inferred Isotopic Temp (°C)	a	dt	a,dt. ref
73017 *	0'C	2.45		- 57.3				
	0C	3.90		- 56.9				
	1C	4.90		- 48.6				
	2C	5.20		- 39.7				
	3C	3.38		- 48.8				
	4C	4.25	27.542 ± 0.288	- 32.3				
	5C	3.95		- 45.3	+ 4.0 ± 6.2			
	6C	4.45		- 58.1				
	7C	4.00		- 28.2				
	8C	3.13		- 40.0				
	9C	3.85		- 47.5				
	10C	----		- 66.3				
	11C	5.20		- 65.5				
	12C	4.95		- 57.8				
	MEAN	4.12 ± 0.83		- 43.2 ± 9.2		6.0	4.2	Harmon et al, '78
77162	1-2-3C	2.58	27.33 ± 0.45	-106.2	- 26.0	6.9	0.3	Evans et al, '78
Lost Johns	1-3-3C	2.90		- 69.3	- 10.1			
77151B Victoria Cave	#1C	0.009	27.00 ± 0.25	- 41.8	+ 5.3	6.9	0.3	
797MP1-NY	-1-2#1C	0.75	23.39	- 94.5	- 6	8	10	Dansgaard, '64
	-1-2#2C	0.42	-----	- 87.0	- 2.5			
807CW6, Iowa	A	0.06	24.52	- 57.2	+ 5.6			
	B	0.06		- 67.1	- 0.9			
807CH1, W.Va.	A	0.13	25.16	- 62.8	+ 0.6			
	B	0.22		- 77.4	- 6.0			

a (ii) Hydrogen

Sample	Number	H ₂ O Content (%)	δ ¹⁸ Oc (%)	δDi (%)	Inferred Isotopic Temp. (°C)	a	d _t	a,dt. ref
Mirror Lake, Pa. (Indian Echo Cavern)	A	0.74	24.06	- 64.0	+ 4.1	8	10	Dansgaard, '64
	B	1.79		- 77.9	- 2.3			
76010 Van.Is.	8	0.27	19.29	-104.0	+ 3.2			
	9	0.35	19.27	-118.2	- 3.2			
	10	0.38	19.34	-108.2	+ 1.3			
	MEAN	0.33 ± 0.06	19.30 ± 0.04	-110.1 ± 7.3	0.4 ± 3.3			
Llano Chiquito	Wood #1	0.47	24.05	- 89.8	- 7.4			

A,B = splits of same sample

C = water extracted by crushing

* Replicates of 73017 (numbers 0C to 12C) extend the same distance along and are stratigraphically above the growth layer of 73017 in Table a(i) (numbers 1 to 10).

b (i) Individual Samples

Sample	No.	H ₂ O Content (‰)	δ ¹⁸ Oc (‰)	δDi (‰)	a	d _t	ref. of a,b.
Mirror Lake, Pa. (Indian Echo Caverns)	#6D	8.59	24.39	-74.3	8	10	Dansgaard, '64
	#7D	3.79	± 0.30	-72.1			
	#ED	4.57		-70.8			
	MEAN	5.55		-72.4 ± 1.8			
	#FCR	1.58		-71.7			
807CW 6 Ia. (Cold Water Cave)	#7D	3.89		-80.7			
	#6CR	--	24.94	-81.0			
	#8CR	1.56	± 0.11	-85.2			
	MEAN			-83.1			
Bone-Norman, W.Va. (Straws)	#2D	3.95		-77.7			
	2'D	3.71		-78.8			
	MEAN	3.83		-78.3			
Friar's Hole, W.Va. Straws	#1'D	1.30		-68.1			
	#2D	1.36		-71.3			
	MEAN	1.33		-69.7			
73107 Bermuda	#1D	8.93	27.54	-41.1	6.0	4.2	Harmon, et al, '78
	#2CR	1.46		-41.0			
75350 Jamaica	#7D	1.78	26.22	-30.7	8	0	Dansgaard, 64
Llano Chiquito	#1'D	3.36	24.05	-54.2	8	10	
Wind Cave, S.Da.	#1D	7.91	20.22	-132.1	8	10	
807CHI, W.Va.	#7	2.37	25.16	-109.7	8	10	
	#3	--		-109.6			

b (i) Individual Samples ... cont'd

Sample	No.	H ₂ O Content (‰)	δ ¹⁸ Oc (‰)	δDi (‰)	a	d _c	ref. of a,b.
77151B Victoria Cave, U.K.	#1	3.14	26.22	-76.9	6.9	0.3	Evans et al., '78
South Georgia	TIP	2.37	26.0	-77.0	8	0	IAEA ppt ⁿ '81
Sub-glacial ppt B.C.	#1	14.66	12.26	-160.7	8	10	Dansgaard, '64
Hydrothermal Calcite	#1	0.08	28.2	-74.1			

b (ii) Profiles

Sample	Number	H ₂ O Content (weight %)	δ ¹⁸ O _c (‰)	δDi (‰)	Isotopic Temp (°C)	δ ¹³ C	No. of Analyses of δ ¹⁸ O & δ ¹³ C
797MP1, NY	5LD	0.360		- 90.1			
	8LD	0.414		- 90.3			
	9LD	0.343		- 90.6			
	11LD	0.350		- 91.0			
	-2LD	0.340		- 90.4			
	-5LD	0.356		- 86.7			
	MEAN	0.361 ± 0.027		- 89.9 ± 1.6	5.1		
	-ILCR	0.211	23.01	- 95.6	3.9	- 9.29	11
	14AD	0.411	23.30	- 97.3	1.0	- 9.12	9
	20AD	0.458	22.85	- 95.1	3.7	- 9.64	9
	30AD	0.650	22.94	- 91.9	6.9	- 9.56	7
	40AD	0.252	23.35	-101.8	-1.2	- 9.14	7
	50AD	0.859	23.10	- 99.3	0.8	-10.03	8
	60AD	0.454	23.18	-102.8	-1.1	- 9.71	8
70AD	0.405	23.15	- 95.1	3.6	- 9.77	10	
	MEAN	0.498 ± 0.197					
75125	(i)AD	0.187		----	---	Gascoyne, '79	
	(ii)AD	0.157	19.63	-123.6	2.4		
	(iii)AD	0.170	19.49	-119.7	4.8		
	(iv)AD	0.191	19.24	-124.6	3.4		
	(v)AD	0.185	19.17	-129.7	1.3		
	(vi)AD	0.159	19.41	-124.8	2.7		
	(vii)AD	0.196	19.10	-129.4	1.7		
	(viii)AD	----	18.88	----	---		
	(ix)AD	0.170	19.17	-116.0	7.9		
	MEAN	0.178 ± 0.014					

b (ii) Profiles ... cont'd

Sample	Number	H ₂ O Content (weight %)	δ ¹⁸ Oc (‰)	δDi (‰)	Isotopic Temp (°C)
76013	Top D	0.266	20.09	-117.5	3.6
	Middle D	0.251	20.02	----	---
	Base D	0.155	20.22	-106.0	8.7
75123	1aD	0.298	19.82	-123.7	1.7
	1CR	0.150		-123.8	
	2A	0.291	19.94	-120.0	3.0
	3A	----	19.40	----	---
	4A	----	19.54	----	---
	5A	0.301	20.13	-117.6	3.4
	6A	0.433	20.06	-116.8	4.0
	7A	0.408	19.94	-118.5	3.7
	2aD	0.266	20.37	-115.4	3.5
		MEAN	0.400 ± 0.075		

* corrected isotopic temperatures

CR= decrepitation of powders

D = decrepitation

1a= sample split from 1, etc.

L = samples taken along growth layer

A = samples taken along speleothem axis

b (ii) Profiles, 74017 Coldwater Cave, Iowa

Sample and No.	Height Above Base (cm)	Water Content (wt. %)	$\delta^{18}\text{O}$ (‰) ^c	δD_1 (‰)	Isotopic Temp (°C)	$\delta^{13}\text{C}$ (‰)
1	53.0	0.860	26.48	- 70.8	1.5	- 8.65
2	52.0	0.896	26.88	- 64.8	3.8	- 8.31
3	50.5	0.930	26.66	- 61.8	5.1	- 8.81
4	49.3	0.890	26.45	- 63.7	5.0	- 8.47
5	48.1	0.901	26.54	- 70.4	1.4	- 8.83
6	44.0	0.778	26.15	- 62.7	6.6	- 8.85
7	40.5	0.790	25.97	- 63.5	6.9	- 8.55
8	37.7	0.710	26.39	- 74.1	0.3	- 8.30
9	36.2	0.682	26.50	- 69.1	3.2	- 8.15
10	34.2	0.696	26.86	- 64.9	2.8	- 7.99
11	33.2	0.648	26.85	- 65.9	2.4	- 8.01
12	32.1	0.572	26.11	- 64.2	6.1	- 7.94
13	29.7	0.911	25.99	- 66.5	5.4	- 8.10
14	27.0	0.680	26.34	- 66.8	3.9	- 7.80
15	24.0	0.674	26.19	- 69.0	3.4	- 7.94
16	21.9	0.644	26.80	- 67.2	2.0	- 7.74
17	19.5	0.600	26.75	- 64.6	3.4	- 8.37
18	15.7	0.634	26.06	- 70.2	3.3	- 8.74
19	11.7	0.600	25.84	- 65.9	6.3	- 8.52
20	8.0	0.672	25.84	- 64.0	7.0	- 8.28
21	4.2	0.640	26.24	- 69.4	3.0	- 7.92
22	0.5	0.564	26.97	- 72.2	-1.0	- 8.80
13	1a	29.7	0.906	26.02	- 67.2	- 8.11
	1b	29.7	0.830	25.94	- 63.0	- 8.04
	3a	29.7	0.916		- 67.4	
	4a	29.7	0.884		- 68.6	
	7b	29.7	1.020		- 66.3	
			0.911 \pm 0.069		- 66.5 \pm 2.1	
Total			0.755 \pm 0.133			

biii) $\delta^{18}\text{O}$ and $\delta^{13}\text{C}$ from Growth Layers of 797MPI and
74017 (Vancouver Island data is in Gascoyne, 1979)

McFails 797MPI

Growth Layer A - outermost layer at 1

	$\delta^{18}\text{O}$	$\delta^{13}\text{C}$	Distance from axis (cm)
A-1	23.23	- 8.54	0
A-2	23.38	- 8.62	2
A-3	23.29	- 8.67	4
A-4	22.84	- 9.76	6
A-5	23.08	- 9.23	8
A-6	23.91	- 9.06	10
A-7	23.30	- 8.90	12
A-8	23.35	- 8.75	14
mean	23.30 \pm 0.30	- 8.94 \pm 0.40	

Growth Layer B at 20

B-1	23.38	- 8.70	- 10
B-2	23.14	- 9.49	- 8
B-3	23.14	- 9.45	- 6
B-4	23.25	- 9.61	- 4
B-5	23.31	- 9.75	- 2
B-6	23.16	- 9.57	0
B-7	23.44	- 8.94	2
B-8	23.40	- 8.73	4
mean	23.28 \pm 0.12	- 9.43 \pm 0.37	

Growth Layer C at 50

C-1	23.35	- 9.80	- 4
C-2	23.45	- 9.63	- 3
C-3	23.35	- 9.97	- 2
C-4	23.59	- 9.96	- 1
C-5	23.24	- 9.98	0
C-6	23.38	- 9.95	1
C-7	23.24	- 9.87	2
C-8	23.52	- 9.44	3
C-9	23.45	- 9.34	4
mean	23.40 \pm 0.12	- 9.76 \pm 0.26	

biii) ... cont'd

74017

	$\delta^{18}\text{O}$	$\delta^{13}\text{C}$	Distance from axis (cm)
1	26.43	- 7.83	0
2	26.47	- 8.47	- 2.5
3	26.61	- 8.37	- 5.0
4	26.37	- 8.45	- 7.5
5	26.42	- 8.66	-10.0
6	26.22	- 9.04	-12.5
7	26.29	- 8.85	-15.0
mean	26.40 \pm 0.13	- 8.52 \pm 0.39	

APPENDIX VIsotope Data of Water from Hydrous and
Hydrothermal Minerals

a) Ore Deposits

b) Granites

a) * = $\delta^{18}O_i$ inferred from $\delta^{18}O$ (quartz) and Sulphur Isotope Temperatures (Ding et al., 1981)

Sample No.	Mineral	δDi	$\delta^{18}O_i^*$	Water Yield(wt %)
004	Calcite	-47.6	- 6.8	0.95
004	Quartz	-46.1		1.58
001	Quartz	-59.9	+ 0.8	1.68
003	Quartz	-45.3	+ 2.1	2.09
013	Barite	-48.7	+ 2.2	0.75
018	Quartz	-47.2	+ 4.4	3.22
020	Barite	-39.0	+ 0.5	0.81
021	Quartz	-46.5	+ 5.0	1.36
022-1	Barite	-34.1	+ 1.8	4.31
022-2	Barite	-37.6		3.36
023-1	Barite	-68.3	- 2.0	3.00
023-2	Barite	-70.5		2.67
031-1	Sphalerite	-31.2	+ 3.7	0.12
031-2	Sphalerite	-31.6		0.14

Overall replication in δDi is \pm 1.3% based on four pairs

b) ** $\delta^{18}O$ of hydroxyl groups (Cramer, et al., 1981)

Sample	No. of Analysis	δD (OH)	$\delta^{18}O$ (OH)**	Water Yield(wt %)
A6 71	1	- 117.4	8.6	162
A6 14	1	- 135.6	8.3	238
A6 49	1	- 121.3	8.7	0.242
A6 53	1	- 128.5	8.5	0.203
A6 177	1	- 127.8	10.0	0.169
A6 260	1	- 128.8	9.0	0.290
A6 281	1	- 108.0	8.2	0.286
A6 142	1	- 108.8	9.5	0.261
A6 140	1	- 102.3	9.7	0.136
A6 197	1	- 126.7	9.6	0.202
A6 261	1	- 137.5	9.7	0.461
	2	- 139.5		--
A6 182	4	- 117.8		0.358
	5	- 119.5	9.2	0.389
	6	- 118.9		0.317
	7	- 119.8		0.466